UNIVERSITY OF BIRMINGHAM

MASS SPECTROMETRY PROFILING OF PROTEINS AND THEIR UBIQUITIN MODIFICATIONS IN AGEING SKELETAL MUSCLE

by

Samuel Oliver Lord BSc, MSc

A thesis submitted to

School of Sport, Exercise and Rehabilitation Sciences

The University of Birmingham

For the degree of

DOCTOR OF PHILOSOPHY

School of Sport Exercise and Rehabilitation Sciences

College of Life and Environmental Sciences

University of Birmingham

September 2024

SUPERVISORS

Dr. Yu-Chiang Lai, Ph.D. (Primary)

Prof. Gareth Wallis, Ph.D. (Secondary)

ASSESMENT COMMITTEE

Dr. Martin Whitham, Ph.D. (Internal examiner)

Dr. Bradley Elliot, Ph.D. (University of Westminster)

Dr. Catarina Rendeiro, Ph.D. (Chair)

ABSTRACT

Skeletal muscle mass and function progressively decline with age. This decline is exacerbated in later life, contributing to the development of sarcopenia which is prevalent in many chronic diseases and a predictor of mortality. The molecular mechanisms driving this decline are not fully understood, slowing the development of pharmaceutical interventions. This thesis uses mass spectrometry to profile age-related changes in proteins and their ubiquitin modifications in mouse skeletal muscle to elucidate potential driving mechanisms of sarcopenia. We begin by reviewing the application of proteomics to study ubiquitylated proteins – termed ubiquitylomics – highlighting its application in skeletal muscle research. We developed a workflow designed to address challenges associated with skeletal muscle proteome profiling, later modifying the protocol to allow for the detection of ubiquitylated sites. Our workflow was applied on skeletal muscle obtained from young (6 month) and old (21-22 month) C57BL/6 male and female mice. Bioinformatics analysis of the proteomics dataset highlighted profound changes to extracellular matrix, mitochondria, energy metabolism, proteostasis, sarcomere and spliceosome proteins. Of note, we show that the unfolded protein response in the endoplasmic reticulum was a male-specific trait in our aged cohort. The ubiquitylomics dataset revealed age-related changes on sites from mitochondrial proteins, histones, ribosomal subunits and UPS-associated proteins. There was no clear relationship between muscle protein abundance and their ubiquitylation status, indicating a more complex mechanism than ubiquitin-mediated degradation. Ubiquitylation of histone H2B – increased during ageing of simpler organisms – was consistently downregulated in both males and females, occurring on an isoform not previously mentioned in the ageing field. Altogether, this thesis improves our mechanistic understanding of ageing skeletal muscle preceding sarcopenia, offering some potential targets for future research.

ACKNOWLEDGEMENTS

Firstly, I would like to thank Dr. Yu-Chaing Lai for being a great supervisor not only across my PhD but also during my undergraduate and master's projects. Without you, I would never have found myself in the position I am now; you truly kick started my passion for research. Your mentorship not only enhanced my technical skills but also inspired me to think critically and creatively. Your attention to detail has allowed me to develop a deeper understanding of the complexities of research and in doing so challenge science – a skill that has proven invaluable throughout my PhD.

To all members of the Lai Lab, past (Alex Seabright, Peter Dawson, Ibrahim Musa and Yusuke Nishimura) and present (Jitpisute Chunthorng-Orn, Bradley Welsh, Jimi Ng and Christina Pan), thank you for your continued support and guidance throughout my PhD. A special mention to Alex and Peter who were so helpful when I first joined the lab and were always willing to answer my never-ending questions. To all other SportExR students past and present that have been a part of my journey, both in the lab and in the office, I am so thankful to have met you all and I wish you all the best in your own careers and I hope to stay in touch. I would like to give a massive shout out to Dr Rahul Samant and Dr Harvey Johnston from the Babraham Institute in Cambridge. I am so grateful for your collaborative efforts over the last 2 years, without you I would certainly not be moving on to a career in proteomics.

To the organisations that have helped during my PhD, I would like to thank the BBSRC for funding this PhD and providing the MIBTP training program, CMAR for providing a pump priming grant to support the ageing research, and the Physiological society for their continued support in attending conferences.

Last but certainly not least, I would like to thank all those in my personal life. A massive shoutout to my parents, thank you for your endless support throughout my academic career. The ride has not always been easy, and you have always been there to offer support and guidance when needed. Despite not explaining my PhD very well in our family chats, you have continued to show interest and provided endless encouragement. Finally, I would like to acknowledge my wonderful fiancée, Matilda. I am so thankful that you made the journey to join me in Birmingham, despite being vocal about how you look forward to us leaving. I cannot thank you enough for your patience and support, having you in my life has truly enriched my PhD experience. This last 4 years has certainly been more than just an academic career and having you in my life is my proudest achievement.

AUTHORS DECLARATION

This thesis has not been submitted, either in full or in part, for any other degree. I hereby declare that except for the following, the content presented in this thesis are the results of my own research.

- Human skeletal muscle tissue sample collection for CHAPTER 3 and CHAPTER 4, which was part of the Elastic band intervention study conducted by Ryan N. Marshall in the School of Sport, Exercise and Rehabilitation Sciences, University of Birmingham.
- Animal work and mouse skeletal muscle tissue sample collection for CHAPTER 5, which was conducted from previous research by Sue Bodine's research group in the Department of Internal Medicine, University of Iowa.
- Offline high-pH reversed-phase fractionation in CHAPTER 5 and Proteome Discoverer analysis for CHAPTER 3, CHAPTER 4 and CHAPTER 5, which were performed by Harvey E. Johnston at the Babraham Institute, Cambridge
- Liquid chromatography coupled with mass spectrometry, which was performed by the Mass Spectrometry core facility at the Babraham Institute, Cambridge

Signed

LIST OF PUBLICATIONS

1. **Lord SO**, Johnston HE, Samant RS, Lai YC. Ubiquitylomics: An Emerging Approach for Profiling Protein Ubiquitylation in Skeletal Muscle. J Cachexia Sarcopenia Muscle. 2024 Sep

2. **Lord SO**, Dawson PWJ, Chunthorng-Orn J, Ng J, Baehr LM, Hughes DC, Sridhar P, Knowles T, Bodine SC, Lai YC. Uncovering the mechanisms of MuRF1-induced ubiquitylation and revealing similarities with MuRF2 and MuRF3. Biochem Biophys Rep. 2024 Jan

3. **Lord SO,** Lai YC. Exercise mediates ubiquitin signalling in human skeletal muscle. FASEB Bioadv. 2022 Feb

4. Podlogar T, Shad BJ, Seabright AP, Odell OJ, **Lord SO**, Salgueiro RB, Civil R, Shepherd EL, Lalor PF, Elhassan YS, Lai YC, Rowlands DS, Wallis GA. Post-exercise muscle glycogen synthesis with glucose, galactose and combined galactose-glucose ingestion. Am J Physiol Endocrinol Metab. 2023 Oct

5. Nishimura Y, Chunthorng-Orn J, **Lord S**, Musa I, Dawson P, Holm L, Lai YC. Ubiquitin E3 ligase Atrogin-1 protein is regulated via the rapamycin-sensitive mTOR-S6K1 signaling pathway in C2C12 muscle cells. Am J Physiol Cell Physiol. 2022 Jul

6. Seabright AP, Fine NHF, Barlow JP, **Lord SO**, Musa I, Gray A, Bryant JA, Banzhaf M, Lavery GG, Hardie DG, Hodson DJ, Philp A, Lai YC. AMPK activation induces mitophagy and promotes mitochondrial fission while activating TBK1 in a PINK1-Parkin independent manner. FASEB J. 2020 May

In progress

1. **Lord SO**, Johnston HE, Baehr LM, Hughes DC, Bodine SC, Samant RS, Lai YC. Discovery proteome and ubiquitylome profiling reveals ageing effect in skeletal muscle. (In preparation for submission).

LIST OF CONFERENCE ABSTRACTS AND COMMUNICATIONS

1. **Characterisation of post-translational modifications in cellular signalling - EMBO workshop (Odense Denmark, May 2022)**: Poster presentation – "Developing a workflow to study the ubiquitylome in skeletal muscle"

2. **CIMA/CMAR conference – Musculoskeletal ageing research from discovery to improved health. (Birmingham UK, May 2023)**: Poster presentation – "Developing a mass spectrometry-based workflow to investigate ubiquitin signalling networks in aged skeletal muscle".

3. **Skeletal muscle metabolism and growth - insight into models and mechanisms - University of Copenhagen PhD Course (Køge Denmark, June 2023):** Poster presentation – "Developing a mass spectrometry-based workflow to investigate ubiquitin signalling networks in aged skeletal muscle".

4. **Physiology conference – The Physiology Society (Harrogate UK, July 2023):** Oral communication – "Developing a Mass Spectrometry-based workflow to study Ubiquitin signalling in ageing skeletal muscle".

5. **The Festival of Genomics & Biodata conference (London UK, January 2024):** Poster presentation – "Discovery proteomics in ageing mouse skeletal muscle".

6. **Proteostasis conference (Cambridge UK, May 2024):** Poster and oral presentation – "Proteomic profiling reveals mechanisms regulating proteostasis in aged skeletal mouse muscle".

7. **New perspectives on the physiological basis of muscle loss conference – The Physiological Society (Exeter UK, September 2024):** Oral presentation – "Discovery proteome and ubiquitylome profiling reveals ageing effect in skeletal muscle".

8. **Ubiquitin and ubiquitin-like proteins in health and disease - EMBO workshop (Cavtat Croatia, September 2024):** Poster presentation – "Discovery proteome and ubiquitylome profiling reveals ageing effect in skeletal muscle".

LIST OF AWARDS AND FUNDING

1. MIBTP studentship funding from BBSRC including bench fees (£12900)

2. Pump-priming grant application from the Centre for Musculoskeletal Ageing Research (CMAR) (£12340)

3. School of Sport, Exercise and Rehabilitation Sciences PGR travel award scheme (£850)

4. UKRI MRC National Musculoskeletal Ageing Network Early / Mid-Career Researcher Travel Award (£300)

5. BLAST Early Career Researcher Travel Bursary Award (£82)

6. Physiological Society Conference Attendance Awards Grant scheme (£500)

7. University of Birmingham School post graduate Research Seminar Prize winner for "Most engaging and best overall presentation".

8. Early Career Researcher Oral Competition Winner – New Perspectives on the Physiological Basis of Muscle Loss conference (Physiological Society) (£200)

TABLE OF CONTENTS

LIST OF FIGURES

Chapter 1

Chapter 2

Chapter 3

Chapter 4

Chapter 5

Chapter 6

LIST OF ABBREVIATIONS

ACC	Acetyl-CoA carboxylase
ACN	Acetonitrile
AGC	Automatic gain control
AKT	Protein kinase B
ALS	Amyotrophic lateral sclerosis
AMPK	Adenosine monophosphate-activated protein kinase
ANXA4	Annexin A4
APEX2	Ascorbate peroxidase 2
AS	Angelman syndrome
ASB2β	Ankyrin repeat and SOCS box protein 2 beta
ASPN	Asporin
Atg5	Autophagy protein 5
Atg7	Autophagy protein 7
ATP	Adenosine triphosphate
BioID	Proximity-dependent biotin identification
BiP	Binding immunoglobulin protein
BMI	Body mass index
BSA	Bovine serum albumin
CID	Collision-induced dissociation
CHAPS	3-[(3-cholamidopropyl)dimethylammonio]-1-propanesulfonate
CHIP	Carboxyl Terminus of HSC70-interacting Protein
CRL	Cullin ring E3 ligase
CRYAB	Crystallin alpha B
CV	Coefficient of variance
DAVID	Database for annotation, visualization, and integrated discovery
DC	Detergent compatible

DDA	Data dependent acquisition
DHTKD1	Dehydrogenase E1 and Transketolase Domain Containing 1
DIA	Data independent acquisition
diGly	Double glycine
DNA	Deoxyribonucleic acid
DTT	Dithiothreitol
DUB	Deubiquitylating enzyme
E-STUB	E3-substrate tagging by ubiquitin biotinylation
ECD	Electron capture dissociation
EDL	Extensor digitorum longus
EDTA	Ethylenediaminetetraacetic acid
EGTA	Ethylene glycol-bis(β-aminoethyl ether)-N,N,N′,N′-tetraacetic acid
ERAD	Endoplasmic reticulum-associated degradation
ESI	Electrospray ionization
ETD	Electron transfer dissociation
FAIMS	Field asymmetric waveform ion mobility spectrometry
FA	Formic acid
FRDA	Friedreich's ataxia
GAD	Gracile axonal dystrophy
GAPDH	Glyceraldehyde 3-phosphate dehydrogenase
GSEA	Gene set enrichment analysis
HCD	High-energy collisional dissociation
HECT	Homologous to E6AP C terminus
HEPES	2-(4-(2-hydroxyethyl)-1-piperazinyl)-ethanesulfonic acid
HS IAP	HS immunoaffinity purification
HSP	Heat shock protein
HSPB5	Heat shock protein beta 5

HSPB7	Heat shock protein beta 7
IKZF1	IKAROS family zinc finger 1
IKZF3	IKAROS family zinc finger 3
iTRAQ	Isobaric tags for relative and absolute quantitation
K-Ɛ-GG	Lysine-epsilon-diglycine
KHL40	Kelch-like family member 40
LC-MS	Liquid chromatography-mass spectrometry
LDS	Lithium dodecyl sulfate
Log	Logarithm
MAFBX	Muscle atrophy F-box
MBP	Maltose binding protein
MG-132	Carbobenzoxy-Leu-Leu-leucinal
MHC	Myosin heavy chain
Mib1	Mind bomb 1
MIST	Myofibril isolation and solubilisation technique
MOPS	3-(N-morpholino)propanesulfonic acid
MPS	Muscle protein synthesis
mRNA	Messenger ribonucleic acid
MS	Mass spectrometry
MS2	Tandem mass spectrometry
mTOR	Mammalian target of rapamycin
mtDNA	Mitochondrial deoxyribonucleic acid
MuRF1	Muscle RING Finger 1
NADP	Nicotinamide adenine dinucleotide phosphate
NBR1	Neighbor of Brca1 gene
NP-40	Nonyl phenoxypolyethoxylethanol
OtUBD	Orientia tsutsugamushi Ubiquitin-Binding Domain

PCA	Principal component analysis
PDI	Protein disulfide isomerase
PMSF	Phenylmethylsulfonyl fluoride
PR-619	2,6-Diamino-3,5-dithiocyanopyridine
PRIDE	Proteomics identification database
PRM	Parallel reaction monitoring
PROTAC	Proteolysis targeting chimera
PSM	Peptide spectral match
PTM	Post translational modification
PTXQC	Proteomics quality control
PVDF	Polyvinylidene fluoride
RBR	Ring between ring
RING	Really interesting new gene
RNA	Ribonucleic acid
Rpt3	Regulatory particle triple-A ATPase 3
RTS	Real time searching
SASP	Senescence-associated secretory phenotypes
SDS	Sodium dodecyl sulfate
SDS-PAGE	Sodium dodecyl sulfate–polyacrylamide gel electrophoresis
sHSP	Small heat shock protein
SILAC	Stable-isotope labeling by amino acids in cell culture
SLRP	Small leucine-rich proteoglycans
SMA	Spinal muscular atrophy
SMOC2	SPARC-related modular calcium-binding protein 2
SP3	Single-pot solid-phase-enhanced sample preparation
SP4	Solvent precipitation SP3
SPS	Synchronous precursor selection

SQSTM1	Sequestosome-1
SRM	Serial reaction monitoring
TA	Tibialis anterior
TBS-T	Tris buffered saline with tween
TCA	Tricarboxylic acid cycle
TEAB	Tetraethylammonium bromide
TFA	Trifluoroacetic acid
TMT	Tandem mass tag
TR-TUBE	Trypsin resistant- tandem ubiquitin binding entities
TRIM25	Tripartite motif-containing protein 25
Tris-HCL	Tris-hydrochloride
TUBE	Tandem ubiquitin binding entities
Ub-AQUA	Ubiquitin absolute quantification
Ub-POD	Proximity & orientation-dependent tagging of ubiquitin
Ub-PSAQ	Ubiquitin protein standard absolute quantification
UBAIT	Ubiquitin-activated interaction traps
UBL	Ubiquitin-like protein
UBQLN1	Ubiquilin-1
UBR4	Ubiquitin protein ligase E3 component N-recognin 4
UCHL1	Ubiquitin carboxy-terminal hydrolase L1
UCHL5	Ubiquitin carboxy-terminal hydrolase L5
UK	United kingdom
Ulk2	Unc-51 like autophagy activating kinase 2
UPR	Unfolded protein response
UPS	Ubiquitin proteosome system
USP	Ubiquitin-specific protease
VCP	Valosin-containing protein

1. GENERAL INTRODUCTION

Portions of the general introduction of this thesis have been utilised in a review article published in Journal of Cachexia, Sarcopenia and Muscle

Lord SO, Johnston HE, Samant RS, Lai YC. Ubiquitylomics: An emerging approach for profiling protein ubiquitylation in skeletal muscle

1.1 Musculoskeletal ageing

1.1.1 Ageing population

The demographic of the human population is shifting dramatically towards older age. Since the 1950's there has been a surge in the number of people aged over 70 years [1]. This surge is expected to continue and by 2050 the proportion of the world's population over 60 years old is expected to double to 22% [2]. A major contributor towards this ageing demographic is the advancement in healthcare that has increased life expectancy [3]. The increase in lifespan has presented new challenges, including the burden on healthspan. Healthspan is the number of years lived disease free, and in 2020 was measured at 64 years which is nearly 10 years less than the average life expectancy [1]. The World Health Organization proclaimed 2021-2030 as the decade of healthy ageing in an effort to improve older individuals' quality of life [4].

1.1.2 Sarcopenia

The maintenance of skeletal muscle function is an important factor for healthy ageing. With age, skeletal muscle experiences an involuntary decline in muscle mass and strength. When this decline reaches a certain threshold, individuals are diagnosed with sarcopenia [5]. Sarcopenia is more prevalent during later life, reported in 5-13% of those aged 60-70 years old and 11-50% in those aged over 80 [6]. Sarcopenia presents significant health concerns for individuals, both physically e.g. frailty and metabolically e.g. insulin resistance [7], [8]. Sarcopenia also has damaging consequences on other tissues and organs, such as increasing the prevalence of cardiovascular disease and cognitive decline [9], [10]. Therefore, it is not surprising that skeletal muscle mass and strength are predictors of longevity [11], [12]. In addition to the detrimental effect on an individual's healthspan, sarcopenia proves extremely costly, with muscle weakness thought to cost the UK an excess of £2.5 billion per year [13].

Therefore, strategies aimed at preserving skeletal muscle throughout lifespan will have profound benefits on healthcare and the economy.

1.1.3 Combatting sarcopenia

Whilst progressive loss of muscle mass and strength with age is inevitable, reaching a state of sarcopenia is influenced by external factors. The age-related loss of muscle mass is exacerbated by periods of muscle disuse, which contributes towards the development of sarcopenia [14]. Not surprisingly, therefore, exercise is proven to promote health muscle ageing and reduce the risk of sarcopenia [15]. In fact, exercise is the only intervention shown to prevent and mitigate sarcopenia in humans [16]. However, physical constraints (e.g. injury and illness) and compliance issues means that exercise as a medicine is unlikely to combat sarcopenia alone. Therefore, pharmaceutical therapeutics that can help prevent or combat sarcopenia are of great value, but currently there are no prescribed first-line drug treatments. To develop such therapeutics requires an in-depth understanding of the mechanisms that under optimal conditions maintain healthy skeletal muscle, and when impaired drive sarcopenia.

Back in 2013, nine hallmarks were put forward that are now considered to contribute towards the ageing process across different cells and tissues [17]. Since then, some additional hallmarks have been added taking the current total to twelve [18]. These hallmarks are genomic instability, telomere attrition, epigenetic alterations, loss of proteostasis, disabled macroautophagy, deregulated nutrient-sensing, mitochondrial dysfunction, cellular senescence, stem cell exhaustion, altered intercellular communication, chronic inflammation and dysbiosis. One of the key criteria for becoming a hallmark of ageing is the opportunity to slow down the normal ageing process by therapeutic interventions. Therefore, these hallmarks offer themselves as ideal candidates for increasing healthspan. Recent efforts have been made

to summarise the hallmarks likely driving sarcopenia [19]. This review concluded that epigenetic alterations, mitochondrial dysfunction and neural dysfunction have strong evidence as hallmarks of human skeletal muscle ageing.

1.2 Skeletal muscle proteins

1.2.1 Importance of proteins in skeletal muscle

Studying the protein response in ageing skeletal muscle is crucial for identifying mechanisms of sarcopenia. While genes provide the blueprint for biology, proteins ultimately determine which actions are carried out within the cell. There are many classifications of proteins which carry out different roles to maintain the function of skeletal muscle. For example, contractile proteins provide strength and movement, structural proteins ensure tissue and organelle integrity, and regulatory proteins drive cellular processes in response to internal and external stimuli. Changes in protein abundance, localisation and activity directly influence changes in cellular function. Identifying how these factors change during skeletal muscle ageing can help pinpoint cellular perturbations that drive sarcopenia.

1.2.2 Protein abundance in skeletal muscle

The abundance of proteins in skeletal muscle is diverse. When considering the total protein mass of skeletal muscle, it was found in mice that 50% is made up of 10 proteins [20]. Given that over 8,000 proteins were identified in this study, the abundance of proteins in skeletal muscle spans a wide range. When assigning protein mass to different functions, over half form part of the contractile machinery and over 30% are involved in metabolism [20]. When considering protein numbers, contractile proteins account for less than 10% [21]. The fact that

contractile proteins make up a large portion of the total mass despite being relatively few in number highlights their high abundance. In fact, myosin and actin contractile proteins are thought to account for 50% of the muscle protein concentration [22]. Myosin and actin belong to the myofibrillar compartment of the muscle, which makes up 60-70% of the muscle protein pool [22]. It is important to note that the abundance of proteins in skeletal muscle is not stationary. The protein pool is in a constant state of flux, regulated by rates of protein turnover – the balance between protein synthesis and degradation. This dynamic process allows for the maintenance and adaptation of muscle composition in response to various physiological and pathological conditions.

1.2.3 Age-related changes in protein abundance

During ageing, there is a growing appreciation that protein turnover is reduced in skeletal muscle, resulting in the accumulation of misfolded and damaged proteins. This has been demonstrated in collagen, whereby the dynamic collagen protein pool is reduced in older muscle [23]. In terms of the dynamic myofibrillar pool, there has been several contradictory findings especially with regards to changes in muscle protein synthesis (MPS), leading to a proposed change in the tracer approach for measuring muscle protein turnover [24]. Nevertheless, over the time course of ageing there is a reduction in the myofibrillar protein pool resulting in muscle atrophy, largely driven by a reduction in fast contractile proteins as part of the oxidative shift in muscle fibres [25]. Proteomics has been an invaluable tool for identifying age-related changes in individual proteins. Early studies revealed changes in metabolism and proteostasis machinery, including increased chaperones that protect against muscle filament aggregation [26], [27], [28]. More recently, it was shown that protein abundance is affected by fibre type, whereby rate-limiting enzymes of glycolysis are upregulated in slow but downregulated in fast muscle fibres of older humans [25]. Despite

decreases in many mitochondrial proteins with age, skeletal muscle in older humans and mice display increases in several mitochondrial enzymes involved in energy metabolism [29], [30]. In 2019, a large-scale proteomics analysis was performed on skeletal muscle across a continuous age range of adult to elderly humans [31]. Amongst other findings, they showed that ageing was associated with profound increases in proteins associated with alternative splicing. Collectively, these studies demonstrate that ageing significantly alters the abundance and turnover dynamics of the skeletal muscle proteome.

1.3 Post-translational modifications (PTMs)

1.3.1 Role of PTMs

Post-translational modifications (PTMs) play a key role in regulating the function of proteins. PTMs act on amino acids residues of proteins through the addition of a chemical, nucleotide sugar, lipid or protein group [32]. There are hundreds of different PTMs in humans, some of which are better characterised than others [33]. These modifications extend the complexity and functional diversity of the proteome, estimated at over 1 million distinct proteoforms [34]. PTMs regulate protein stability, activity, interactions, and location which allows the fine-tuning of biological processes. As a result, disruptions in PTMs can be deleterious and is seen in many diseases [35].

1.3.2 Different types of PTMs

PTMs each play a different role in regulating protein function. The most extensively researched PTM is phosphorylation, which regulates protein activity through the addition of a phosphate group. In skeletal muscle, this has an important role to play in signal transduction, allowing the muscle to activate different biological pathways in response to different stimuli including

mechanical stress, growth factors and inflammatory cytokines [36]. Acetylation is a PTM best known for modification of histones for gene transcription. In skeletal muscle, histone acetylation increases in response to immobilised-induced skeletal muscle atrophy [37]. Under the same atrophy condition, acetylation decreases on contractile proteins such as myosin heavy chain (MHC) [37]. Acetylation modifies 80% of contractile proteins and the removal of essential enzymes for catalysing acetylation (acetyltransferases) impairs the contractile function of skeletal muscle [38], [39]. Ubiquitylation is another PTM which has received interest in skeletal muscle due to its key role in protein degradation [40]. Muscle disuse increases the ubiquitylation of contractile proteins, which is presumably signalling for their degradation [37]. Degradation of contractile proteins influences the muscle protein balance and subsequently skeletal muscle mass. As a result, dysregulated ubiquitylation likely has a direct influence on sarcopenia and other muscle mass-related diseases. The roles of ubiquitylation extend to non-degradative processes, including signal transduction [41], DNA repair [42] and protein transport [43]. Therefore, ubiquitylation is a PTM which regulates many diverse biological processes in the cell.

1.3.3 Protein ubiquitylation

Protein ubiquitylation involves the covalent attachment of ubiquitin — a 76 amino acid protein — via its C-terminal, predominantly onto internal lysine residues of target proteins (although the presence of N-terminal protein ubiquitylation is also well established). Recent work has discovered that ubiquitin can also target internal cysteine, serine and threonine sites, or even non-protein molecules [44], [45]. Protein ubiquitylation requires sequential ATP-driven enzymatic reactions, involving ubiquitin-activating (E1), ubiquitin-conjugating (E2) and ubiquitin-ligating (E3) enzymes **(Figure 1a)**. Protein ubiquitylation can also be removed by deubiquitylases (DUBs). At present count, there are two E1s, nearly 40 E2s, more than 600

E3s and approximately 100 DUBs encoded in the human genome [46]. Proteins can be ubiquitylated in many ways: on a single amino acid by a single ubiquitin moiety (monoubiquitylation), on multiple amino acid residues by single ubiquitin moieties (multi-monoubiquitylation) or on single or multiple amino acids by covalently linked ubiquitin chains (polyubiquitylation). Polyubiquitin chains exhibit distinct topologies, determined by the internal lysine (K6, K11, K27, K29, K33, K48, K63) or N-terminal methionine (M1) used for chain elongation [47] **(Figure 1b)**.

1.3.4 Ubiquitin code

Characterising the nature of ubiquitin modification is an important step in determining its physiological consequences. The recognition of ubiquitylation topology is mediated by ubiquitin binding domains. Proteins equipped with these ubiquitin binding domains, often referred to as 'readers', play a pivotal role in transducing the ubiquitin signal into downstream outputs [48] **(Figure 1c)**. Ubiquitylation can signal for various biological processes; therefore, ubiquitin binding domains often appear to be linkage-specific, contributing to the complex network of ubiquitin signalling known as the ubiquitin code [49]. For instance, K48-linked ubiquitin chains signal for proteasomal degradation, a process not generally attributed to homotypic K63-linked ubiquitin chains [50]. Instead, K63-linked ubiquitylation has a major role in diverse signalling responses including autophagy, endocytosis, DNA damage and immune response [51]. The role of other lysine-linked ubiquitin chains are less well characterised but have roles in autophagy, cell cycle, DNA damage, immunity, degradation and protein trafficking [52]. M1-linked ubiquitin chains (linear ubiquitylation) are heavily involved in inflammatory signalling through NF-kB pathway [53]. The role of other non-lysine ubiquitylation (serine, threonine or cysteine) is still an emerging field, with a role in endoplasmic reticulum-associated degradation (ERAD) and beyond [44], [54]. However, it is

essential to note that our current understanding of the ubiquitin code is derived from cellular models; the extent to which the same diversity exists in skeletal muscle requires further investigation.

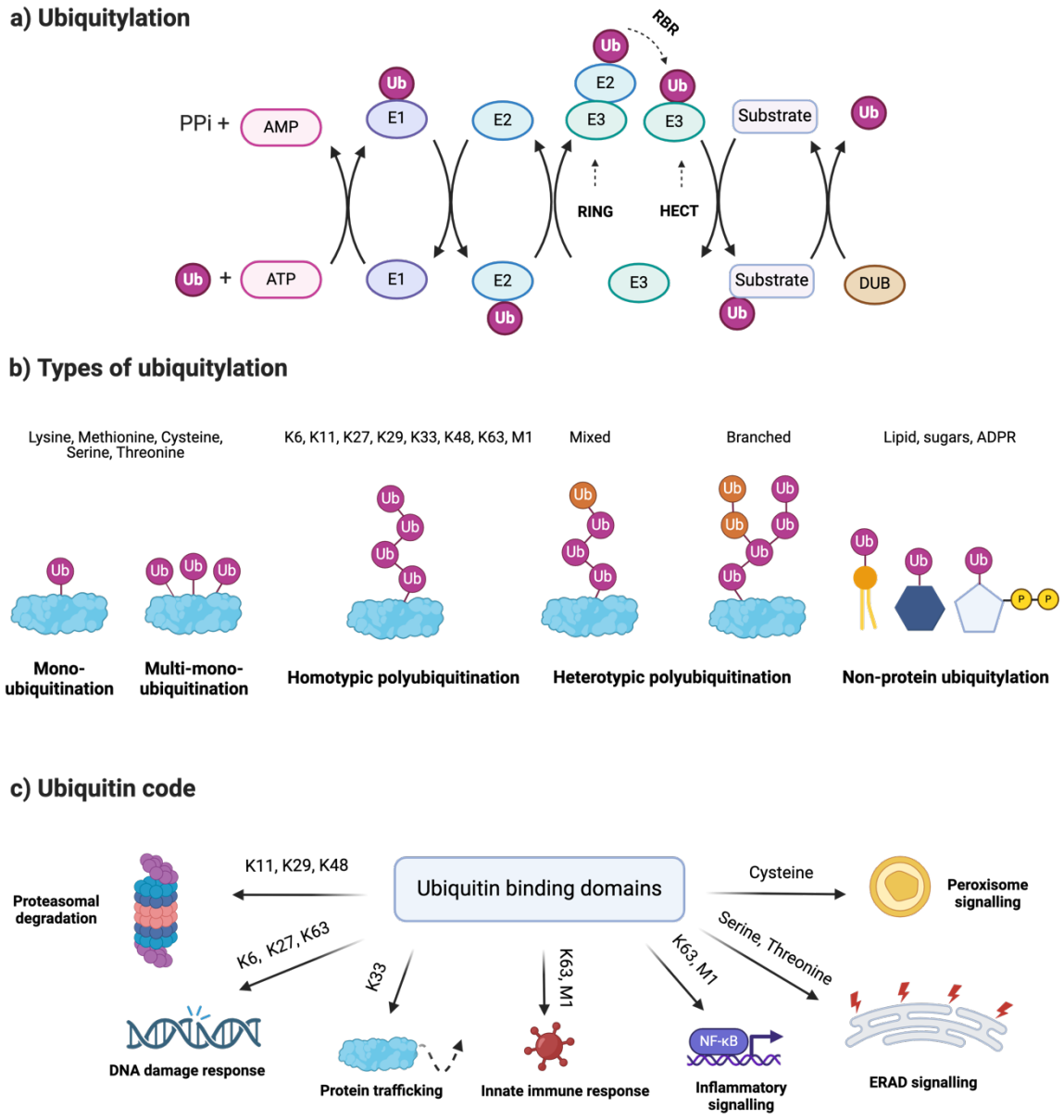

Figure 1. Protein ubiquitylation. a) Enzymatic cascade of reactions that occur during ubiquitylation. E3 ligases can be divided into three families: RING-finger, HECT, and Ring-Between-Ring (RBR). Each have unique capabilities for transferring ubiquitin to the substrate. b) The versatility of ubiquitylation, from different linkage sites (Lysine, Methionine, Cysteine, Serine, Threonine), chain topology (homotypic and heterotypic) and substrates (protein and non-protein). c) The ubiquitin code that uses ubiquitin binding domains (known as readers) to recognise specific ubiquitin-linkage types which signal for different biological processes in cells. Image created using biorender.com

1.4 Evolution of ubiquitin

Ubiquitin can be expressed either fused to ribosomal proteins or as a polyubiquitin precursor, resulting in different ubiquitin-expressing genes. The ubiquitin protein encoded by the different genes are identical providing evolutionary stability and stronger buffering against mutations [55]. Ubiquitin is remarkably conserved between species, with humans and yeast ubiquitin sharing 96% sequence identity [56]. As a result, ubiquitin is often studied in many different organisms, with findings often applicable to humans. However, it is important to note that while ubiquitin itself is highly conserved, the ubiquitin system's complexity and regulation can vary between species. Whilst humans and mice share 335 homologous E3 ubiquitin ligases (~70%), the yeast genome encodes only encodes ~50 E3 ubiquitin ligases of which 7 were highly conserved between all three species [57].

1.5 Ubiquitylation in ageing skeletal muscle

1.5.1 Ubiquitin

Early observations into age-regulated protein ubiquitylation in skeletal muscle focused on changes in total ubiquitin. In 2004, one group observed increased ubiquitin in the extensor digitorum longus (EDL) muscle of 24-month-old rats and in quadricep muscle biopsies of 70-79 year old humans compared to younger subjects [58]. 2 years later, another group identified increased ubiquitin levels in 24-month-old rats when studying the tibialis anterior (TA) muscle, which underwent significant loss of mass relative to body weight [59]. This began the concept that ubiquitin could be contributing towards the development of sarcopenia, particularly in fast-twitch muscle which undergoes the most extensive atrophy. More recently, it was observed that the soleus muscle (slow-twitch) of 20-month-old rats also display elevated levels of ubiquitin compared to younger subjects [60]. Reports have also shown no change in total

ubiquitin levels in both TA and soleus between 9-month and 29-month-old rats, suggesting it is not a consistent ageing effect [61].

1.5.2 E3 ligases

E3 ligases are often seen as the key drivers of ubiquitylation, responsible for selecting proteins to be modified. In skeletal muscle, the focus of ubiquitylation research has often been around muscle atrophy given its role in protein degradation. As a result, there have been many studies aimed at identifying which E3 ligases are responsible for driving muscle atrophy, subsequently given the title 'atrogenes'. The first E3 ligases termed atrogenes were MuRF1 and MAFbx (also called atrogin-1), displaying increased mRNA expression following immobilisation, denervation and hindlimb suspension [62] and fasting and disease-induced atrophy – MAFbx only [63]. However, neither mRNA or protein levels appear to change consistently with age and so their abundance is not thought to be a driver of sarcopenia [64].

Other E3 ligases do appear to play an important role in driving sarcopenia, which has been covered in a recent review article [64]. Mind bomb-1 (Mib1) is an E3 ligase that ubiquitylates and degrades α-actinin 3 (Actn3), in order to maintain sarcomeric structure in skeletal muscle [65]. In aged mouse muscle, Mib1 protein abundance is reduced, resulting in the accumulation of Actn3 which disrupts fast glycolytic fibres and accelerates muscle atrophy [65]. Parkin is an E3 ligase recruited by PINK1 to ubiquitylate outer mitochondria membrane proteins, providing a docking site for autophagy receptors [66]. Whilst Parkin expression in aged skeletal muscle increases, its localisation to the mitochondria decreases [67]. Genetic alteration of Parkin in skeletal muscle has provided insight into the importance of this E3 ligase in suppressing sarcopenia. For example, overexpression of Parkin protected age-related losses of skeletal muscle mass and strength [68] and the absence of Parkin causes a decrease in mitochondrial

function and muscle specific force [69]. The E3 ligase UBR4 is increased at both mRNA and protein level in mouse skeletal muscle during ageing [70]. To test whether loss of UBR4 could rescue age-associated muscle wasting, the authors depleted the levels of UBR4 in the muscle and examined its effect on the muscle phenotype. Whilst they found that reducing UBR4 induced myofiber hypertrophy, it also resulted in reduced muscle force and protein quality control. Together, these findings illustrate that age-related alterations in E3 ligase protein abundance can influence the development of sarcopenia in skeletal muscle.

E3 ligases have been known to ubiquitylate lifespan regulators which influence the longevity of different organisms. For example, the E3 ligase CHIP ubiquitylates the insulin receptor, increasing its turnover and reducing insulin signalling [71]. Reduced insulin signalling extends lifespan in both insects and mammals and therefore is recognised as a mediator of longevity [72]. CHIP deficiency in *C. elegans*, *Drosophila* and mice and accelerated age-related pathologies and leads to a reduced lifespan [71], [73]. Interestingly in rats, CHIP was found to be upregulated in the gastrocnemius with age [74]. The authors speculate that age-increases in CHIP may occur to ubiquitylate and remove damaged and misfolded proteins that arise in skeletal muscle. In support, another group found that CHIP was upregulated in mice TA muscle following the loss of UBR4 which they hypothesised was an adaptive response, responding to the loss of protein quality control [70].

1.5.3 Deubiquitylating enzymes (DUBs)

Ubiquitylation is a reversible PTM that can be removed through DUBs. DUBs are present on the proteasome and remove the ubiquitin chains before the protein is degraded, allowing ubiquitin to be recycled [75]. Beyond this, DUBs can also remove ubiquitin from a protein before it reaches its intended target or partially cleave ubiquitin chains to alter its signal [76].

DUBs can display high levels of specificity for both substrates and ubiquitin chain types, offering themselves as effective drug targets [77].

In skeletal muscle, there are few studies that have researched the role of DUBs, with most of the work conducted on the ubiquitin-specific protease (USP) family. In aged sarcopenic rats, the protein content of USP14 — a proteasome-associated DUB — is upregulated when compared with adult controls [74]. USP19 is another DUB well studied in the context of muscle atrophy by Simon Wing's laboratory. They have shown that removing USP19 protects against dexamethasone and denervation induced muscle wasting in mice [78]. They later found that removal of USP19 increases insulin sensitivity and decreased glucocorticoid signalling which protects the muscle from atrophy [79]. Whilst there is no direct evidence for its role in sarcopenia, pharmacological inhibition of USP19 could present itself as a useful treatment to reduce loss of muscle mass with age. Interestingly, when measuring the activity levels of different DUBs, 11 increased in aged rat muscle [74]. Following this trend, increased DUB activity was seen in aged *C. elegans* and inhibiting their activity increased lifespan [80]. This is not to say that reducing the abundance or activity of all DUBs is realistic option for treating sarcopenia, as they have important roles in cellular homeostasis, such as preventing uncontrolled induction of autophagy [81].

1.5.4 Ubiquitin Proteasome System (UPS)

The most well-recognised role of protein ubiquitylation is to initiate protein degradation. This is largely conducted by the ubiquitin proteasome system (UPS), also referred to as the 26S proteasome. The UPS is made of two main compartments: The 19S regulatory complex and the 20S catalytic core. The 19S regulatory complex recognises the protein, primarily those which contain a polyubiquitin chain attached and the 20S catalytic core is responsible for the

degradation of the proteins into peptides [82]. The two compartments allow the UPS to perform selective degradation of proteins to remove unwanted proteins and replenish the pool of amino acids for synthesis of new proteins. However. excessive degradation of muscle proteins would result in muscle atrophy. Accordingly, the activity of UPS must be finely balanced in skeletal muscle.

Most tissues display age-related reductions in UPS activity [83], [84], [85]. This is thought to be due to proteasomal overload and a subsequent switch towards more promiscuous degradation mechanisms such as selective macroautophagy [86]. In skeletal muscle, the age-related changes in UPS activity are more disputed. Many rodent studies have found a reduction in UPS activity in skeletal muscle with age [87], [88], [89], [90], [91], [92], one report in human muscle found no changes [93] and a few rat studies have shown an increase with age [74], [94]. There are many factors that could explain this disparity, one of which is muscle type analysed. The Bodine lab found decreased UPS activity in aged gastrocnemius [92], no difference in aged soleus muscle and increases in the TA muscle [61]. One group suggested that fast and slow muscle groups have different strategies to combat age-related loss of protein quality control which could explain differences in UPS activity [95]. Another factor is the age of the muscle, as one study reported an increase in UPS activity in rat muscle up to 29 months which declined at 34 months [96]. Finally, and perhaps most importantly, the method for measuring UPS activity and whether both 19S and 20S components were analysed. Nevertheless, whilst the altered capacity of UPS in aged skeletal muscle may be disputed, impairments towards the UPS with age are detrimental. For example, muscle-specific knock-out of the 26S proteasome subunit Rpt3 in mice impaired muscle function and resulted in reduced lifespan [97].

1.5.5 Autophagy signalling

Beyond the proteasome, cells have another degradative system called autophagy. Autophagy is used for the degradation of protein aggregates and damaged organelles such as mitochondria (mitophagy). Autophagy-mediated degradation involves lysosomes which engulf proteins and sometimes entire organelles e.g. mitochondria (mitophagy), recycling the material to support the cell e.g. energy production by supplying amino acids, glucose, and fatty acids [98]. Autophagy can be separated into selective and non-selective degradation, with the former often involving ubiquitylation [99]. Selective autophagy involves a selection of receptors that signal for degradation, such as p62 (SQSTM1) and NBR1. These receptors contain ubiquitin binding domains, which allow these receptors to bind to ubiquitylated proteins to facilitate their degradation [100]. Therefore, ubiquitin is recognised as a degradation signal for both the proteasome and autophagy [101].

Autophagy plays a protective role during sarcopenia, preventing satellite cell senescence, relieving oxidative stress and reducing inflammatory signalling [102], [103]. Therefore, it is not surprising that activating autophagy is an effective countermeasure for sarcopenia. Exercise can activate autophagy through Akt and AMPK signalling to alleviate sarcopenia [104], [105]. Activation of mitophagy through overexpression of Parkin has been shown to protect muscle from sarcopenia [68]. On the other hand, disrupted autophagy signalling impairs skeletal muscle function. Deletion of autophagy related genes, Atg5 and Atg7 in the muscle results in decreased muscle force and strength [106], [107]. Mice deficient in the muscle-enriched autophagy related gene ULK2 (required for the degradation of ubiquitylated protein aggregates) experienced impaired muscle force and developed muscle atrophy and degeneration [108]. Overall, this demonstrates the importance of autophagy signalling to protect against sarcopenia.

1.6 Knowledge gaps in the current literature

Over the past few decades, studies have identified age-related changes in proteins and investigated the role of ubiquitylation in skeletal muscle. Rodent models have significantly contributed to this field, offering valuable insight into mechanisms driving sarcopenia. However, a critical limitation in rodent studies is the frequent use of exclusively male cohorts. As a result, our molecular understanding of muscle ageing is bias towards male physiology, overlooking differences in the ageing process between sex. Furthermore, much of our understanding of age-related ubiquitin regulation is based on total ubiquitin levels, the abundance of E3 ligases and DUBs, or proteasome/autophagy content and activity. There is a significant knowledge gap regarding the ubiquitylated substrates that are altered by age in skeletal muscle. Identifying these substrates is crucial to understand biological processes effected by ubiquitin and the broader implication this might have on sarcopenia.

1.7 Specific objectives of the thesis

The overarching aim of this thesis is to provide a more comprehensive understanding of how proteins and their ubiquitin modifications change in skeletal muscle during age, and whether this differs between males and females. To deliver this, we opted to use liquid chromatography coupled with mass spectrometry (LC-MS) as this provides large-scale, unbiased analysis of proteins and allows the identification of PTMs. This approach allowed us to perform data-driven analysis in an attempt order to capture the most biologically meaningful data.

In **Chapter 2** we highlight the use of LC-MS to study global changes in protein ubiquitylation, termed ubiquitylomics, in skeletal muscle. In **Chapter 3** we develop a workflow for studying the skeletal muscle proteome using LC-MS. In **Chapter 4** we modify this workflow to allow the identification of ubiquitylated proteins. Finally in **Chapter 5** we employ these workflows

to study age-related changes in the proteome and ubiquitylome of skeletal muscle from male and female mice.

1.8 Introduction to mass spectrometry

Mass spectrometry (MS) is a highly sensitive analytical instrument, well designed for comprehensive protein analysis. MS typically analysis smaller fragments of proteins called peptides that can be identified based on their mass to charge ratio (m/z). To obtain such depth requires tandem MS – spectral information is first provided on the entire peptide (MS^1) and then on the fragmented peptide (MS^2). By using available databases, software converts spectral information into peptides (referred to as a peptide spectral match) which can then be assigned to a given protein(s). Spectral data is obtained by the mass analyser, of which there are different approaches such as measuring the speed of an ionised peptide across an electric field (e.g., time of flight) or measuring oscillation frequency in an ion trap (e.g., orbitrap and FTCIR). The choice of mass analyser determines the accuracy, resolution and speed of spectral data obtained [109]. Peptides are identified and quantified using either data-dependent or data-independent acquisition (DDA or DIA). DDA only selects the most abundant peptides (based on their precursor intensity) from the MS^1 scan for fragmentation, whereas DIA works independently of the MS^1 data to (theoretically) fragment all peptides. The choice of mass analyser and data acquisition depends on the experiment at hand e.g., sample complexity, number of samples and method of quantification. MS quantification is broadly separated into label free or label-based quantification. Label free quantification compares the MS signal intensity of a peptide across runs, whereas label-based quantification uses unique stable isotopes to quantify peptides within a single run.

2. Ubiquitylomics: An emerging approach for profiling protein ubiquitylation in skeletal muscle

Ubiquitylomics: An emerging approach for profiling protein ubiquitylation in skeletal muscle

Samuel O. Lord [1], Harvey E. Johnston [2], Rahul S. Samant [2], Yu-Chiang Lai,[1,3,4]

[1] School of Sport, Exercise and Rehabilitation Sciences, University of Birmingham, Birmingham, UK

[2] Signalling Programme, The Babraham Institute, Cambridge, UK

[3] MRC Versus Arthritis Centre for Musculoskeletal Ageing Research, University of Birmingham, Birmingham, UK

[4] NIHR Birmingham Biomedical Research Centre Sarcopenia and Multimorbidity, University of Birmingham, Birmingham, UK

Corresponding Author: Dr. Yu-Chiang Lai, School of Sport, Exercise and Rehabilitation Sciences University of Birmingham, Birmingham, B15 2TT, Email: y.lai.1@bham.ac.uk

Published in: Journal of Cachexia, Sarcopenia and Muscle

DOI: https://doi.org/10.1002/jcsm.13601

2.1 Abstract

Skeletal muscle is a highly adaptable tissue, finely tuned by various physiological and pathological factors. Whilst the pivotal role of skeletal muscle in overall health is widely acknowledged, unravelling the underlying molecular mechanisms poses ongoing challenges. Protein ubiquitylation, a crucial post- translational modification, is involved in regulating most biological processes. This widespread impact is achieved through a diverse set of enzymes capable of generating structurally and functionally distinct ubiquitin modifications on proteins. The complexity of protein ubiquitylation has presented significant challenges in not only identifying ubiquitylated proteins but also characterising their functional significance. Mass spectrometry enables in-depth analysis of proteins and their post-translational modification status, offering a powerful tool for studying protein ubiquitylation and its biological diversity: an approach termed ubiquitylomics. Ubiquitylomics has been employed to tackle different perspectives of ubiquitylation, including but not limited to global quantification of substrates and ubiquitin linkages, ubiquitin site recognition and crosstalk with other post-translational modifications. As the field of mass spectrometry continues to evolve, the usage of ubiquitylomics has unravelled novel insights into the regulatory mechanisms of protein ubiquitylation governing biology. However, ubiquitylomics research has predominantly been conducted in cellular models, limiting our understanding of ubiquitin signalling events driving skeletal muscle biology. By integrating the intricate landscape of protein ubiquitylation with dynamic shifts in muscle physiology, ubiquitylomics promises to not only deepen our understanding of skeletal muscle biology but also lay the foundation for developing transformative muscle-related therapeutics. This review aims to articulate how ubiquitylomics can be utilised by researchers to address different aspects of ubiquitylation signalling in skeletal muscle. We explore methods used in ubiquitylomics experiments, highlight relevant literature

employing ubiquitylomics in the context of skeletal muscle and outline considerations for experimental design.

Key words: Ubiquitin, diGly, Proteomics, Mass spectrometry, Skeletal muscle

2.2 Methods for studying protein ubiquitylation

Defining ubiquitin-mediated signalling networks is complicated by several sources of difficulty in capturing ubiquitylation events. Ubiquitylation can be a very transient modification due to the removal of ubiquitin linkages by DUBs. Recent work has shown that DUBs regulate at least 40000 unique sites on ubiquitylated proteins [110]. In addition, given that protein ubiquitylation is widely used to target proteins for degradation, the window for detecting such proteins is reduced by their high turnover rates. In human cell lines, the median half-life of global ubiquitylation sites is 12 min, which is substantially shorter than the bulk of the cellular protein repertoire, where over 95% have a half-life greater than 8 h [111], [112]. As a consequence, ubiquitylated proteins have a low stoichiometry when compared to non-ubiquitylated proteins.

For this reason, preserving protein ubiquitylation at the point of sample collection is an essential step in obtaining a robust readout. DUBs display promiscuous activity when released in tissue or cell homogenates. Including DUB inhibitors such as EDTA/EGTA (inhibit metallo-proteinases) and 2-chloroacetamide/Iodoacetamide/N-ethylmaleimide/PR-619 (inhibit cysteine proteinases) in the lysis buffer ensures that ubiquitylated proteins are kept as they were in the intact cell or tissue. Unlike the addition of protease inhibitors, it is not standard practice to include DUB inhibitors in lysis buffers, at least not at the recommended concentrations

[113]. Including sufficient concentrations of DUB inhibitors is particularly important when using non-denaturing lysis buffers and when handling samples outside of low temperatures. To try and capture degradation-borne proteins, proteasome inhibitors such as bortezomib and MG-132 are often added into cells for a short period prior to lysis. However, due to the damaging consequences of preventing protein degradation, proteasome inhibitors are less suitable for in vivo studies. Furthermore, proteasome inhibitors display off-target effects including an increase in compensatory degradation pathways, such as autophagy [114], and a decrease in non-degradative ubiquitylation signals, such as histone ubiquitylation [115].

Considerations should be made for the choice of sample preparation. Sample preparation should ensure the proteins of interest are solubilised and retained for analysis. Certain proteins can be difficult to analyse due to their intrinsic properties. For example, transmembrane proteins are more hydrophobic than globular proteins [116]. Protocols have been developed to ensure optimal extraction and recovery of membrane-bound proteins [117], [118]. Capturing such proteins may be desirable as ubiquitylation plays a major role in the secretory pathway and plasma membrane protein transport [119]. Therefore, the chosen method of sample preparation should be tailored towards the type of proteins at the focus of each study.

To date, most studies have relied upon antibody-based detection (e.g., western blotting) to investigate protein ubiquitylation in skeletal muscle. Whilst these approaches can provide semi-quantitative analysis of ubiquitylation, they do have limitations. A notable limitation is antibody availability; for instance, not every ubiquitin linkage type has a commercially available antibody and therefore cannot be detected by immunodetection assays (e.g., western blotting, immuno-cytochemistry/histochemistry) [120]. Commercialised ubiquitin-linkage-specific antibodies were first developed for K48- and K63-linked ubiquitin chains [121], which

is a major contributing factor towards why these ubiquitin chains are best studied and comparatively better understood than other chain types. To our knowledge, in contrast with much smaller PTMs such as protein phosphorylation, there are very few commercially available antibodies that allow detection of a specific protein only when it is ubiquitylated at a given amino acid. Therefore, to determine whether a protein has been ubiquitylated, one must first include an enrichment step to selectively capture ubiquitylated proteins before blotting for the protein of interest, or vice versa.

Most commonly, ubiquitin enrichment from biological material involves the use of ubiquitin binding domains from various proteins that evolved to recognise ubiquitin signals (e.g., the proteasome shuttle-factors Dsk2 from yeast *S. cerevisiae* or UBQLN1 from humans). Through the recombinant expression of ubiquitin binding domains with different intrinsic binding specificities and/or the fusion of multiple ubiquitin binding domains into repeating units, for example, MultiDsk [122], [123], tandem ubiquitin binding entities (TUBEs) [123] and OtUBD [124], researchers have successfully generated reagents with enhanced and selective affinity towards monoubiquitin or polyubiquitin chains of different lengths and/or linkages [113]. Even after successful enrichment, researchers may be forced to focus on proteins with the most specific and sensitive antibodies available for detection. Subsequently, many proteins become neglected simply because they are more difficult to investigate, which slows down progress in the field, or at the very least, builds an incomplete model.

Tackling many of these issues, LC-MS has emerged as a powerful tool for in-depth analysis of protein ubiquitylation (‘ubiquitylomics’). LC-MS has the potential to identify thousands of ubiquitylated proteins and provide the ubiquitylation site on each peptide. Accordingly, LC-

MS is responsible for the detection of many novel ubiquitylated substrates and sites that were previously limited by the detection tools available [125]. Furthermore, protein groups and biological pathways enriched in ubiquitylomics datasets can be identified through computational tools such as gene set enrichment analysis (GSEA) [126]. Such findings create new research avenues to explore previously neglected roles of protein ubiquitylation.

The aim of this review is to articulate how ubiquitylomics can be utilised to study protein ubiquitylation events in skeletal muscle. We first highlight methodological approaches available within ubiquitylomics workflows and their applications for understanding biology and developing drug targets. Next, we review studies that employ ubiquitylomics to advance our molecular understanding of muscle biology. Finally, we discuss the challenges associated with performing ubiquitylomics in skeletal muscle and outline key considerations for experimental design.

2.3 Mass spectrometry (MS)-based ubiquitylomics

LC-MS is a highly sensitive tool for detecting whether a protein has been ubiquitylated, simply by a change in peptide mass. This most commonly involves bottom-up proteomics, in which proteins are first cleaved into smaller peptides at the carboxyl side of arginine and lysine residues by trypsin. Following trypsin digestion, peptides that have been ubiquitylated will retain a double glycine remnant (‘diGly’) protruding from the site of ubiquitylation. The diGly remnant adds 114.04 Da to the peptide mass, distinguishing itself from the unmodified parent peptide. This mass shift was first utilised in 2003 to identify 110 ubiquitylation sites on 72 proteins [127]. Due to the low stoichiometry of protein ubiquitylation, this study along with those conducted over the next several years relied on non-native expression of tagged ubiquitin

to selectively enrich ubiquitylated proteins. Whilst ground-breaking, these early studies suffered from high protein background and were limited to cell-based experiments where non-native ubiquitin could be expressed. Over the last decade, considerable developments at the level of biochemical ubiquitin tools, MS instrumentation and computational methodologies have spurred a growing interest in the use of ubiquitylomics.

2.3.1 Ubiquitin remnant peptide enrichment

Perhaps the most consequential development that revolutionised the ubiquitylomics field came in 2010, allowing ubiquitylated sites to be selectively enriched using an antibody [125]. Since most protein ubiquitylation occurs on lysine residues, this antibody was developed to recognise the lysine epsilon diGly (K-ε-GG) ubiquitin remnant motif. This antibody was developed for peptide immunoprecipitation, that is, to selectively enrich ubiquitylated peptides after trypsin digestion, prior to MS-based bottom-up proteomics. A year later, this antibody enrichment platform was used to recognise over 10 000 ubiquitylation sites on ~5000 proteins in human cell lines [50], [115]. These studies illustrated the tremendous potential of LC-MS for large scale analysis of protein ubiquitylation. Various protocols have since been developed to improve the efficiency and versatility of K-ε-GG antibody enrichment, including chemical cross-linking to the beads [128], on-antibody TMT labelling [129], magnetic beads and automated processing [130].

Since the development of the K-ε-GG antibody, a few other antibodies have been developed to enrich different ubiquitin remnants on peptides. One group has developed an antibody termed UbiSite that has greater specificity for ubiquitylated peptides over similar peptides with ‘ubiquitin-like’ (UBL) PTMs [131]. This antibody recognises a larger 13-residue remnant

(after Lys-63 in the ubiquitin sequence) which is brought about following digestion with LysC instead of trypsin. This reliance on a larger ubiquitin remnant epitope presents two main advantages to UbiSite when compared with K-ε-GG: (1) UbiSite recognises a broader range of ubiquitylation sites, not just those formed on a lysine residue, and (2) UbiSite does not recognise other UBL PTMs, such as NEDDylation and ISGylation, both of which are indiscriminately enriched by the K-ε-GG antibody. The second point is likely more important when dealing with UBL-activating conditions such as inflammation, as whilst ubiquitin makes up ~95% of total ubiquitin and UBL signal in resting cells, ISGylation significantly increases under interferon stimulation [50]. More recently, another group has developed an antibody specifically targeting diGly remnants on the N-terminus of peptides, corresponding to N-terminus ubiquitylation [132]. Together, these ubiquitin remnant motif antibody enrichment tools have overcome barriers previously encountered in ubiquitylomics analysis.

2.3.2 Ubiquitin chain analysis

A major limitation with the bottom-up proteomics approach, such as those used for ubiquitin remnant peptide enrichments, is the loss of ubiquitin architecture following the digestion of proteins into peptides. The enzymatic cleavage disassembles ubiquitin linkages, preventing the determination of ubiquitin chain topology on identified substrates **(Figure 2.1)**. This complicates the inference of the biological impact associated with each ubiquitylation site, given that the ubiquitin chain determines its function **(Figure 1c)**. Alternative methods must be considered if obtaining information of ubiquitin chain types is paramount.

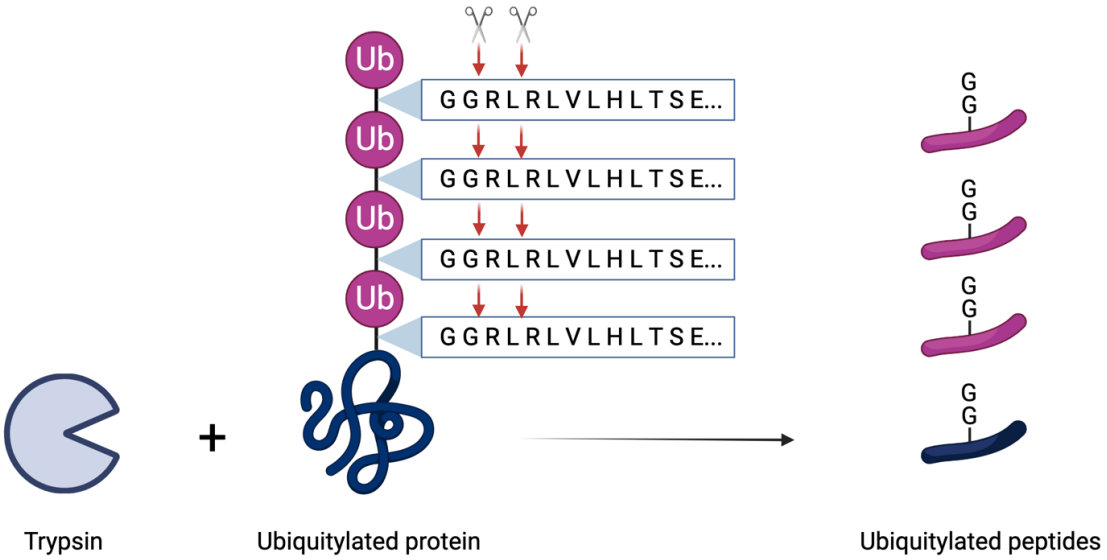

Figure 2. 1. Digestion of ubiquitylated proteins. Trypsin cleaves at the C-terminal side of Arginine (R) and Lysine (K) residues, which are found throughout the ubiquitin sequence. During trypsin treatment, ubiquitin chains are therefore digested into multiple peptides. Digested ubiquitin chains can be identified by the signature double glycine (GG) remnant on ubiquitin peptides; however, the substrate is no longer attached and cannot be identified in a complex mixture. Image created using biorender.com.

One strategy is to take advantage of chain-specific TUBEs, affimers or antibodies to selectively enrich for proteins with specific ubiquitin chain types prior to LC-MS [133]. These enrichment techniques enable the acquisition of chain-type linkage information for each protein. However, ubiquitin chain enrichment tools can suffer from cross-reactivity and require larger amounts of starting material. In addition, it is important to note that protein-level enrichments are less suitable for identifying ubiquitylation sites, given their low stoichiometry in relation to non-ubiquitylated sites within a protein's amino acid sequence. Additional methods for assessing ubiquitin chain topology include Ub-clipping and/or middle-down MS to retain some of the ubiquitin chain architecture via limited proteolysis [134], [135], and Ub-ProT, which utilises Trypsin-Resistant TUBE (TR-TUBE) to protect ubiquitin chains from digestion [136]. These techniques give researchers the unique ability to investigate the ubiquitin code during different conditions.

Alternatively, isotopically labelled peptides corresponding to diGly-modified residues in the ubiquitin protein sequence can be introduced to a biological sample as a reference during MS quantification. The inclusion of these synthetic peptides enables the absolute quantification of all ubiquitin chain-linkages in a sample: an approach termed 'Ub-AQUA' [137]. Rather than just a fold change, Ub-AQUA provides the stoichiometry of ubiquitin chains—a major advantage over relative quantification. Interestingly, the Ub-AQUA technique has unveiled that, in skeletal muscle obtained from 8- to 12-week-old mice, 8.7% of total ubiquitin is formed by polyubiquitin chains and over half of these are K33-linked [138]. The high stoichiometry of K33-linked polyubiquitin chains was a distinct feature of muscle, as most other mouse tissues were dominated by K48-linked polyubiquitin chains. Ubiquitin protein standard absolute quantification (Ub-PSAQ) is another method for absolute quantification of ubiquitin [139]. Ub-PSAQ uses isotopically labelled protein standards corresponding to free ubiquitin and ubiquitin conjugates which are added to lysates before digestion. By including affinity reagents selective for capturing specific polyubiquitin chains, Ub-PSAQ is capable of providing absolute quantification of ubiquitin chains.

2.4 Applications of ubiquitylomics

Ubiquitylomics is a tool that can be employed to investigate different biological questions. Most commonly, ubiquitylomics is employed to uncover signalling networks and protein interactions but can also be used for drug discovery and biomarker identification, showcasing its effectiveness in both experimental and clinical settings.

2.4.1 Analysing the dynamics of ubiquitylation

Ubiquitylated proteins often have a short life-expectancy as many are degraded by the proteasome. Proteasome inhibition enables the capture of ubiquitylated proteins destined for proteasomal degradation, thereby capturing highly dynamic ubiquitylated proteins. As a result, proteasome inhibition can increase the detection of ubiquitylated peptides two to three fold following K-ε-GG antibody enrichment [140]. Of note, proteasome inhibition induces proteotoxic stress which creates additional ubiquitylated substrates for protein quality control. To distinguish dynamic and protein quality control ubiquitylation, one ubiquitylomics study employed an 8-hour time-course with the proteasome inhibitor bortezomib [50]. The authors reasoned that ubiquitylated proteins which increased exclusively at the later 8-hour time-point most likely arose from proteotoxic stress rather than dynamic regulatory ubiquitylation. Of note, the ubiquitylation sites in this group outnumbered the sites which increased only at the 2-hour treatment time-point. Therefore, longer treatments of proteasome inhibition may capture more proteotoxic ubiquitylation created by the treatment as opposed to naturally occurring dynamic ubiquitylation.

2.4.2 Capturing substrates of ubiquitin-regulating enzymes

Mapping an E3 ligase or DUB to specific ubiquitylation sites on a substrate remains the holy grail in ubiquitylation research. Modern mass spectrometers are well equipped to identify whether a substrate has become ubiquitylated or deubiquitylated; but identifying the enzymes responsible presents a greater challenge. This is mainly because ubiquitylation can be regulated by approximately 600 E3 ligases and 100 DUBs in humans [46], with partially overlapping substrates and varying degrees of redundancy.

Studies have utilised chemical or genetic modification methods to heighten or suppress the expression or activity of an E3 ligase or DUB, followed by subsequent ubiquitylomics. Proteins that undergo significant changes in their ubiquitylation status following the altered expression/activity of an E3 ligase or DUB can be deemed as potential substrates. This approach has been used to study the substrates of the largest family of E3 ligases called the Cullin-RING E3 ligases (CRL) [141]. Chemical inhibition of this E3 ligase family coupled with ubiquitylomics identified 410 candidate substrates, with 108 also displaying altered stability. Potential substrates of E3 ligases implicated in muscle atrophy have also been identified using a similar approach. For example, the overexpression of MuRF1, ASB2β and mutant KHL40 in mouse or zebrafish coupled with ubiquitylomics revealed potential substrates of these E3 ligases in skeletal muscle [142], [143], [144]. To the best of our knowledge, identification of DUB substrates using ubiquitylomics has yet to be performed in skeletal muscle. In the case of cellular models, genetic manipulation of DUBs coupled with ubiquitylomics analysis has been conducted to identify USP30 substrates, demonstrating that USP30 targets multiple mitochondrial proteins involved in the regulation of mitophagy [145]. Since then, the same approach has been used to study many other DUB substrates, contributing to the establishment of a database of DUB substrates [146].

Other approaches attempt to 'capture' E3 ligase or DUB substrates through protein–protein interactions. Affinity-based capture such as co-immunoprecipitation are often used to capture protein–protein interactions; however, a major disadvantage is the difficulty in identifying transient and low-affinity interactions. To overcome these pitfalls, synthetic fusion proteins can be expressed in cells to 'trap' protein interactions. E3 ligase–substrate interactions can be captured through fusion of ubiquitin to the E3 ligase, a reagent known as Ubiquitin-Activated Interaction Traps (UBAITs) [147]. Substrate trapping can also be performed through

exogenous co-expression of an E3 ligase fused with a TUBE [148]. TUBEs bind to polyubiquitylated substrates in cells, protecting them from DUBs and proteasome-mediated degradation. Afterwards, immunoprecipitation (often targeting the tag fused to the TUBE e.g. anti-FLAG) can be used to selectively enrich ubiquitylated substrates prior to LC-MS. TR-TUBE offers an additional advantage by protecting both the TUBE and ubiquitin from trypsin digestion [149]. This is beneficial as digested peptides from TUBE and ubiquitin can introduce a substantial source of background noise during MS analysis.

Proximity labelling enzymes, such as APEX2, BioID and TurboID, have also been successfully deployed for capturing putative E3 ligase or DUB substrates in cells. When fused to an E3 ligase or DUB, proximity labelling enzymes typically work by labelling nearby proteins with biotin in live cells. Biotinylated proteins (representing putative substrates) can then be enriched through streptavidin affinity pull-down and analysed using LC-MS. The development of more catalytically efficient proximity labelling enzymes means it is now possible to label interacting proteins within a few minutes, enabling capture of transient signalling responses [150]. It should be noted, however, that this method will also label non-substrates that come into proximity with the E3 ligase or DUB of interest and so further validation steps (such as *in vitro* ubiquitylation/deubiquitylation assays) should be performed to confirm authenticity. To improve specificity for capturing ubiquitylated substrates and mitigate non-substrate capture, recent studies have implemented additional modifications to these proximity labelling enzymes, for example, BioE3, E-STUB and Ub-POD [151], [152], [153].

2.4.3 Targeted protein degradation

Ubiquitylomics has also been used to detect substrates of E3 ligases in the context of targeted protein degradation. Small molecules such as proteolysis targeting chimera (PROTAC) and

molecular glues have been developed to redirect E3 ligases for the degradation of non-native substrates (known as neo-substrates) associated with disease [154]. However, one concern regarding the effectiveness of PROTACs and molecular glues as therapeutic agents is how selective the redirected E3 ligase will be to its target neo-substrate. Any off-target ubiquitylation could result in the unwanted degradation of physiologically important proteins. Ubiquitylomics has been used to profile protein ubiquitylation following targeted protein degradation to determine the specificity of PROTACs/molecular glues. To give a classic example, quantitative ubiquitylomics analysis revealed that Lenalidomide—a drug used to treat multiple myeloma—works as a molecular glue by selectively ubiquitylating and degrading the transcription factors IKZF1 and IKZF3 [155].

2.4.4 Post-translational modification (PTM) crosstalk

The proteome-wide crosstalk between ubiquitylation and other PTMs can be explored using LC-MS. Interplay between different PTMs on a single protein, termed PTM crosstalk, adds an additional layer of complexity to cellular regulation. Beyond the impact of individual PTMs, their inter-regulation influences signalling pathways, contributing to the intricate maintenance of cellular homeostasis. PTM crosstalk can be assessed by LC-MS through additional steps such as serial enrichment and deep fractionation [156]. Serial enrichment is a popular approach for analysing multiple PTMs in the same sample, utilising the flow-through of one PTM enrichment for subsequent enrichment of another PTM [157], [158]. Whilst serial enrichment allows for smaller sample input, this approach can result in the loss of PTM information. In one comparison, prior enrichment of phosphorylated peptides reduced the detection of ubiquitylated peptides by 13% when compared to isolated enrichments [157]. Although some of these losses could be a result of the additional handling steps required, it is also likely that other losses occur due to both PTMs co-existing on the same peptide, which is captured in the

initial enrichment and thus absent from subsequent enrichments. Therefore, consideration should be taken over the most appropriate enrichment order to reduce loss of PTM information, for example, perhaps prioritising the least abundant PTM. At the instrument level, coupling MS with high-field asymmetric ion mobility spectrometry (FAIMS) represents a technological advance that uses multiple forms of online peptide separation to improve the dynamic range of detection for less abundant PTM-containing peptides [159].

When dealing with different PTMs, it is important to use the appropriate ion fragmentation technique. To identify the location of each PTM, peptides must first be fragmented to expose regions of amino acids. Fragmentation is performed but imparting internal energy, typically through an inert gas such as helium or nitrogen (collision-induced dissociation (CID) and high-energy collisional dissociation (HCD)) or electrons (electron capture dissociation (ECD) and electron transfer dissociation (ETD)). The identification of PTMs can be influenced by the method of peptide fragmentation, for instance to retain more labile PTMs such as phosphorylation, a softer fragmentation like ECD and ETD is used to preserve the modification [160]. In contrast, ubiquitin is bound through a covalent bond and so can withstand the energy of an inert gas whilst benefiting from superior peptide fragmentation.

The application of LC-MS has substantially improved our understanding of the occurrence and functional importance of PTM crosstalk with ubiquitylation. For example, one study investigated the directionality of PTM crosstalk, identifying conserved phosphorylated sites which precede ubiquitylation [161]. This crosstalk directionality occurs with phosphodegrons, in which protein phosphorylation is recognised by an E3 ligase, leading to subsequent ubiquitylation and protein degradation. Phosphorylation can also regulate substrate ubiquitylation independent of protein degradation, for example during DNA repair [162]. On

the other hand, there are examples of phosphorylation preventing protein ubiquitylation [163]. Beyond phosphorylation, there are many other PTMs that display crosstalk with ubiquitylation, highlighted more comprehensively in another review [164]. One example worth noting is the crosstalk between ubiquitylation and acetylation—both occurring on lysine residues. A lysine residue harbouring an acetyl modification may prevent ubiquitin attachment at this position. By comparing ubiquitylome and acetylome datasets obtained from human cell lines, it was revealed that 30% of acetylated lysines can also be modified by ubiquitin [115]. In patient-derived tumour tissue, a subset of lysine sites were inversely modified by ubiquitylation and acetylation, suggesting these two modifications work in an antagonistic manner [129]. In agreement with this finding, acetylation at both lysine and N-terminal residues has been reported to protect proteins from ubiquitin-mediated degradation [165], [166]. Lysine acetylation also occurs on ubiquitin itself, which can inhibit polyubiquitin chain assembly, thus impacting chain architecture [167]. These studies demonstrate how different PTMs communicate to alter ubiquitin signalling. Therefore, coupling ubiquitylomics with other PTM-enriched proteomics will help identify 'switches' of ubiquitylation that regulate health and disease, offering targets for therapeutic intervention.

2.5 Ubiquitylomics in skeletal muscle

Ubiquitylomics is evidently a powerful tool for studying protein ubiquitylation, with continuous advancements in methodological approaches providing new ways to unravel the complexities of ubiquitylation in cellular biology. In skeletal muscle, ubiquitylomics is commonly framed in the context of change induced by various forms of perturbation, including pathological, physiological or interventional **(Figure 2.2)**.

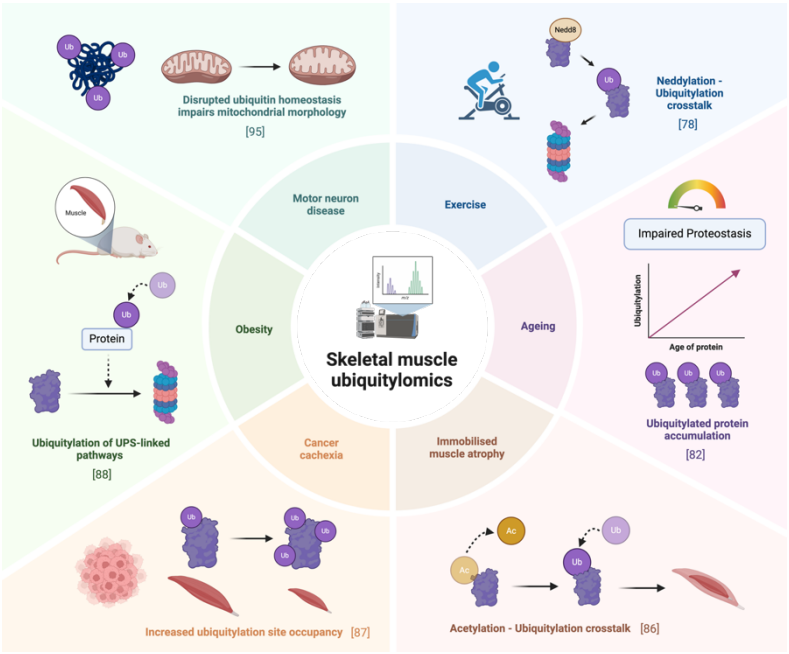

Figure 2. 2. Schematic displaying the results of skeletal muscle ubiquitylomics experiments in different physiological or pathological states. Image created using biorender.com.

2.5.1 Exercise

Exercise undoubtedly stands out as the most well-established method for maintaining skeletal muscle health, known to induce many signalling pathways in response to changes in the cellular environment. Exercise attenuates the degenerative ageing hallmarks [168], and can slow down the progression of skeletal muscle atrophy through improving protein quality control [169]. In skeletal muscle, strenuous exercise activates the UPS, presumably to remove damaged proteins [170]. To understand the potential mechanisms responsible for this increase, one study employed diGly peptide enrichment to investigate the effect of an acute bout of intense aerobic exercise on the skeletal muscle ubiquitylome [171]. GSEA revealed that several pathways, including muscle contraction and glycolysis, displayed altered protein ubiquitylation during exercise. Future work is required to determine whether ubiquitylation of these proteins regulates exercise-induced improvements in muscle mass and energy metabolism. Rapid

alterations in protein ubiquitylation were found alongside increases in NEDDylation, leading the authors to hypothesise that crosstalk between these two PTMs is involved in UPS activation. Changes in ubiquitylated proteins were not seen 2 h after exercise, highlighting the dynamic and transient nature of protein ubiquitylation. This is in stark contrast to the phospho-proteome, in which nearly 3000 phospho-sites were differentially regulated even 3 h after intense sprint exercise [172]. To date, there is no study looking into the ubiquitylome following resistance or endurance exercise; given the utilisation of different metabolic and contractile proteins during sprint, endurance and resistance exercise, one might expect unique changes in protein ubiquitylation with each exercise bout.

2.5.2 Ageing

During ageing, there is a decline in protein quality control, resulting in an accumulation of protein aggregates and a global loss of proteostasis—a well-established hallmark of ageing also seen in skeletal muscle [17], [19]. Given the role of ubiquitylation in regulating protein quality control, ubiquitylomics has been employed to identify ubiquitin-mediated impaired proteostasis in aged skeletal muscle. When combined with stable isotope labelling, ubiquitylomics analysis revealed an age-related increase of long-lived ubiquitylated proteins in *Drosophila* muscle [173]. To our knowledge, this method has not been applied in mammalian skeletal muscle tissue; however, similar results were observed in mouse liver tissue [174]. These long-lived ubiquitylated proteins could represent protein aggregates that are ubiquitylated but not efficiently degraded in skeletal muscle. The relationship between protein aggregates and ageing in skeletal muscle has not been extensively studied. Nevertheless, LC-MS has revealed tissue-specific aggregates in aged African killifish *N. furzeri* and found DHTKD1, a mitochondrial enzyme involved in the degradation of several amino acids, is

aggregation-prone in skeletal muscle [175]. Performing ubiquitylomics analysis on insoluble aggregates would enable the identification of ubiquitylated proteins that contribute towards age-related impaired muscle proteostasis.

2.5.3 Muscle atrophy and disease

Protein ubiquitylation has long been known to contribute towards muscle atrophy, promoting myofibrillar protein degradation through the UPS. Aligning with this concept, ubiquitylomics studies conducted in denervated- and immobilised-induced muscle atrophy show global increases in myofibrillar protein ubiquitylation [37], [176]. By integrating these findings with additional data obtained by LC-MS, both studies were able to provide novel mechanistic insights. For example, actin and myosin heavy/light chain became ubiquitylated following immobilisation and were also deacetylated [37]. Therefore, the antagonistic crosstalk between acetylation and ubiquitylation appears to be involved in immobilised-induced muscle atrophy. Furthermore, denervation altered the expression of 105 proteins associated with ubiquitylation, including the upregulation of E3 ligase Trim25, which had not previously been associated with muscle atrophy [176]. By obtaining large datasets for both total and ubiquitylated proteins, this study offers a valuable resource to study potential targets of ubiquitin-associated enzymes during denervation-induced atrophy.

Tumour-bearing mice display increasing protein ubiquitylation as they experience muscle atrophy (cancer cachexia), suggesting that ubiquitylation correlates with the reduction in muscle mass [177]. Interestingly, the authors were able to show that ubiquitylation increased most on additional sites of proteins already ubiquitylated before muscle atrophy occurred. Therefore, during cancer, proteins ubiquitylated at early stages may be targets for additional

ubiquitylation during muscle atrophy. Most of these sites were dependent upon the E3 ligase MuRF1, and GSEA revealed they belonged to proteins involved in muscle contraction, cytoskeleton, sarcoplasmic reticulum and glycolysis.

As a highly metabolic tissue, skeletal muscle undergoes changes in response to metabolic health. Obesity causes a deterioration in metabolic health which compromises the function of skeletal muscle, e.g. insulin resistance. Based on the observation that the activity of the UPS is greater following a high-fat diet, one group investigated the effects of this change on the mouse skeletal muscle ubiquitylome [178]. They found that, whilst the total number of ubiquitylated proteins and ubiquitylated sites remained largely unchanged, individual protein ubiquitylation changes were evident, including those involved in proteasome-mediated degradation. This emphasises the importance of employing ubiquitylomics to identify such individual differences in an unbiased way. This work made parallels between UPS activation and energy metabolism in obesity by utilising a multi-omics approach. By combining RNAseq, proteomics, ubiquitylomics and metabolomics, they found the UPS activator Nfe2l1, which promotes degradation of K48-linked ubiquitylated proteins, encourages glycolytic metabolism in fast-twitch muscle fibres. These findings illustrate how protein ubiquitylation can shape the landscape of energy metabolism in skeletal muscle.

Loss of motor neuron function can also contribute towards skeletal muscle atrophy. Disrupted ubiquitin signalling and subsequent loss of proteostasis is a feature of many neuromuscular diseases [179]. For instance, lack of the DUB Uchl1 in Gracile Axonal Dystrophy (GAD) impairs the synaptic transmission at neuromuscular junctions, loss of function in the E3 ligase coding gene Ube3a disrupts proteasome activity in Angelman Syndrome (AS), the E3 ligase

Rnf126 degrades frataxin which is reduced in Friedreich Ataxia (FRDA), reduced levels of the E1 ubiquitin-activating enzyme Uba1 disrupts myelin protein expression in Schwann cells isolated from Spinal Muscular Atrophy (SMA) mice and the accumulation of ubiquitylated protein inclusions in neuronal cells disrupts proteostasis in Amyotrophic Lateral Sclerosis (ALS) [180], [181], [182], [183], [184]. Ubiquitylomics has been employed on different cell models of ALS, identifying targets of altered ubiquitylation which may contribute towards the pathology. For instance, cells expressing misfolded superoxide dismutase 1 experienced increased ubiquitylation of mitochondrial proteins corresponding to mitochondrial defects [185]. Moreover, cells lacking functional Cyclin-F impaired the ubiquitylation of Hsp90ab1, disrupting its chaperone capabilities [186].

2.6 Challenges of ubiquitylomics in skeletal muscle

Whilst ubiquitylomics-based experiments have identified ubiquitin signalling networks that drive biological processes in skeletal muscle, the number of these studies is substantially lower than in many cells and tissues. This is most likely due to the difficulties in achieving a deep coverage of the muscle ubiquitylome.

The number of ubiquitylated proteins identified by LC-MS is largely affected by the abundance distributions (or dynamic range) of proteins in the sample. Until recently, MS-based proteomics typically employed data-dependent acquisition (DDA), in which only the most-abundant peptides observed by the MS are analysed further. Highly abundant proteins contribute to a large proportion of the total peptides injected into the LC-MS, supressing the detection of less abundant peptides. This problem is particularly apparent when analysing skeletal muscle tissue, which is composed of large and abundant structural and contractile proteins that make up a

sizeable proportion of the total peptide content. For example, the structural protein titin is the largest protein in the human proteome, comprising ~30 000 amino acids and exceeding 3000 kDa. Therefore, peptides derived from titin are very abundant and frequently detected throughout the MS detection period. Based on the sum of mass spectra, one study found that the 10 most abundant proteins in skeletal muscle make up half of the total protein mass in skeletal muscle, with titin accounting for 16% [20].

This skewed detection of a select few proteins has often prevented the deep coverage of ubiquitylated proteins. For instance, ubiquitylomics comparison across different murine tissues revealed skeletal muscle contained the lowest number of ubiquitylated sites [187]. When comparing ubiquitylomics data from human skeletal muscle and two different human cell lines [115], fewer proteins in muscle contributed to a larger proportion of the total ubiquitylation site coverage **(Figure 2.3)**. Given the high abundance of ubiquitylation sites on a few structural and contractile proteins, the coverage of ubiquitylated proteins may well be lowered by less frequent observation of lower abundance sites due to limits in the dynamic range of detection. Therefore, a substantial proportion of the ubiquitylated proteome in skeletal muscle is likely undetected by MS.

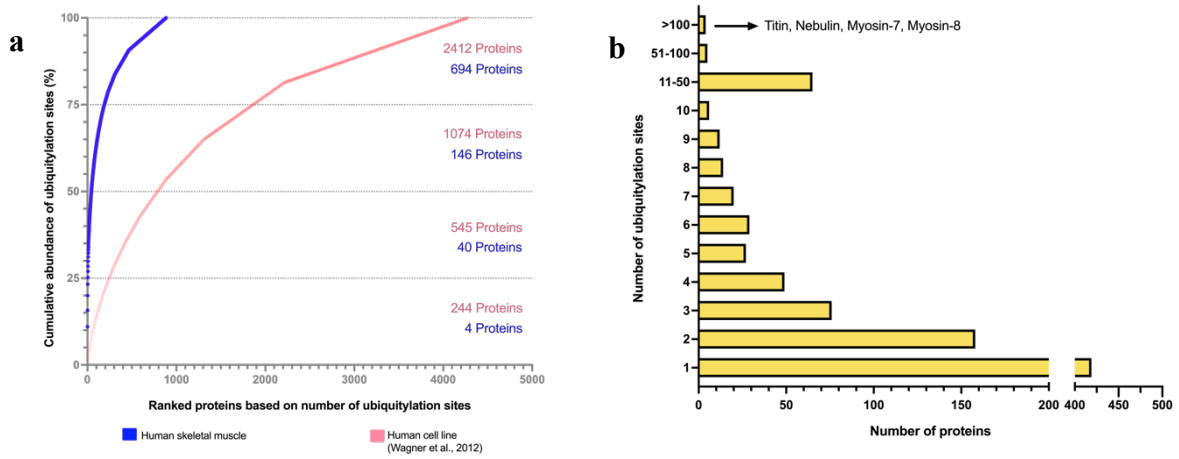

Figure 2. 3. Dynamic range in the number of ubiquitylation sites detected on each protein in skeletal muscle. (a) Ubiquitylomics data from human skeletal muscle (n = 3) was compared against published data combined from two human cell lines (HEK293T and MV4-11)[115]. Proteins were ranked based on the number of ubiquitylation sites detected (including only those with at least 1 site), and the cumulative abundance of ubiquitylation sites was calculated from highest to lowest rank. Each circle represents an individual protein; the number of proteins contributing to each cumulative quartile are displayed. (b) Proteins from human skeletal muscle were categorised based on the number of ubiquitylation sites detected. Each bar represents the number of proteins that contain the given number of ubiquitylation sites.

2.7 Considerations for ubiquitylomics analysis in skeletal muscle

To improve the depth of protein coverage detected by LC-MS, strategies have been developed to reduce sample complexity. A common method is orthogonal peptide fractionation (e.g., at high pH, or with strong cation exchange chromatography), which separates the sample into simpler mixtures, increasing the number of peptides that can be observed during DDA cycles [188]. When utilised in plasma, which like skeletal muscle contains a challenging protein dynamic range, high pH reverse-phase fractionation improves the depth of protein coverage [189]. Notably, high pH reversed-phase fractionation has been shown to improve the detection of ubiquitylation sites [190].

Studies have tried including additional fractionation steps to simplify the protein pool even further. In skeletal muscle, researchers have attempted to separate proteins based on their

solubility prior to proteomics [191], [192], [193], [194]. Due to their large size and highly connected structure, highly abundant proteins in the myofiber are more difficult to solubilise. Centrifugal separation of insoluble proteins allows less-abundant soluble proteins to be analysed separately from the more-abundant insoluble proteins—increasing the total number of proteins detected. Through this approach, one study detected 1490 proteins in the soluble supernatant of mouse skeletal muscle that were not detected in whole tissue analysis [192]. More recently, nanoparticle protein interaction has been employed for separation of muscle proteins to further improve depth of coverage [30]. Together, these studies show the available methods for reducing sample complexity to enhance the coverage of proteins detected in skeletal muscle.

Given that protein ubiquitylation detection in skeletal muscle is dominated by a few highly abundant proteins **(Figure 2.3)**, employing fractionation strategies promises to be especially fruitful for ubiquitylomics analysis. However, it should be noted that, more recently, the proteomics field is broadly moving away from such fractionation approaches as advances in instrument speeds and sensitivity offer greater dynamic ranges of detection. It remains to be seen if these advancements will provide similar impacts on the challenges of skeletal muscle proteomics and ubiquitylomics.

The method employed for data acquisition on the mass spectrometer also plays a crucial role in determining the depth of protein coverage. As mentioned earlier, DDA characterises a limited number of peptides based on abundance. Recently, data-independent acquisition (DIA) has emerged as a powerful alternative to DDA. DIA fragments all peptide ions within a mass to charge window, resulting in less bias towards highly abundant proteins. As a result, DIA has been able to identify up to 70 000 ubiquitylated peptides, significantly increasing the detection

limit in a single LC-MS run [195], [196]. DIA will likely improve the number of ubiquitylated peptides/proteins detected in skeletal muscle, combating the underrepresentation of less-abundant proteins often seen in DDA.

2.8 Conclusions

With the trajectory of methodological advancements, the analysis of thousands of ubiquitylated peptides in skeletal muscle has become feasible. Therefore, it may be of interest for researchers to become familiarised with the technical and analytical steps involved **(Figure 2.4)**. More detailed information on these steps is covered in other reviews [197], [198], [199], [200]. One major challenge of ubiquitylomics is to understand how each ubiquitylation site integrates into the biological system. Integrating this method into a multi-omics framework for parallel analysis of nucleic acids, proteins and metabolites could help establish mechanistic insight into the order of molecular events. The next phase of ubiquitylomics could also uncover the spatial and temporal regulation of skeletal muscle ubiquitylation, harnessing technologies developed in other -omics fields, for example, stable isotope tracers for flux analysis, and MS imaging for spatial resolution [201], [202]. User-friendly web-based computational tools, such as MSstatsShiny, WebGestalt and CURTAIN, make ubiquitylomics data analysis far more accessible to muscle physiologists and exercise scientists with limited bioinformatics experience [203], [204], [205]. Even if not directly engaged in ubiquitylomics-based experiments, researchers should make use of the rich datasets provided by ubiquitylomics studies, deposited in accessible databases such as PRIDE [206]. Searching through ubiquitylomics datasets to determine whether specific proteins in skeletal muscle are

ubiquitylated in certain conditions is likely to prove beneficial in both clinical and experimental settings.

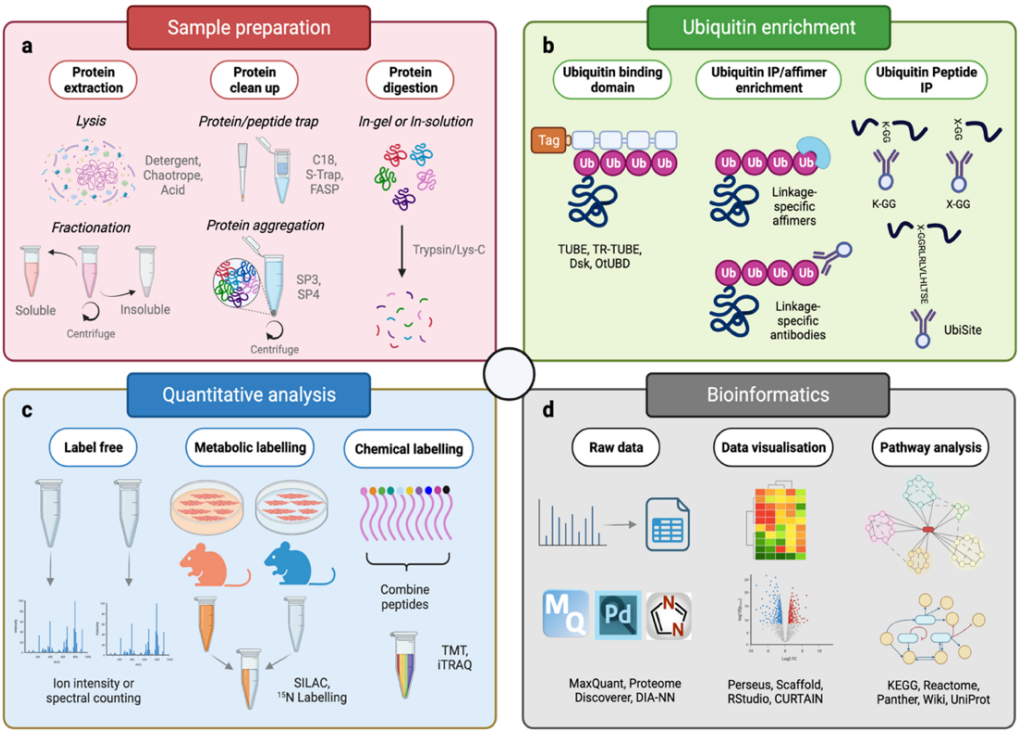

Figure 2. 4. Schematic displaying the key steps when performing MS-based ubiquitylomics experiments. (a) Sample preparation is used to ensure sample compatibility with proteolysis, LC and MS. Protein extraction and solubilisation requires the use of harsh chemical agents, for example, detergents and chaotropes, that can interfere with typical bottom- up proteomics workflows. Various clean- up methods are available for isolating proteins or peptides, for example, protein aggregation or trapping, allowing the removal of contaminants. (b) Ubiquitin enrichment is used to deplete non-ubiquitylated peptides/proteins that would interfere with detection. Multiple tools are available for ubiquitin enrichment at both the protein and peptide level, such as ubiquitin binding domains, antibodies and affimers, each with different advantages and disadvantages. (c) Quantitative analysis is performed to identify relative abundance differences in ubiquitylated peptides/proteins between samples. The label- free approach compares either ion intensities or spectral number of a given protein. Data-independent acquisition (DIA) is mostly limited to label- free quantification, whilst data- dependent acquisition (DDA) allows for label- based quantification and multiplexing. Metabolic labelling involves the use of 'heavy' and 'light' isotopes, which are incorporated into proteins (e.g., in lysine and arginine residues for SILAC), and relative quantification is performed by comparing the isotope intensities of a given protein's peptides. Chemical labelling modifies all peptides covalently with isobaric tags, conferring identical chemical properties, but reporter ions differentiated by isotopic distributions. The intensities of the reporter ions (which are cleaved off during MS fragmentation) is used to infer relative quantification of a given protein. (d) Bioinformatics is required for the deconvolution of spectral data obtained from the mass spectrometer. Various software is available which deal with raw MS data and employ database searching and filtering for the identification and quantification of peptides/proteins and their modifications, for example, diGly for ubiquitylation. Biologically meaningful data can then be visualised through different displays, for example, volcano plots and heatmaps, using programs that often include statistical testing. Pathway analysis can also be employed to search for biological pathways driven by differentially regulated ubiquitylated proteins. Image created using biorender.com.

3. Developing a method to study the proteome of skeletal muscle

3.1 Abstract

Proteomics is capable of identifying and quantifying thousands of proteins in skeletal muscle. At this scale, proteomics can provide a holistic overview of mechanistic changes that occur during ageing. Identifying thousands of proteins requires a well optimised workflow, catered to the sample of interest, which in skeletal muscle can provide additional complications (as outlined in chapter 2). We set out to develop a reliable and reproducible workflow that could perform large-scale proteome profiling in skeletal muscle tissue. The aim of this chapter was to critically evaluate the effectiveness of different stages in the proteomics workflow. Our workflow employed muscle fractionation, separating highly abundant myofibrillar proteins from sarcoplasmic proteins. We employed a cost-effective protein precipitation clean up method to remove contaminants in the lysate whilst delivering high protein recovery. Quality control checks confirmed our sample preparation enabled high quality peptide identification by LC-MS. Our method identified 2163 proteins, an additional 273 proteins when compared to whole tissue analysis. Many of these additional proteins were exclusively found in the soluble fraction, with a notable presence of plasma membrane proteins. In summary, we have developed a robust proteomics workflow designed for large-scale analysis of the skeletal muscle proteome.

3.2 Background

Proteomics is the large-scale study of proteins, typically involving LC-MS instrumentation to identify and quantify proteins. While methods exist for analysing proteins in their intact form, the depth of coverage is improved when dealing with peptides, a process termed bottom-up proteomics. One of the major advantages of bottom-up proteomics is the ability to provide untargeted analysis. This is valuable for discovery-based research when researchers are

uncertain about proteins present in their sample or how a condition may have altered their abundance. In addition, the high sensitivity of modern LC-MS instruments means bottom-up proteomics can be performed on very small amounts of peptide (< 1 μg). This is especially beneficial when working with primary tissue such as skeletal muscle, where material is often limited. As with any method there are also drawbacks that need to be considered, and if possible minimised. A significant challenge of bottom-up proteomics is managing high sample complexity. Analysing peptides derived from skeletal muscle requires advanced separation techniques and high-resolution instrumentation, which can increase both the time and cost of analysis. Furthermore, the high sensitivity of LC-MS is problematic when exposed to contaminants. Trace amounts of contaminants such as salts or detergents interfere and compete with peptides for detection. Removing contaminants is an essential methodological step for ensuring high coverage of the proteome. Therefore, an essential step before performing proteomics on valuable biological samples is ensuring that the workflow is optimised.

To tackle the challenging dynamic range of muscle proteins, our approach involved separating abundant highly abundant myofibrillar proteins from sarcoplasmic proteins. To achieve good fractionation of sarcoplasmic and myofibrillar proteins, we took advantage of their solubility properties. A low percentage of Triton X-100 detergent (0.5%) was added in our 'sarcoplasmic' soluble lysis buffer as it has been shown to solubilise proteins in mitochondria, sarcolemma and sarcoplasmic reticulum without interfering with contractile proteins in the myofiber [207]. The most effective lysis buffer for solubilising myofibrillar proteins is less well characterised, therefore we decided to compare the effectiveness of two different lysis buffers. The first method known as 'MIST' was taken from a muscle fractionation methods paper, which includes a solubilising agent called spermidine [193]. The second method comes from a

proteomics protocol paper which increases the detergent concentration to 5% to aid protein solubilisation [208].

Following lysis of muscle tissue, the next stage step was to remove any contaminants that would interfere with the detection of peptides. MS detects peptides by measuring charged ions brought about by ionisation. However, other charged substances such as ionic detergents and salts will compete with peptides for ionisation and subsequently reduce peptide detection [209]. Furthermore, their non-volatile nature affects droplet formation during electrospray ionization (ESI) which reduces the number of charged ions [210]. As a result, if these compounds are present during LC-MS analysis, this will result in ion suppression and severely effect the efficiency of the machine. Detergents and salts are included in our lysis buffers to help solubilise proteins, for example our lysis buffer includes five different detergents (Triton X-100, Tween 20, NP-40 substitute, SDS (Sodium dodecyl sulfate) and sodium deoxycholate) and 2 different salts (sodium orthovanadate and sodium chloride). Therefore, it is important that we remove these compounds before LC-MS analysis.

Different strategies have been developed to remove various salts and detergents from biological samples including filtration and affinity-based methods [211], [212], [213], [214]. These methods can be costly and are often applied in combination e.g., detergent clean up prior to digestion, followed by desalting of peptides [208]. Sample clean up represents a large source of sample loss and so minimising the number of clean up steps is preferable. Protein precipitation-based methods can remove a range of contaminants in a single stage using organic solvents such as ethanol, acetone or acetonitrile (ACN). Typically, magnetic beads are included which bind to proteins after exposure to solvents through a proposed mechanism similar to hydrophilic-interaction-liquid-chromatography (HILIC). This process is known as single-pot,

solid-phase-enhanced sample preparation (SP3) [208]. Alternatively, beads can be omitted if you employ centrifugation after solvent exposure. Organic solvents remove the water surrounding soluble proteins, which at high concentrations causes protein aggregation through non-covalent interactions (**Figure 3.1**). Aggregated proteins can then be pelleted due to their high mass and contaminants in the supernatant can be removed. This method of protein aggregation is driven entirely by solvent precipitation, and was termed SP4 [118].

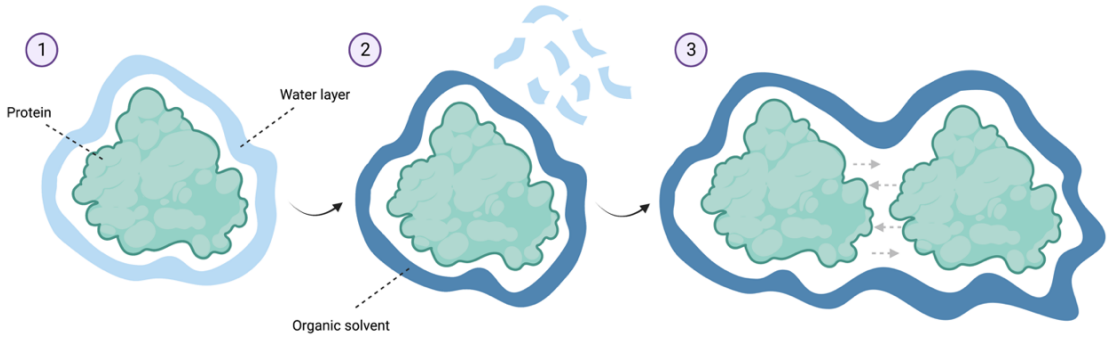

Figure 3. 1. Schematic demonstrating the process of protein precipitation using organic solvents. Step 1: Protein is water soluble. Step 2: Water layer is dispersed by organic solvent, bringing protein out of solution. Step 3: Insoluble proteins bind together forming insoluble aggregates. Image created using biorender.com.

It is worth mentioning, given that SP4 capture is driven by hydrophobic interactions, reports have shown the hydrophilic protein pool is better retained with SP3 [215]. However, overall protein yields are similar as it enhances hydrophobic protein capture, for instance membrane-bound proteins [118]. Given that SP4 offers a cheaper approach, we opted to go for this method. There are certain conditions that need to be considered when optimising SP4-based clean up. Firstly, although protein precipitation is used to remove salts and detergents, their presence provides ionic strength that promotes efficient protein precipitation [216]. Secondly, high protein concentrations are recommended during SP4 to ensure sufficient precipitate formation and reduce protein adhesion to tube-wall [118]. Finally, from our experience, higher protein

content is also beneficial for protein pellet visualisation to avoid contact and potential losses during wash stages.

The next stage was to determine whether our sample preparation workflow is compatible with LC-MS. Our method of choice was bottom-up proteomics, which meant we first had to digest our proteins into peptides for accurate identification. Therefore, the performance of our workflow depends on the ability for the LC-MS to detect peptides instead of background noise. To check the quality of the peptide-level data, we used a Proteomics Quality Control (PTXQC) R-based pipeline [217]. This pipeline provides a report of different quality control metrics, including a built-in scoring system to provide a performance overview. We could then identify which areas of our workflow were working sufficiently and whether any aspects were underperforming. Finally, we wanted to determine if our fractionation workflow improved the detection of the muscle proteome when compared to a whole tissue lysis approach. At this stage, we performed more in-depth analysis of the fractionation workflow to confirm good separation of proteins, before quantifying differences in the proteome coverage with the whole tissue approach.

3.3 Methods

3.3.1 Collection of skeletal muscle

Muscle samples were provided by Dr Ryan Marshall and Prof Leigh Breen. Muscle biopsies were taken from quadricep (Vastus Lateralis) of three human participants (24-27 years, BMI: 22-26) and frozen in liquid nitrogen before being stored at -70 °C until lysis. Ethical approval was obtained through the East Midlands - Derby Research Ethics Committee (18/EM/0004),

conformed to the requirements of Research Governance at the University of Birmingham and was conducted in accordance with the Declaration of Helsinki.

3.3.2 Fractionation of skeletal muscle

Separation of soluble and insoluble fractions was performed by two different methods. The first method was based on the optimised muscle fractionation protocol [193]. Briefly, 50 mg of frozen muscle tissue was powdered using a mallet and crusher. A 10-fold volume of ice-cold lysis buffer 1 (25 mM Tris, pH 7.2, 0.5% Triton X-100, 100 mM 2-chloroacetamide, 1 mM sodium orthovanadate, 1x cOmplete Mini EDTA-free protease inhibitor (11836170001, Roche, Switzerland)) was added to each sample. The powdered muscle was homogenised using a TissueLyser II (Qiagen, Netherlands) with 5 mm stainless steel beads during 2 x 2-minute cycles at 30 Hz. To collect the soluble fraction, the lysate was centrifuged at 1500 g (4 °C) for 10 minutes and the supernatant was collected. To obtain the insoluble fraction the pellets were first washed in 10 volumes lysis buffer 1 and then resuspended in 15 volumes of ice-cold lysis buffer 2 (20 mM Tris–HCl, pH 7.2, 100 mM potassium chloride, 20% glycerol, 1 mM DTT, 50 mM spermidine, 100 mM 2-chloroacetamide, 1 mM sodium orthovanadate, 1x cOmplete Mini EDTA-free protease inhibitor (11836170001, Roche, Switzerland)) and placed in the TissueLyser II (Qiagen, Netherlands) with 5 mm stainless steel beads for 2 x 2-minute cycles at 30 Hz. To collect the insoluble fraction a quick 1 min spin was performed on a desktop centrifuge and the supernatant was transferred to a new tube. The second method was based on a stringent detergent-based lysis method [203]. The soluble fraction was obtained as described in the first method, however the washed pellet was resuspended in 15 volumes of ice-cold 5% detergent lysis buffer (50 mM HEPES pH 8.0, 1% SDS, 1% Triton X-100, 1% NP-40, 1% Tween 20, 1% sodium deoxycholate, 50 mM NaCl, 1mM DTT, 5mM EDTA, 1% (w/v) glycerol, 100 mM 2-chloroacetamide, 1 mM sodium orthovanadate, 1x cOmplete Mini EDTA-

free protease inhibitor (11836170001, Roche, Switzerland)) and placed in the TissueLyser II (Qiagen, Netherlands) with 5 mm stainless steel beads for 2 x 2-minute cycles at 30 Hz. The lysate was incubated at 95 °C for 5 mins, cooled for 10 mins at room temperature. Lysates from both supernatant and pellet were sonicated at 4 °C for 12 x 5-second bursts with 5 second intervals. Finally, both lysates were cleared at 16000 g for 10 minutes and the supernatant from both soluble and insoluble fraction was collected. For whole tissue lysis, the same protocol was followed as described in the second method without prior fractionation of the soluble fraction. This way the only difference between the fractionation and whole tissue approach should be the separation of proteins and not protein solubility, allowing a fair comparison.

3.3.3 Protein concentration assay

Protein lysate concentrations were determined by a DC assay (5000111, Bio-Rad, USA) using an FLUOstar Omega plate reader (BMG Labtech, UK) according to manufacturer's instructions. Concentrations were read at an absorbance of 750 nm.

3.3.4 Coomassie staining and western blotting

100 µg lysate was prepared for western blot analysis by adding 4x LDS sample buffer (NP0008, Thermo Scientific, USA) containing 5% β-mercaptoethanol to final concentration 1x and 1.25% respectively and left overnight to denature. 10 µg of each sample was loaded into 10% Bis-Tris gels and separated using SDS-PAGE gel electrophoresis. Gels were run in 1x MOPS buffer for approximately 90 minutes at 140V. For Coomassie staining, gels were incubated in PageBlue protein staining solution (24620, Thermo Scientific, USA) for 1 hour before rinsing in double distilled water as per manufacturer's instructions. For western blotting, proteins were transferred onto PVDF membranes (10600021, Amersham, USA) for 1 hour at 100V.

Membranes were blocked in 5% bovine serum albumin (BSA) (BP9704100, Thermo Scientific, USA) diluted in Tris-buffered saline Tween 20 (TBS-T) and incubated overnight at 4 °C with the appropriate primary antibody: MHC (#M4276, 1:1000, Merck Millipore, USA), Actin (#A2103, 1:1000, Merck Millipore, USA), Desmin (#5332, 1:1000, Cell Signaling Technology, USA), ACC (#3676, 1:1000, Cell Signaling Technology, USA), GAPDH (#5174, 1:25000, Cell Signaling Technology, USA), Citrate synthase (#14309, 1:1000, Cell Signaling Technology, USA) and Histone H3 (#9715, 1:1000, Cell Signaling Technology, USA). Membranes were then washed in TBS-T three times prior to incubation in horseradish peroxidase-conjugated secondary antibodies (1:10000, Cell Signaling Technology, USA) at room temperature for 1 hour. Membranes were washed a further three times in TBS-T prior to antibody detection using enhanced chemiluminescence horseradish peroxidase substrate detection kit (WBKLS0500, Millipore, UK). Imaging was undertaken using a G:BOX Chemi-XR5 (Syngene, UK).

3.3.5 LC-MS sample preparation

Sample preparation was performed using a modified version of the SP4 protocol [118]. Lysates were prepared at 4 mg/mL and 200 µg of each sample was aliquoted into 1.5 mL LoBind tubes. Samples were reduced by 5 mM DTT for 45 minutes at 25 °C and then alkylated by 10 mM 2-chloroacetamide for 45 minutes at 25 °C in the dark. Proteins were precipitated by adding four volumes of 100% ACN followed by gentle mixing at 500 rpm for 5 seconds and left for 5 minutes at room temperature. Precipitated proteins were pelleted by centrifugation for 5 minutes at 16000 g at room temperature. To maximise pellet density, the tube was first orientated with the hinge inwards for 2.5 minutes and then turned 180° for the final 2.5 minutes. The supernatant was carefully discarded. The pellet was washed three times in 1.5x total precipitation volume of 80% ethanol, each time samples were centrifuged at 16000 g at room

temperature. After the final wash, the protein pellet was resuspended in 1x total precipitation volume of 50 mM ammonium bicarbonate containing trypsin (V5280, Promega, USA) at 1:100 enzyme:protein ratio. Sonication and vortexing was performed periodically until the protein pellet were resuspended. Proteins were left to digest for 18 hours at 37 °C shaking at 1000 rpm. Samples were centrifuged at 16000 g for 2 minutes and the peptide containing supernatant was collected into a fresh Eppendorf tube. Peptides were dried using a SpeedVac Concentrator plus (12884952, Eppendorf, Germany) at room temperature.

3.3.6 LC-MS

Peptides were resuspended in 2% ACN 0.1% trifluoroacetic acid (TFA) and ~500 ng peptides were analysed and acquired by an Orbitrap Eclipse (Thermo Scientific, USA) coupled with a Dionex UltiMateTM 3000 nanoHPLC system (Thermo Scientific, USA) at the Babraham Mass Spectrometry Core Facility. Briefly, peptides were loaded onto a trap column at a flow rate of 2 µL/min for 10 minutes and separated on a reversed-phase nanoLC column (150 × 0.075mm; Reprosil-Pur C18AQ, Dr Maisch) using a 2-hour gradient of 2 to 35% ACN, 0.1% FA with a flow rate of ~300 nL/min. Mass spectra were acquired with the following parameters for MS1: resolution 120,000, scan range 350-1,800 m/z, automatic gain control (AGC) target 4×10^5, and maximum injection time 50 ms. MS2 spectra were acquired in DDA mode using: Top speed of 3 seconds, HCD fragmentation, resolution 30,000, AGC 5×10^4, maximum injection time 100 ms, isolation window 1.6 m/z, and normalized collision energy of 30.

3.3.7 Data analysis

Data analysis was performed on both MaxQuant [218] and Proteome Discoverer. MaxQuant was used to analyse the original fractionated proteome data for protein quality control checks

using PTXQC pipeline [217]. Proteome Discoverer was used on the comparison of fractionation vs whole tissue analysis.

MaxQuant: MaxQuant was performed with Andromeda peptide search engine (default settings). Spectra were analysed against human proteins in the Swiss-Prot Reference Proteome database. Precursor and fragment ion tolerance was set to 4.5 and 20 ppm and a maximum of two missed cleavages were considered. Methionine oxidation and N-termini acetylation were variable modifications, whilst cysteine carbamidomethylation was set as a fixed modification. Matching between runs was enabled – 0.7 minutes matching time and 20 minutes alignment time window. Only proteins with at least one unique or razor peptide were included for further analysis.

Proteome Discoverer: Data analysis was performed on Proteome Discoverer by a post-doctoral researcher at the Babraham institute (information not available). Protein abundance values were determined by label free quantification in DDA mode. Protein-level data was log2 transformed and normalised by scaling against the sample average. Any missing values were imputed using probabilistic minimum imputation on Excel [219]. Statistical analysis was performed on RStudio using the Limma R package with empirical Bayes, including multiple hypothesis testing correction using the Benjamini and Hochberg method.

3.4 Results

3.4.1 Assessing lysis methods for muscle fractionation

To decide which lysis method was most effective for muscle fractionation, we wanted to determine both the solubilisation and separations of proteins. If proteins have not been

solubilised, they will be removed during centrifugation stages required for high fractionation purity and will not be analysed on the LC-MS. Incomplete solubilisation is often seen when lysing skeletal muscle tissue because myofibrillar and extracellular matrix proteins are large in size and highly connected [193]. To compare how well each lysis method solubilises the proteins, we analysed the protein yield using a DC assay. As we used the same amount of muscle tissue and lysis buffer, we can infer that any change in concentration reflects a change in protein solubility. We found that the concentration of the insoluble fraction was 6.6 µg/µL for the MIST lysis buffer and 6.4 µg/µL for the detergent lysis buffer. Therefore, from this measurement it appears both lysis buffers were equally effective at solubilising proteins.

To visualise proteins which had been solubilised from either lysis buffer, we performed SDS-PAGE gel electrophoresis followed by Coomassie protein staining. The insoluble fractions from both lysis methods contained a greater abundance of high weighted proteins which likely reflect MHC **(Figure 3.2a)**. We then performed western blotting to confirm the presence of specific proteins found in the sarcoplasm (soluble) or myofibrillar (insoluble) compartment. As anticipated, MHC and actin were more abundant in the insoluble fractions, whereas Acetyl-CoA carboxylase (ACC) and Glyceraldehyde 3-phosphate dehydrogenase (GAPDH) were more abundant in the soluble fractions **(Figure 3.2b)**. Interestingly, the intermediate filament protein Desmin was only detected in the insoluble fraction obtained by the high detergent lysis method **(Figure 3.2b)**. It was noticeable from both the Coomassie stain and the western blots that the MIST method resulted in a smearing effect that altered how the proteins moved through the gel. This could indicate some alteration to the protein structure caused by a chemical in the MIST lysis buffer. One possibility is the addition of spermidine which as a polyamine, increases the positive charged state of proteins which could affect their separation during SDS-PAGE electrophoresis. Alternatively, because a low-speed centrifugation is used to clear the

lysate [188], these samples may still contain insoluble proteins which might cause proteins to migrate slower down the gel.

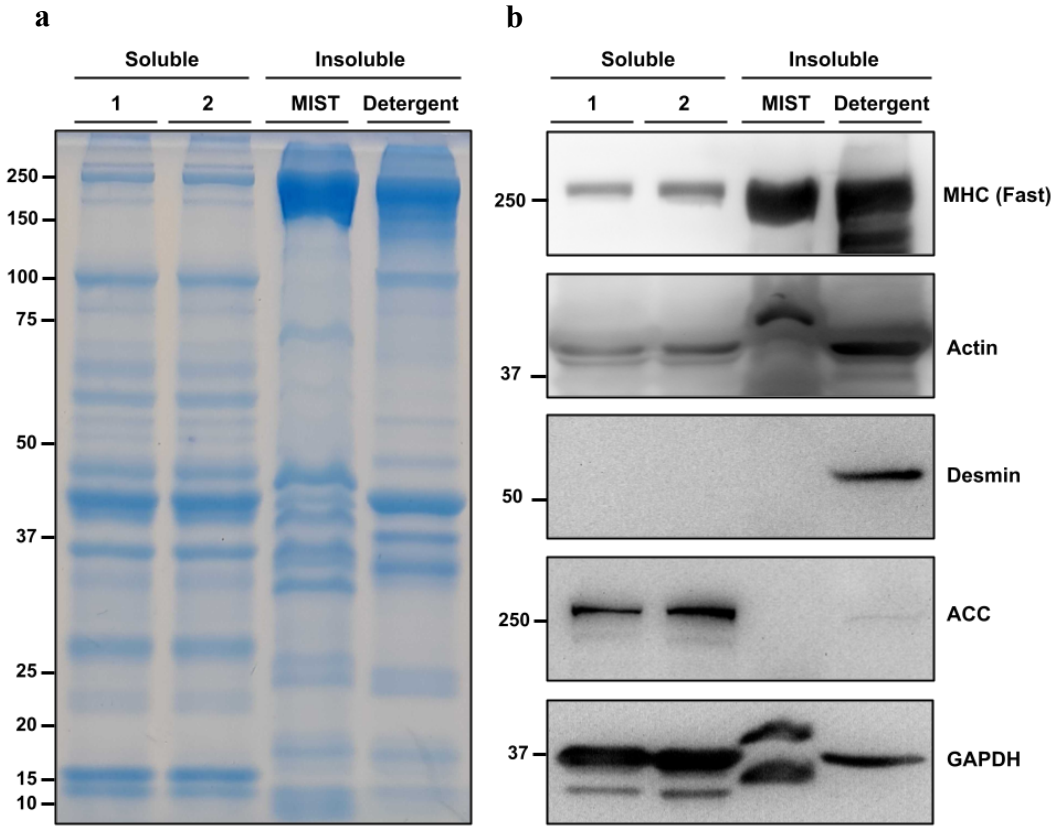

Figure 3. 2. Comparison of skeletal muscle fractionation. Spare human muscle tissues were fractionated using centrifugation. Muscles were first homogenised in 0.5% detergent lysis buffer, centrifuged to separate the proteins into pellet (insoluble) and supernatant (soluble) fractions. The pellet was then homogenised in either MIST or 5% detergent buffer. Samples were subjected to a) Coomassie protein staining and b) Western blotting to confirm separation of soluble and insoluble proteins.

3.4.2 Assessing the recovery of proteins during sample clean-up

Components of the lysis buffer can influence the efficiency of downstream protein clean up methods. Therefore, before deciding on our lysis buffer of choice we wanted to determine compatibility with SP4 by assessing protein recovery. Coomassie staining was used to visualise the protein content in the pellet and supernatant following ACN-induced protein aggregation,

relative to the crude lysate (pre-SP4). We decided to use 80% ACN as our solvent as this was previously shown to be optimal for driving protein aggregation [118]. We found that the supernatant in the soluble fractions and detergent-based insoluble fraction contained minimal protein, however the supernatant from the MIST-based insoluble fraction contained similar amounts of protein as the pellet **(Figure 3.3)**. This tells us that detergent lysis buffer results in greater protein recovery following SP4. Therefore, moving forward we decided to use 5% detergent buffer to lyse the insoluble fraction.

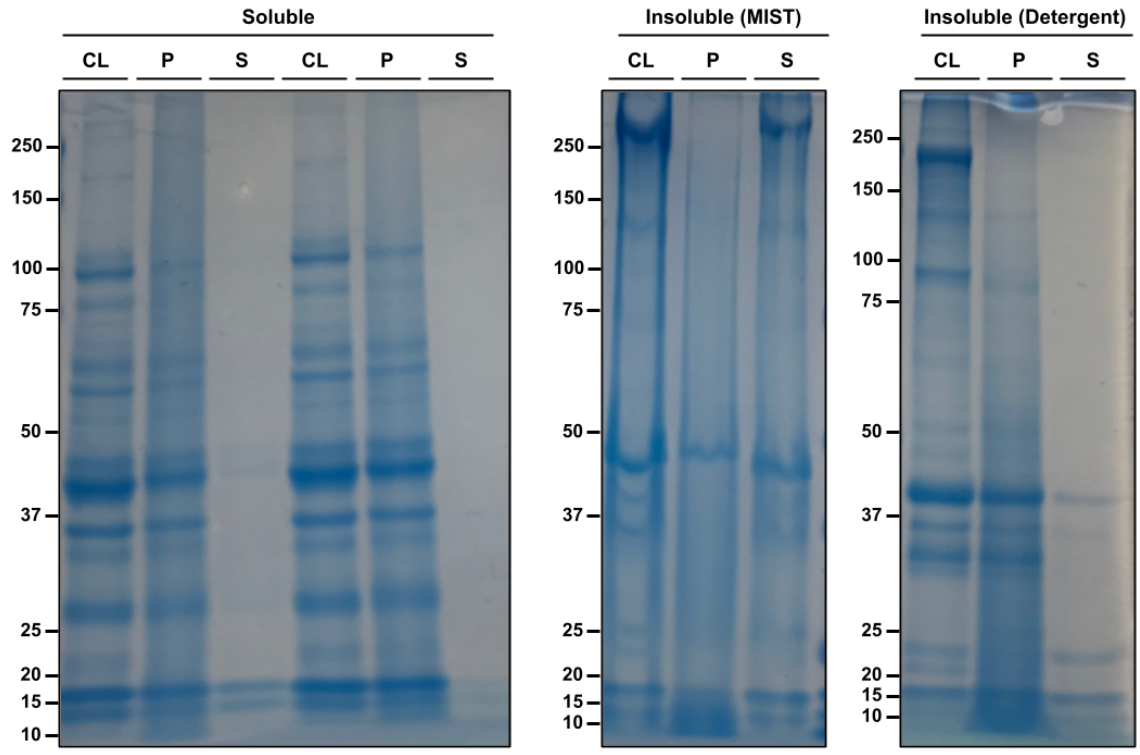

Figure 3. 3. Comparison of protein recovery during precipitation. SP4 was performed on lysate obtained from the soluble and insoluble fractions. Coomassie protein staining was used to visualise protein present at each stage: CL = Crude lysate, P = Pellet, S = Supernatant.

3.4.3 Assessing workflow compatibility for bottom-up proteomics

Following SP4 protein clean-up we digested our proteins with trypsin and ran the reconstituted peptides through LC-MS. The raw files were then analysed using MaxQuant software to

convert spectral data into protein-level data. To check the quality of the data, the output from MaxQuant was submitted to the PTXQC R-based pipeline. Based off the scoring system, most quality control measures came out with the best score, with the failed measures relating to peptide and protein count which at this stage we were not attempting to optimise **(Figure 3.4a)**. We were interested in keeping the number of contaminants very low, which was the case for both fractions – contributing to less than 2% of the total ion intensity **(Figure 3.4b)**. The report also showed that the percentage of missed cleavages were below the recommended threshold limit **(Figure 3.4c)**. Missed cleavages arise from incomplete digestion, which can cause issues with protein identification. Therefore, this report provides reassurance that trypsin is effectively digesting our proteins for efficient bottom-up proteomics. Overall, we were happy with the quality of the data and confident that we had successfully developed a reliable workflow.

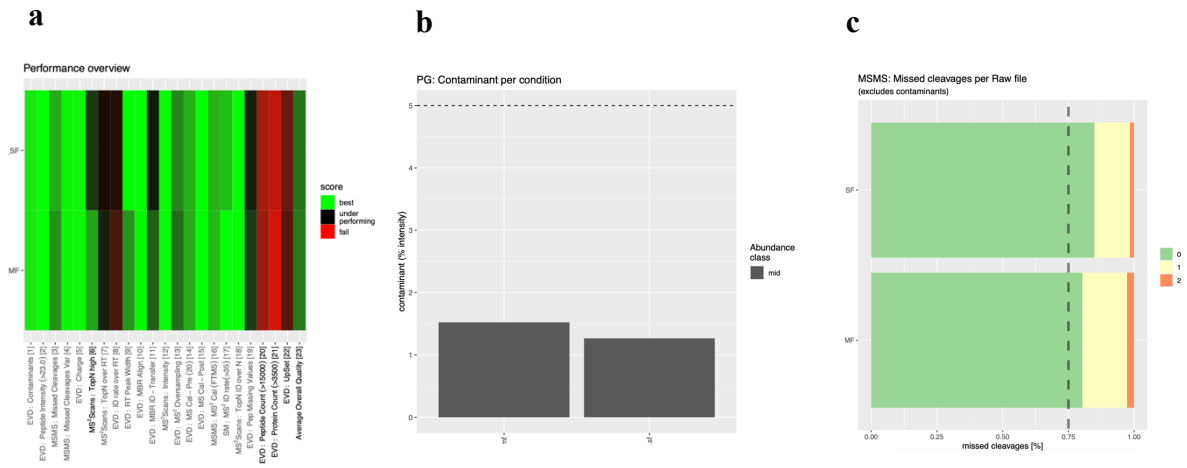

Figure 3. 4. Proteomics quality control measures. All figures generated using the PTXQC pipeline on RStudio. a) Heatmap displaying the performance overview using the colour-graded scoring system. b) Bar plot displaying the percentage of proteins classed as a contaminant. c) Bar plot to show the number of missed cleavages displayed as a percentage. SF = soluble fraction and MF = insoluble fraction.

3.4.4 Assessing workflow performance for improving proteome coverage

Our next task was to determine whether our fractionation workflow improved the detection of the muscle proteome when compared to a whole tissue lysis approach. Samples were initially subjected to Coomassie protein stain and western blot analysis to confirm fractionation and compare the results to whole tissue lysis. Coomassie protein staining revealed a very similar distribution of proteins between both insoluble and whole tissue samples **(Figure 3.5a)**. Notable similarities came from thick bands at the predicted weight of actin (~43 kDa) and MHC (~220 kDa) which was confirmed by western blotting (**Figure 3.5a and Figure 3.5b**). This is not surprising given that these myofibrillar proteins enriched in the insoluble fraction make up a large proportion of the muscle proteome [20]. Surprisingly, we were only able to detect ACC in the soluble fraction and not whole tissue, whereas GAPDH detectable in both (**Figure 3.5b**). We also wanted to confirm that we had successfully solubilised different organelles and determine in which fraction this had occurred. We blotted for citrate synthase and histone H3 to confirm the solubilisation of mitochondria and nucleus respectively. Citrate synthase was present in both fractions, which is not surprising seen as mitochondria are present as both subsarcolemmal and intermyofibrillar organelles (**Figure 3.5b**). Nevertheless, citrate synthase was more abundant in the soluble fraction which suggests that most mitochondria were solubilised by the initial low detergent lysis buffer. On the other hand, histone H3 was not detected in the soluble fraction and enriched in the insoluble fraction (**Figure 3.5b**). This suggests that a high amount of detergent was required to solubilise the nucleus.

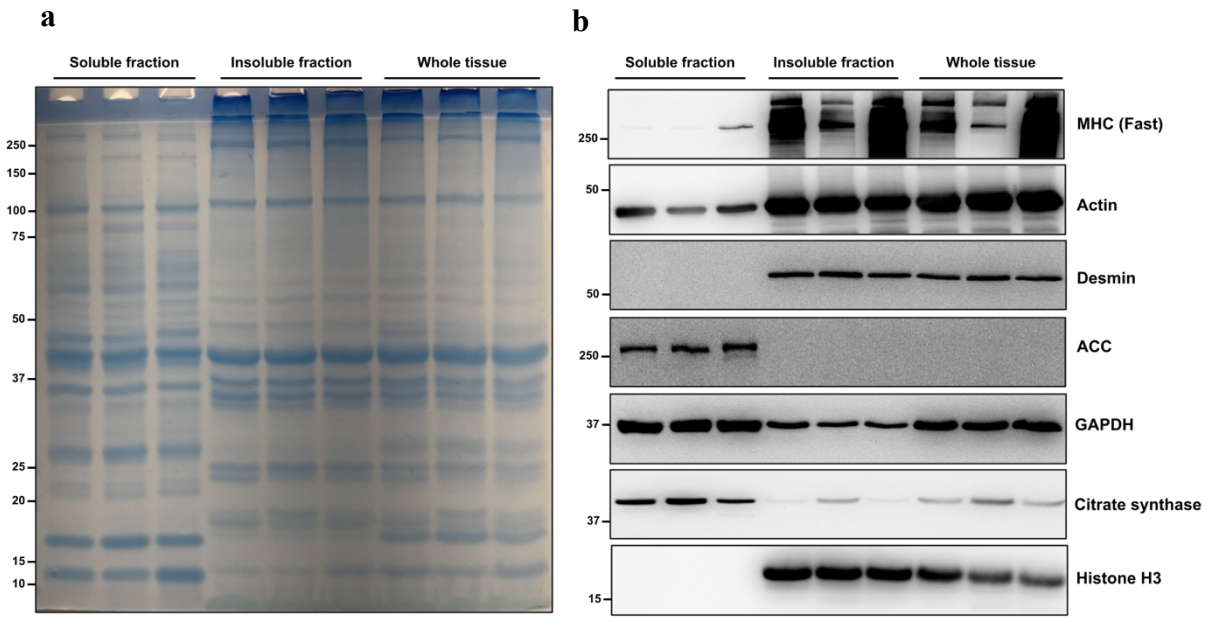

Figure 3. 5. Comparison of skeletal muscle fractionation vs whole tissue lysis. Spare human muscle tissues were powdered and split 50:50 for either fractionation or whole tissue lysis. Samples were then subjected to a) Coomassie protein staining and b) Western blotting to visualise proteins.

Contaminants from the lysis buffer were then removed using SP4, proteins digested and peptides analysed by LC-MS. Before investigating the coverage of the proteome, we first wanted to perform some quality control checks. A key priority of our workflow was the reproducibility, therefore we wanted to ensure the variation between replicates would be low. To check this, we performed principial component analysis (PCA) which transforms abundance values from the thousands of proteins we identified and produces a 2-dimensional visual summary of the variation. The PCA plot shows 3 tight clusters which represent the three different samples that have been analysed (soluble fraction, insoluble fraction and whole muscle) (**Figure 3.6a**). This informs us that there was little variation in protein abundance values between all replicates, indicating reproducible workflows. The clusters from soluble and insoluble samples were spread out across Principal component 1 (PC1) (**Figure 3.6a**). PC1 accounted for 72% of the total variance which means that a large proportion of the variation in

the data was due to the differences between these two fractions. This is not surprising given that these two fractions are essentially two separate parts of the muscle proteome.

To visualise the distribution of proteins that contribute towards the clusters seen with PCA, we used heatmaps. Heatmaps provide a great visual representation of protein distribution, helping to identify trends, correlations, and outliers when dealing with thousands of hits across multiple comparisons. The heatmap shows two large clusters of proteins that were inversely correlated between the soluble and insoluble fractions (**Figure 3.6b**). The heatmap of the whole tissue samples follow a similar pattern to the insoluble fraction, although a cluster of proteins were less abundant in the insoluble fraction. Together, this demonstrates that individual protein abundance values differ significantly between the two fractions, while the insoluble fraction and the whole tissue samples have similar protein profiles.

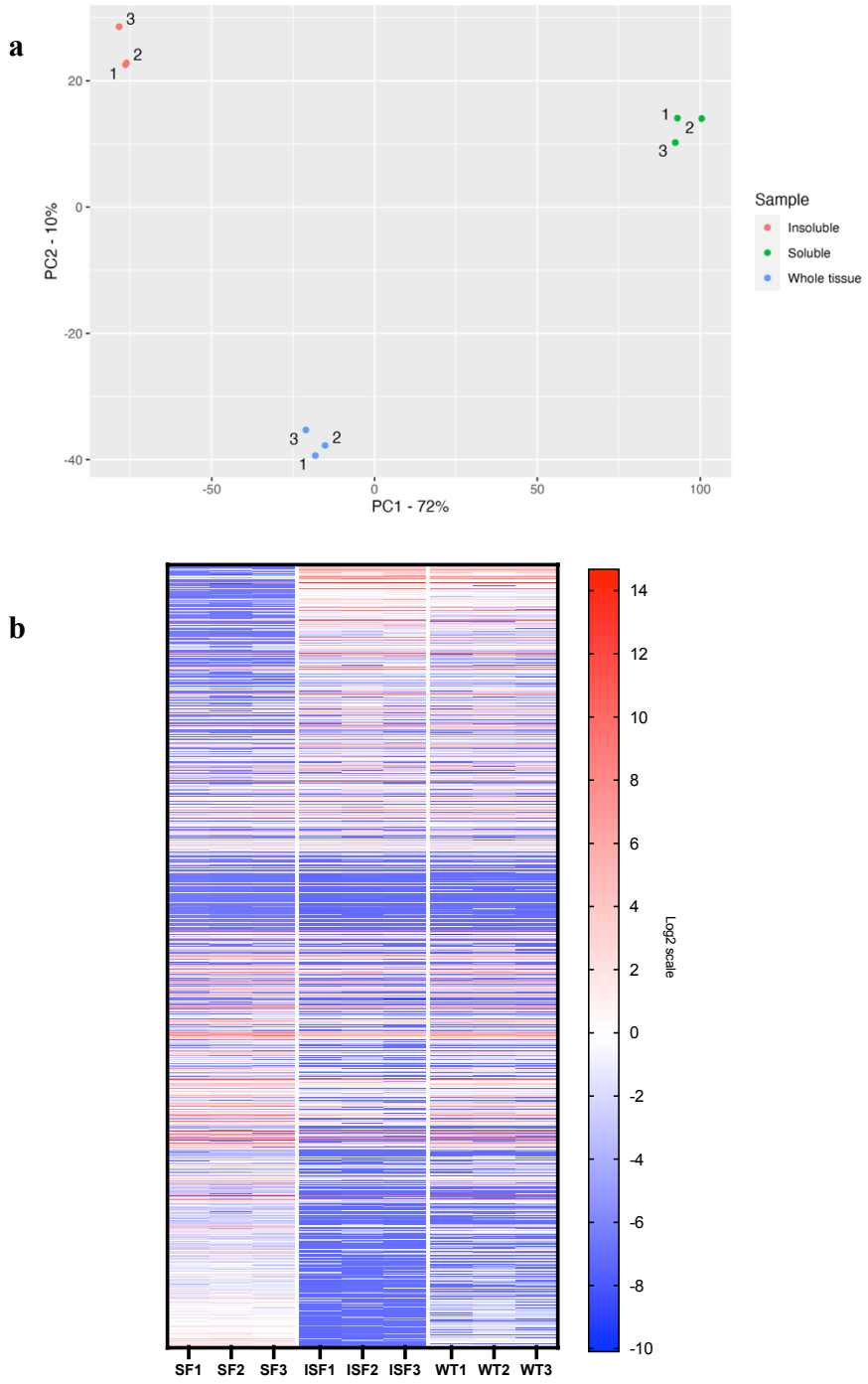

Figure 3. 6. Protein abundance variation between samples. a) PCA plot displaying the variation in protein abundance values both within and between samples. b) Heatmap showing the log2FC values for each protein across all samples quantified by label free quantification. SF = Soluble fraction, ISF = Insoluble fraction, WT = Whole tissue.

Having established a large variation in protein abundance values between the two muscle fractions, we aimed to determine the specific proteins contributing to this difference. To do so, we performed statistical analysis to identify proteins had been significantly enriched into either fraction. Statistical analysis was performed using the Limma R package with empirical Bayes method. Limma was chosen because it uses linear modelling that is designed to handle large numbers of genes or proteins effectively [220]. Empirical bayes method was employed because it enhances statistical power by sharing information across features which is important when dealing with small samples sizes [221]. To correct for multiple testing and reduce the false discovery rate, we used the Benjamini and Hochberg method. We opted for this method as it is less stringent that other over other multiple correction tests that can indirectly introduce type 2 errors (false negative). We decided that any protein that displayed greater than 2-fold change in abundance between fractions (Log2FC > 1 or Log2FC < -1) with an adjusted *P* value < 0.05 would be deemed as significantly enriched. To calculate the protein fold change between fractions, we had to ensure that there were no missing values in our data. Missing values are common in label-free proteomics and even more prevalent in our dataset as we have fraction-specific proteins. To overcome this issue, we employed data imputation on the missing values using the probabilistic minimum imputation method [219]. Whilst this introduces artificial data, these values are close to the limit of detection and therefore fold change values should not be largely affected by this imputation method. Therefore, for the purpose of identifying significantly enriched proteins we deemed this a suitable method.

Using these criteria, we found that of the 2163 proteins detected, 507 proteins were enriched in the insoluble fraction and 943 proteins were enriched in the soluble fraction (**Figure 3.7a**). To understand the type of proteins that were enriched into either fraction, we performed GSEA. We opted to rank proteins based on fold change values using the identified proteins as

background to determine biological terms with the greatest magnitude of change. The insoluble fraction was enriched with proteins involved in translation and actin binding, whereas the soluble fraction was enriched with proteins involved in cell redox homeostasis and organic acid binding (**Figure 3.7b**). Insoluble enriched proteins were localised to the ribosome and contractile fibres, whereas soluble enriched proteins were located in transport vesicles and peptidase complex (**Figure 3.7b**). This reinforces the point that our fractionation procedure was able to separate contractile proteins in the myofiber from regulatory proteins in the sarcoplasm.

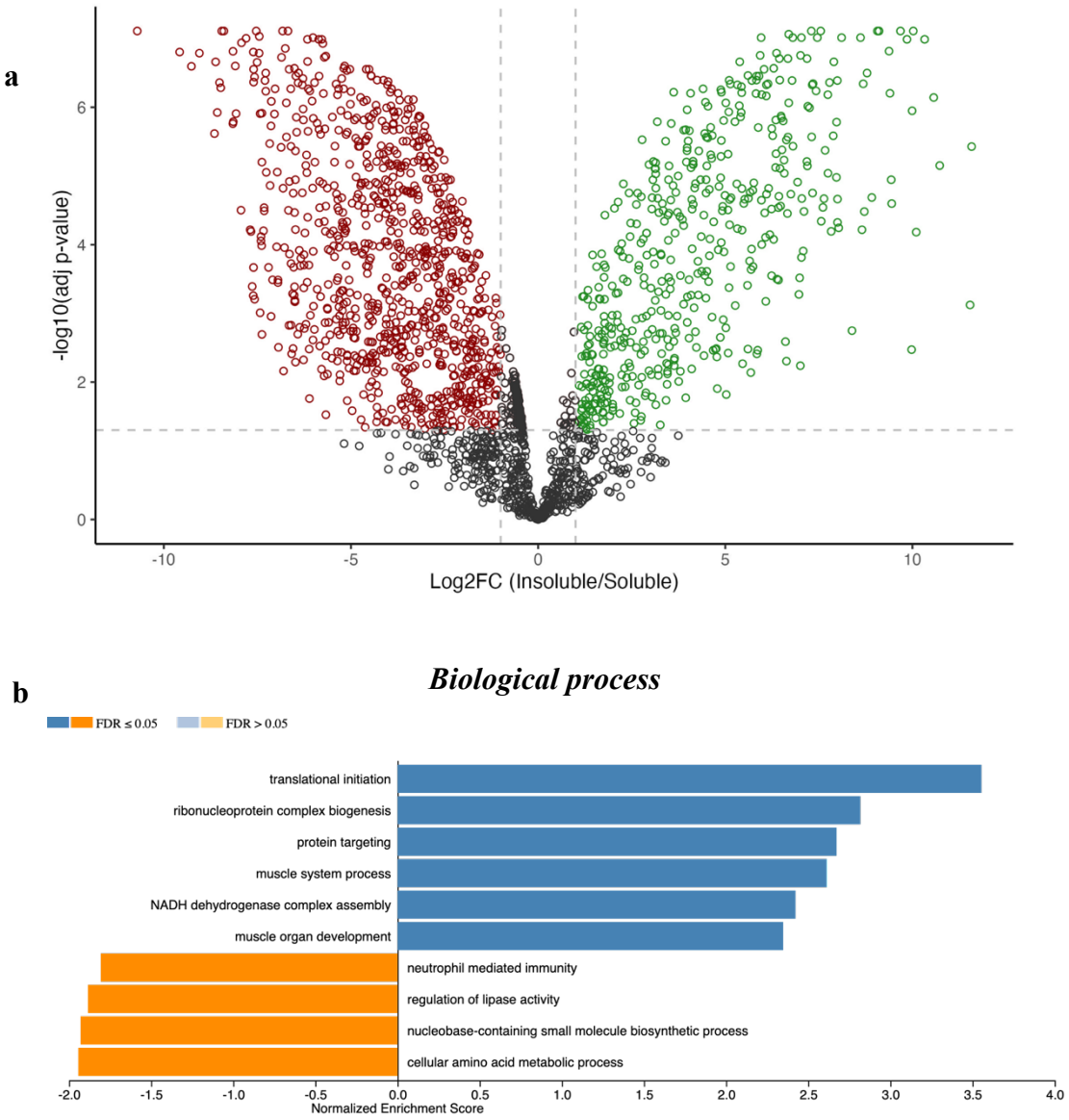

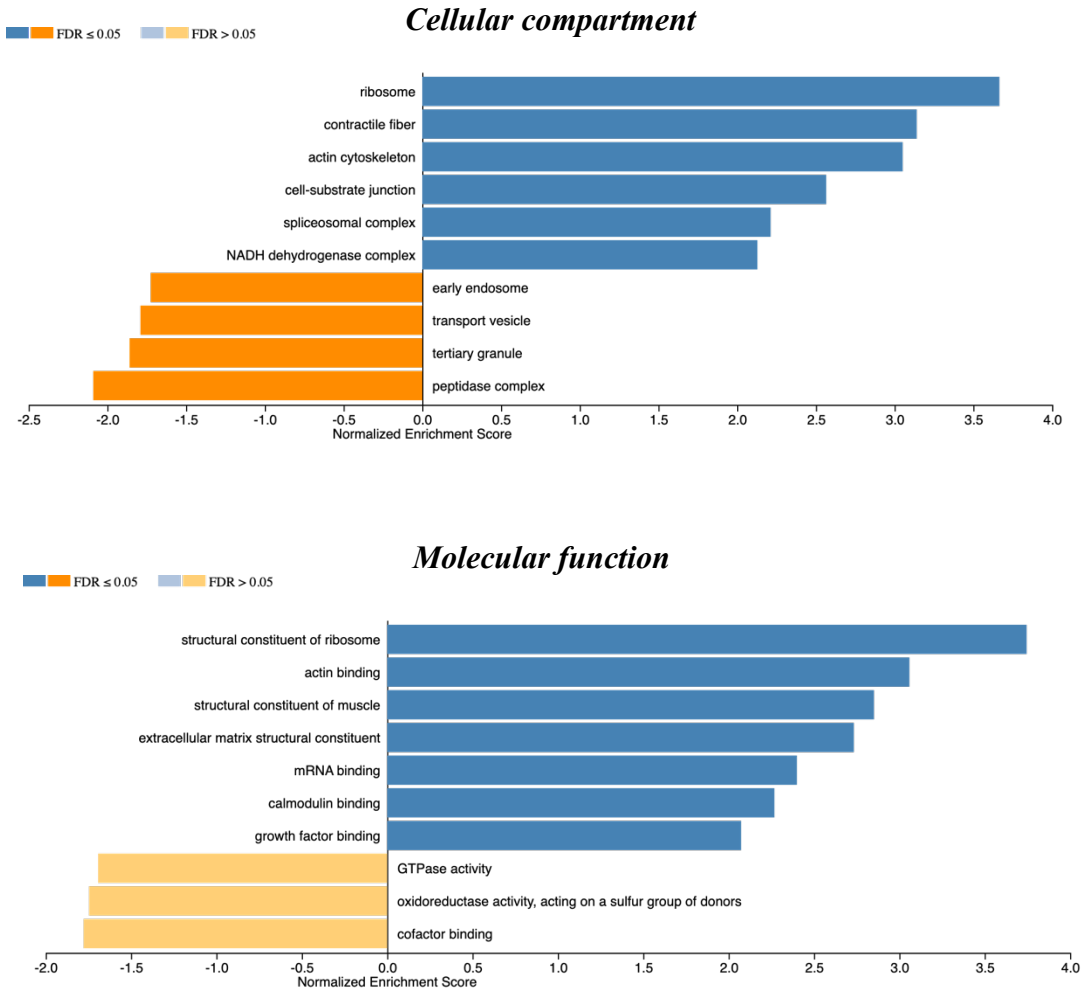

Figure 3. 7. Fraction enriched proteins. a) Volcano plot showing the fold change and statistical significance of protein abundance values between fractions. Significantly enriched proteins are highlighted: Red = soluble enriched (Log2FC < -1 + adjusted *P* value < 0.05), Green = insoluble enriched (Log2FC > 1 + adjusted *P* value < 0.05). b) Gene set enrichment analysis was performed on all quantified proteins which were ranked based on their fold change value between fractions. Gene ontology analysis of enriched terms relating to a biological process, molecular function or cellular compartment was determined using WEB-based Gene SeT AnaLysis Toolkit (WebGestalt). Blue = enriched in the insoluble fraction, Orange = enriched in the soluble fraction.

After confirming successful separation of proteins in our fractionated samples, we wanted to determine whether fractionation improved the coverage of proteins detected by the LC-MS. To answer this, we used the following criteria: Proteins that appeared as “Not Found” in all three replicates were removed and the remaining proteins were counted for that sample. As we were dealing with presence or absence, we did not use the data imputation method. We then plotted

a Venn diagram for each protein retained in a sample. With fractionation (soluble + insoluble), we were able to detect 2163 proteins whereas with whole tissue lysis we detected 1890 proteins (273 fewer) (**Figure 3.8a**). The soluble fraction contained the highest number of proteins not detected in the whole tissue analysis. To identify which proteins were only detected in the soluble fraction, we submitted these proteins to DAVID functional analysis with the total detected proteome as the background. Gene ontology analysis revealed an enrichment of membrane proteins, notably 29% belonged to the plasma membrane (**Figure 3.8b**). Therefore, fractionation was particularly beneficial for detecting plasma membrane proteins.

a

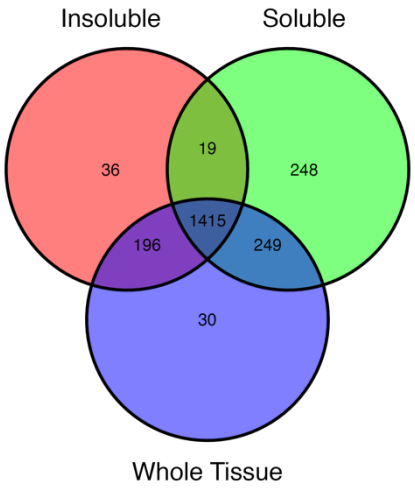

b

Cellular compartment	Count	%
Plasma membrane	71	28.51405622
Intracellular membrane-bounded organelle	20	8.032128514
Golgi membrane	14	5.62248996
Lysosomal membrane	11	4.417670683
Ruffle membrane	7	2.81124498
Early endosome membrane	6	2.409638554
High-density lipoprotein particle	5	2.008032129
Chromosome, centromeric region	4	1.606425703
Tertiary granule membrane	4	1.606425703
Condensed chromosome, centromeric region	3	1.204819277
Integrin complex	3	1.204819277

Figure 3. 8. Coverage of the proteome. a) Venn diagram showing the overlap of proteins detected in the soluble, insoluble and whole tissue samples. b) Table displaying enriched cellular compartments from DAVID Gene ontology analysis of proteins only detected in the soluble fraction.

3.5 Conclusions

Overall, this chapter has shown that we were able to develop a workflow that enabled the separation of soluble and insoluble proteins from skeletal muscle tissue for enhanced detection of the muscle proteome. Importantly, we appear to have successfully solubilised myofibrillar proteins and ensured the removal of harmful contaminants with minimal loss to protein content. Given the challenging nature of muscle proteins, this is an important step to ensure we can perform reliable proteomics experiments in the future. Given that we identified a greater number of proteins when performing fractionation, we deemed it appropriate to continue with this method. However, another study which compared fractionation vs whole tissue analysis of the proteome identified 1490 proteins that were only quantified in the soluble fraction [192]. They also found that many of these proteins were found in the nucleus rather than in the plasma membrane. The reason for this discrepancy could be due to the buffer used for the insoluble fraction and whole tissue lysis, in which they opted for urea over detergent which will lead to different composition of extracted proteins. It would be interesting to directly study the skeletal muscle proteome identified when comparing urea to detergent-based lysis of the insoluble fraction to determine which method is optimal for protein extraction.

4. Developing a method to study the ubiquitylome of skeletal muscle

4.1 Abstract

Proteomics is capable of identifying and quantifying PTMs such as ubiquitylation. LC-MS is typically used as it can detect the mass shift brought about by ubiquitin modifications on peptides. Importantly, the high sensitivity of LC-MS means the exact site of ubiquitylation can be determined. Having developed a fractionation workflow compatible with LC-MS that allowed for increased depth of the muscle proteome, our next task was to modify the workflow to allow for the detection of ubiquitylated proteins (ubiquitylome). The aim of this chapter was to critically evaluate the effectiveness of different stages in the ubiquitylomics workflow. Our workflow employed immunoprecipitation to enrich for ubiquitylated (diGly-modified) peptides. In doing so, our fractionated ubiquitylomics workflow identified 5172 diGly-modified peptides, 448 more than when performing a whole tissue ubiquitylome analysis. Interestingly, on average 48% of peptides identified contained the diGly-modification, but in the soluble fraction this dropped to 39%. To improve enrichment efficiency, we modified the immunoprecipitation protocol to reduce non-specific binding by including less antibody and increasing the stringency of the washes. Furthermore, we found trypsin was still active after overnight digestion which could be interfering with antibody-efficiency during immunoprecipitation. By heating the peptides after digestion for 30 minutes, we successfully inhibited trypsin activity. With these modifications, we have addressed the shortcomings of our initial ubiquitylomics workflow in an attempt to improve the detection of ubiquitylated peptides.

4.2 Background

Ubiquitylomics is the study of protein ubiquitylation on a proteome-wide scale. Ubiquitylomics employs LC-MS to identify and quantify ubiquitin modifications on proteins. This approach has proven invaluable for uncovering novel ubiquitylated substrates, mapping ubiquitylation sites, and revealing changes in ubiquitylation patterns under various conditions [198]. As a result, ubiquitylomics provides researchers insight into the ubiquitin landscape within cells or tissues, serving as a rich resource for further investigation. Utilising this information, targeted mechanistic studies can be designed to determine the biological consequence of ubiquitylated proteins, potentially leading to biomarker identification and therapeutic targets. The full potential of ubiquitylomics requires optimised protocols tailored to specific research objectives. This thesis looks to quantify age-related changes in ubiquitylated substrates within skeletal muscle. Therefore, the aim of this chapter is to develop a robust method that would enable quantitative analysis of the skeletal muscle ubiqutylome.

As mentioned in Chapter 2, the low stoichiometry of protein ubiquitylation relative to total protein means a ubiquitin enrichment procedure is commonly performed prior to LC-MS analysis to provide sufficient detection. We opted to use K-ε-GG immunoprecipitation which allows for the selective enrichment of peptides that contain a double glycine remnant (diGly) on a lysine residue, which occurs after ubiquitylated proteins have been digested by trypsin (**Figure 4.1**). There is a recommended workflow offered by Cell Signaling Technology, however as this protocol is typically used in cell lines we had to evaluate its effectiveness with skeletal muscle. We conducted K-ε-GG immunoprecipitation on both the fractionated and whole tissue lysate, to determine if separating soluble and insoluble proteins improved the coverage of the ubiquitylome. To do so, we made use of the same peptide batch used for

proteomics analysis in Chapter 3. An in-depth examination of the diGly-enriched dataset was carried out to confirm good separation of ubiquitylated proteins, before quantifying differences in the ubiquitylome coverage with the whole tissue approach.

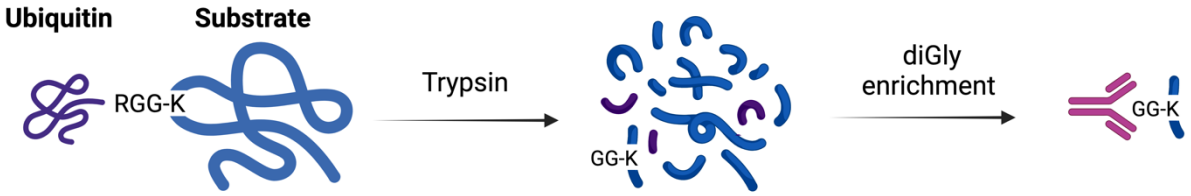

Figure 4. 1. diGly-modified peptide enrichment. Schematic showing the process of site-specific ubiquitin enrichment from peptides generated by trypsin. Image created using biorender.com.

4.3 Methods

4.3.1 Collection of skeletal muscle

Muscle samples were provided by Dr Ryan Marshall and Prof Leigh Breen. Muscle biopsies were taken from quadricep (Vastus Lateralis) of three human participants (24-27 years, BMI: 22-26) and frozen in liquid nitrogen before being stored at -70 °C until lysis. Ethical approval was obtained through the East Midlands - Derby Research Ethics Committee (18/EM/0004), conformed to the requirements of Research Governance at the University of Birmingham and was conducted in accordance with the Declaration of Helsinki.

4.3.2 Fractionation of skeletal muscle

Separation of soluble and insoluble fractions was carried out in Chapter 3 (section 3.4.4). Briefly, 50 mg of frozen muscle tissue was powdered using a mallet and crusher. A 10-fold volume of ice-cold lysis buffer 1 (25 mM Tris, pH 7.2, 0.5% Triton X-100, 100 mM 2-chloroacetamide, 1 mM sodium orthovanadate, 1x cOmplete Mini EDTA-free protease

inhibitor (11836170001, Roche, Switzerland)) was added to each sample. The powdered muscle was homogenised using a TissueLyser II (Qiagen, Netherlands) with 5 mm stainless steel beads during 2 x 2-minute cycles at 30 Hz. To collect the soluble fraction, the lysate was centrifuged at 1500 g (4 °C) for 10 minutes and the supernatant was collected. To obtain the insoluble fraction, the pellet was first washed in 10 volumes lysis buffer 1 and then resuspended in 15 volumes of ice-cold 5% detergent lysis buffer (50 mM HEPES pH 8.0, 1% SDS, 1% Triton X-100, 1% NP-40, 1% Tween 20, 1% sodium deoxycholate, 50 mM NaCl, 1 mM DTT, 5 mM EDTA, 1% (w/v) glycerol, 100 mM 2-chloroacetamide, 1 mM sodium orthovanadate, 1x cOmplete Mini EDTA-free protease inhibitor (11836170001, Roche, Switzerland)) and placed in the TissueLyser II (Qiagen, Netherlands) with 5 mm stainless steel beads for 2 x 2-minute cycles at 30 Hz. The lysate was incubated at 95 °C for 5 minutes, cooled for 10 minutes at room temperature. Lysates from both supernatant and pellet were sonicated at 4 °C for 12 x 5-second bursts with 5 second intervals. Finally, both lysates were cleared at 16000 g for 10 minutes and the supernatant from both soluble and insoluble fraction was collected. For whole tissue lysis, the same protocol was followed without prior fractionation of the soluble fraction.

4.3.3 Protein concentration assay

Protein lysate concentrations were determined by a DC assay (5000111, Bio-Rad, USA) using an FLUOstar Omega plate reader (BMG Labtech, UK) according to manufacturer's instructions. Concentrations were read at an absorbance of 750 nm.

4.3.4 Coomassie staining

Samples were prepared for SDS-PAGE gel electrophoresis by adding 4x LDS sample buffer (NP0008, Thermo Scientific, USA) containing 5% β-mercaptoethanol to final concentration 1x

and 1.25% respectively and left overnight to denature. Sample were loaded into 10% Bis-Tris gels and separated by gel electrophoresis in 1x MOPS buffer for approximately 90 minutes at 140V. Gels were incubated in PageBlue protein staining solution (24620, Thermo Scientific, USA) for 1 hour before rinsing in double distilled water as per manufacturer's instructions.

4.3.5 LC-MS sample preparation

Sample preparation was performed using a modified version of the SP4 protocol [118]. Lysates were prepared at 4 mg/mL and 2 mg of each sample was aliquoted into 1.5 mL LoBind tubes. Samples were reduced by 5 mM DTT for 45 minutes at 25 °C and then alkylated by 10 mM 2-chloroacetamide for 45 minutes at 25 °C in the dark. Proteins were precipitated by adding four volumes of 100% ACN followed by gentle mixing at 500 rpm for 5 seconds and left for 5 minutes at room temperature. Precipitated proteins were pelleted by centrifugation for 5 minutes at 16000 g at room temperature. To maximise pellet density, the tube was first orientated with the hinge inwards for 2.5 minutes and then turned 180° for the final 2.5 minutes. The supernatant was carefully discarded. The pellet was washed three times in 1.5x total precipitation volume of 80% ethanol, each time samples were centrifuged at 16000 g at room temperature. After the final wash, the protein pellet was resuspended in 1x total precipitation volume of 50 mM ammonium bicarbonate containing trypsin (V5280, Promega, USA) at 1:100 enzyme:protein ratio. The pellet was sonicated and vortexed periodically to disrupt the pellet. Proteins were left to digest for 18 hours at 37 °C shaking at 1000 rpm. Samples were centrifuged at 16000 g for 2 minutes and the peptide containing supernatant was collected into a fresh Eppendorf tube. Peptides were dried using a SpeedVac Concentrator plus (12884952, Eppendorf, Germany) at room temperature.

4.3.6 diGly immunoprecipitation

Enrichment of ubiquitylated peptides was performed using PTMscan HS Ubiquitin/SUMO Remnant Motif (K-ε-GG) magnetic immunoaffinity beads (59322, Cell Signaling Technology, USA). First, peptides were resuspended in 1.5 mL of HS IAP Bind buffer and sonicated in a water bath for 5 minutes to ensure complete solubilisation. The peptide solution was centrifuged at 16000 g for 5 minutes to remove any insoluble material and then transferred to a 20 µL aliquot of K-ε-GG remnant magnetic immunoaffinity beads. The bead-peptide mixture was incubated end-over-end on a rotator for 2 hours at 4 °C. The mixture was then spun at 2000 g for 5 seconds to bring down the beads and then placed on a magnetic stand for 10 seconds. The peptide solution containing unbound peptides were removed. The beads were washed four times in 1 mL of HS IAP Wash buffer and twice in LC-MS grade water (85189, Thermo Scientific, USA) by inverting 5 times to mix, centrifuged at 2000 g for 5 seconds before being placed on a magnetic stand for 10 seconds to remove all solution. During the final wash, the beads were transferred to a fresh LoBind tube. 50 µL of 0.15% TFA was added to the beads and mixed at 500 rpm on a thermomixer (Eppendorf, Germany) at room temperature for 10 minutes. The tube was then centrifuged at 2000 g for 5 seconds and placed on a magnetic rack. The eluted peptide solution was transferred to a glass vial. The elution process was repeated and both eluates were combined in the same glass vial. Peptides were dried using a SpeedVac Concentrator plus (12884952, Eppendorf, Germany) at room temperature.

4.3.7 LC-MS

Peptides were resuspended in 10 µL 2% ACN 0.1% TFA and 4 µL were analysed and acquired by an Orbitrap Eclipse (Thermo Scientific, USA) coupled with a Dionex UltiMateTM 3000 nanoHPLC system (Thermo Scientific, USA) at the Babraham Mass Spectrometry Core

Facility. Briefly, peptides were loaded onto a trap column at a flow rate of 2 µL/min for 10 minutes and separated on a reversed-phase nanoLC column (150 × 0.075mm; Reprosil-Pur C18AQ, Dr Maisch) using a 3-hour gradient of 2 to 35% ACN, 0.1% FA with a flow rate of ~300 nL/min. Mass spectra were acquired with the following parameters for MS1: resolution 120,000, scan range 350-1,800 m/z, AGC target 4×10^5, and maximum injection time 50 ms. MS2 spectra were acquired in DDA mode using: Top speed of 3 seconds, HCD fragmentation, resolution 30,000, AGC 5×10^4, maximum injection time 100 ms, isolation window 1.6 m/z, and normalized collision energy of 30.

4.3.8 Data analysis

Data analysis was performed on Proteome Discoverer by a post-doctoral researcher at the Babraham institute (information not available). Protein-level data was then log2 transformed and normalised by scaling against the sample average. Any missing values missing values were imputed using probabilistic minimum imputation on Excel [219]. Statistical analysis was performed using the Limma R package with empirical Bayes, with multiple hypothesis testing corrected using the Benjamini and Hochberg method.

4.4 Results

4.4.1 Enriching the ubiquitylome

Before analysing the coverage of the ubiquitylome, it was important to determine the quality of the data. To determine how successful the enrichment of diGly-modified peptides had been, we quantified the number of diGly-modified peptides as a percentage of the total peptide coverage. This calculation provides an enrichment efficiency that we can compare to other studies to determine a relative success rate of diGly enrichment. Enrichment efficiency across

all samples was 48% (5423 diGly-modified peptides out of 11295 total peptides) (**Figure 4.2**). To determine the success of this enrichment efficiency score, we wanted to compare the result to other studies using K-ε-GG immunoprecipitation in skeletal muscle. There are only a handful of studies that used this method in skeletal muscle and even fewer who report their enrichment efficiency score. One study used K-ε-GG immunoprecipitation in multiple murine tissues, including skeletal muscle and found their average enrichment efficiency rate across all tissues was 35% [187]. They also found the least number of ubiquitylated sites in skeletal muscle when compared to 4 other tissues, which could be due to worse enrichment efficiency. Therefore, whilst we were unable to provide a majority pool of ubiquitylated peptides in our sample, our enrichment efficiency exceeded what one group had been able to achieve in skeletal muscle.

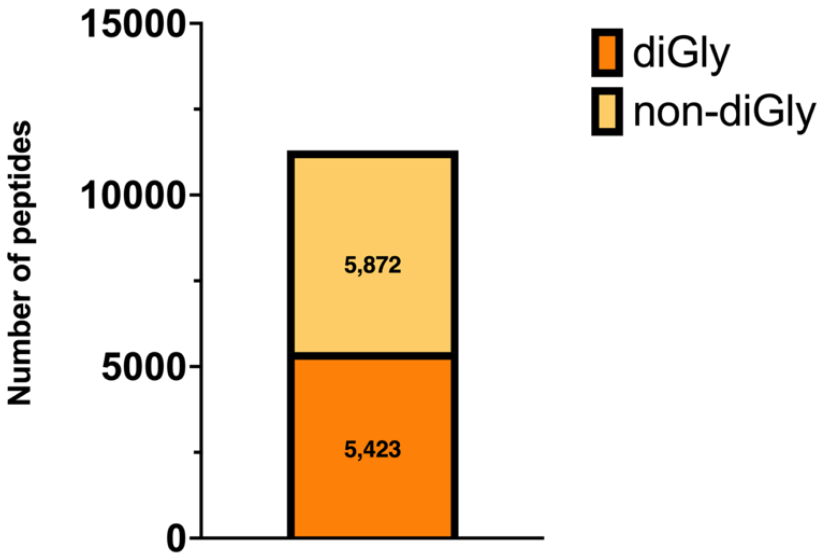

Figure 4. 2. diGly-modified peptide enrichment efficiency. Stacked bar plot displaying the total number of diGly-modified peptides and non-diGly modified peptides detected across all samples (soluble, insoluble and whole tissue).

A limitation of introducing antibody enrichment, is the batch-to-batch variation this can introduce. PCA plots revealed three clusters belonging to the soluble, insoluble and whole tissue samples (**Figure 4.3a**). The clusters were less tight than in the total proteome PCA plot,

indicating that diGly enrichment introduced greater variation. This was most apparent across PC2 of the insoluble fraction. To check if there was one replicate causing more of the variation, we plotted protein abundance values of each replicate against one another and measured the correlation using Pearson Correlation Coefficient test (**Figure 4.3b**). All replicates had an R value greater than 0.81, but the highest score was found between replicate 1 and 3 of the insoluble fraction (0.88). Therefore, replicate 2 of the insoluble fraction was causing the most variation in this sample. It is worth noting, that all proteins were included in this analysis irrespective of if they contained a diGly modification or not. Therefore, we wanted to determine if the variation was driven by the ubiquitylated peptides, non-ubiquitylated peptides or both. When calculating the coefficient of variance (CV) we found values were greater in peptides without a diGly modification (**Figure 4.3c**). Therefore, the variance brought about in this replicate is likely due to variability in the ubiquitin enrichment process rather than ubiquitylation itself. However, overall, there was no dramatic outlier that we deemed as failing the quality control check, so we were able to include all three replicates in our analysis.

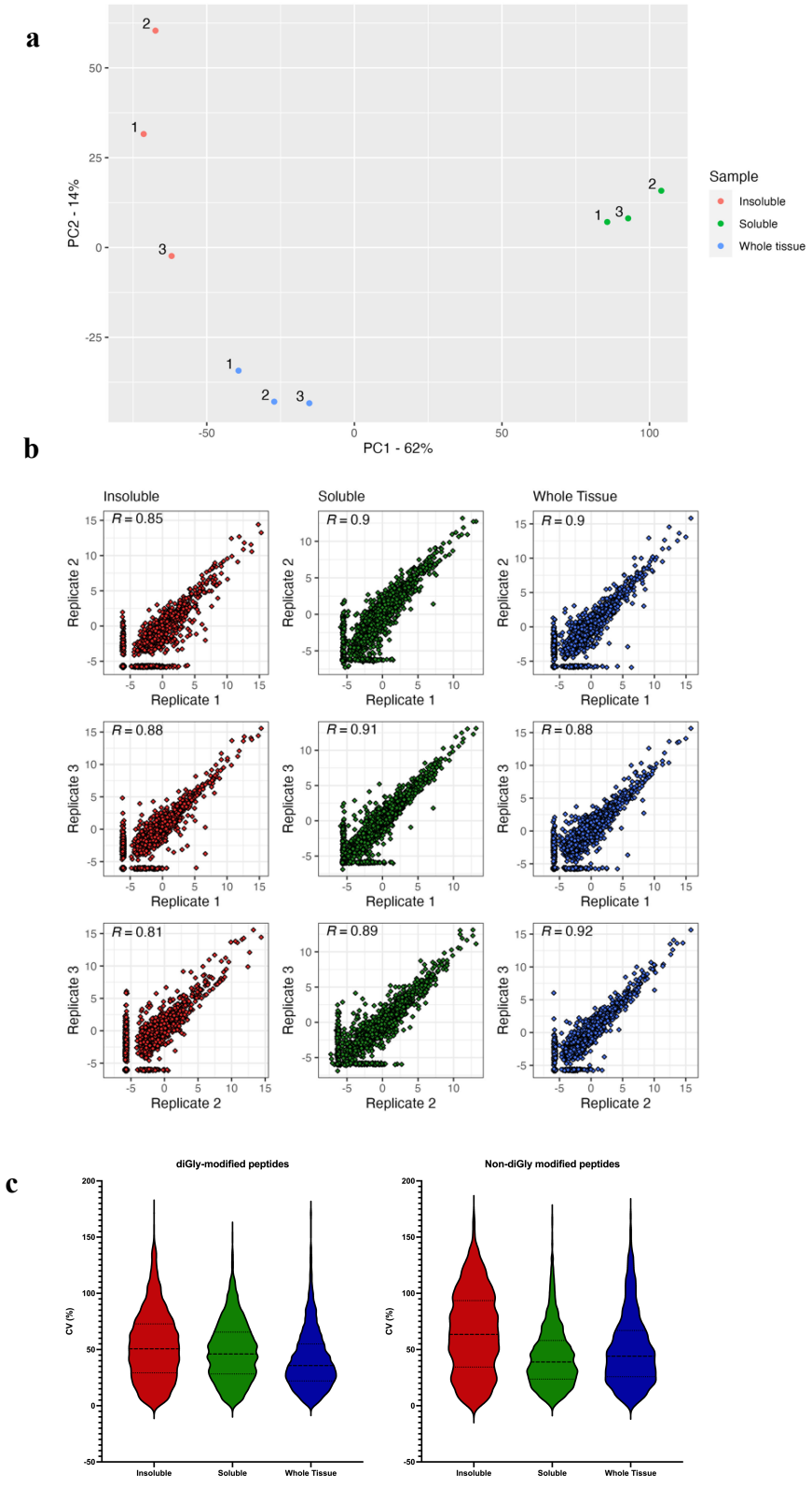

Figure 4. 3. Protein abundance variation after diGly enrichment. a) PCA plot displaying the variation in protein abundance both within and between samples. b) Scatterplot showing the correlation in protein abundance values between replicates, each dot represents an individual protein. c) Violin plots showing the median, quartiles and range of CV% values of peptides within each sample.

4.4.2 Fractionation of the muscle ubiquitylome

The largest variation in protein abundance came between the soluble and insoluble fractions, as depicted by the spread across PC1 (**Figure 4.3a**). To understand the impact of our fractionation workflow, we aimed to identify the ubiquitylated peptides that contributed most to this variation. To do this, we filtered the ubiquitylomics data so that only peptides that contained a diGly-modification were included. Statistical analysis was performed as per the previously described protocol in Chapter 3 using probabilistic minimum imputation followed by Limma. In total 3985 diGly-modified were analysed, of which 973 and 822 were significantly enriched into the insoluble or soluble fraction, respectively (**Figure 4.4**). Therefore, nearly half of the diGly-modified peptides were enriched into either fraction. When looking at the top enriched diGly-modified peptides, the insoluble fraction was mostly sarcomeric proteins, whilst peptides enriched in the soluble fraction were mostly enzymatic proteins (**Figure 4.4**). These results indicate that our fractionation procedure was effective in separating ubiquitylated myofibrillar proteins from ubiquitylated regulatory proteins.

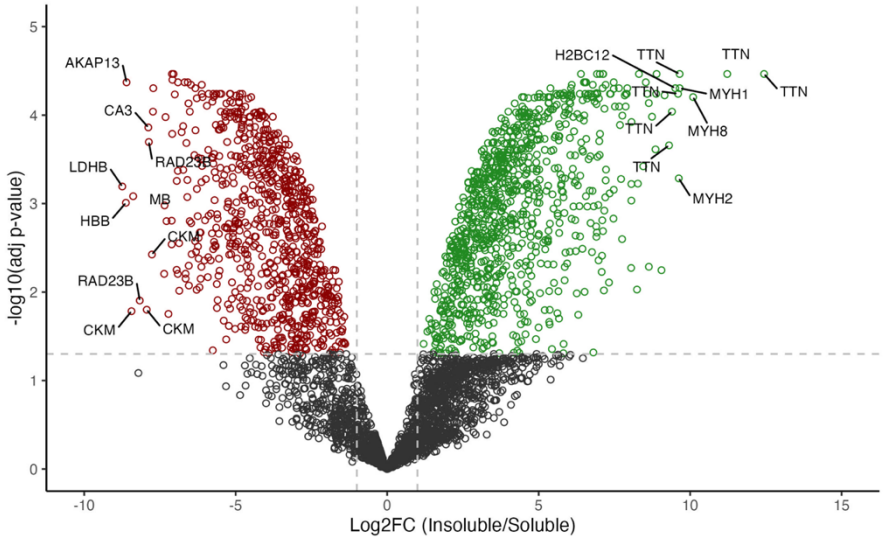

Figure 4. 4. Fraction enriched ubiquitylated peptides. a) Volcano plot showing the fold change and statistical significance of diGly-modified peptide abundance values between fractions. Significantly enriched diGly-modified peptides are highlighted: Red = soluble enriched (Log2FC < -1 & adjusted *P* value < 0.05), Green = insoluble enriched (Log2FC > 1 & adjusted *P* value < 0.05). Top 10 enriched peptides were annotated.

Next, we wanted to uncover which proteins experienced the most ubiquitin modifications. Five proteins had more than 100 diGly-modified sites, all of which were more abundant in the insoluble fraction (**Figure 4.5a)**. Due to the large size of titin, it did not come as a surprise to see that this protein was heavily ubiquitylated. However, it was intriguing to see that titin was ubiquitylated on 737 different lysine residues which was over two and a half times more sites than the protein with the second highest ubiquitylation site count (nebulin). Due to the high abundance of ubiquitylation sites on titin, we wanted to know how many diGly-modified peptides from titin were detected in each fraction. When looking at the number of diGly-modified peptides identified in at least one replicate per fraction, we found 759 in the insoluble fraction and 145 in the soluble fraction (**Figure 4.5b**). The reduction of diGly-modified titin in the soluble fraction will decrease the dynamic range of abundance values. As a result, this will enhance the detection of less abundant diGly-modified peptides in the soluble fraction.

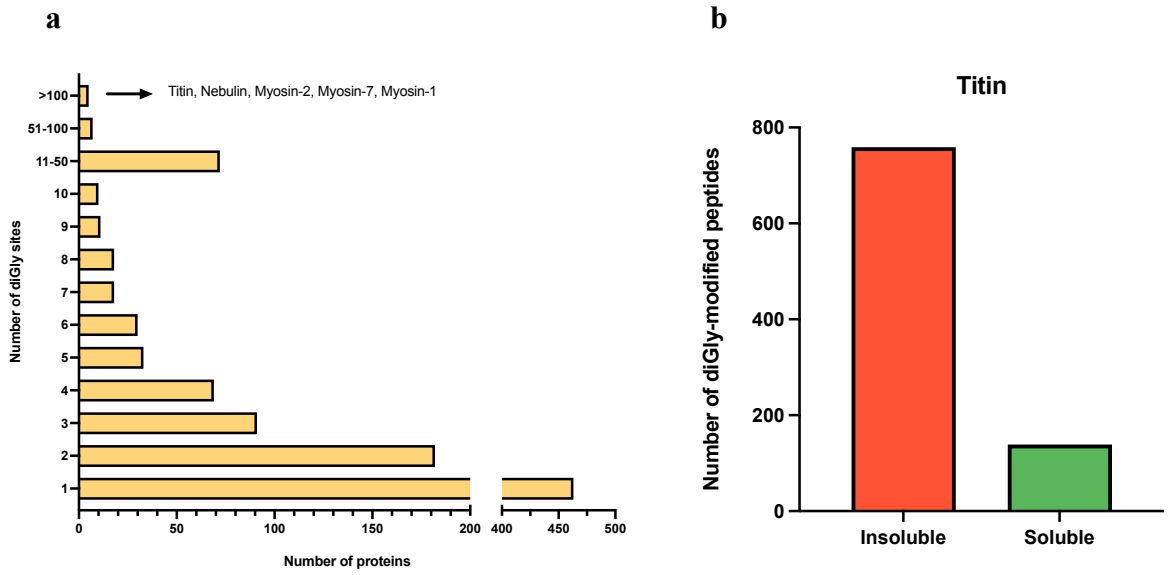

Figure 4. 5. Titin is the most ubiquitylated protein. a) Ubiquitylated proteins were categorised based on the number of ubiquitylation sites detected. Each bar represents the number of proteins that contain the given number of ubiquitylation sites detected in all samples (soluble, insoluble and whole tissue). b) Bar plot showing the number of diGly-modified peptides belonging to titin in either fraction.

4.4.3 Assessing workflow performance for improving ubiquitylome coverage

We have now confirmed the K-ε-GG immunoprecipitation was capable of enriching diGly-modified peptides, and that highly abundant ubiquitylated proteins such were enriched into the insoluble fraction. Next, we wanted to determine if fractionation improved the detection of the ubiquitylome. In total, we identified 4724 diGly-modified peptides without muscle fractionation and 5172 diGly-modified peptides with muscle fractionation (**Figure 4.6b**). From these peptides, we identified 955 proteins without muscle fractionation and 972 proteins with muscle fractionation (**Figure 4.6e**). Overall, muscle fractionation did improve the identifications of ubiquitylated peptides and proteins, however this difference was lower than we anticipated. Despite the reasonable overall enrichment efficiency (**Figure 4.2**), we did observe large variability between samples. The most noticeable issue lay with the soluble fraction, in which only 39% of the peptides contain a diGly remnant. This was much lower than the insoluble fraction and whole tissue which had a 59% and 57% enrichment efficiency score respectively. The reason for this discrepancy appears to be due to an increase in non diGly-modified peptides in the soluble fraction. We detected 5001 non diGly-modified peptides in this fraction, compared to 3039 and 3514 in the insoluble fraction and whole tissue, respectively (**Figure 4.6c**). Therefore, poor diGly enrichment efficiency in the soluble fraction is likely lowering the detection of the fractionated ubiquitylome.

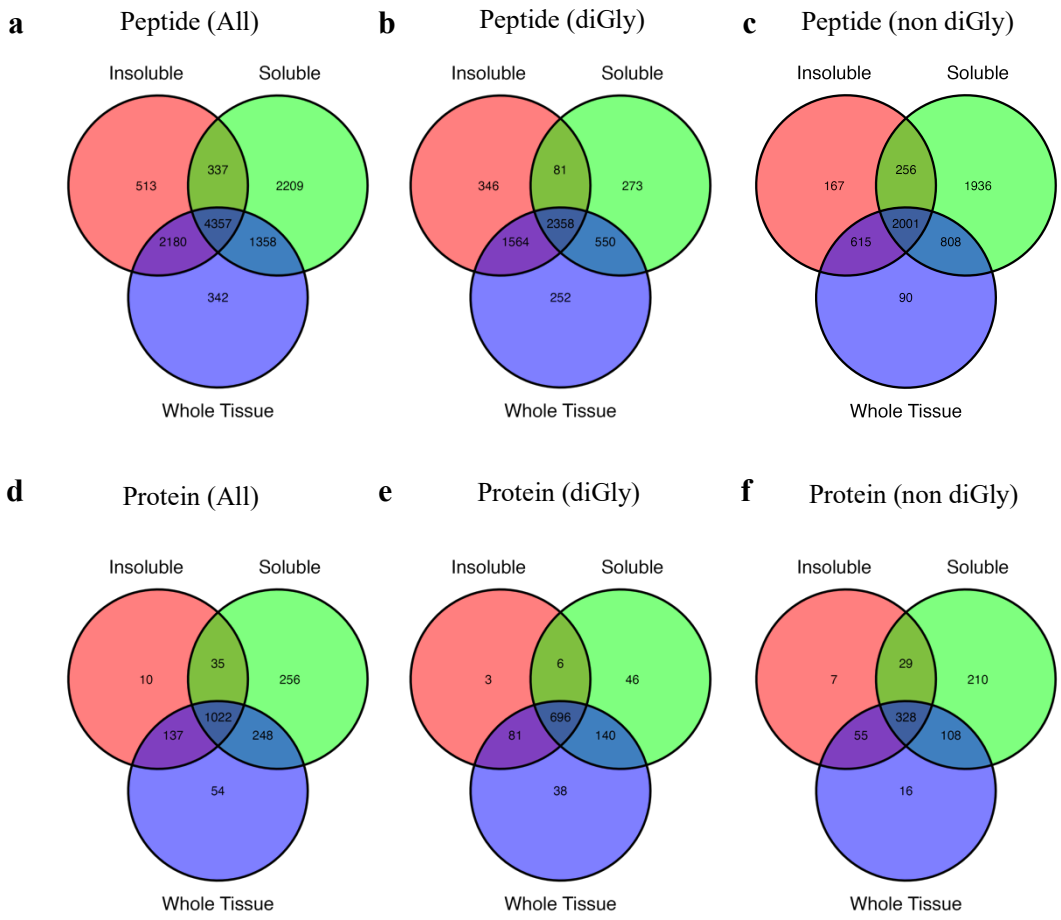

Figure 4. 6. Total number of ubiquitylated peptides and proteins identified in each sample. Venn diagram showing the distribution of peptides and proteins in the soluble, insoluble and whole tissue samples. a-b) All peptides/proteins included, c-d) Only includes peptides/proteins containing at least 1 diGly remnant, e-f) Only includes peptides/proteins that do not contain any diGly remnants.

To ensure that the worse enrichment efficiency in the soluble fraction was not due to a single replicate outlier, we compared the number of peptides without a diGly modification for each replicate. Despite some variation among replicates, the soluble fraction consistently contained more non-diGly-modified peptides compared to any insoluble or whole tissue sample (**Figure 4.7**). This may indicate that the K-ε-GG immunoprecipitation protocol is less effective with the soluble fraction.

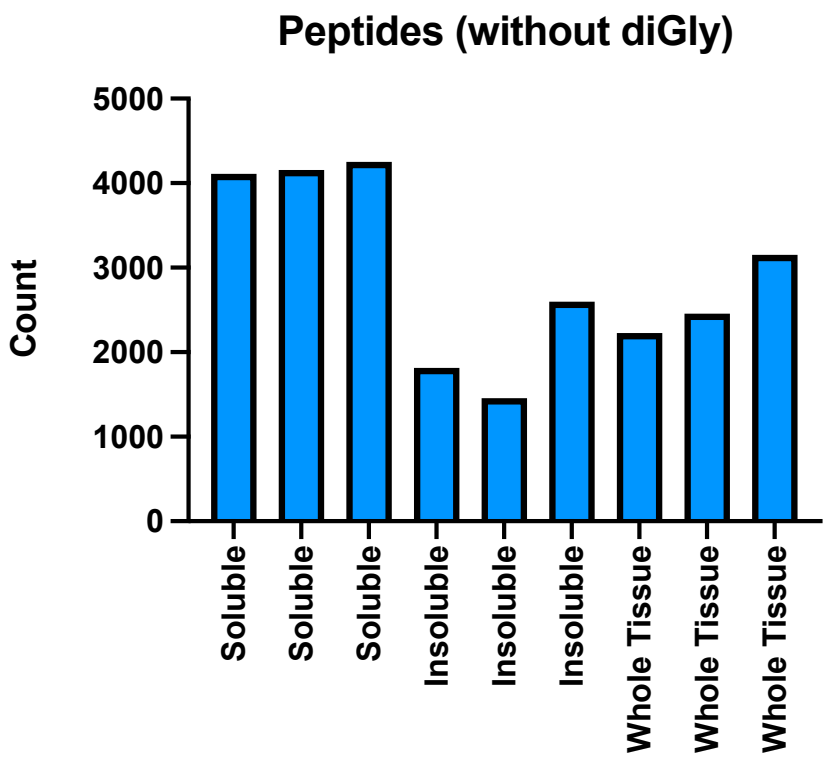

Figure 4. 7. Number of peptides without diGly modification. Bar chart showing the number of non-diGly-modified peptides identified in each replicate following K-ε-GG immunoprecipitation.

4.4.4 Optimising the ubiquitylomics workflow

Whilst the reason for the high abundance of non-diGly-modified peptides in the soluble fraction is unknown, it may be due to unspecific peptides binding to the immunoaffinity beads. If this was the case, increasing the stringency of the bead washes and reducing the number of beads in the reaction could help lower the levels of unspecific peptide binding. When using automated handling of beads used for K-ε-GG immunoprecipitation, one study found that increasing the stringency of the wash stages helped to improve antibody efficiency. By including 50% ACN and 0.01% CHAPS in the wash buffer they were able to improve bead handling, subsequently increasing the number of diGly-modified peptides detected [130]. Whilst we were not able to include the automated procedure, we decided to include the modified wash buffers in our protocol. Of note, whilst CHAPS is a detergent and therefore acts as a contaminant for LC-MS

analysis, it has been reported that 0.01% CHAPS does not interfere with the LC-MS signal and therefore we were confident that no additional clean up step would be required [209]. Moreover, we reduced the number of K-ε-GG immunoaffinity beads by changing the volume from 20 µL to 15 µL per sample in an attempt to lower non-specific binding.

K-ε-GG immunoprecipitation may have also been affected by the presence of active trypsin. Immunoprecipitation involves the use of antibodies, which are proteins and therefore can be digested by trypsin. If this occurs, the antibodies will no longer be effective and will not be able to selectively enrich for ubiquitylated peptides. Therefore, it is important that we have no active trypsin present when performing K-ε-GG immunoprecipitation. To assess the presence of trypsin, we subjected peptides obtained from an overnight trypsin digest of proteins to an SDS-PAGE gel electrophoresis and visualised protein content using a Coomassie stain. We discovered that our sample still contained trypsin, suggesting this enzyme had not undergone complete autodigestion and would be present during K-ε-GG immunoprecipitation (**Figure 4.8a)**. To determine if the trypsin was still active, we mixed the digested sample with proteins and incubated them overnight at 37 °C. After running a Coomassie stain, we found that the molecular weight of proteins had been significantly reduced, suggesting they had been digested into peptides by trypsin (**Figure 4.8b**). Consequently, our current workflow suffers from residual trypsin activity which may interfere with K-ε-GG immunoprecipitation and could partially explain the relatively low yield of diGly-modified peptides in our samples.

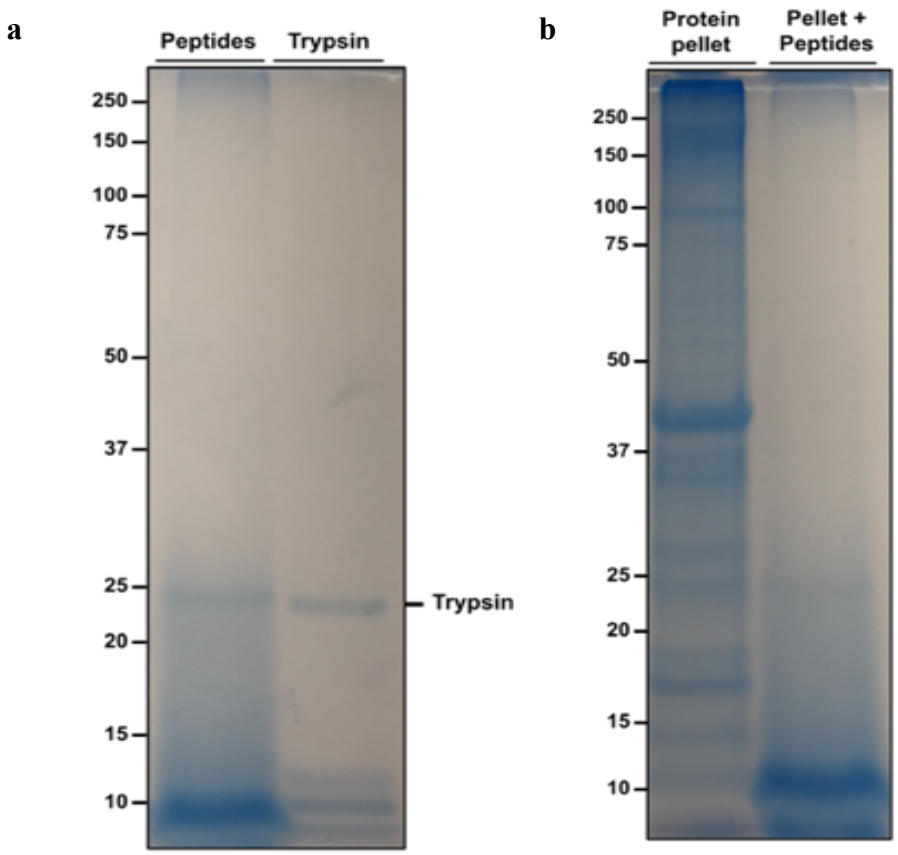

Figure 4. 8. Trypsin remains active after digestion. a) The presence of intact trypsin in peptides following overnight digestion of 50 µg protein. Trypsin alone was loaded as a positive control b) The residual activity of trypsin following overnight digestion, tested by incubating digested product with 50 µg protein overnight at 37 °C.

To try and address this, we first decided to test different sources of trypsin. Up to this point, we had been using Trypsin Gold sourced from Promega, which includes the addition of methyl groups to lysine residues on trypsin making it more resistant to autolytic digestion. We decided to test Sequence Grade Trypsin (also from Promega) and a plant-based trypsin (known as Trypzean) to see whether they were less resistant to auto-digestion. We found that both sources of animal trypsin remained equally active after digestion, whilst trypzean appeared to display reduced activity, illustrated by the greater presence of protein remaining after overnight incubation with peptides digested with this enzyme (**Figure 4.9a**). However, trypzean also suffered from worse digestion efficiency when compared to both sources of animal trypsin,

illustrated by the incomplete digestion of proteins incubated overnight with this enzyme (**Figure 4.9a**). We wondered whether increasing the concentration of trypzean could help ensure complete digestion of proteins whilst retaining lower residual activity. We found that increasing the concentration of trpyzean to a ratio of 1:10 increased the digestion of proteins (**Figure 4.9b**). However, this higher concentration of trypzean suffered from increased residual activity, similar to that of animal trypsin (**Figure 4.9c**).

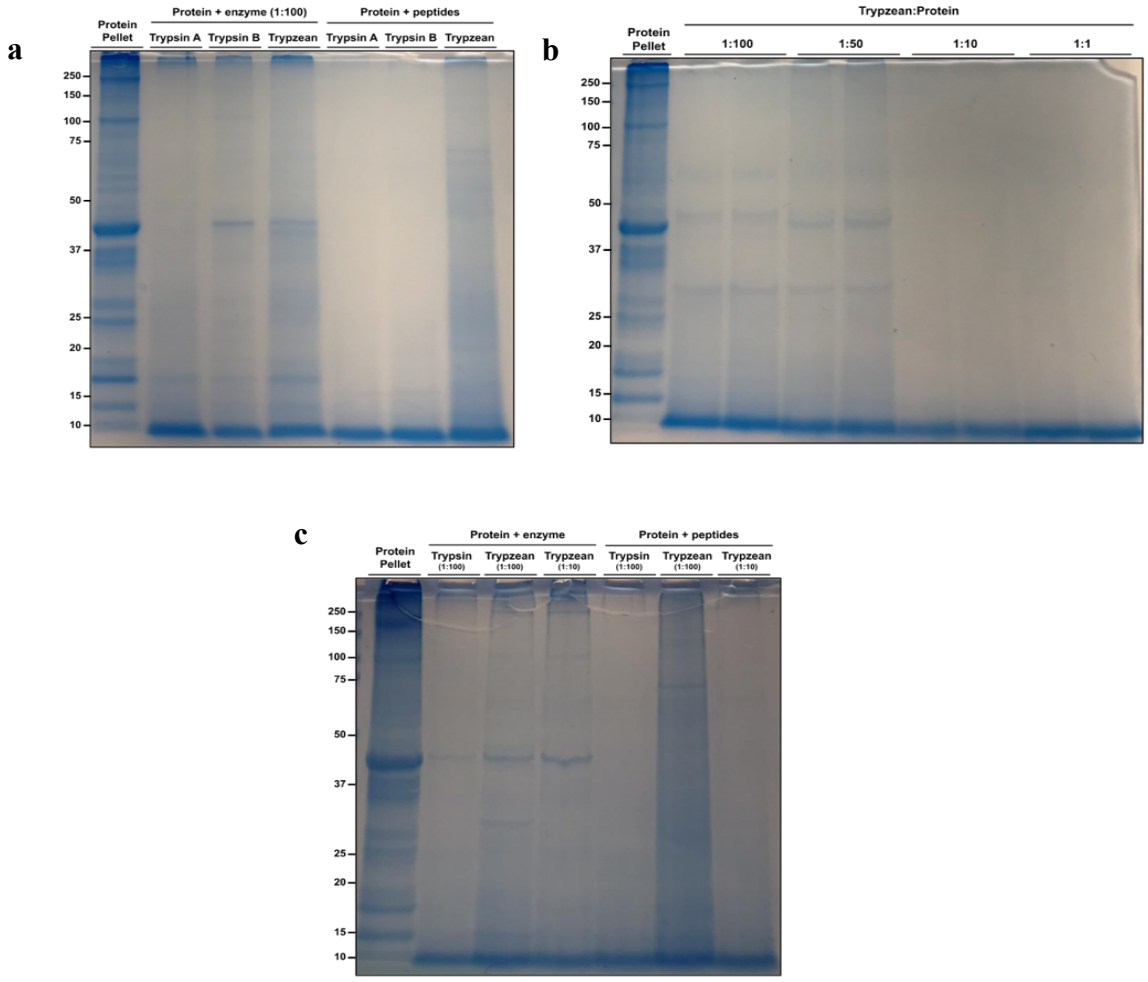

Figure 4. 9. Alternative sources of trypsin insufficient for reducing residual activity. All reactions were performed on proteins derived from human skeletal muscle. a) Digestion efficiency (Lanes 2-4) and residual activity (Lanes 5-7) of Promega trypsin (A = gold, B = sequence grade) and trypzean tested on 50 µg protein. b) Digestion efficiency of different concentrations of trypzean when incubated overnight with 50 µg protein. c) Digestion efficiency (Lanes 2-4) and residual activity (Lanes 5-7) of trypsin gold and trypzean at different protein to enzyme concentrations.

As we were unable to identify an effective alternative to trypsin, we decided instead to include an additional stage after digestion to irreversibly inhibit the enzyme. This way we maintain the high digestion efficiency that trypsin provides whilst also eliminating any residual activity this enzyme appears to carry over. Commonly used methods to inhibit trypsin include acidification and freezing, however these are both reversible. K-ε-GG immunoprecipitation does not work in acidic nor frozen conditions and therefore the activity of trypsin would be restored. We opted for more harsh conditions, by permanently inhibiting trypsin through serine protease inhibitors or heat denaturation. Trypsin is a serine protease and there are available inhibitors, such as phenylmethylsulfonyl fluoride (PMSF) and a protease inhibitor cocktail, which act irreversibly to block its catalytic activity. Alternatively, denaturing trypsin with heat will permanently alter its conformational shape, preventing trypsin from carrying out its proteolytic function and thus inhibiting its activity.

First, we tested increasing concentrations of PMSF and protease inhibitor cocktail up to their recommended working concentration. We opted to use BSA as our protein substrate to save muscle tissue for future experiments. No concentration of PMSF we tested was able to completely inhibit trypsin activity (**Figure 4.10a**)**.** When trypsin was incubated with the highest concentration of PMSF (1 mM), only 29% of the original BSA protein remained, which means that 71% was degraded into peptides (**Figure 4.10d**). The protease inhibitor cocktail was more effective at reducing trypsin activity, however the recommended working concentration (1x) still resulted in a 53% reduction in BSA protein (**Figure 4.10a and Figure 4.10d**). Heat denaturation appeared a much more effective method of inhibiting trypsin activity as after 30 minutes of heating at 95 °C, trypsin was no longer able to degrade BSA (**Figure 4.10b and Figure 4.10d**). To confirm that 30 minutes of heating is sufficient to inactivate any residual trypsin present in our ubiquitylome experiments, we performed a scaled-up version using 20

µg trypsin and 2 mg BSA. The digested BSA peptides were heated and incubated with a fresh 20 µg of BSA protein. When performing 30 minutes of heating to the peptides, BSA protein was not digested, illustrating that residual trypsin was inactivated (**Figure 4.10c and Figure 4.10d**). Therefore, moving forward we implemented a 30-minute heating stage after overnight digestion to denature trypsin and inhibit its activity prior to K-ε-GG immunoprecipitation.

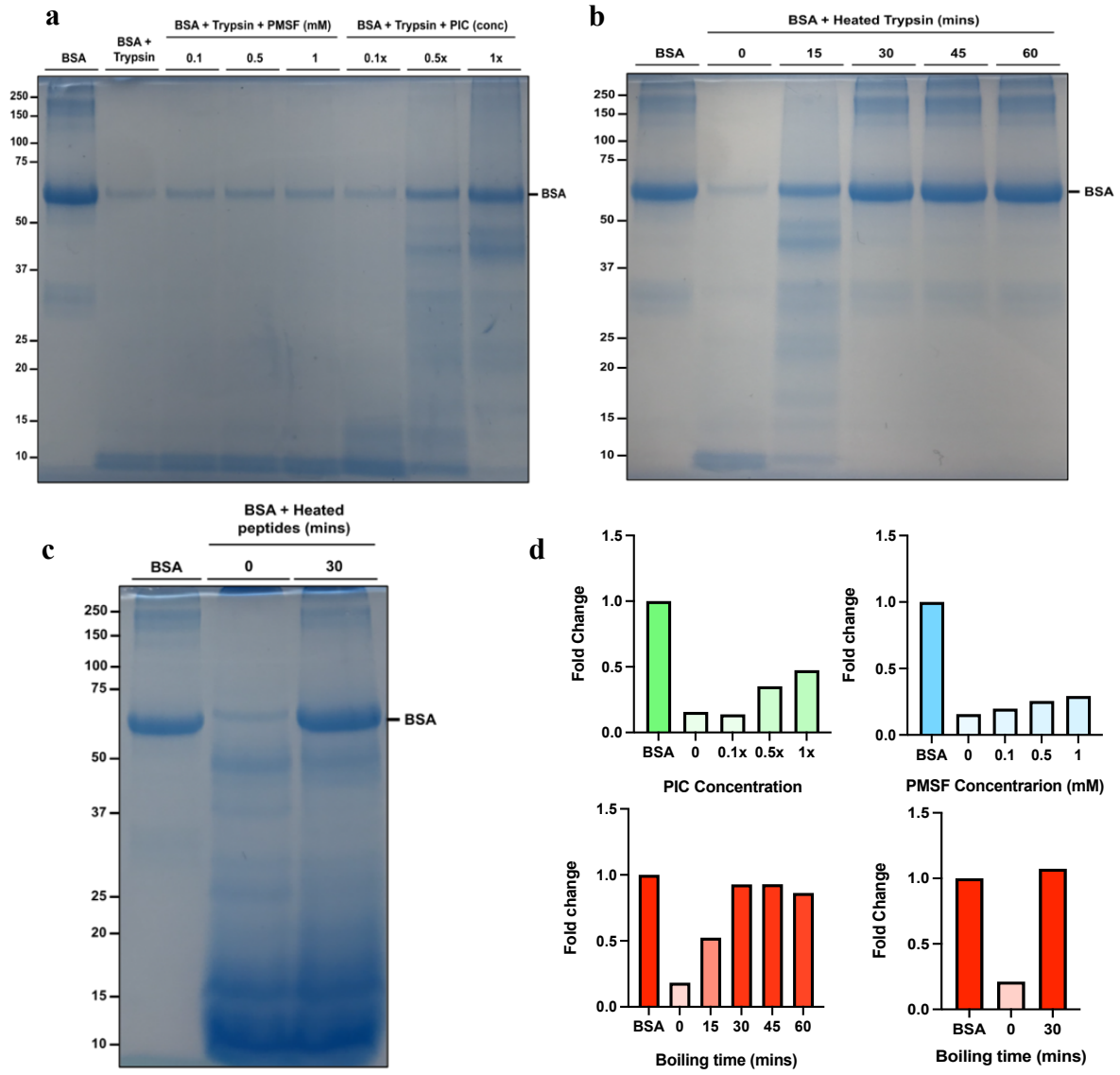

Figure 4. 10. Coomassie protein staining to determine the success of trypsin inhibition. a) 0.2 µg trypsin was incubated for 1 hour on ice with different concentrations of PMSF or protease inhibitor cocktail (PIC) prior to overnight incubation with 20 µg BSA. b) 0.2 µg trypsin was heated at 95 °C for different amounts of time prior to overnight incubation with 20 µg BSA BSA. c) 2 mg BSA was incubated overnight with 20 µg trypsin and digested product was heated at 95 °C for 30 minutes and incubated overnight with 20 µg BSA. d) ImageJ was used to quantify bands and results were displayed on GraphPad Prism.

Moving forward, we also wanted to address the issue of missing values in our current workflow. Only 39% and 58% of ubiquitylated peptides were identified in all insoluble or soluble samples respectively. The large number of missing values is likely due to the stochastic nature of DDA, in which low abundant MS signals can be missed between runs. Most missing values were present in the insoluble fraction, which is likely due to the highly abundant myofibrillar proteins that reduce the signal of the remaining proteins. To address this issue, we wanted to use multiplexing which allows for the simultaneous analysis of multiple samples in a single MS run [222]. This method involves labelling proteins or peptides from each sample with specific tags, which serve as internal standards that can be differentiated during MS analysis. The samples can then be pooled meaning only one LC-MS run needs to be performed, thereby removing run-to-run variation.

There are two different types of multiplexed labelling, metabolic and chemical. Metabolic labelling uses heavy and light stable isotopes which are incorporated into the protein during synthesis. This isotopic label alters a peptides mass to charge ratio and therefore a peptide can be differentiated based on whether it has a heavy or light label. This is commonly used for cell culture-based experiments (SILAC) when looking for a different in two conditions. Chemical labelling (most commonly TMT or iTRAQ) uses isobaric tags that have identical overall masses but vary in their individual group masses. Each tag can be differentiated during MS2 fragmentation as the reporter groups gets separated, causing a mass change. Both labelling methods can be used for relative quantification: By comparing the isotope intensities of a given protein's peptides (metabolic) or by comparing the reporter ion intensities for each peptide fragment (chemical). Chemical labelling can be easily employed in tissue samples and has the added advantage of labelling up to 18 different samples. Moreover, due to their identical mass during prior to MS2 fragmentation, each peptide ion is combined from multiple samples which

increases the MS1 signal. For example, a TMT 6 plex will increase the peptide signal ~6 times relative to label free quantification. As a result, more peptides reach the DDA signal threshold limit for quantification, meaning less starting material is required. This is particularly important for ubiquitylated peptides as they have a lower stoichiometry and so peptides are less likely to reach the signal threshold. TMT labelling of ubiquitylated peptides is most effective whilst still bound to the K-ε-GG immunoaffinity bead to prevent TMT binding to the diGly remnant [129]. Therefore, moving forward we decided to use on bead TMT labelling for quantitative analysis of the ubiquitylome. The modified ubiquitylomics workflow is shown in **Figure 4.11.**

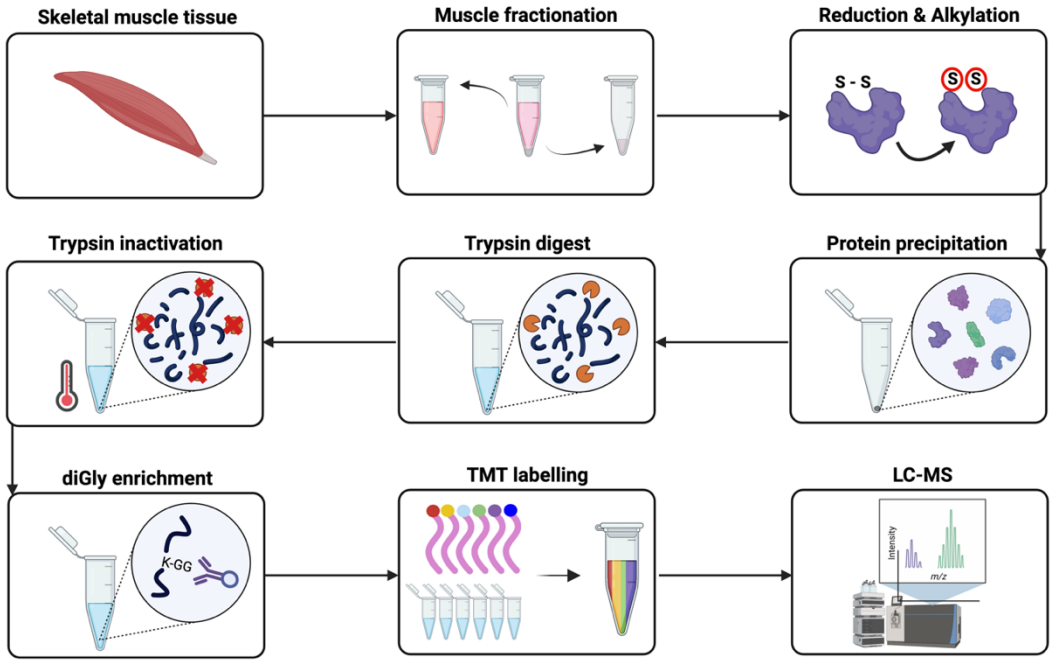

Figure 4. 11. Schematic showing the optimised workflow for studying the ubiquitylome in skeletal muscle. Image created using biorender.com

Whilst TMT labelling was employed to improve the coverage of ubiquitylated peptides, it is important to be aware of the limitations. Firstly, labelling must be performed after enrichment of ubiquitylated peptides because otherwise the labels would bind to the primary amine on the diGly remnant and prevent the K-ε-GG antibody from binding [129]. Due to the batch-to-batch

variation in diGly enrichment efficiency, this can introduce non-biological variation during quantitative analysis. Furthermore, TMT quantification can reduce the true difference in abundance values between samples. During MS2 peptide selection for TMT quantification, co-eluting peptides that are within the isolation window are also fragmented, thus contributing towards quantification. This is known as co-isolation interference and these interfering peptides will generally favour a 1:1 abundance ratio, suppressing the true difference of the intended peptide [223]. To minimise the issue of ratio suppression, we will incorporate offline fractionation prior to LC-MS analysis. This additional fractionation separates peptides based on their hydrophobic interactions using a high pH reversed-phase chromatography [224]. This method is orthogonal to the low pH reversed-phase separation technique employed in the LC column attached to the MS. As a result, you obtain a greater separation of peptides and reduce the risk of co-isolation interference during MS2 quantification. Additionally, by using a high-resolution orbitrap instrument coupled with ion mobility separation (FAIMS) we aim to further decrease the occurrences of co-isolation [225]. Although not included in our workflow, MS3 scanning also provides a method to reduce co-isolation effect using synchronous precursor selection (SPS) or real time searching (RTS) which help ensure that the selected precursor ions are indeed part of the target peptide [226], [227]. However, we did not apply MS3 scanning as previous work has shown MS2 with FAIMS detects threefold more diGly-modified peptides [129].

4.5 Conclusions

Overall, this chapter has shown that we were able to develop a workflow that enabled the identification of diGly-modified peptides. The original K-ε-GG immunoprecipitation method was able to provide nearly 50% enrichment efficiency, allowing us to identify many ubiquitylated peptides that would otherwise go undetected due to their low stoichiometry.

Unsurprisingly, muscle proteins such as nebulin, myosin and titin were amongst the most ubiquitylated. We observed a clear separation of titin ubiquitylation in our two fractions, indicating that our fractionation procedure has depleted highly abundant myofibrillar ubiquitylated peptides from our soluble fraction. At first glance, it was therefore surprising that fractionation did not greatly increase the detection of ubiquitylated peptides in skeletal muscle. By analysing the diGly enrichment efficiency of each sample, it was clear that the soluble fraction performed poorly. By increasing the diGly enrichment efficiency, we aimed to significantly improve the detection of ubiquitylated peptides. Therefore, moving forward we have implemented modifications to the K-ε-GG immunoprecipitation protocol. This includes the inactivation of trypsin to prevent antibody digestion, and a reduced volume of immunoaffinity beads with more stringent wash steps to reduce the amount of unspecific binding. A further modification to our protocol was including TMT labelling, in order to reduce the presence of missing values and improve the quantitative capacity and accuracy.

5. Discovery proteome and ubiquitylome profiling reveals ageing effect in skeletal muscle

5.1 Abstract

Ageing is characterised by a progressive decline in skeletal muscle function, yet the underlying molecular mechanisms are not fully understood. Ubiquitylation, a post-transcriptional modification, plays a crucial role in regulating the proteome and orchestrates diverse biological processes. To elucidate the molecular changes associated with ageing, we performed mass spectrometry-based proteomics on skeletal muscle from young (6 month) and old (21-22 month) male and female mice, assessing the abundance of proteins and ubiquitin-related modifications. Our proteomics analysis revealed extensive age-related alterations in multiple cellular components, including extracellular matrix, mitochondria, nuclear spliceosome, sarcomere and endoplasmic reticulum. We observed sex-specific ageing effects, particularly in the unfolded protein response in which only males show an increase in pro-folding chaperones. Our ubiquitylomics dataset revealed age-dependent modifications on various proteins, including those associated with mitochondria, ribosome, the ubiquitin-proteasome system and histones. Notably, we found a marked reduction in ubiquitylation of a histone H2B isoform at K121 in both sexes. These findings provide a comprehensive resource of age-associated protein and ubiquitin-related modification changes in mouse skeletal muscle, offering insights into potential mechanisms of sarcopenia.

5.2 Introduction

Ageing is associated with a decline in skeletal muscle mass, strength and metabolic function, ultimately leading to a loss of overall muscle function. The extent of this age-related decline is influenced by various lifestyle and biological factors, including sex [228]. The deterioration of muscle function has widespread adverse effects on whole-body health, contributing to metabolic and cognitive decline [8], [10], while also increasing the risk of mortality [229]. Understanding the molecular mechanisms underlying skeletal muscle ageing is crucial for developing therapeutic strategies to mitigate these health challenges.

Rodents are valuable models for studying the mechanisms of human ageing due to their shorter lifespans and controlled environments. However, a significant limitation with current ageing research in rodents is the underrepresentation of female subjects. Male cohorts are often favoured in studies because they provide fewer hormonal fluctuations compared to females [230]. This bias has resulted in a molecular understanding of muscle ageing that is predominantly centred on male physiology, overlooking important sex-specific differences in the ageing process.

MS-based proteomics is a powerful tool for investigating the molecular changes associated with muscle ageing. Proteomics has identified fibre-type-specific age-related changes in human muscle and demonstrated a disconnect between transcription and translation in mice muscle [25], [231]. Despite these advancements, there remains a critical need to explore how PTMs contribute to muscle ageing. Ubiquitylation, a PTM that regulates most biological processes, is primarily known for targeting proteins for degradation through the proteasome and autophagy-mediated pathway [101]. This process is crucial for maintaining protein quality control, removing damaged and misfolded proteins that accumulate with age.

Ubiquitylomics research has already provided significant insights into the relationship between protein ubiquitylation and ageing across different model organisms. In aged *C. Elegans,* ubiquitylomics identified a decrease in the ubiquitylation of proteasomal targets, leading to their accumulation causing a subsequent reduction in longevity [80]. In *Drosophila*, ubiquitylomics revealed an age-modulated increase in the ubiquitylation of long-lived proteins such as histone 2A that was shown to be an evolutionary conserved biomarker of ageing [173]. In aged mouse brains, over one-third of the changes observed by ubiquitylomics could be replicated by inhibiting the proteasome, suggesting an age-related impairment in protein clearance capacity [232]. Therefore, it is evident that ubiquitylomics provides critical insights into the molecular mechanisms driving age-related functional decline. In this chapter, we used ubiquitylomics to analyse age-related changes in skeletal muscle tissue, aiming to understand how protein ubiquitylation contributes to the decline in muscle function and the development of sarcopenia.

To address some of the existing knowledge gaps with muscle ageing, we investigated both the proteome and ubiquitylome (ubiquitin-enriched proteome) of skeletal muscle from young (6 month) and old (21-22 month) male and female mice. Utilising centrifuge-based fractionation to enhance protein coverage [233], we generated separate datasets for the soluble and insoluble muscle fraction. We identified proteins and ubiquitin modifications that were differentially regulated with age and assessed the impact of sex. Our findings reveal both established and novel signatures of ageing muscle, providing a comprehensive resource to further explore the mechanisms driving sarcopenia.

5.3 Methods

5.3.1 Collection of skeletal muscle

Gastrocnemius complex muscle (Plantaris, Soleus and Gastrocnemius) was obtained from 8 young (6 months) and 8 old (21-22 months) C57BL/6 mice, snap-frozen and stored at -70 °C. In both age groups, there were 3 males and 5 females. The Institutional Animal Care and Use Committee at the University of California, Davis, approved all animal protocols used in this study.

5.3.2 Fractionation of skeletal muscle

100 mg of frozen gastrocnemius complex muscle was powdered on dry ice using a mallet and crusher. The powdered tissue was first lysed in a 10-fold volume of ice-cold lysis buffer A (50 mM HEPES pH 8.0, 0.5% Triton X-100, 5 mM EDTA, 100 mM 2-chloroacetamide, 10 µM PR-619, 1 mM sodium orthovanadate, 1x cOmplete Mini EDTA-free protease inhibitor (11836170001, Roche, Switzerland)) using the TissueLyser II (Qiagen, Netherlands) with 5 mm stainless steel beads for 4 x 2-minute cycles at 30 Hz. The lysate was then centrifuged at 1500 g for 10 minutes (4 °C) and the supernatant was collected. The remaining pellet was washed in 1 mL of ice-cold lysis buffer A and the supernatant discarded. The pellet was then resuspended in a 15-fold volume of ice-cold lysis buffer B (50 mM HEPES pH 8.0, 1% SDS, 1% Triton X-100, 1% NP-40, 1% Tween 20, 1% sodium deoxycholate, 50 mM NaCl, 5 mM EDTA, 1% (w/v) glycerol, 100 mM 2-chloroacetamide, 10 µM PR-619, 1 mM sodium orthovanadate, 1x cOmplete Mini EDTA-free protease inhibitor (11836170001, Roche, Switzerland)) and placed in the TissueLyser II (Qiagen, Netherlands) with 5 mm stainless steel beads for 2 x 2-minute cycles at 30 Hz. Lysates from both supernatant and pellet were sonicated at 4 °C for 12 x 5-second bursts with 5 second intervals. Finally, the lysates were cleared at 16000 g for 10 minutes and the supernatant from both soluble and insoluble fraction was

collected. Protein concentrations from each sample were determined by a DC assay (5000111, Bio-Rad, USA) using an FLUOstar Omega plate reader (BMG Labtech, UK) according to manufacturer's instructions. Concentrations were read at an absorbance of 750 nm.

5.3.3 Coomassie staining and western blotting

100 µg of protein was prepared for SDS-PAGE gel electrophoresis by adding 4x LDS sample buffer (NP0008, Thermo Scientific, USA) containing 5% β-mercaptoethanol to final concentration 1x and 1.25%, respectively, and left overnight at room temperature to denature. 10-30 µg of protein was loaded into 10% Bis-Tris gels and separated in 1x MOPS buffer for approximately 90 minutes at 140V. For Coomassie protein staining, gels were incubated in PageBlue protein staining solution (24620, Thermo Scientific, USA) for 1 hour before rinsing in double distilled water as per manufacturer's instructions. For western blots, proteins were transferred onto PVDF membranes (10600021, Amersham, USA) for 1 hour at 100V. Membranes were blocked in milk powder diluted to 5% in TBS-T for 1 hour, rinsed in TBS-T and incubated overnight at 4 °C with the appropriate primary antibody: MHC (#M4276, 1:1000, Merck Millipore, USA), Actin (#A2103, 1:1000, Merck Millipore, USA), Desmin (#5332, 1:1000, Cell Signaling Technology, USA), ACC (#3676, 1:1000, Cell Signaling Technology, USA), GAPDH (#5174, 1:25000, Cell Signaling Technology, USA), Total OXPHOS (#ab110413 1:1000, Abcam, UK), CRYAB (#15808-1-AP 1:2000, ProteinTech, USA), HSPB7 (#15700-1-AP, 1:1000, ProteinTech, USA), PDI (#3501, 1:1000, Cell Signaling Technology, USA). Membranes were then washed in TBS-T three times for 10 minutes prior to incubation in horseradish peroxidase-conjugated secondary antibodies (1:10000, Cell Signaling Technology, USA) at room temperature for 1 hour. Membranes were washed a further three times for 10 minutes in TBS-T prior to antibody detection using enhanced chemiluminescence horseradish peroxidase substrate detection kit (WBKLS0500, Millipore,

UK). Imaging was undertaken using a G:BOX Chemi-XR5 (Syngene, UK). ImageJ was used to quantify protein bands which were normalised to total protein through ponceau staining **(Supplementary Figure 13)**.

5.3.4 LC-MS sample preparation

For consistency, 3 male and 3 female young and old mice were used for LC-MS analysis. Sample preparation was performed using a modified version of the SP4 protocol [118]. 2 mg of protein was reduced by 5 mM DTT for 45 minutes at 25 °C and then alkylated by 10 mM 2-chloroacetamide for 45 minutes at 25 °C in the dark. Proteins were precipitated by adding four volumes of 100% ACN followed by gentle mixing at 500 rpm for 5 seconds and left for 5 minutes at room temperature. Precipitated proteins were pelleted by centrifugation for 5 minutes at 16000 g at room temperature. To maximise pellet density, the tube was first orientated with the hinge inwards for 2.5 minutes and then turned 180° for the final 2.5 minutes. The supernatant was carefully discarded and the remaining pellet was washed three times in 1.5 mL of 80% ethanol, each time samples were centrifuged at 16000 g at room temperature. After the final wash, the protein pellet was resuspended in 100 mM Tetraethylammonium bromide (TEAB) and sonicated at 4 °C in intervals until the protein pellet disrupted. Trypsin (V5280, Promega, USA) was added at a 1:100 enzyme to protein ratio before incubating at 37 °C for 18 hours, shaking at 1000 rpm. Samples were centrifuged at 16000 g for 2 minutes and the peptide containing supernatant was collected. An aliquot was taken for Coomassie protein staining to ensure complete digestion. Samples were heated at 95 °C for 30 minutes to inactivate trypsin. 50 µg of peptides (2.5%) were aliquoted into a separate LoBind tube for proteomics analysis and the remaining peptides were used for K-ε-GG immunoprecipitation prior to ubiquitylomics analysis. Peptides were dried using a SpeedVac Concentrator plus

(12884952, Eppendorf, Germany). Downstream analysis was performed separately for males and females.

5.3.5 Quantitative proteomics

TMT labelling: Dried peptides were resuspended in 25 µL 100 mM TEAB (pH 8.5). 200 µg of TMT 6plex reagents (90061, Thermo Scientific, USA) dissolved in 10 µL anhydrous ACN was transferred directly to the peptides. Tubes were shaken at 700 rpm for 1 hour at room temperature and centrifuged at 2000 g for 5 seconds. The reaction was quenched with the addition of 2 µL 5% hydroxylamine for 15 minutes shaking at 700 rpm at room temperature. Labelled peptides were combined into a 0.5 mL LoBind tube and dried down using a SpeedVac Concentrator plus (12884952, Eppendorf, Germany).

Off-line peptide fractionation: 150 µg of combined peptides were fractionated using the Pierce High pH Reversed-Phase Peptide Fractionation Kit (84868, Thermo Scientific, USA) as per the manufacturer's recommended protocol. Briefly, vacuum concentrated peptides were solubilised in 200 µL of 0.1% TFA and passed through a prepared column twice at 1000 g for 2 minutes, washed in 4% ACN, 0.1% triethylamine and eluted in 100 µL of 6, 8, 10, 12, 14, 16, 18, 20, 25, 30, 40, 50 % ACN, 0.1% triethylamine. Eluted peptides were vacuum concentrated and resuspended in 30 µL of 5% ACN, 0.1% formic acid (FA).

LC-MS analysis: 3 µL (~750 ng peptides) of each TMT-labelled high-pH peptide fractions were analysed and acquired using a Q-Exactive Plus Orbitrap MS (Thermo Scientific, USA) coupled with a Dionex UltiMate^{TM} 3000 nanoHPLC system (Thermo Scientific, USA). Peptides were separated on a reversed-phase nanoLC column (150 × 0.075mm; Reprosil-Pur C18AQ, Dr Maisch, Germany) using a 180 min gradient of 2-35% ACN, 0.1% FA with a flow rate of ~300 nl/min. Mass spectra were acquired with the following parameters for MS^1: resolution 70,000, scan range 350-1,800 m/z, AGC target 3×10^6, and maximum injection time

50 ms. MS2 spectra for 2+ and above charged species were acquired using: HCD fragmentation, top 10, resolution 17,500, AGC 5×10^4, maximum injection time 100 ms, isolation window 0.7 m/z, and normalised collision energy of 35. The minimum AGC target was set at 1×10^4.

5.3.6 Quantitative ubiquitylomics

diGly peptide enrichment & TMT labelling: Enrichment of ubiquitylated peptides was performed using the modified UbiFast manual protocol [130]. Peptides were resuspended in 1.5 mL of HS IAP Bind buffer (containing 0.01% CHAPS) and sonicated for 5 minutes to ensure complete solubilisation. Suspended peptides were centrifuged at 16000 g for 5 minutes to remove any insoluble material. 15 µL of PTMscan HS Ubiquitin/SUMO Remnant Motif (K-ε-GG) magnetic immunoaffinity beads (59322, Cell Signaling Technology, USA) were added into each peptide solution. The bead-peptide mixture was incubated for 1 hour at 4 °C using an end-over-end rotator. The mixture was centrifuged at 2000 g for 5 seconds to bring down the beads and placed on a magnetic stand. The unbound peptide solution was discarded and the beads were washed four times in 1 mL of modified HS IAP Wash buffer (50% HS IAP Wash buffer and 50% ACN, containing 0.01% CHAPS) and two times in LC-MS grade water (85189, Thermo Scientific, USA). After washing and immediately before labelling, the beads were resuspended in 200 µL 100 mM HEPES (pH 8.5) and transferred to a fresh 1.5 mL LoBind tube. 200 µg of each TMT 6plex reagent (90061, Thermo Scientific, USA) was dissolved in 10 µL anhydrous ACN and transferred directly to the resuspended bead solution. Tubes were shaken at 1400 rpm for 10 minutes at room temperature and centrifuged at 2000 g for 5 seconds. The reaction was quenched with 8 µL 5% hydroxylamine shaking for 5 minutes at 1400 rpm at room temperature. Excess reagent was washed away once with 1.3 mL and twice with 1.5 mL HS IAP Wash buffer (containing 0.01% CHAPS). After washing, each of the TMT

labelled samples were individually resuspended in 90 µL HS IAP Wash Buffer (containing 0.01% CHAPS) and combined whilst still bound to the beads. The beads were mixed and allowed to settle on a magnetic rack where the supernatant was then removed. The original tubes were serially washed with 1.5 mL HS IAP Wash Buffer (containing 0.01% CHAPS) to collect any remaining beads, and this wash was added to the final sample. Two final washes with 1.5 mL LC-MS grade water (85189, Thermo Scientific, USA) were performed. TMT-labelled enriched peptides were eluted from the beads with 50 µL 0.15% TFA for 10 minutes on a thermomixer at 500 rpm at room temperature. Samples were centrifuged at 2000 g for 5 seconds and placed on a magnetic rack. The solution containing the eluted peptides were transferred to a 0.5 mL LoBind tube. The elution process was repeated and both eluates were combined.

Peptide desalting: diGly-enriched peptides were dried down using a SpeedVac Concentrator plus (12884952, Eppendorf, Germany). Peptides were cleaned by a 10 µL C18 stage tip (single 16g punch of Empore C18, 66883-U, USA). Tips were activated with 10 µL of 100% ACN, and twice with 10 µL 0.1% TFA. Vacuum concentrated diGly-modified peptides were solubilised in 10 µL of 2% ACN, 0.1% TFA and passed through a stage tip twice at 500 x g, washed twice with 10 µL of 0.1% TFA and eluted in 50% ACN, 0.1% TFA. Eluted peptides were vacuum dried and resuspended in 12 µL of 5% ACN, 0.1% FA.

LC-MS analysis: 5 µL of TMT-labelled diGly-enriched peptides were analysed and acquired using a Orbitrap Eclipse MS (Thermo Scientific, USA) coupled with a Dionex UltiMate 3000 nanoHPLC system (Thermo Scientific, USA). Peptides were separated on a reversed-phase nanoLC column (450 mm × 0.075 mm; ReprosilPur C18AQ, Dr Maisch, 3 µm particles, Germany) at 40 °C using a 300 minute gradient of 2-35% ACN, 0.1% FA with a flow rate of 300 nl/min. Mass spectra were acquired with FAIMS at -45, -55, -65, -75, and by: MS^1 - 120000 resolution, maximum injection time 50ms, AGC target 400000; MS^2 HCD fragmentation,

isolation window 0.7 m/z, collision energy 38%, 50000 resolution, maximum injection time 200 ms, AGC target 125000.

5.3.7 Data processing

LC-MS raw files were processed with Proteome Discoverer software v.2.5 (Thermo Scientific, USA). Spectra were searched using SequestHT (v.2.0.0.24), with Percolator (v.2.0). The search was performed against the Mouse UniProt database (Mus musculus, Taxonomy ID=10090, v2022-08-03) and a contaminant protein database provided by the manufacturer (PD_Contaminants_2015_5.fasta). Search criteria were set for a maximum of 2 missed cleavage sites, peptide length range of 6 to 144, a precursor mass tolerance of 10 ppm and a fragment mass tolerance of 0.02 Da. For whole peptides search, cysteine carbamidomethylation and lysine/N-termini TMT-labels were set as fixed modifications whilst methionine oxidation, N-terminal acetylation, N-terminal methionine loss and N-terminal methionine loss + acetylation were set as variable modifications. For diGly-modified peptides search, cysteine carbamidomethylation was set as fixed modifications, whilst methionine oxidation, lysine diGly remnant, lysine/N-termini TMT-labels, N-terminal acetylation, N-terminal methionine loss and N-terminal methionine loss + acetylation were set as variable modifications. Proteome Discoverer was used to determine peptide spectral match (PSM) intensity values.

5.3.8 Statistical analysis

Statistical analysis of the proteomics dataset was performed using MSstatsTMT, an open-source R/Bioconductor package [234]. Briefly, global median normalisation (equalising the medians across all the channels) was performed on log2 transformed PSM intensity values. Resulting values were then summarised to protein values using the default MSstats method,

which first imputes missing values with accelerated failure time model and then performs protein-level summarisation using Tukey's median polish. Differential abundance analysis of each protein between ages was calculated by a linear mixed-effects model using a pairwise contrast matrix with empirical Bayes inference. Resulting *P* values adjusted for multiple hypothesis testing by the Benjamini–Hochberg FDR procedure. We determined significantly enriched proteins using the criteria of adjusted *P* value < 0.05. To determine age-by-sex effects, we unlogged the protein abundance values and compared each old replicate against every young replicate within sex, resulting in nine ratios for each protein. These ratios were log2 transformed a pairwise comparison between sex was performed using a Limma moderated t-test with empirical Bayes inference. We determined significantly enriched proteins using the criteria of adjusted *P* value < 0.05. To focus on those proteins most likely to be true sex-specific age effects, we also applied a -0.5 > log2FC > 0.5 cut-off. Of note, we did encounter proteins that were only identified in one dataset which were removed from this analysis.

Statistical analysis of the ubiquitylomics dataset was performed using MSstatsPTM, an open-source R/Bioconductor package [235]. Briefly, global median normalisation was performed on log2 transformed PSM intensity values from both ubiquitylomics and proteomics datasets separately. Resulting values of the ubiquitylomics dataset were then summarised up to the peptide level whilst the proteomics dataset was summarised up to the protein level. For this process, we did not employ missing value imputation before Tukey's median polish summarisation. Differential abundance analysis of each diGly-modified peptide was calculated by a linear mixed-effects model using a pairwise contrast matrix with empirical Bayes inference. Model-based inferences regarding the diGly-modified peptide and the total protein abundances were combined, and diGly-modified peptide values were adjusted for changes in overall protein abundance. We determined significantly enriched proteins using the criteria of

P value < 0.05. This was selected over the adjusted *P* value due to high CV values which meant the Benjamini–Hochberg correction was too stringent.

5.3.9 Data visualisation

Data was visualised using R software (v4.4.1) with RStudio (v2024.04.2) and GraphPad Prism (v.10). For volcano plots, we used -0.3 > log2FC > 0.3 cut-off which has been used in TMT-based quantification to adjust for ratio compression [231]. GSEA was performed on ranked proteins (based on fold change values) to determine enrichment of Gene Ontology terms by cellular compartment using WEB-based GEne SeT AnaLysis Toolkit (WebGestalt) online tool [204]. Functional network analysis was performed with STRING (v.12). MitoCarta 3.0 inventory was used for categorising proteins to mitochondrial pathways [236]. Proteostasis human consortium network (v2.0) was used for categorising components of proteostasis. Epithelial Systems Biology Laboratory (ESBL) was used for obtaining a database of E3 ligases [237] and DUBs [238]. Spliceosome database was used for obtaining spliceosome complex proteins [239]. IBS 2.0 was used to visualise ubiquitylation positioning across Rpl19 [240].

5.4 Results and Discussion

5.4.1 Quantitative analysis of the skeletal muscle proteome and ubiquitylome

Coomassie protein staining and western blots revealed distinct differences in the protein composition of the soluble and insoluble skeletal muscle fractions **(Supplementary Figure 1)**. Western blots confirmed enrichment of sarcoplasmic proteins such as ACC and GAPDH in the soluble fraction, whereas myofibrillar proteins such as MHC and actin were enriched in the insoluble fraction **(Supplementary Figure 1)**. Quantitative analysis of the young and old

muscle proteome and ubiquitylome was performed after confirmation of successful fractionation (**Figure 5.1a**). PCA plots revealed variation by age in both total protein and diGly-modified peptides (**Supplementary Figure 2**). For the male mice, we quantified 4186 proteins and statistical analysis revealed that 523 soluble and 92 insoluble proteins were significantly regulated by age (563 in total when removing overlapping proteins), indicating that 13.5% of the detectable muscle proteome was affected by age (**Figure 5.1b**). Among the significantly regulated proteins also exhibiting an absolute Log2FC > 0.3, 75% from soluble fraction and 87% from insoluble fraction were upregulated. This indicates that most age-related proteins are increased in old relative to young mice which aligns with previous proteomics findings in human skeletal muscle [30], [31], [241]. For the female mice, we quantified 3194 proteins and statistical analysis revealed only 20 were significantly regulated (1 soluble and 19 insoluble proteins), which is less than 1% of the detectable proteome (**Figure 5.1b**). Previous studies have reported less age-related changes in female mice at both the gene and protein level [242], [243]. We believe the dramatically lower significance, particularly in the soluble fraction, has arisen from a greater variability in the old mice, as displayed in the PCA plots. Our ubiquitylomics workflow identified 1548 and 845 diGly-modified peptides in male and female mice, respectively (**Figure 5.1c**), but given the higher degree of variability between replicates we were not able to identify statistically significant results. However, without multiple testing corrections, 127 and 67 diGly-modified peptides were significantly regulated by age in male and female mice, respectively (**Supplementary Figure 3**).

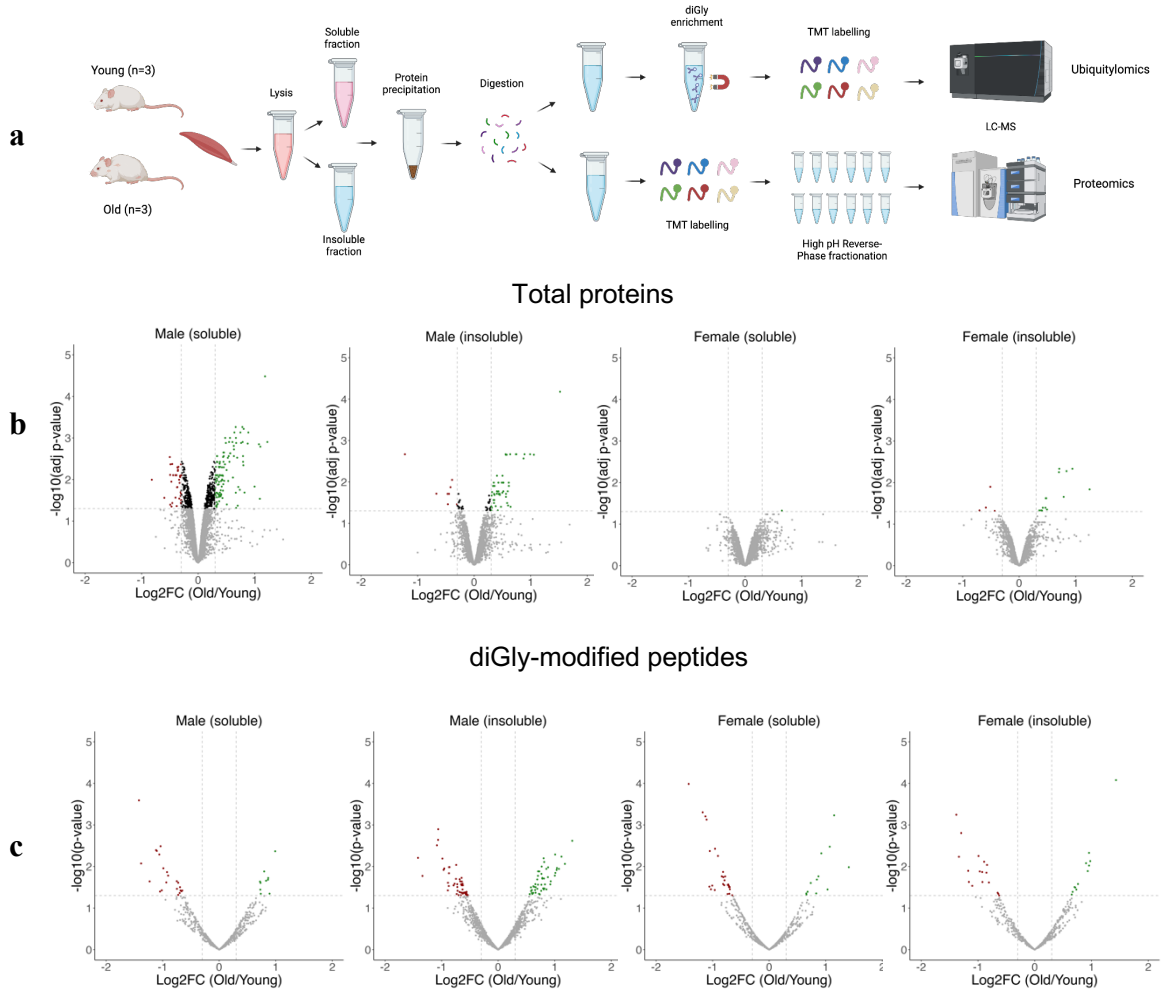

Figure 5. 1. Coverage of the ageing muscle proteome and ubiquitylome. a) Overview of proteomics and ubiquitylomics workflow which was performed separately for male and female mice. b) Volcano plot from both soluble and insoluble male and female proteome showing the Log2FC (Old/Young) plotted against the –Log10 adjusted *P* value highlighting significantly regulated proteins (green: Log2FC > 0.3 & adjusted *P* value < 0.05, red: Log2FC < 0.3 & adjusted *P* value < 0.05). c) Volcano plot from both soluble and insoluble male and female ubiquitylome showing the Log2FC (Old/Young) plotted against the –Log10 *P* value highlighting significantly regulated peptides (green: Log2FC > 0.3 & *P* value < 0.05, red: Log2FC < 0.3 & *P* value < 0.05).

5.4.2 Biological functions of age-related proteins

GSEA of the male and female proteomics data revealed several cellular compartments affected by age-related protein changes (**Figure 5.2).** We identified overrepresented compartments (FDR ≤ 0.05) in both sexes (extracellular matrix, nuclear spliceosome and plasma membrane), male only (endoplasmic reticulum, contractile fibres, actin cytoskeleton and secretory granule)

and female only (endosomes and apical membrane). Consistently across both fractions, mitochondrial proteins were underrepresented in both male and female mice. STRING analysis of protein-protein interaction networks performed on significantly regulated male proteins revealed notable changes in enzymatic networks in the soluble fraction **(Supplementary Figure 4a)**. Mitogen-activating protein kinases and phosphorylase kinases were downregulated in older muscle as were enzymes involved in glycolysis and AMP metabolism. In contrast, key enzymes promoting nucleotide metabolism and fatty acid oxidation were upregulated. Moving forward, we investigated the enriched biological pathways in more detail, combining the ubiquitylomics data to outline potential mechanisms of ageing skeletal muscle that are worth investigating further.

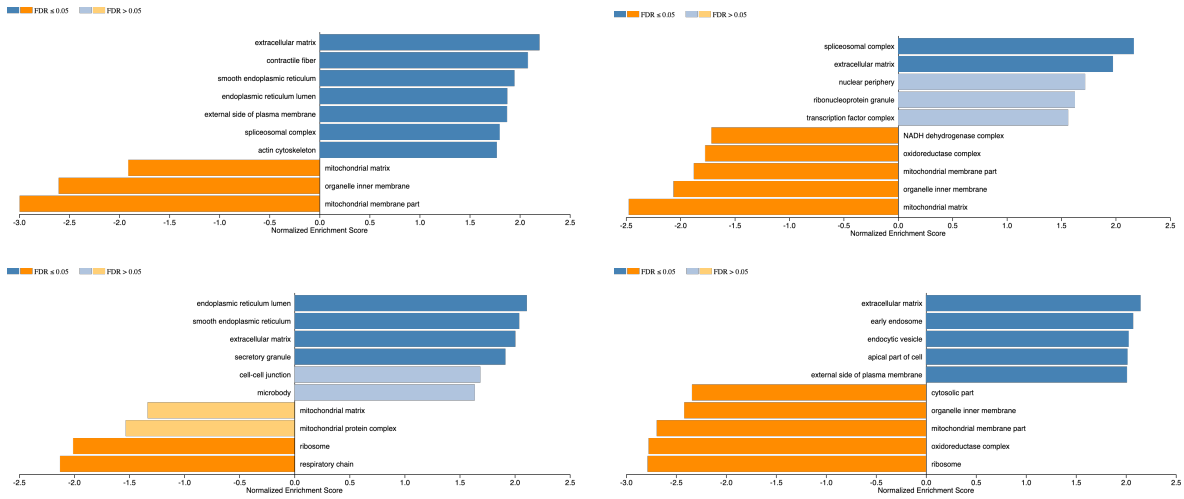

Figure 5. 2. Enriched terms of the ageing skeletal muscle proteome. GSEA from both soluble (upper) and insoluble (lower) male (left) and female (right) proteome, highlighting enriched cellular compartments from Gene Ontology analysis.

5.4.3 Increased extracellular matrix proteins

The extracellular matrix surrounds muscle fibres, important for force transmission, structural support and muscle regeneration. Older mice displayed an increase in extracellular matrix protein abundance in both fractions across both sexes (**Supplementary Figure 5**). We identified large fold change increases with age in different collagen proteins across both fractions, with Col6a1 significantly increasing in both sexes (**Figure 5.3a**). Given that collagen proteins increase in the soluble muscle fraction of older mice, the accumulation of these proteins is not likely caused by aggregation, a concept previously reported in ageing muscle [23], [244]. Small leucine-rich proteoglycans (SLRPs), regulate collagen fibrillogenesis during extracellular matrix remodelling [245]. Previous work has shown an age-increase in SLRPs in skeletal muscle of male mice [246]. We identified an increase in SLRP protein abundance in both males and females, particularly in asporin (Aspn) which was significantly increased in both sexes (**Figure 5.3b**). Of note, we also identified age-related increases in SPARC-related modular calcium-binding protein 2 (Smoc2), particularly in male mice (**Figure 5.3c**). Increased Smoc2 impairs muscle stem cell functionality and has previously been reported in skeletal muscle of older male, not female, mice [231], [243], [247]. We did not detect any significant changes in extracellular matrix diGly-modified peptides, so the protein changes appear independent of ubiquitylation.

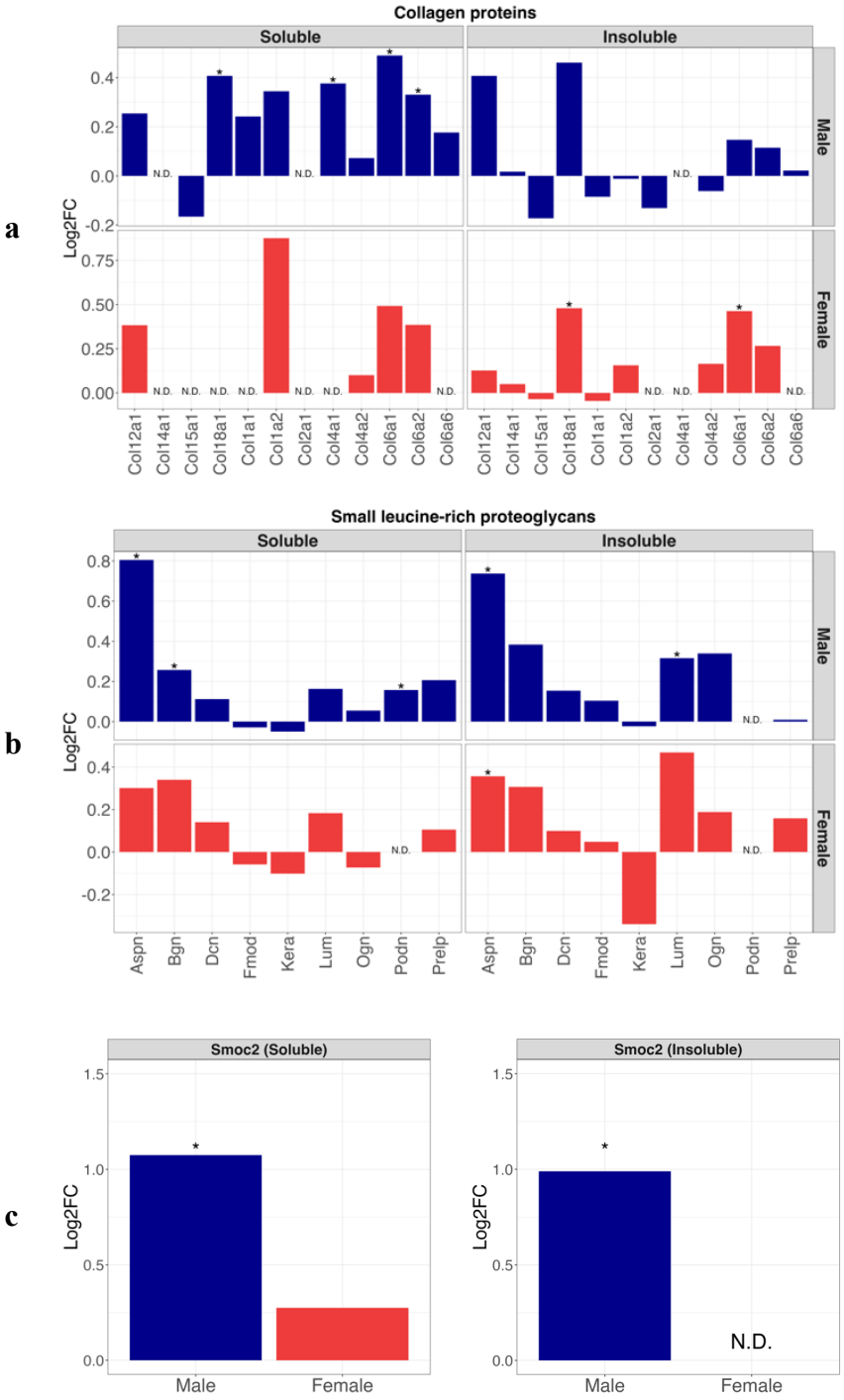

Figure 5. 3. Increased abundance of extracellular matrix proteins. Bar plot showing the Log2FC (Old/Young) values for a) collagen proteins and b) small leucine rich proteoglycan proteins, detected in the soluble and insoluble fraction of male and female mice. Statistically significant proteins (adjusted *P* value < 0.05) between young and old muscle were marked with an asterisk (*). N.D. = not detected., c) Smoc2 protein detected in the soluble and insoluble muscle fraction of male and female mice. Statistically significant proteins (adjusted *P* value < 0.05) between young and old muscle were marked with an asterisk (*).

5.4.4 Decreased mitochondrial ribosomes

The decline of mitochondrial function is a key hallmark of ageing, and is a prominent feature of ageing skeletal muscle [19]. In both male and female mice, we detected an age-related trend decline in mitochondrial proteins in skeletal muscle (**Supplementary Figure 6)**. In male mice this trend was significant, especially in the soluble fraction whereby 51 out of the 67 significantly regulated proteins were downregulated with age.

To investigate which mitochondrial proteins were most affected by age in male mice, we took advantage of the MitoCarta 3.0 inventory which categorises mitochondrial proteins by their pathways. For each pathway, we quantified the number of proteins that were upregulated, downregulated, or unchanged with age in the soluble fraction **(Supplementary Figure 7a)**. Mitochondrial proteins involved in metabolism and the central dogma accounted for nearly 75% of all downregulated mitochondrial proteins in the soluble fraction of male mice **(Supplementary Figure 7a)**. Whilst 13 mitochondrial proteins involved in metabolism were also upregulated, Apex1 was the only central dogma protein that significantly increased with age **(Supplementary Figure 7a)**. The mitochondria central dogma is involved in the translation of mitochondrial DNA (mtDNA) to protein [248]. In older male mice, 60% of the downregulated proteins in the central dogma were mitochondrial ribosomes. Most mitochondrial ribosomes identified in male mice had a negative fold change value and all significantly regulated mitochondrial ribosomes were downregulated in both fractions **(Figure 5.4a)**. The female mice exhibited a similar trend of decreasing mitochondrial ribosomal proteins in both muscle fractions, emphasising their age-related reduction in skeletal muscle **(Figure 5.4a)**.

Mitochondrial ribosomes express a distinct set of proteins which make up part of the oxidative phosphorylation complex. In both male and female mice, we identified 11 of the 13 mitochondrial expressing proteins. Across both muscle fractions we saw a general age-related decline in these proteins across males and females, with Mtco2 (Complex IV) significantly decreasing in the male soluble fraction **(Figure 5.4b)**. When blotting for the oxidative phosphorylation complex, we found a significant reduction in Mtco1 (Complex IV) in the soluble fraction of both male and female mice **(Supplementary Figure 7b)**. Work by others have suggested that reduced translation of mtDNA in older muscle is caused by less engagement with the mitochondrial ribosomes [249]. Our results suggest that the decline in mitochondrial ribosomal proteins may also contribute to the reduction in mtDNA translation.

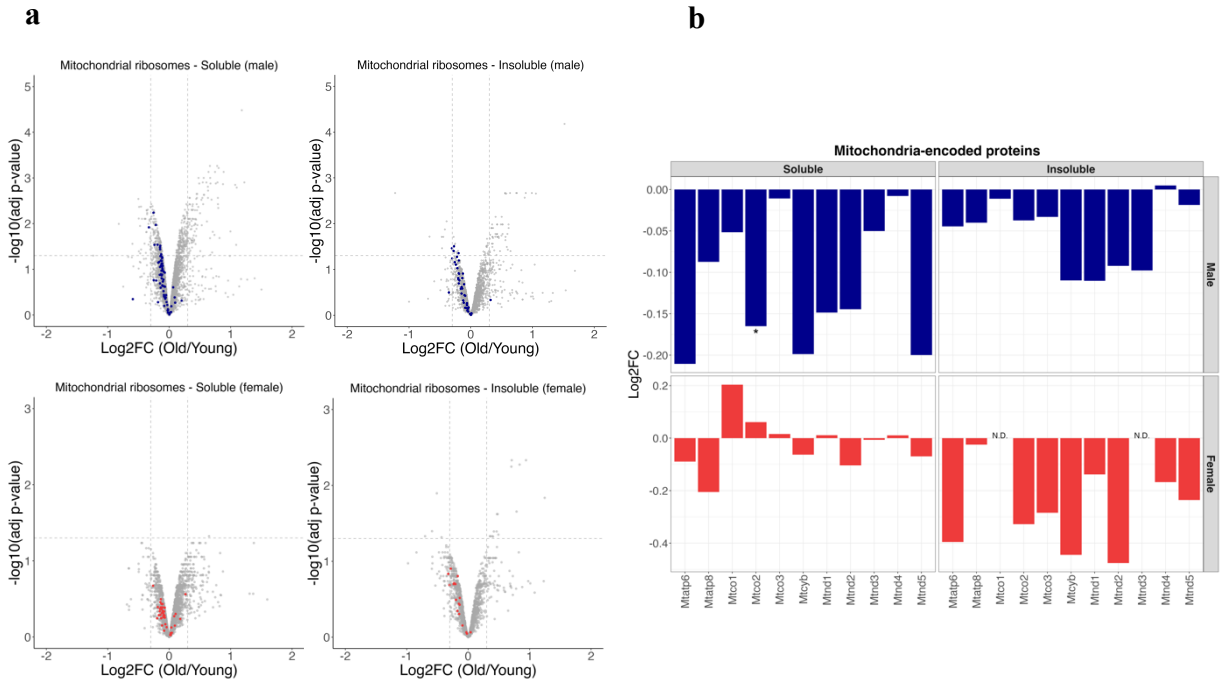

Figure 5. 4. Decreased abundance mitochondrial ribosomes and encoded proteins. a) Volcano plot highlighting mitochondrial ribosome proteins (Blue) in the soluble and insoluble muscle fraction of male and female mice. Log2FC (Old/Young) plotted against the –Log10 adjusted *P* value. b) Barplots displaying the Log2FC (Old/Young) values of mitochondrial-encoding proteins in the soluble and insoluble muscle fraction of male and female mice. Statistically significant fold change values (adjusted *P* value < 0.05) are marked with an asterisk (*).

5.4.5 Decreased ubiquitylation of oxidative phosphorylation complex

We found a general decline in diGly-modified peptides from mitochondrial proteins. After adjusting for changes in total protein abundance, 22 mitochondrial diGly-modified peptides remained significant in either fraction of which 10 and 9 were downregulated in older males and females, respectively (**Figure 5.5**). Downregulated diGly-modified peptides were found on voltage-dependent anion channels – Vdac1 (K33) and Vdac2 (K40, K73), and solute carrier proteins – Slc25a3 (K290) and Slc25a4 (K43, K166) (**Figure 5.5**). These proteins allow substrates of oxidative phosphorylation to be transported through the outer membrane, across the inner membrane and into the matrix compartment [250], [251]. One diGly-modified peptide was downregulated in Idh3a (K58) (**Figure 5.5**), a crucial enzyme linking products of the TCA cycle to oxidative phosphorylation. Another diGly-modified peptide was downregulated in Tbrg4 (K442) (**Figure 5.5**), a protein which stabilises mitochondrial RNA, thereby affecting the protein expression of mtDNA and subsequently components of oxidative phosphorylation [252]. diGly-modified peptides from oxidative phosphorylation complex proteins were also reduced by age. diGly sites on Atp5po (complex V) (K51, K70), Ndufa4 (complex IV) (K77) and Uqcrfs1 (complex III) (K163) decreased with age (**Figure 5.5**). Interestingly, two diGly sites were altered on Uqcrc2 (complex III), one decreased in the insoluble fraction (K98), but the other increased in the soluble fraction (K92) (**Figure 5.5**). Taken together, there appears to be an age-effect of reduced ubiquitylation on proteins involved in oxidative phosphorylation.

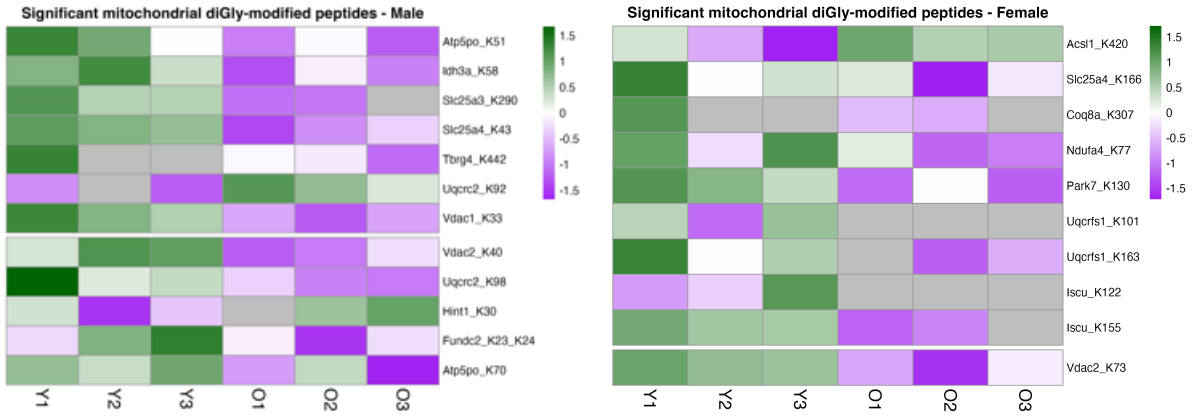

Figure 5. 5. Downregulation of diGly-modified mitochondrial proteins. Heatmap displaying Log2 abundance values scaled by z-scoring of significantly regulated diGly-modified peptides belonging to the mitochondria (including those only found in one age category). Grey colour represents missing values, and break divides soluble fraction (upper) from insoluble fraction (lower).

5.4.6 Altered lipid and glucose metabolism

Three proteins (Hadha, Hadhb and Acss1) involved in mitochondrial fatty acid oxidation metabolism were significantly upregulated in male mice **(Figure 5.6a and Figure 5.6b)**. All 3 are enzymes which help to produce acetyl-CoA through the breakdown of fatty acids, which can be used in the TCA cycle for energy production. In agreement with our findings, Hadha and Hadhb protein abundance has previously been reported to be greater in human and mouse skeletal muscle of older subjects [29], [30]. The increased abundance of Hadha, Hadhb and Acss1 might be a compensatory adaptive response against the decline in glycolytic enzymes **(Figure 5.6c)**, shifting away from glucose metabolism to a greater reliance on lipid metabolism. In female mice, we detected the same trend decline in glycolytic enzymes without an increase in mitochondrial fatty acid oxidation proteins **(Figure 5.6a and Figure 5.6c)**. Of note, we did observe increased diGly modification of Acsl1 (K420) in the soluble muscle fraction of female mice (**Figure 5.5**). Acsl1 catalyses long-chain fatty acids to acyl-CoAs which can be used for fatty acid oxidation. In both sexes there was a significant increase in Acox1, a protein that aids in fatty acid oxidation within the peroxisome. As this process is not

directly involved in ATP generation, this response might serve a different purpose in dealing with accumulation of intramuscular lipids commonly observed in aged muscle [253], [254]. Together, these changes in total and ubiquitylated proteins offer potential mechanisms of muscle lipid metabolism changes with age.

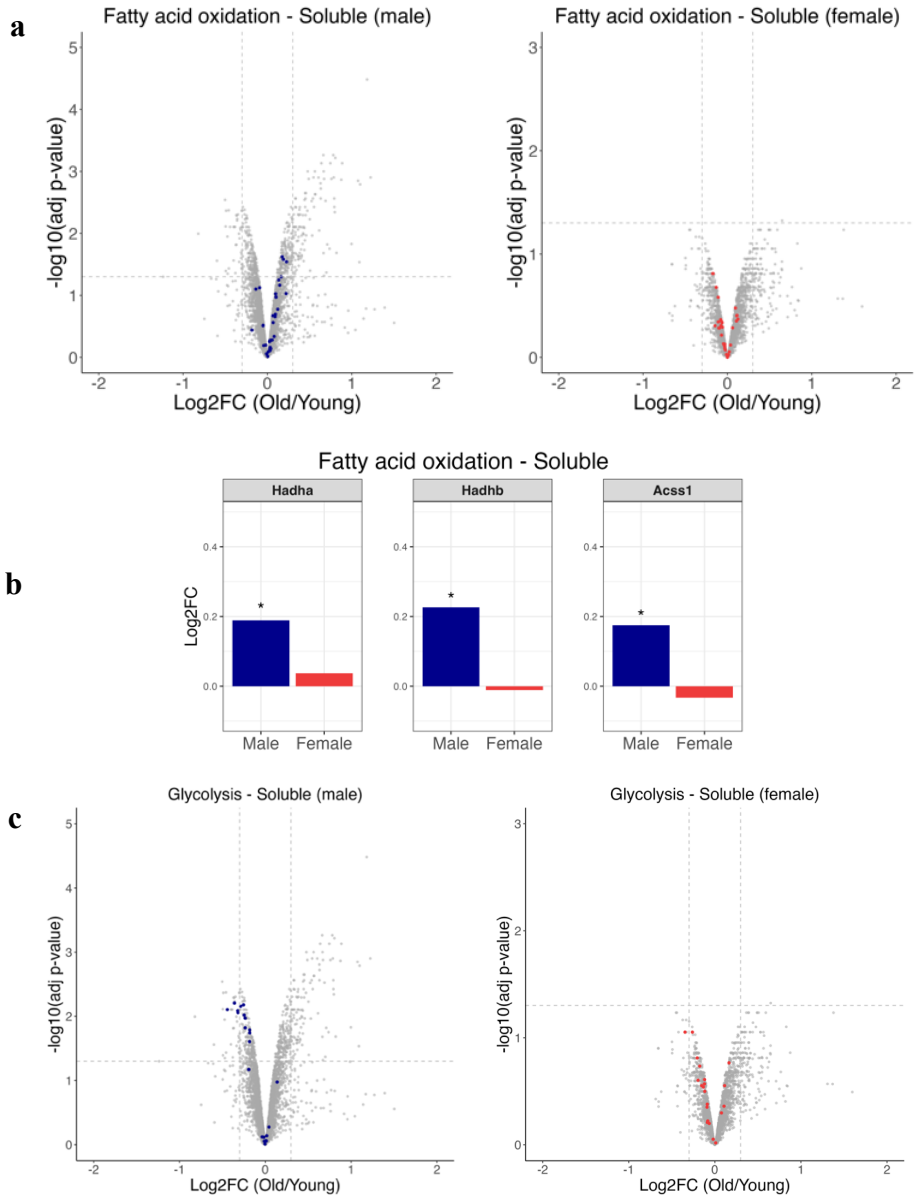

Figure 5. 6. Abundance of proteins involved in lipid and glucose energy metabolism. a) Volcano plot highlighting fatty acid oxidation proteins (MitoCarta 3.0) in the soluble fraction of male (blue) and female (red) mice. Log2FC (Old/Young) plotted against the –Log10 adjusted *P* value.. b) Bar plot showing the Log2FC (Old/Young) values for Hadha, Hadhb and Acss1 detected in the soluble fraction of male and female mice. Statistically significant changes (adjusted *P* value < 0.05) in protein abundance levels between young and old muscle were marked with an asterisk (*). C) Volcano plot highlighting glycolysis-regulating proteins in the soluble fraction of male (blue) and female (red) mice. Log2FC (Old/Young) plotted against the –Log10 adjusted *P* value.

5.4.7 Decreased histone H2B ubiquitylation

Histone modifications including acetylation, methylation and ubiquitylation play essential roles in DNA organisation and epigenetic regulation, and have been implicated in lifespan regulation [255]. In the insoluble fraction of both male and female mice, there was a stark age-reduction in the diGly-modification of histone H2B type 1-K (H2bc12) at lysine (K) 121 (**Figure 5.7a**). The sequence of this peptide (AVT**k**YTSAK) occurs at the C-terminus and shares 100% alignment with histone H2B type 2-E (H2bc21) but differs from most H2B isoforms which contain alanine-to-serine swap at the penultimate amino acid [256]. To verify that the correct sequence has been assigned, we analysed MS2 spectra for AVT**k**YTSAK and AVT**k**YTSSK (**Supplementary Figure 8**). The fragmented TMT reporter ions show a reduced abundance of AVT**k**YTSAK in the older sample, which was not evident for AVT**k**YTSSK. Therefore, the age-related decline in histone H2B ubiquitylation at K121 is specific for the H2bc12/H2bc21 isoform. Of note, we did not quantify an unmodified peptide unique to H2bc12, which meant we could not determine the abundance of H2bc12 total protein. Therefore, we cannot discount the possibility that H2bc12 protein levels also decreased.

Histone H2B ubiquitylation at site K121 is important for transcriptional activation and DNA damage repair [257], [258]. Not much is known about the role of histone H2B K121 ubiquitylation in skeletal muscle, although it is reduced during myogenic differentiation [259]. However, these studies do not differentiate between histone H2B isoforms, so it is difficult to know if K121 ubiquitylation on H2bc12 has the same effect. Interestingly, ubiquitylation of the mammalian histone H2B K121 homolog in yeast (K123) and *Drosophila* (K118) has been reported to increase with age [173], [260]. However, neither organism contains H2B isoforms with the serine-to-alanine swap, so their findings are not based on H2bc12 (**Figure 5.7b**). To

our knowledge, we are the first study to show age-related decrease in H2B K121 ubiquitylation in specific isoforms containing a penultimate alanine amino acid.

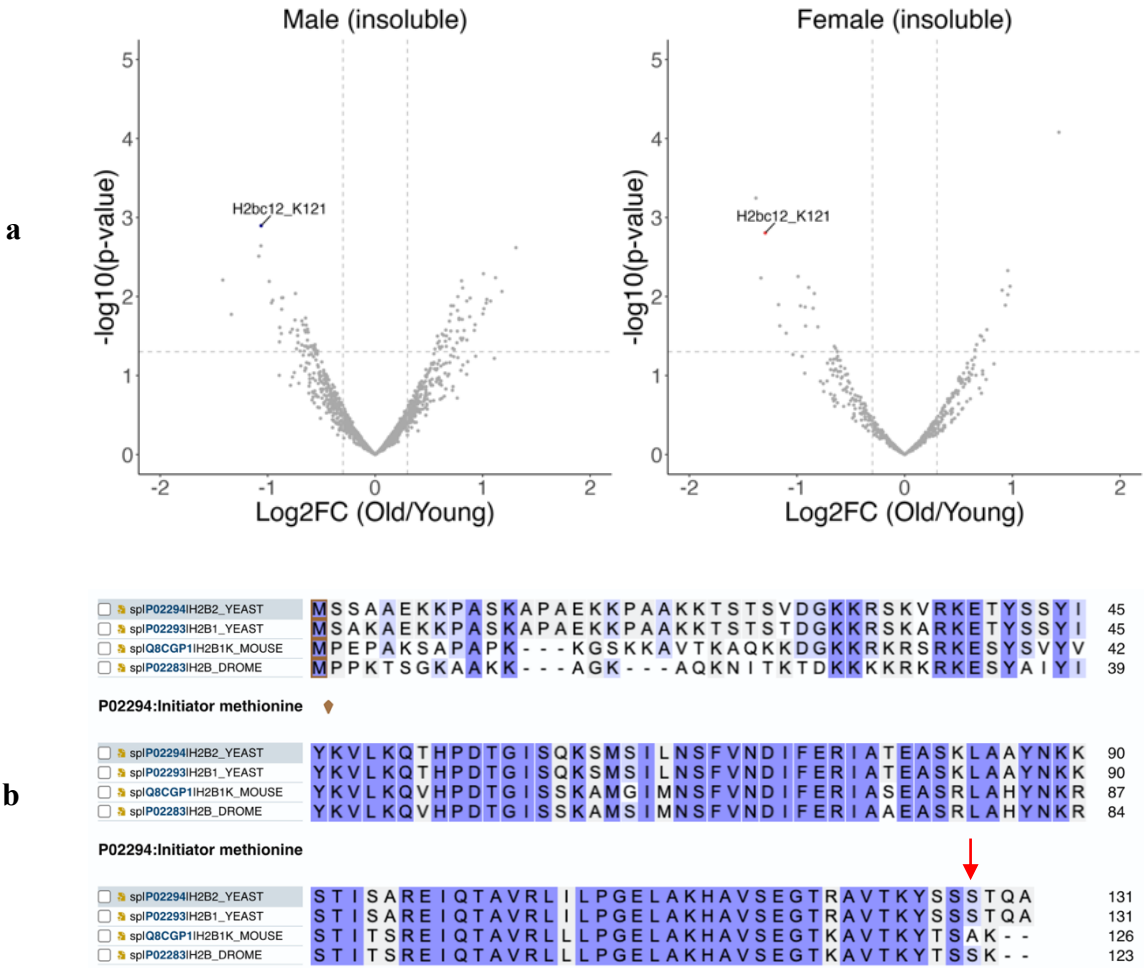

Figure 5. 7. Effect of age on Histone H2B isoform-K (H2bc12) ubiquitylation in males and females. a) Volcano plot from both male (left) and female (right) insoluble ubiquitylome showing the Log2FC (Old/Young) of diGly-modified peptides plotted against the –Log10 P value. H2bc12 diGly-modified peptide at site K121 is highlighted. b) UniProt peptide alignment comparing the H2bc12 isoform in mice (H2B1K) to the H2B isoforms in yeast and *Drosophila.* Red arrow indicates the sequence variation in either serine or alanine amino acid.

5.4.8 Increased solubility of sarcomeric proteins

Although inherently insoluble, myofibrillar proteins can appear in the soluble fraction when they detach from the sarcomere, observed prior to their degradation [261]. In older male

muscle, sarcomeric proteins belonging to the contractile fibre and actin cytoskeleton were enriched in the soluble fraction only of male mice (**Figure 5.2**). These findings encouraged us to identify age-related sarcomeric proteins and compare their fold change values across both muscle fractions.

In male mice, the soluble fraction exhibited a significant enrichment of 20 sarcomeric proteins with age, compared with 8 in the insoluble fraction (**Figure 5.8a**). In female mice, despite an age-related trend increase in muscle proteins in the soluble fraction, the only significant changes came from increases in the insoluble fraction. Proteins exclusively enriched in the soluble fraction of male mice included structural components of the Z-disk (Actn2, Actn3, Myoz1, Nebl, Pdlim5 and Tcap) and contractile components (Myh1, Myh3, Myl3, Mybpc2, Tnnt3 and Tpm2) (**Figure 5.8b**).

We hypothesised that age-related increases in soluble contractile and structural proteins are likely damaged or dysfunctional and need to be degraded. Given the role of ubiquitylation for signalling damaged proteins for degradation, we anticipated that soluble sarcomeric proteins increasing with age, would also display increased diGly-modifications. Interestingly, after adjusting for changes in total protein abundance, no diGly-modified peptides from sarcomeric proteins significantly increased in the soluble fraction, albeit diGly-modified peptides from Nrap (K192) and Flnc (K1832) were only detected in the soluble fraction of older mice suggesting their ubiquitylation increased by age. In fact, we found no correlation between age-related abundance of soluble sarcomeric proteins and their diGly-modification in males or females **(Figure 5.8c)**. The absence of a clear relationship between protein and ubiquitylation abundance has previously been observed during skeletal muscle atrophy [143]. Under the assumption that soluble sarcomeric proteins are damaged and detrimental for muscle

proteostasis, our results suggest less efficient targeting for ubiquitin-mediated degradation in older mice. However, it is also plausible that soluble sarcomeric proteins are not degradation-borne, for instance they could be newly synthesised proteins awaiting incorporation into the sarcomere during myofibrillogenesis.

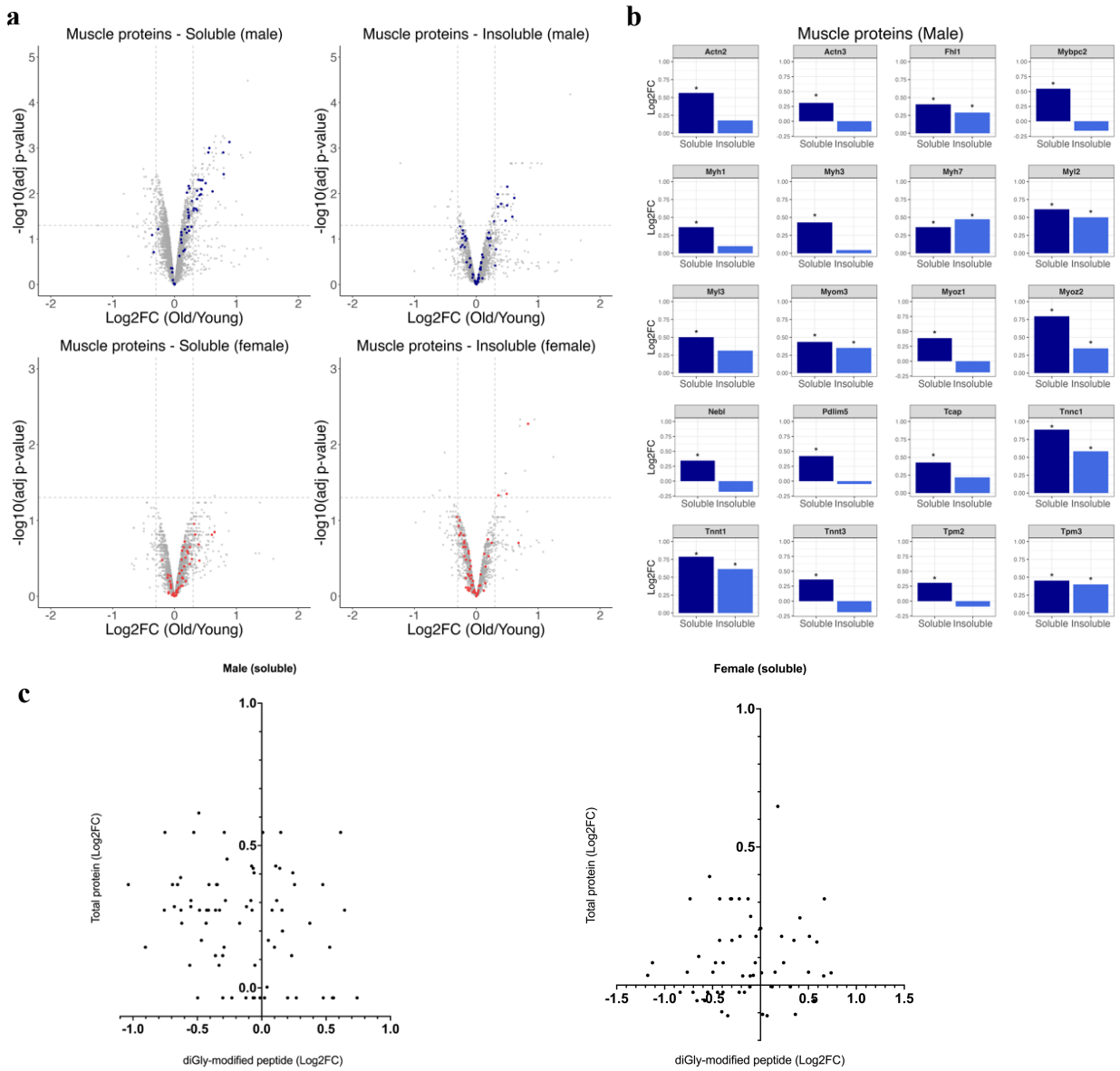

Figure 5. 8. Alterations in the abundance of total and ubiquitylated sarcomeric proteins with age. a) Volcano plot highlighting skeletal muscle proteins from the soluble and insoluble fraction of male (blue) and female (red) mice, showing the Log2FC (Old/Young) plotted against the –Log10 adjusted *P* value. b) Bar plot showing the Log2FC (Old/Young) values for muscle proteins that passed the significance (adjusted *P* value < 0.05) and fold change cut-off (absolute Log2FC value > 0.3) in the soluble fraction of male mice and their respective values in the insoluble fraction. Statistically significant proteins between young and old muscle were marked with an asterisk (*). c) Log2FC (Old/Young) values of contractile and structural proteins and their diGly-modified peptides in the soluble fraction of male or female mice.

5.4.9 Alterations in splicing and translational machinery

The nuclear spliceosome is a complex array of proteins responsible for pre-mRNA splicing, required for generating mature, functional mRNA molecules ready for translation into proteins. Previous studies in ageing human skeletal muscle have shown increases in spliceosome complex proteins [30], [31]. Our results also show an age-related increase in spliceosome components in the soluble fraction of both male and female mice (**Figure 5.9a and Figure 5.9b**). Alternative splicing has been implicated in muscle fibre senescence, so increased spliceosome proteins may contribute to the ageing phenotype of skeletal muscle [262]. Ribonucleoproteins are heavily involved in RNA processing [263]; we found many spliceosome proteins increasing with age belong to either the small or heterogenous ribonucleoproteins (**Figure 5.9c)**. It has previously been reported that aged mice possess more alternative spliced genes than younger counterparts [264], which could be driven by age-related increases in ribonucleoproteins.

Ribosomal proteins are the cells machinery for synthesising mature mRNA into new proteins. Whilst we were able to quantify over 82 cytosolic ribosome subunit proteins across both males and females, only four were significantly regulated by age, all of which increased in the soluble fraction of male mice (Rps7, Rps27a, Rpl19 and Rpl22) (**Supplementary Figure 9**). Rpl22 displayed the largest fold change increase of any ribosomal subunit in the soluble fraction of female mice. Rpl22 has been reported to suppress its paralog Rpl22l [265], and whilst this protein was detected in female mice, it was not reduced in the old cohort. The insoluble fraction of male mice did not display any clear changes in ribosomes, whereas in the female mice there was an age-related trend decline (**Supplementary Figure 9**). An age-related decline of ribosome proteins has previously been reported in human skeletal muscle [31]. Across both males and females, we were able to quantify 50 diGly-modified peptides from 28 cytosolic

ribosome subunits, 7 of which were significantly regulated by age in male mice only. Notably, four of the five diGly-modified peptides quantified on Rpl19 were significantly downregulated with age in male mice (all located towards the C-terminus) (**Figure 5.9d**). Rpl19 diGly-modification at K186 was decreased in the soluble fraction along with an increase in total protein, suggesting this site may regulate ubiquitin-mediated degradation of Rpl19.

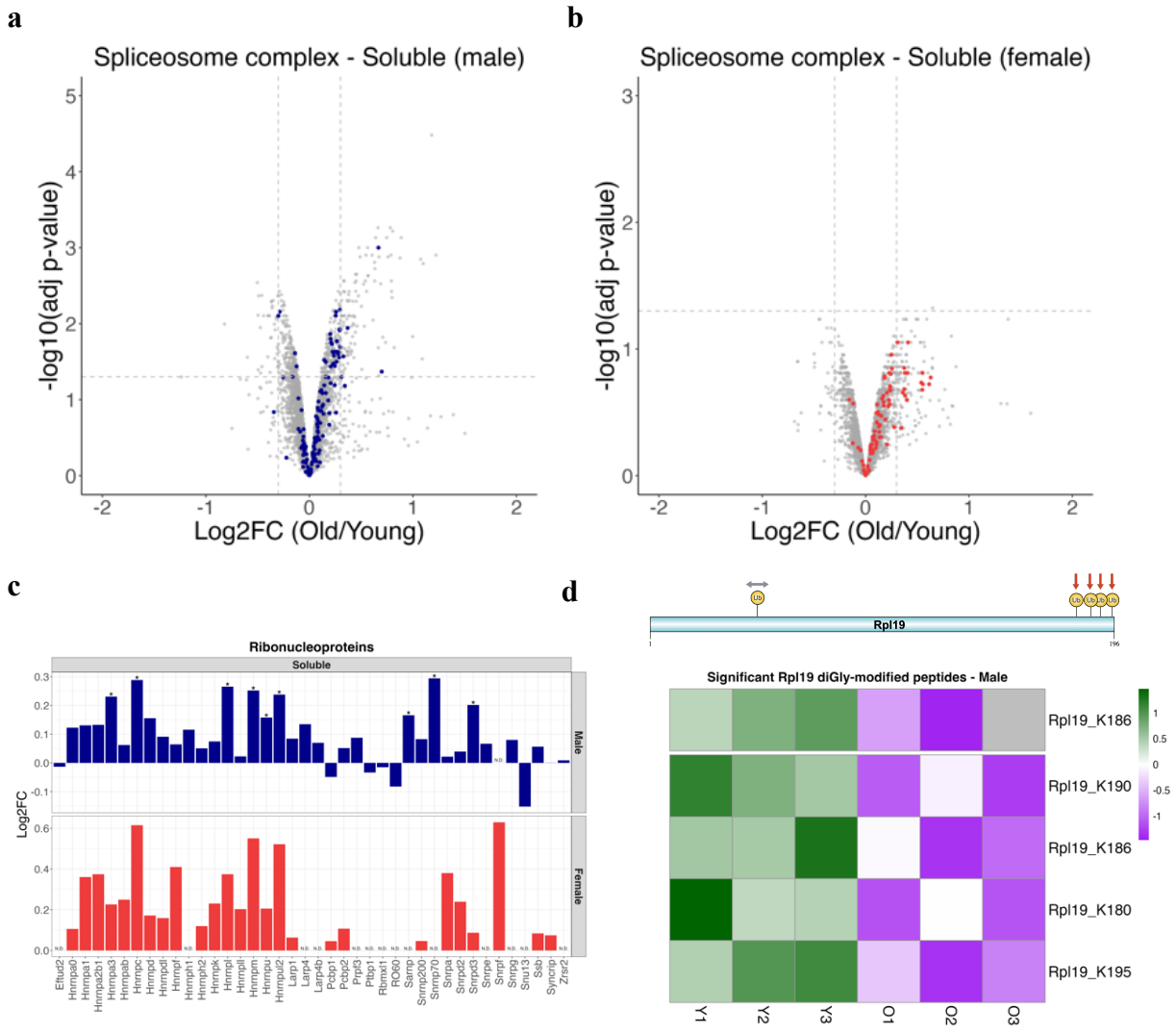

Figure 5. 9. Alterations in the abundance of spliceosome and ribosome proteins. Volcano plot highlighting spliceosome proteins (Orange) from the soluble muscle fraction of a) male and b) female mice, showing the Log2FC (Old/Young) plotted against the –Log10 adjusted *P* value. c) Bar plot showing the Log2FC values for each ribonucleoprotein detected in the soluble muscle fraction of male and female mice. Statistically significant proteins (adjusted *P* value < 0.05) between young and old muscle were marked with an asterisk (*). d) All diGly-modifications identified on Rpl19 (Created with IBS 2.0) with a heatmap displaying Log2 abundance values scaled by z-scoring. Grey colour represents missing values, and break divides soluble fraction (upper) from insoluble fraction (lower).

5.4.10 Increased small heat shock proteins

Chaperones play a critical role in cellular proteostasis, particularly with protein folding. We identified 20 significantly regulated chaperones in the soluble fraction of male mice, 14 of which were upregulated **(Supplementary Figure 10a)**. Heat shock proteins (Hsp) assist in the folding of newly synthesised proteins and refolding mature damaged proteins [266]. 13 of the 15 significantly upregulated chaperones belong to the Hsp family or act as their co-chaperone/nucleotide exchange factor (NEF) inhibitor **(Supplementary Figure 10b)**. The largest family of Hsp's that were upregulated belonged to the Hsp20 family, also known as small heat shock proteins (sHsp). sHsp are a family of ATP-independent chaperones which prevent the formation of larger deleterious aggregates through binding to exposed regions of proteins [267]. Proteomics analysis detected all seven sHsp known to be expressed in muscle, of which four were significantly upregulated in the soluble fraction of aged muscle **(Figure 5.10a)**. The same trend was observed in female mice, of which all seven sHsp's had a positive Log2FC value **(Figure 5.10b)**. Hspb7 and Hspb5 (Cryab) displayed the largest increase in males, which were validated with western blots in both sexes **(Figure 5.10c)**. Hspb7 and Hspb5 (Cryab) are both involved in muscle filament maintenance [268], [269], and have previously shown to increase in aged rat muscle [26]. Increased abundance of these sHsp's support the argument that sarcomeric proteostasis is impaired in age mice, particularly in males.

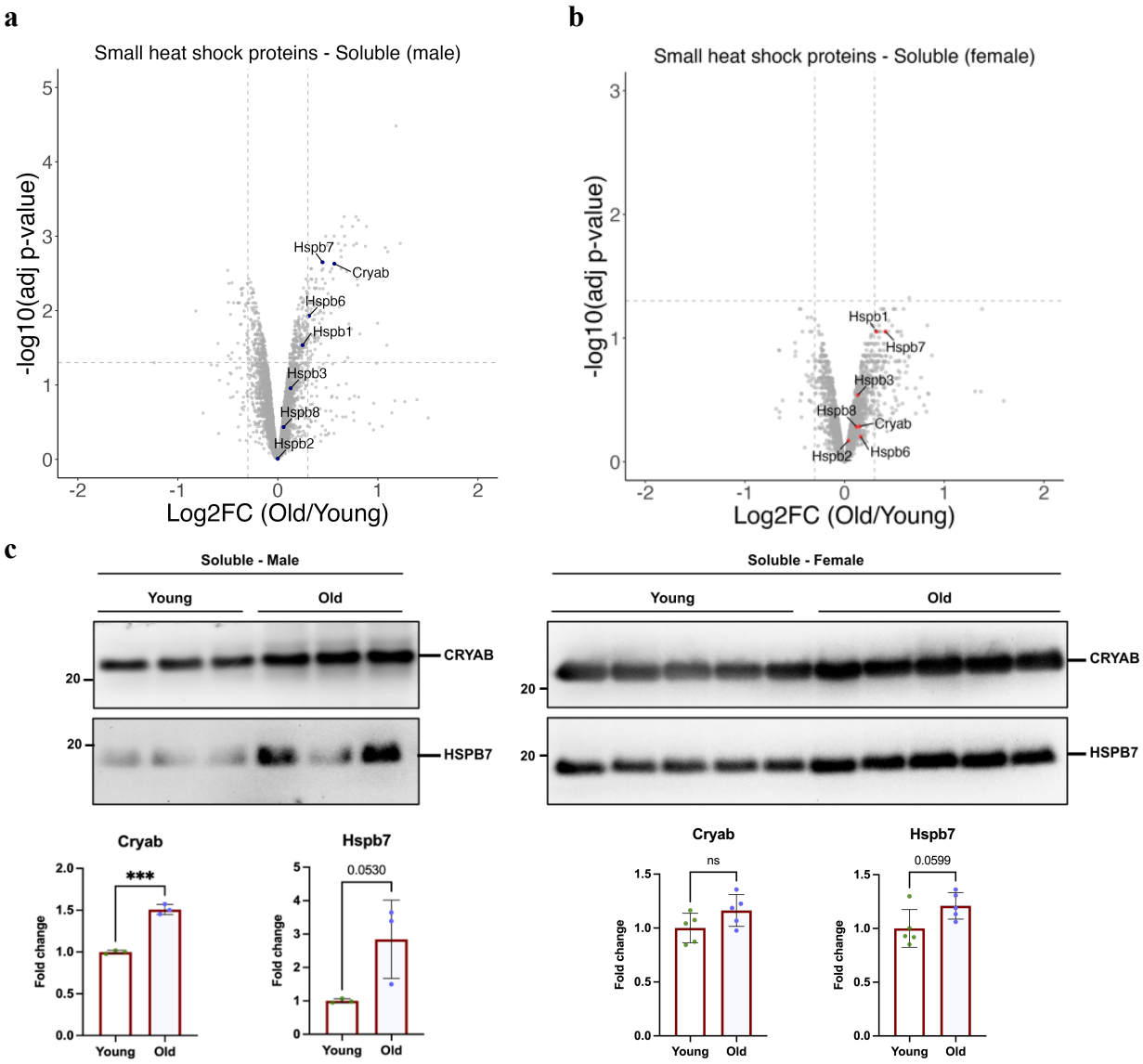

Figure 5. 10. Small heat shock response with age. Volcano plot highlighting small heat shock chaperone proteins (red) from the soluble fraction of a) male and b) female mice, showing the Log2FC (Old/Young) plotted against the –Log10 adjusted *P* value. c) Western blots and quantification of Cryab and Hspb7 protein abundance in young and old skeletal muscle from male (left) and female (right) mice. Data was visualised on GraphPad Prism using unpaired t-test to confirm significance (*** = $P < 0.001$) with standard deviation bars.

5.4.11 Increased unfolded protein response in males

The unfolded protein response (UPR) is a signalling pathway aimed at restoring proteostasis in the endoplasmic reticulum by promoting protein folding, reducing protein synthesis and enhancing proteolysis through ERAD [270]. In older male mice, the master regulator of the

UPR, Hspa5 (also known as BiP), is upregulated along with other endoplasmic reticulum chaperones: Hsp90b1, Calreticulin (Calr) and Hyou1 **(Figure 5.11a)**. Additionally, the family of protein disulfide isomerase (PDI) folding enzymes were also upregulated **(Figure 5.11a)**. This demonstrates that protein folding capacity in the endoplasmic reticulum is enhanced in older male mice, likely responding to impaired proteostasis. In females, these UPR proteins displayed a much smaller degree of change between ages, especially for Pdia1 which we validated with western blotting **(Figure 5.11b)**. In support of this finding, endoplasmic reticulum UPR markers such as PDI and BiP have been previously reported to be a male specific ageing response in mouse skeletal muscle [243]. Proteins assisting in ERAD, such as Bcap31, Erlin2, Ubxn4 (also known as Erasin) and Ube2g2 were also increased in older male mice **(Figure 5.11a)**. Overall, our proteomics data suggests older male mice experience dysregulated proteostasis in the endoplasmic reticulum of skeletal muscle, resulting in the activation of the UPR. Despite no changes in protein levels, female mice did display increased ubiquitylation of VCP/p97 — an ATP-dependent chaperone which can function to promote ERAD — at 3 sites which did not occur in males **(Supplementary Figure 11)**.

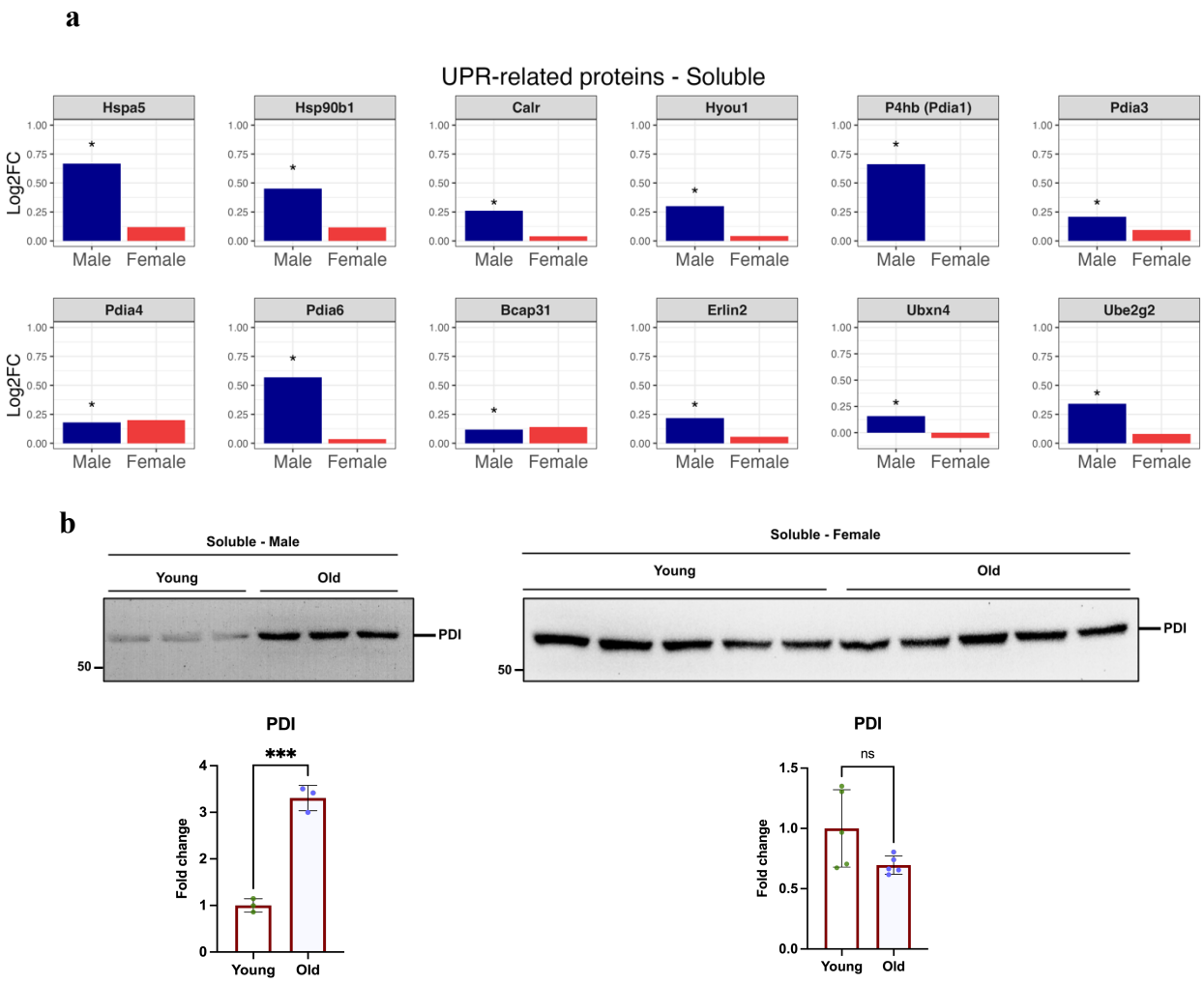

Figure 5. 11. Age-alterations in UPR markers. a) Bar plots displaying the Log2FC (Old/Young) values of significantly regulated UPR related proteins in the soluble fraction of male mice and the corresponding values in female mice. Statistically significant fold change values (adjusted *P* value < 0.05) are marked with an asterisk (*). b) Western blots and quantification of PDI (detects Pdia1) protein abundance in young and old skeletal muscle from male (left) and female (right) mice. Data was visualised on GraphPad Prism using unpaired t-test to confirm significance (*** = $P < 0.001$) with standard deviation bars.

.

5.4.12 Decreased ubiquitylation of UPS-binding proteins

Protein degradation is typically carried out by the UPS or autophagosome. There was little change in the average abundance of proteasome- or autophagy-related proteins **(Figure 5.12a and Figure 5.12b)**, suggesting that these two degradation machineries remain relatively intact with age. Interestingly, there was an age-reduction in ubiquitylation of UPS-binding proteins.

diGly-modified peptides of insoluble Adrm1 (K42), Rad23a (K78) and soluble Psmc3 (K75) were significantly downregulated in older male mice (**Figure 5.12c**). It has been reported that Adrm1 ubiquitylation impairs the proteasome's ability to bind and degrade substrates [271], Inhibiting Rad23 ubiquitylation at the ubiquitin binding domain (includes K78) impairs degradation of its target substrates [272], and ubiquitylation of Psmc3 by the E3 ligase Not4 halters proteasome assembly [273]. Therefore, despite general stability in proteasome protein levels, the decreased ubiquitylation of UPS-binding proteins could be affecting UPS activity and assembly in older skeletal muscle in male mice.

5.4.13 Alterations in E3 ligases and DUBs

CRL are the largest E3 ligase family and crucial for ubiquitin-mediated proteasomal degradation [274]. In male mice, analysis of the soluble muscle fraction revealed age-related protein changes in several components of CRL complexes. Cul3 protein levels showed a modest decrease, while its substrate adaptor Klhl40 moderately increased (**Supplementary Figure 12**). Different substrate-recognition components of other CRL complexes exhibited varied changes: Cul5-associated Asb10 increased, whereas Asb15 moderately decreased, as did the Cul1-associated Fbxo40 (**Supplementary Figure 12**). Across different muscle fractions of both male and female mice, we also observed age-related changes in diGly-modified CRL complexes. In male mice, diGly-modified Cul5 (K724) increased in the soluble fraction (**Figure 5.12d**), whilst in the insoluble fraction diGly-modified Cul3 (K262) was only detected in young mice. The activity of CRL is dependent on Cullin neddylation, which in our workflow will also produce a diGly remnant on peptides. By utilising Phosphositeplus, we found Cul5 K724 has been reported as a neddylation site, whereas Cul3 K262 is a commonly reported ubiquitylation site [275]. In older mice, diGly-modified Cul3 substrate adaptors: Kctd10 (K32) and Klhl41 (K471) increased in the soluble fraction of males and females,

respectively (**Figure 5.12d**). Other E3 ligases involved in UPS-mediated degradation with age-related changes in diGly-modifications include Mkrn2 (decreased on K334), Trim47 (increased on K261) and Ube3a – also known as E6AP – (decreased on K859) (**Figure 5.12d**). Of note, Ube3a influences UPS activity and is known to associate with the proteasome in skeletal muscle of older mice [74], [181].

When searching for the response of DUBs, we found Uchl1 protein increased in both fractions of older male mice **(Supplementary Figure 12)**. The increased expression of Uchl1 has been previously reported in male mice under atrophic models [142], [176]. Even after adjusting for increases in total protein, diGly-modified Uchl1 (K4) significantly increased with age (**Figure 5.12d)**. Uchl5 is associated with the 19S regulatory subunit of the proteasome, playing an essential role in promoting UPS-mediated degradation [276]. Despite not reaching significance (adjusted *P* value = 0.09), Uchl5 displayed a large fold change increase in the insoluble fraction of older male mice **(Supplementary Figure 12)**. Overall, there appears to be age-related changes of both total protein and ubiquitylation of certain E3 ligases and DUBs involved in UPS-mediated protein degradation, likely responding to changes in muscle proteostasis.

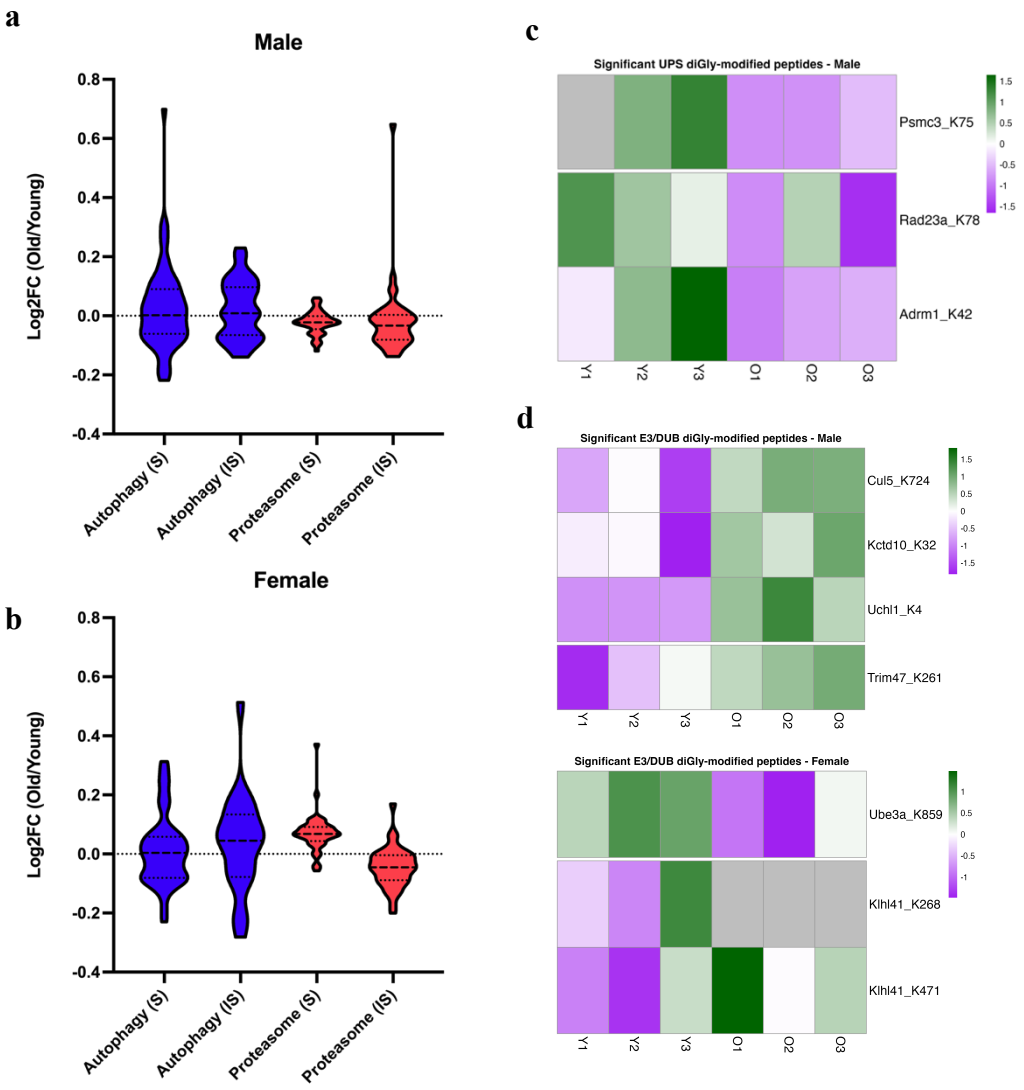

Figure 5. 12. Response of protein degradation markers with age. Violin plot displaying the median, quartile and range of Log2FC values of each protein from the soluble (S) and insoluble (IS) fraction of a) male and b) female mice belonging to the UniProt key terms 'Autophagy' or 'Proteasome'. Heatmap displaying Log2 abundance values scaled by z-scoring of significantly regulated diGly-modified peptides belonging to the c) UPS or d) E3 and DUBs, scaled by z-scoring. Grey colour represents missing values, and break divides soluble fraction (upper) from insoluble fraction (lower).

5.4.14 Significant age-by-sex effects

Previously, it has been shown that sex differences in the ageing skeletal muscle proteome are driven by changes in male mice [243]. In agreement, we have reported many proteins that only display age-related changes in male mice. However, up until now we have not determined which age-by-sex differences are significant. To perform this analysis, we had to address the

LC-MS run-to-run variation of the male and female protein abundance values. Typically, this is achieved by normalising against a reference channel, however this was not included in our workflow. As an alternative, we normalised the datasets by creating ratios of old:young protein abundance values between each replicate within sex. From our proteomics dataset, we were able to generate ratios for 2723 soluble proteins and 1792 insoluble proteins. Of these, 1061 soluble and 715 insoluble proteins exhibited statistically significant differences between males and females. After applying a fold change cut-off, this resulted in 44 soluble and 33 insoluble proteins with significantly regulated age-by-sex effects (**Figure 5.13a**). Log2FC values provide the magnitude of the age-by-sex effect, but not the specific pattern of change. For example, a positive Log2FC (male/female) can occur from an increase in protein with age in males but not females, or from a decrease in protein with age in females but not males. To distinguish between these occurrences, we visualised the individual ratio abundance values of significantly regulated age-by-sex proteins in a heatmap (**Figure 5.13b**). What is apparent is most age-by-sex differences in the soluble fraction are caused by proteins which increase rather than decrease with age. Very few proteins display a strong inverse response to age i.e. increase in one sex and a decrease in another. Nnt (NAD(P) transhydrogenase) is one protein that does display an inverse relationship with age, increasing in the males but decreasing in the females in both fractions. Previous work in human skeletal muscle found Nnt decrease with age, although they did not distinguish between sex [31]. Nnt functions as a proton pump in the mitochondrial membrane to reduce $NADP^+$ to NADPH and support antioxidant defence [277]. Therefore, the age-related mitochondrial response to oxidative damage in skeletal muscle appears sex specific. Overall, this analysis demonstrates that the protein response to ageing in skeletal muscle is different between male and female mice, highlighting the importance of considering sex as a biological variable in future research.

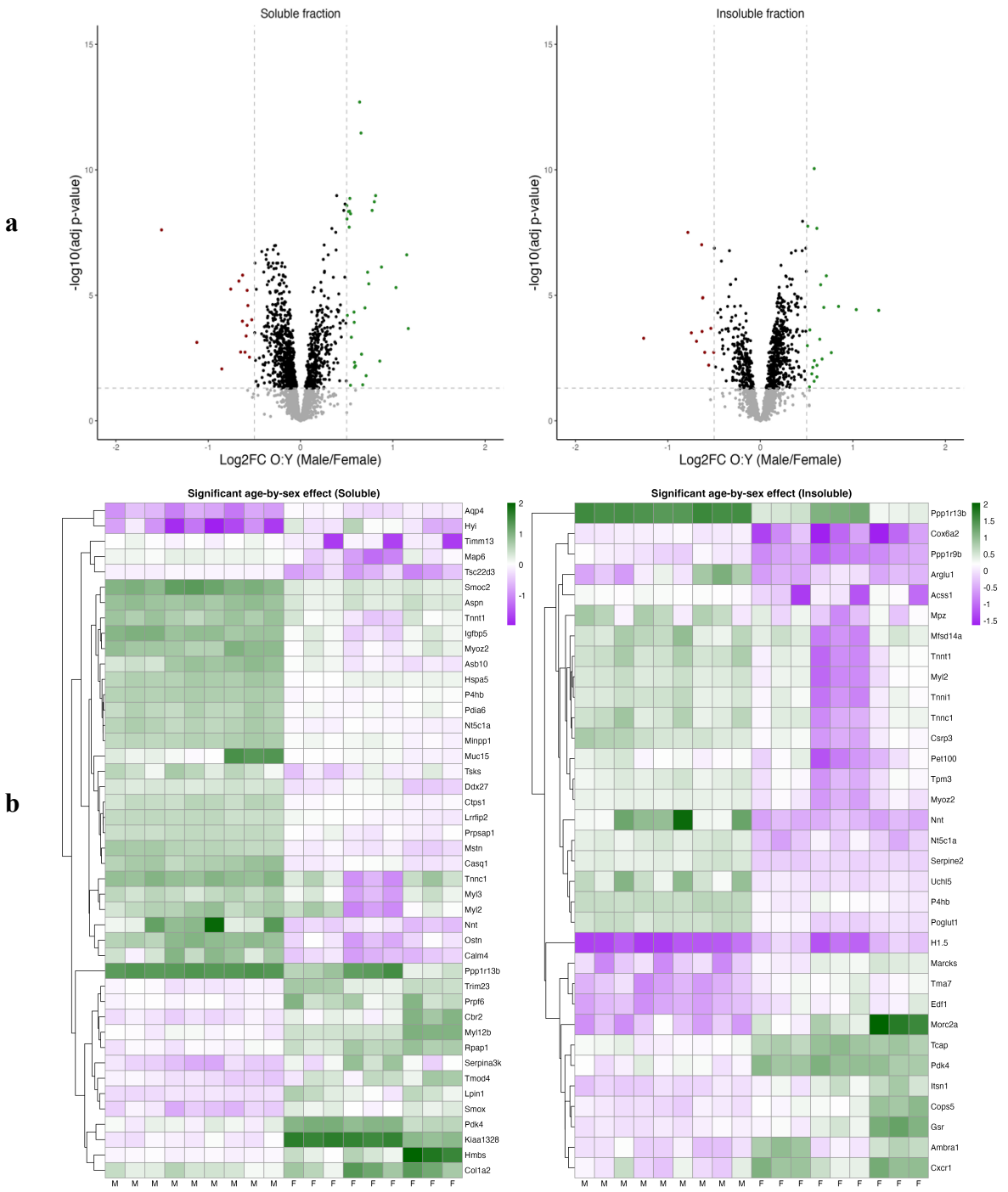

Figure 5. 13. Significant age-by-sex effects in mouse skeletal muscle. a) Volcano plot from both soluble (left) and insoluble (right) proteome showing the Log2FC (Male/Female) of the Old:Young ratios plotted against the –Log10 adjusted *P* value highlighting significantly regulated proteins (green: Log2FC > 0.5 & adjusted *P* value < 0.05, red: Log2FC < 0.5 & adjusted *P* value < 0.05). b) Heatmap showing individual Log2 Old:Young ratios of proteins displaying significant age-by-sex effect (adjusted *P* value < 0.05 and absolute Log2FC > 0.5) in either soluble (left) and insoluble (right) proteome. M = male, F = female. Given that the original scale of the data is meaningful and necessary for interpretation, we did not scale the rows by the z-scoring.

5.5 Conclusions

Here we provide new insights into the molecular mechanisms of skeletal muscle ageing through a comprehensive quantitative proteomics and ubiquitylomics analysis of young and old mice. Our study identified age-related changes previously observed in human skeletal muscle, including decline in mitochondrial proteins and increase in spliceosome components [31], while also uncovering novel changes, including a reduction in mitochondrial ribosomes and an increase in soluble sarcomeric proteins. This is the first study to conduct ubiquitylomics analysis in ageing skeletal muscle, highlighting age-related modifications in various proteins, such as mitochondrial proteins, ribosomal subunits, histone proteins and UPS-binding proteins. Importantly, our study addresses the gender imbalance prevalent in rodent studies, revealing that the disruption of protein homeostasis in the endoplasmic reticulum is a male-specific characteristic. Our finding provides a valuable resource for exploring molecular mechanisms contributing to age-related decline in skeletal muscle function in both males and females. This work lays the foundation for future studies to investigate these mechanisms and develop strategies to mitigate against sarcopenia.

Supplementary figures

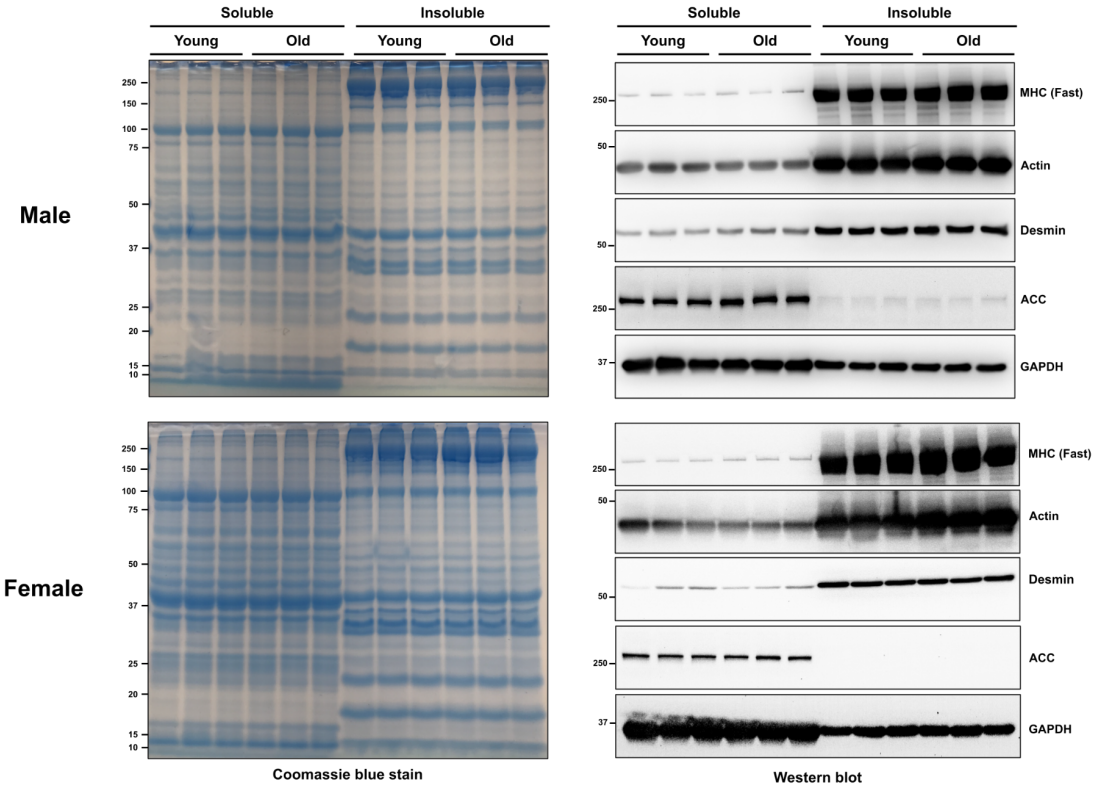

Supplementary Figure 1. Validation of skeletal muscle fractionation prior to LC-MS analysis. Gastrocnemius complex muscle from young (5-6 month) and old (21-22 month) male and female mice were fractionated using centrifugation. Muscles were first homogenised in a 0.5% detergent lysis buffer, centrifuged to separate the proteins into pellet (insoluble) and supernatant (soluble) fractions. The pellet was then homogenised in a 5% detergent buffer. Samples were subjected to Coomassie protein staining and western blotting to confirm separation of soluble and insoluble proteins.

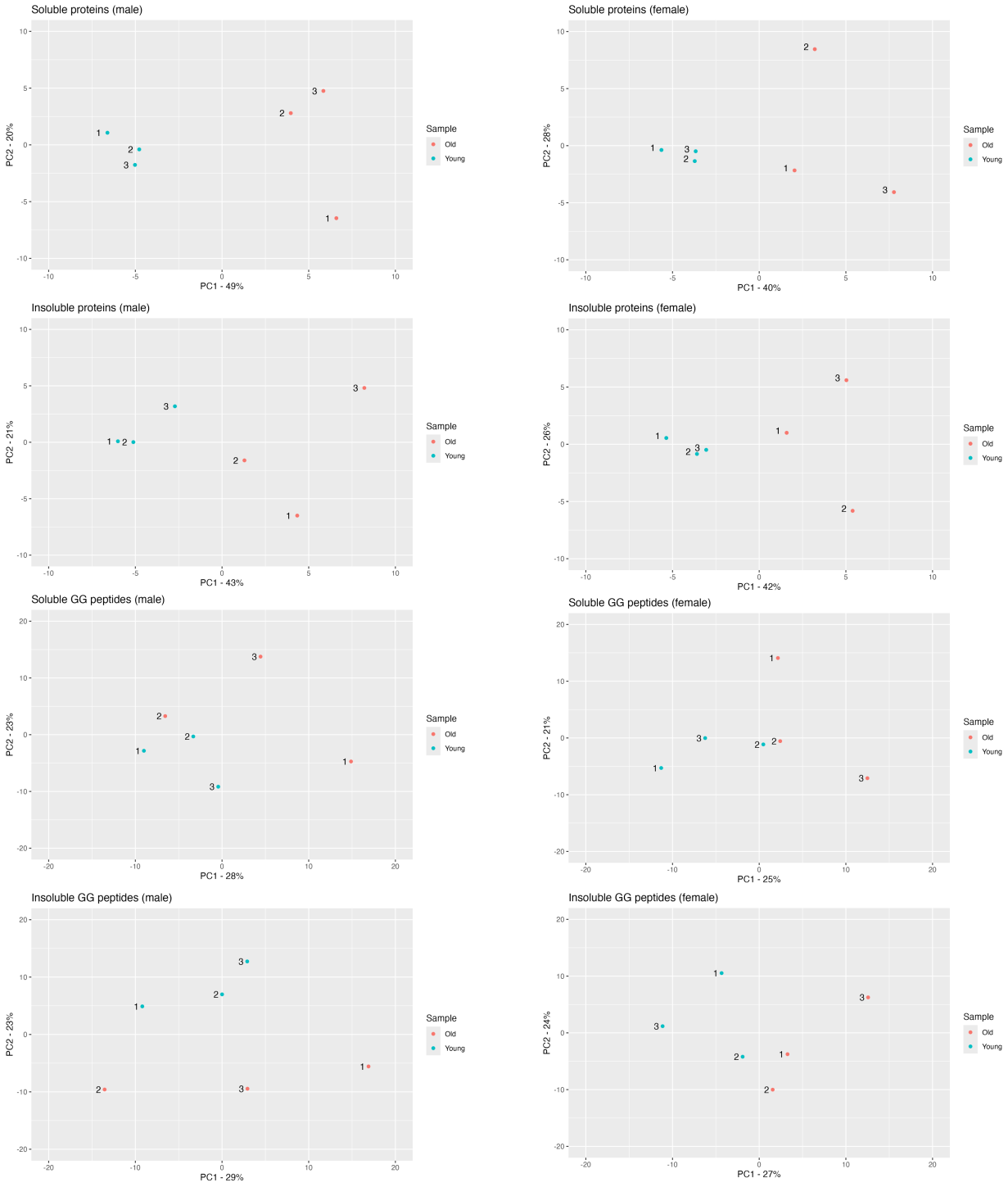

Supplementary Figure 2. Sample variation in protein or diGly-modified peptide abundance. PCA plots displaying the variation in abundance values from both total protein and diGly-modified peptides generated from both soluble and insoluble fractions of male and female mice. Each dot represents a different sample replicate (n=3).

a

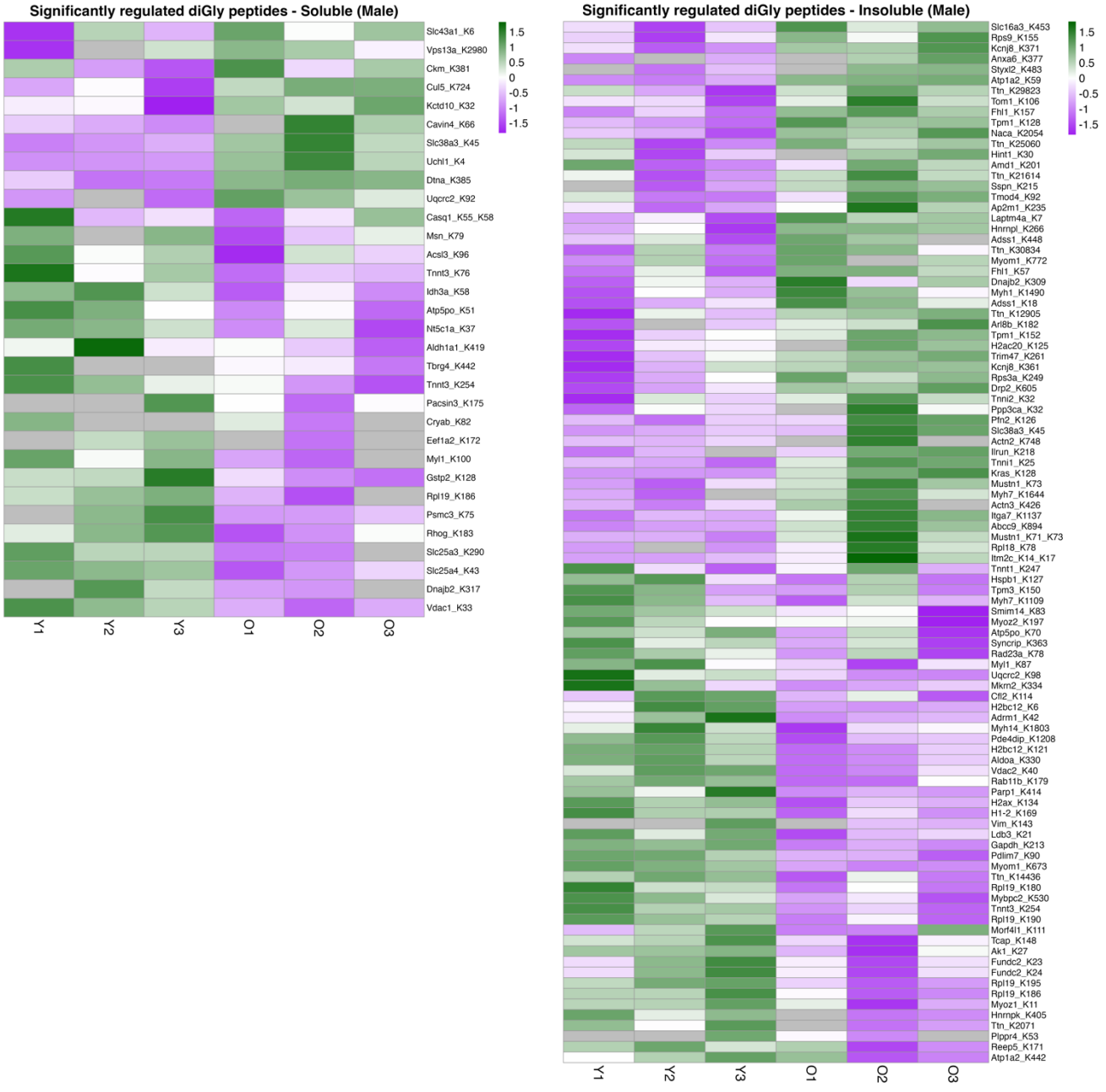
Significantly regulated diGly peptides - Soluble (Male)
Slc43a1_K6
Vps13a_K2980
Ckm_K381
Cul5_K724
Kctd10_K32
Cavin4_K66
Slc38a3_K45
Uchl1_K4
Dtna_K385
Uqcrc2_K92
Casq1_K55_K58
Msn_K79
Acsl3_K96
Tnnt3_K76
Idh3a_K58
Atp5po_K51
Nt5c1a_K37
Aldh1a1_K419
Tbrg4_K442
Tnnt3_K254
Pacsin3_K175
Cryab_K82
Eef1a2_K172
Myl1_K100
Gstp2_K128
Rpl19_K186
Psmc3_K75
Rhog_K183
Slc25a3_K290
Slc25a4_K43
Dnajb2_K317
Vdac1_K33
Y1
Y2
Y3
O1
O2
O3
1.5
1
0.5
0
-0.5
-1
-1.5
Significantly regulated diGly peptides - Insoluble (Male)
Slc16a3_K453
Rps9_K155
Kcnj8_K371
Anxa6_K377
Stxbl2_K483
Atp1a2_K59
Ttn_K29823
Tom1_K106
Fhl1_K157
Tpm1_K128
Naca_K2054
Ttn_K25060
Hint1_K30
Amd1_K201
Ttn_K21614
Sspn_K215
Tmod4_K92
Ap2m1_K235
Laptm4a_K7
Hnrnpl_K266
Adss1_K448
Ttn_K30834
Myom1_K772
Fhl1_K57
Dnajb2_K309
Myh1_K1490
Adss1_K18
Ttn_K12905
Arl8b_K182
Tpm1_K152
H2ac20_K125
Trim47_K261
Kcnj8_K361
Rps3a_K249
Drp2_K605
Tnni2_K32
Ppp3ca_K32
Pfn2_K126
Slc38a3_K45
Actn2_K748
Ilrun_K218
Tnni1_K25
Kras_K128
Mustn1_K73
Myh7_K1644
Actn3_K426
Itga7_K1137
Abcc9_K894
Mustn1_K71_K73
Rpl18_K78
Itm2c_K14_K17
Tnnt1_K247
Hspb1_K127
Tpm3_K150
Myh7_K1109
Smim14_K83
Myoz2_K197
Atp5po_K70
Syncrip_K363
Rad23a_K78
Myl1_K87
Uqcrc2_K98
Mkrn2_K334
Clt2_K114
H2bc12_K6
Adrm1_K42
Myh14_K1803
Pde4dip_K1208
H2bc12_K121
Aldoa_K330
Vdac2_K40
Rab11b_K179
Parp1_K414
H2ax_K134
H1-2_K169
Vim_K143
Ldb3_K21
Gapdh_K213
Pdlim7_K90
Myom1_K673
Ttn_K14436
Rpl19_K180
Mybpc2_K530
Tnnt3_K254
Rpl19_K190
Morf4l1_K111
Tcap_K148
Ak1_K27
Fundc2_K23
Fundc2_K24
Rpl19_K195
Rpl19_K186
Myoz1_K11
Hnrnpk_K405
Ttn_K2071
Plppr4_K53
Reep5_K171
Atp1a2_K442
Y1
Y2
Y3
O1
O2
O3
1.5
1
0.5
0
-0.5
-1
-1.5

b

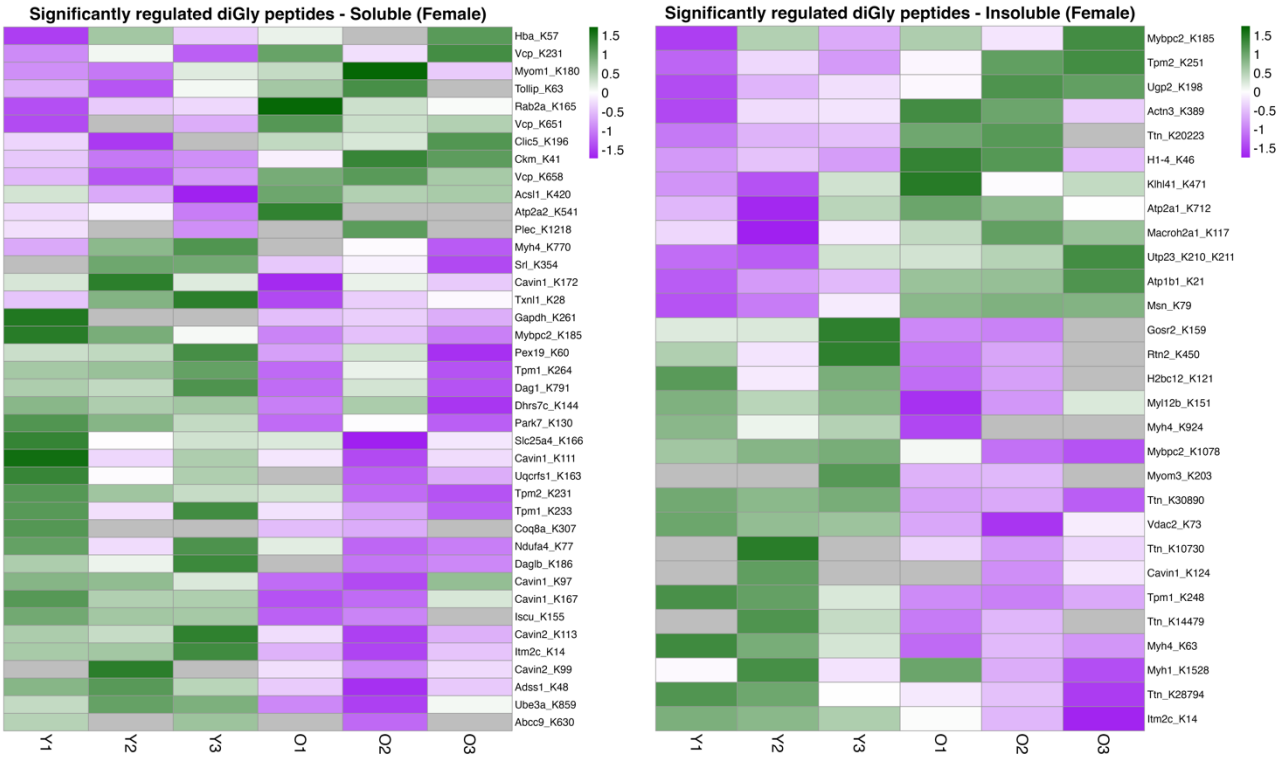

Supplementary Figure 3. Age-related changes in diGly-modified peptides. Heatmap displaying Log2 abundance values scaled by z-scoring of significantly regulated diGly-modified peptides (*P* value < 0.05) of young and old a) male and b) female mice in both soluble (left) and insoluble (right) fractions. Grey colour represents missing values.

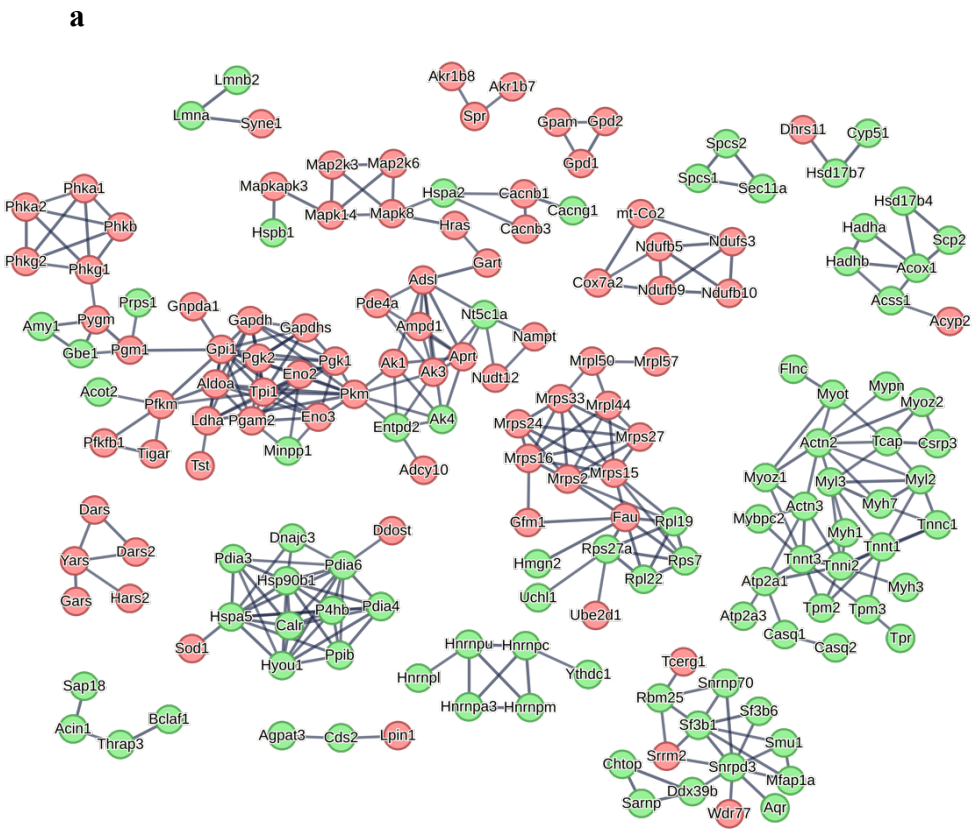

Supplementary Figure 4. Protein-protein interaction networks of the ageing male muscle proteome. Statistically significant proteins (adjusted *P value* < 0.05) from the male dataset were inputted to STRING from a) soluble and b) insoluble fraction. Connections shown for protein interactions with the high confidence score (0.9). Only interactions of more than 2 are shown. Green = greater in old vs young, Red = greater in young vs old.

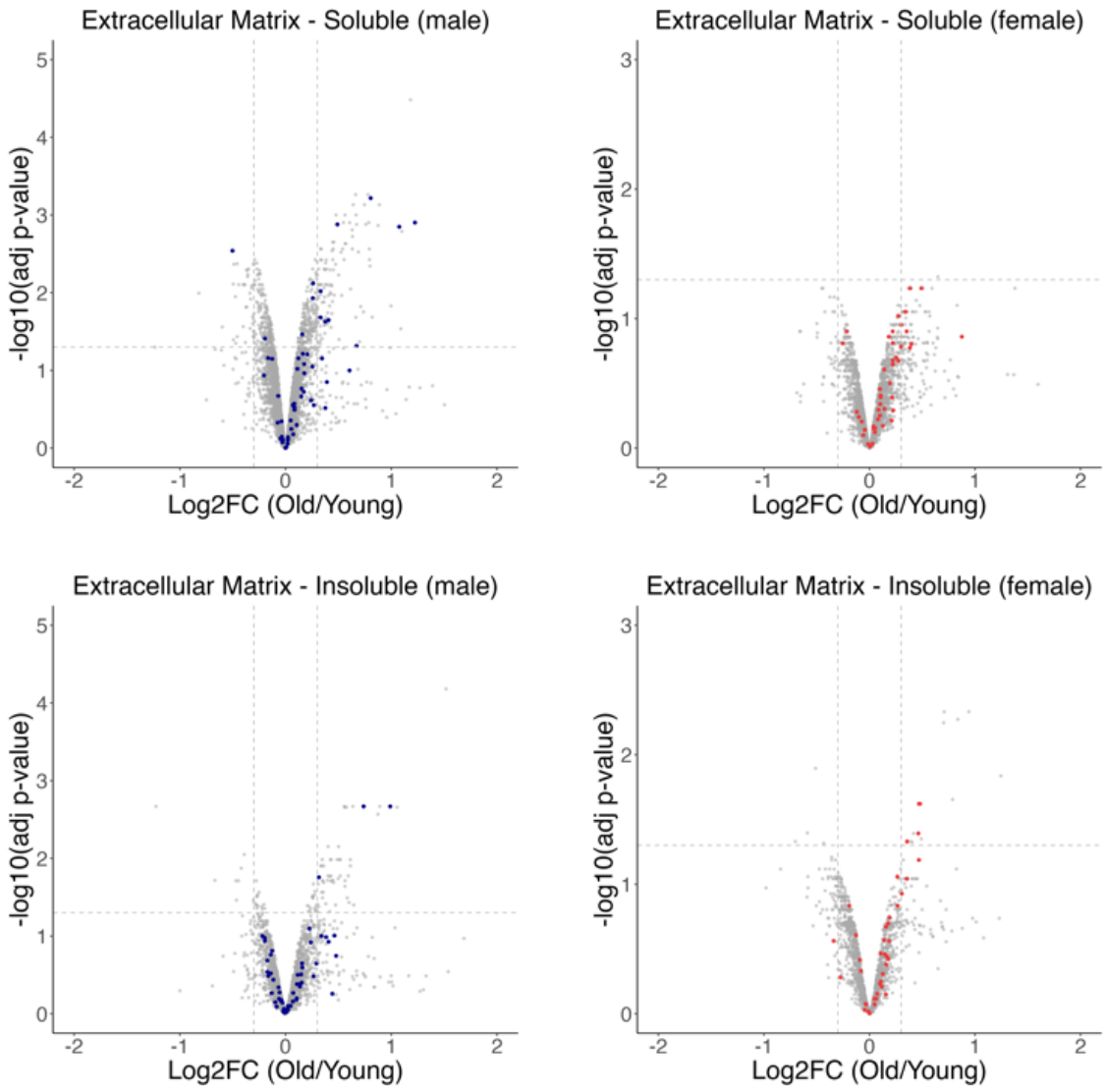

Supplementary Figure 5. Quantitative analysis of extracellular matrix protein abundance with age. Volcano plot highlighting extracellular matrix proteins (Teal) from the soluble and insoluble muscle fraction of male and female mice, showing the Log2FC (Old/Young) plotted against the –Log10 adjusted *P* value.

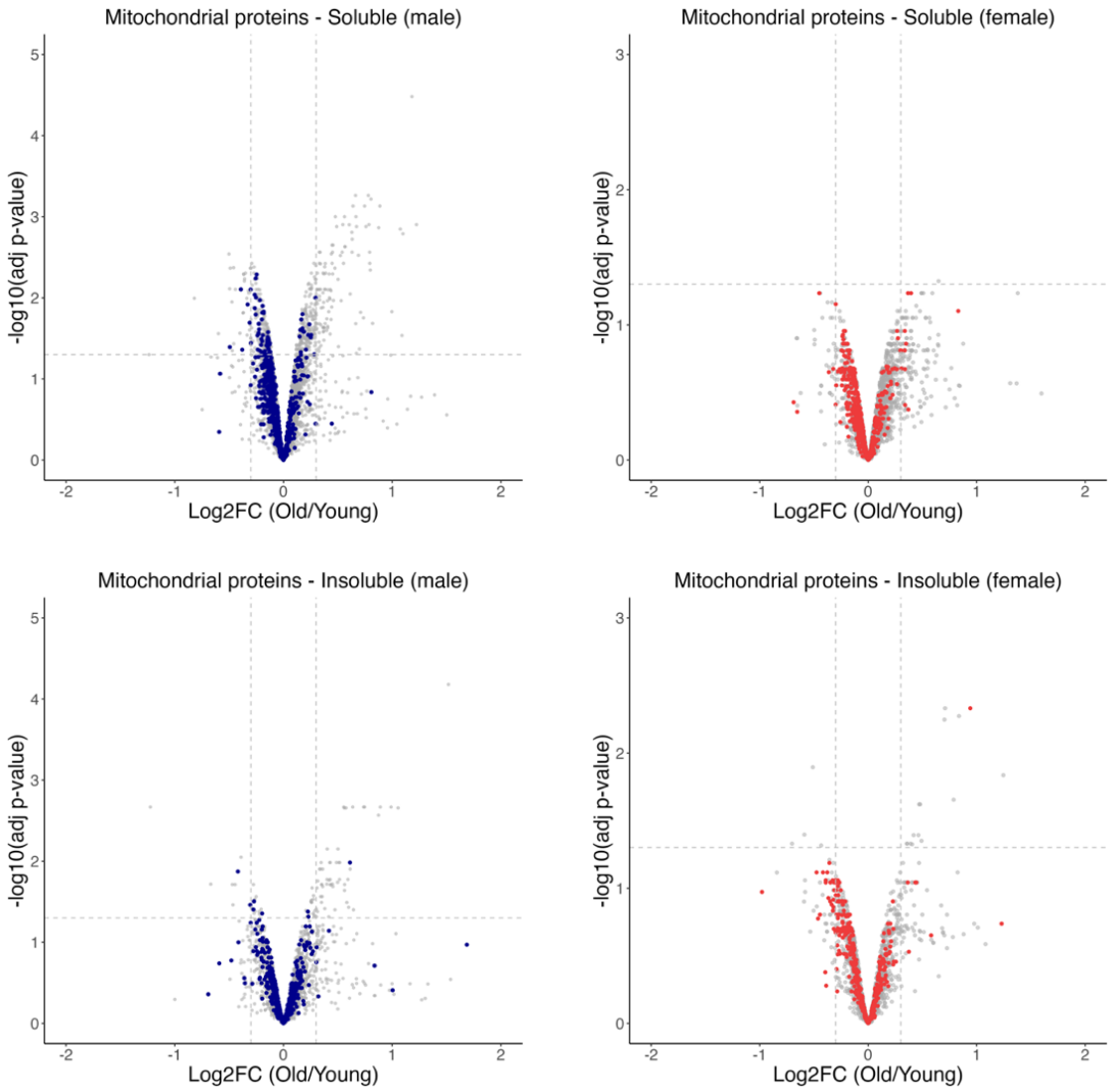

Supplementary Figure 6. Quantitative analysis of mitochondrial protein abundance with age. Volcano plot highlighting mitochondrial proteins (Blue) from the soluble and insoluble muscle fraction of male and female mice, showing the Log2FC (Old/Young) plotted against the –Log10 adjusted *P* value.

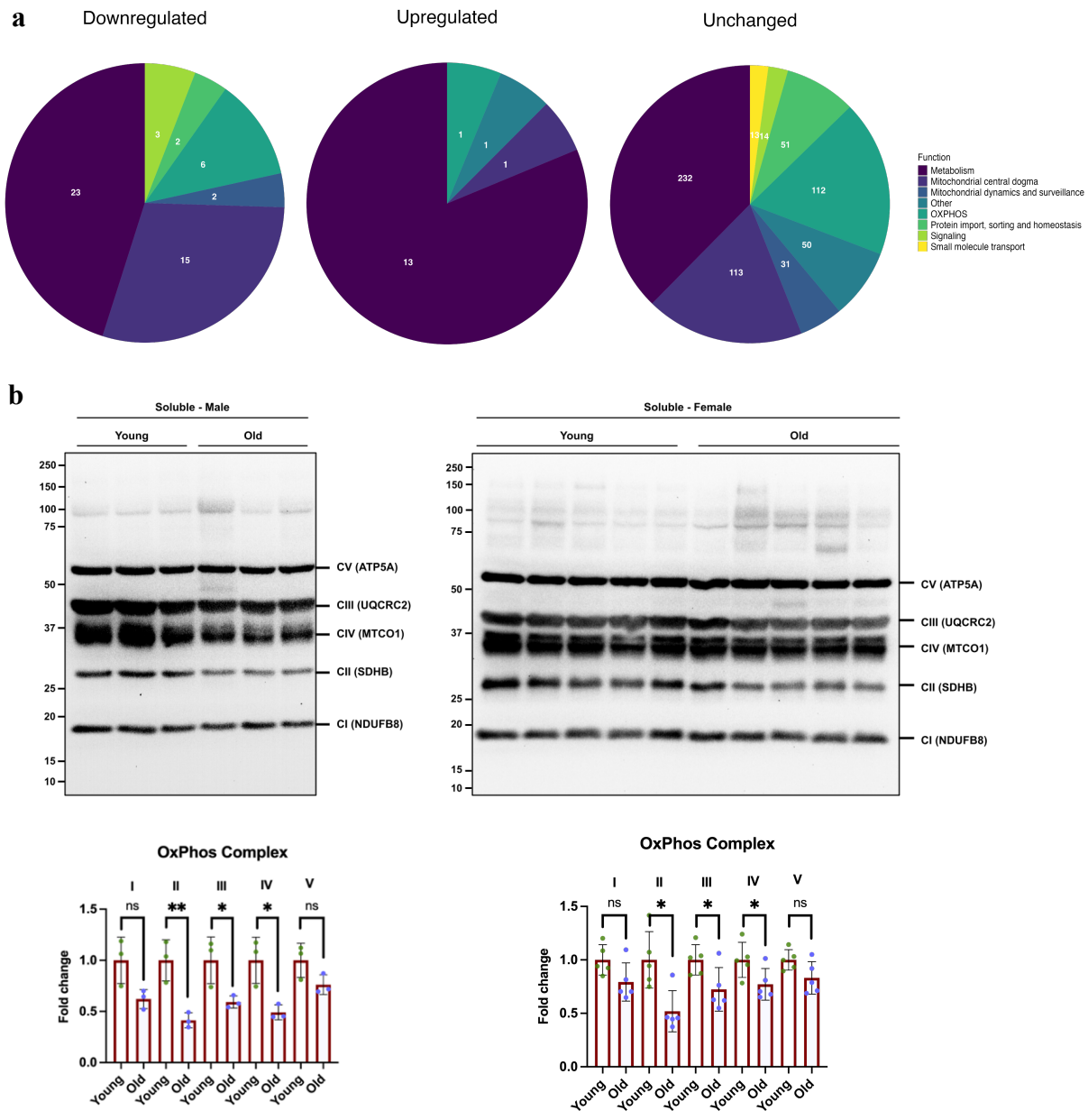

Supplementary Figure 7. Functional analysis of age-related soluble mitochondrial proteins in male mice. a) Pie chart showing the proportion of significantly downregulated (adjusted *P* value < 0.05, Log2FC < 0), upregulated (adjusted *P* value < 0.05, Log2FC > 0) or unchanged (adjusted *P* value > 0.05) mitochondrial proteins in the soluble fraction of male mice belonging to a specific mitochondrial pathway (termed function). The number of proteins in each function are labelled within the Pie charts. b) Western blots and quantification of the oxidative phosphorylation complex in the soluble fraction of male (left) and female (right) mice.

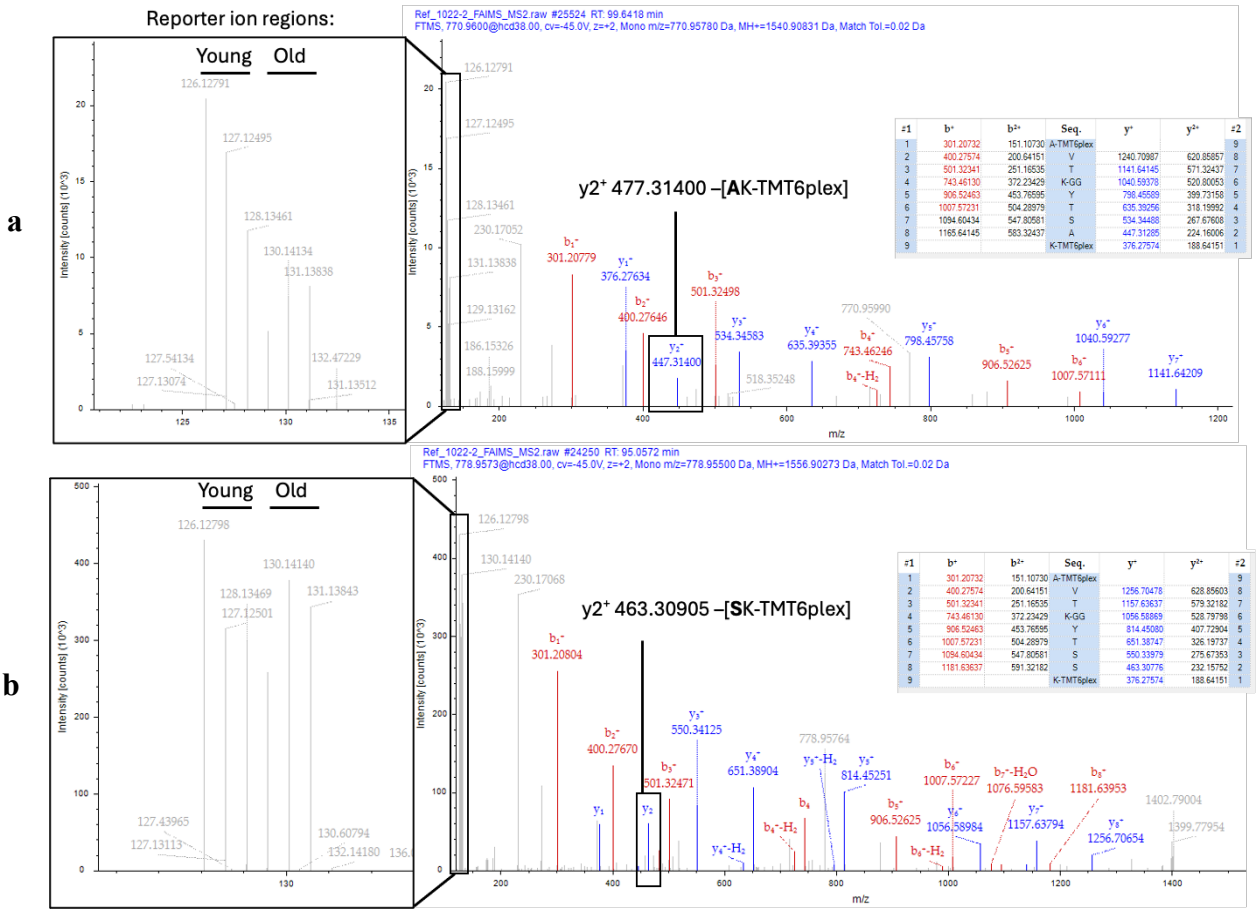

Supplementary Figure 8. MS2 spectra from ubiquitylated Histone H2B C-terminus peptides. Spectral information obtained from fragmented a) AVTkYTSAK or b) AVTkYTSSK peptides in the insoluble fraction of male mice. Spectra shows the b and y ions created following HCD fragmentation. Ions have been matched to an amino acid within 0.02 Da. y2 ion reflects the C-terminus fragment beginning with an alanine or serine amino acid, distinguishing the two H2B peptides. Reporter ion regions display the quantitative abundance value of the peptide in each sample (TMT 126:131).

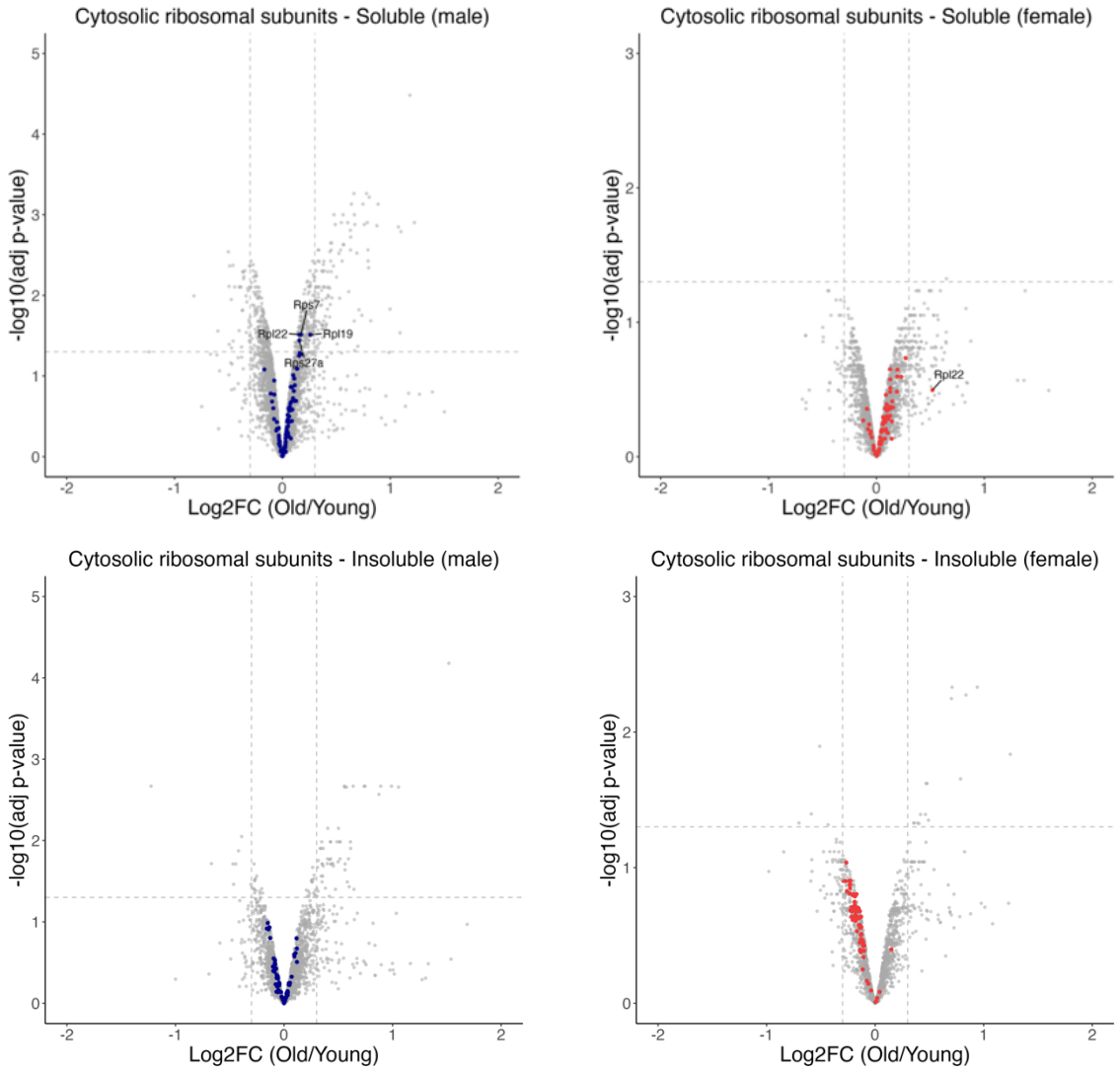

Supplementary Figure 9. Quantitative analysis of cytosolic ribosome subunit proteins with age. Volcano plot highlighting cytosolic ribosome subunits (Orange) from the soluble and insoluble muscle fraction of male and female mice, showing the Log2FC (Old/Young) plotted against the –Log10 adjusted *P* value. Annotations were performed for those that surpassed the significance or fold change threshold.

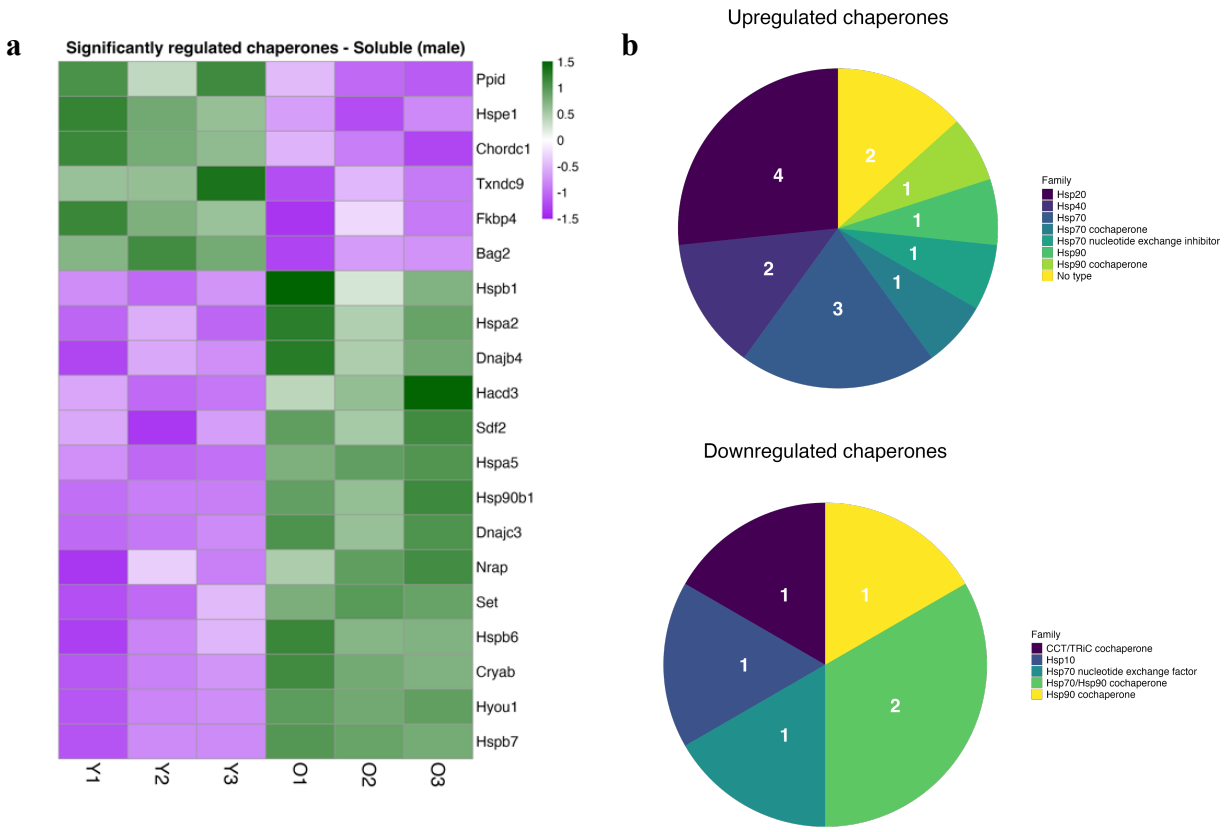

Supplementary Figure 10. Significantly regulated chaperone proteins in male mice. a) Heatmap displaying Log2 abundance values scaled by z-scoring of significantly regulated proteins belonging to the chaperone class of the proteostasis network. b) Pie chart showing the proportion of significantly upregulated and downregulated chaperone protein families as characterised by the Human Proteostasis Annotation Network. The number of proteins in each family are labelled within the Pie charts.

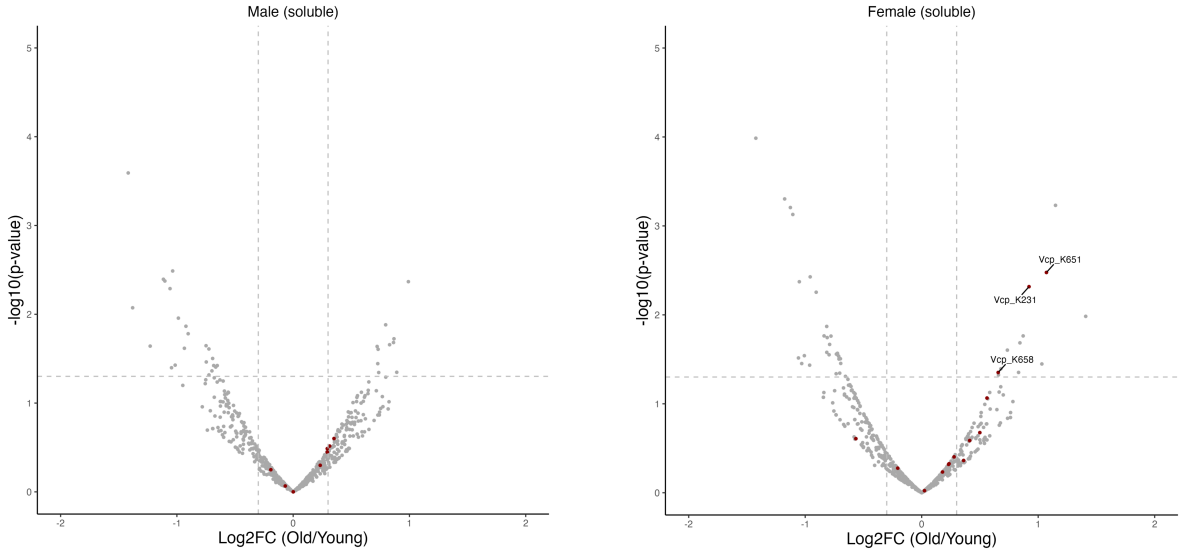

Supplementary Figure 11. Quantitative analysis of ubiquitylated VCP with age. Volcano plot highlighting diGly-modified peptides from Vcp (Red) from the soluble muscle fraction of male and female mice, showing the Log2FC (Old/Young) plotted against the –Log10 *P* value. Annotations were performed for those that surpassed the significance threshold.

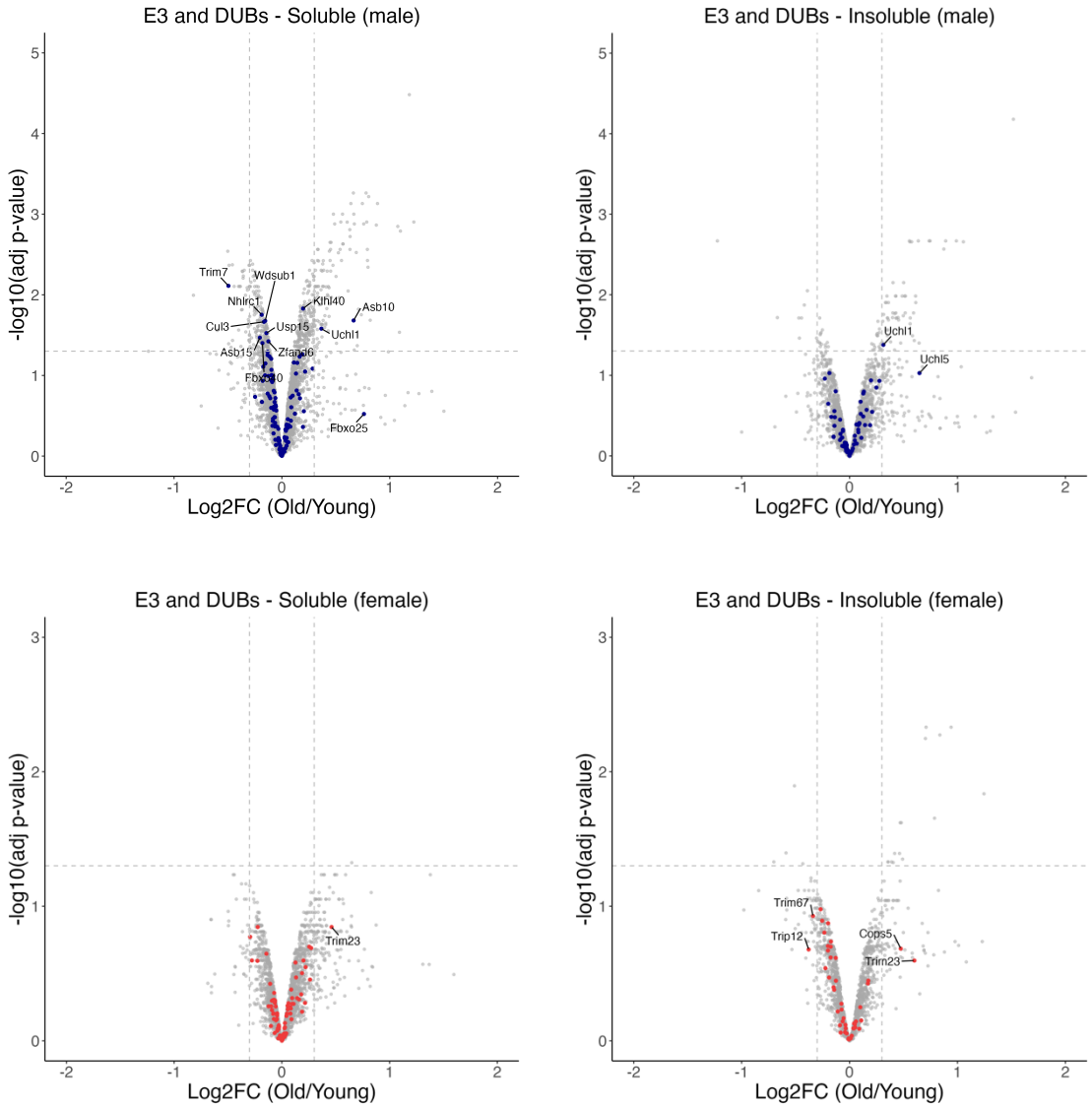

Supplementary Figure 12. Quantitative analysis of E3 and DUB protein abundance with age. Volcano plot highlighting E3 ligase and DUBs (Green) from the soluble and insoluble muscle fraction of male and female mice, showing the Log2FC (Old/Young) plotted against the –Log10 adjusted *P* value. Annotations were performed for those that surpassed the significance or fold change threshold. E3 ligase and deubiquitylase databases were taken from the Epithelial Systems Biology Laboratory (ESBL) and converted from human to mouse using UniProt.

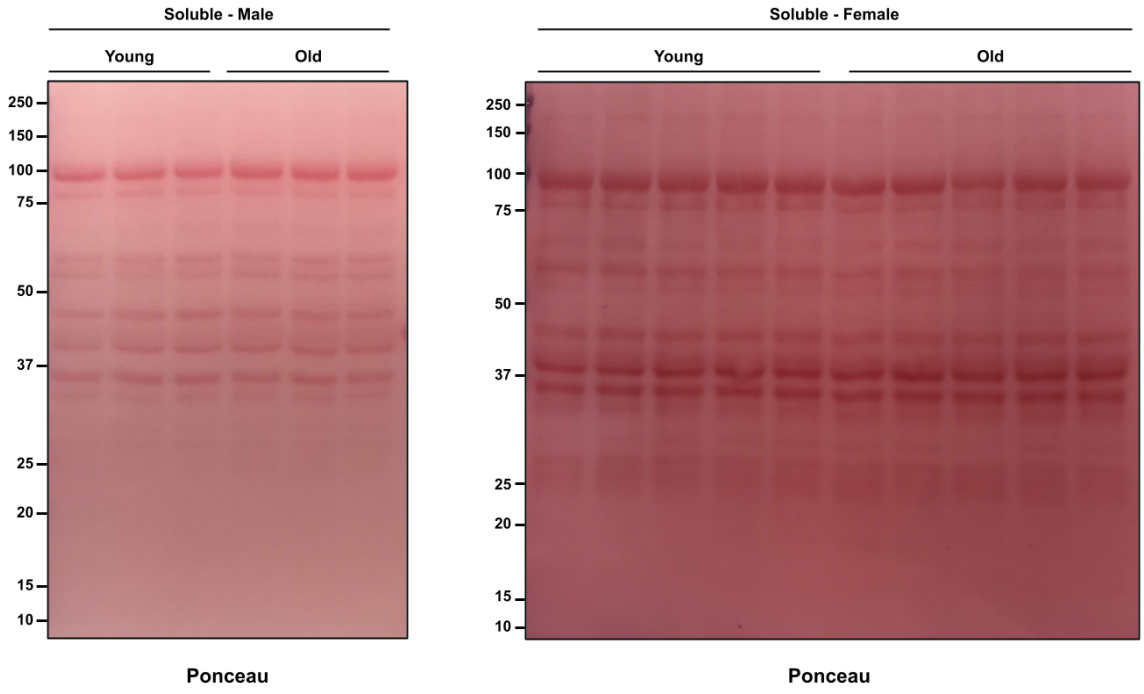

Supplementary Figure 13. Total protein staining. Representative ponceau stain of the soluble fraction from male and female mice used to normalise protein bands which have been quantified after western blotting.

6. Discussion

Ageing results in functional decline across all tissues, creating many challenging diseased states to combat in order to achieve healthy living at older age. Skeletal muscle decline is linked to many physiological and metabolic disorders that occur during ageing and as a result is a predictor of longevity [7], [11]. Gaining a deeper understanding of the molecular mechanisms that drive skeletal muscle decline with ageing will aid the development of future therapeutic interventions aimed at achieving healthy skeletal muscle ageing.

LC-MS offers an invaluable technique for discovering age-related protein changes. In theory, LC-MS can identify and quantify the entire set of proteins expressed in a given biological system. The high sensitivity of LC-MS enables the detection of many different PTMs that regulate protein function. Together, this enables a highly comprehensive, unbiased approach to study protein abundance and their modifications simultaneously.

In the field of ageing skeletal muscle research, LC-MS has seen limited application for studying PTMs. To date, our understanding is that protein phosphorylation is the only PTM that has been examined in this context [278], [279]. We were particularly interested in using LC-MS to study age-related changes in protein ubiquitylation. A key rationale was ubiquitin-regulating enzymes (E3 ligases and DUBs) have proven important in ageing skeletal muscle (see chapter 1.4). Furthermore, ubiquitin-mediate processes such as the UPS and autophagy are essential for protein quality control, which undergoes significant stress during ageing resulting in a decline in protein homeostasis [280]. Moving forward, our goal was to determine how proteins and their ubiquitin modifications are altered in skeletal muscle by age. Therefore, the main purpose of this thesis was twofold:

i. Develop a MS-based workflow that enables quantitative analysis of proteins and their ubiquitin modifications

ii. Investigate changes in total protein and ubiquitylated protein abundance in skeletal muscle of male and female mice during ageing.

The present chapter will present a summary of the key findings of this thesis. Based on findings from **CHAPTER 3 to 5**, I will discuss methodological recommendations for future studies aiming to conduct proteomics or ubiquitylomics in skeletal muscle. Whilst this is partly described in **CHAPTER 2**, this section will be more tailored towards my workflow and the challenges that I faced. From the study described in **CHAPTER 5,** I will outline how our findings improve the current knowledge of protein and ubiquitin-regulation in ageing skeletal muscle. I will also discuss the limitations of this experiment and provide ideas for future directions.

6.1 Methodological recommendations for future studies

The success of any experiment relies on the quality of the data. You can have the best experimental idea to tackle critical questions in the scientific field, but if you end up with poor quality data then you will end up with unreliable and misleading findings. Poor data quality often comes from issues with sample input. The phrase "garbage in, garbage out" is often used to describe this phenomenon, and it is very relatable for MS-based proteomics experiments. LC-MS is very good at giving lots of data but is highly sensitive to sample quality issues e.g. contaminants or inconsistent protein amounts. Therefore, if the quality of your sample input is poor, you will end up with lots of 'rubbish' data. Avoiding this situation is particularly important with MS-based proteomics, given the time and cost of running these experiments.

Based on findings from this thesis, I will provide some recommendations for future studies who want to conduct a proteomics or ubiquitylomics experiments in skeletal muscle.

6.1.1 Fractionation

Detection of the skeletal muscle proteome is significantly hindered by the large dynamic range of protein abundance values. In our work, we opted to employ fractionation to separate out highly abundant proteins found in the myofibrillar fraction. Whilst we believe this is an appropriate method of choice, especially for beginners in proteomics as it is relatively user-friendly, it does bring in some new challenges that users need to be aware of.

Firstly, muscle fractionation is designed to separate highly abundant myofibrillar proteins from less abundant proteins, however the separation is not pure. Whilst inherently insoluble, some myofibrillar proteins are detected in our soluble fraction as displayed in our western blot validations. Although pure separation is not required for good protein coverage, it can become an issue if the fractionation efficiency varies between samples. For instance, if one soluble fraction contains more myofibrillar proteins, the abundance of its remaining proteome will be suppressed, introducing technical variation when comparing protein abundance values. Therefore, when performing muscle fractionation, it is important to check the abundance values of the highly abundant myofibrillar proteins such as titin, myosin and actin in each soluble fraction.

A notable limitation of our fractionation method is that we were not able to completely solubilise the entire insoluble fraction. Therefore, we are not able to access the entire insoluble proteome of skeletal muscle, so our analysis is still bias to proteins that are ‘easier’ to solubilise. This is a particular issue in the context of ageing where protein aggregates which are inherently

difficult to solubilise become more abundant [281]. Therefore, our analysis is likely unable to detect protein aggregates that might be significant in the ageing process. Our fractionation method could solubilise more proteins when we included a heating step on the insoluble fraction. Without sufficient heat, some proteins remain in their native state and cannot be accessed by the solubilising agents. Heating at 95 °C for 5 minutes helps denature the proteins and aids solubilisation. Whilst the presence of detergent and reducing agents should prevent the high temperatures from driving protein aggregation, protocols also recommend lower temperatures for longer time periods e.g. 60 °C for 30 minutes, perhaps to reduce the risk of protein aggregation [208].

6.1.2 Sample clean-up

Sample clean-up is an essential step of any proteomics workflow, ensuring contaminants (e.g., detergents, chaotropes, salts) do not enter the LC-MS system. There are many different sample clean up methods, designed for specific applications [282]. We opted for SP4, which is not limited by the composition of lysis buffer (work with detergents, chaotropes or acids), can be performed with minimal handling without expensive materials and in theory removes all contaminants [118]. The latter avoids the need for multiple clean up steps e.g. peptide desalting that introduce additional losses. However, this can only be achieved by resuspending the pellet in reagents compatible with downstream analysis e.g. ammonium bicarbonate, which are not as effective at resolubilising proteins. Physical disruption of the pellet through sonication can help disrupt the pellet, reported to be sufficient for trypsin to digest the proteins into soluble peptides [118]. However, in our workflow we did experience some inconsistencies in digestion efficiency, presumably due to a poorly disrupted protein pellet following SP4 which required additional trypsin incubations **(Figure 6.1)**. Given that ubiquitylomics requires a high amount of protein, the pellet created during SP4 is likely too large to disrupt with sonication, preventing

full access for trypsin digest. Incomplete digestion will reduce the number of peptides produced and will compromise the performance of K-ε-GG immunoprecipitation and LC-MS if intact proteins are carried over. Therefore, to avoid these complications with SP4, we recommend future experiments consider employing longer or more concentrated trypsin digests and use Coomassie protein stains to check the presence of intact proteins.

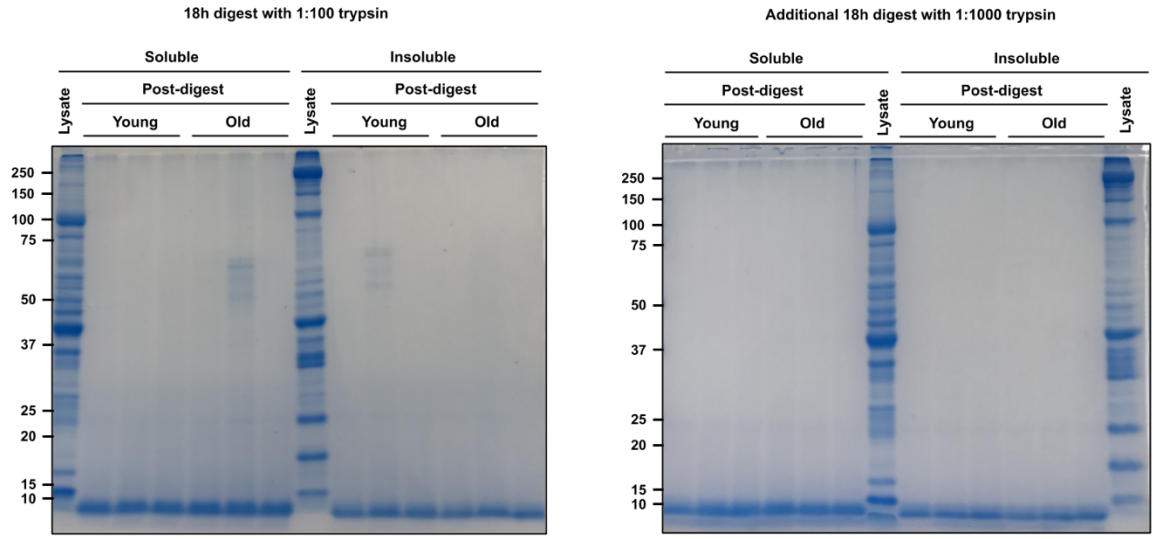

Figure 6. 1. Digestion efficiency following protein precipitation. Coomassie protein stain performed following 18-hour trypsin digestion (left), followed by an additional 18 hour incubation (right). The same amount of theoretical protein was loaded as a reference for both muscle fractions. Peptides can be identified at the bottom of the gel due to their smaller size.

6.1.3 Ubiquitin enrichment

Detection of the skeletal muscle ubiquitylome is significantly hindered by the low stoichiometry of ubiquitylated proteins relative to total proteins. Therefore, to obtain good coverage of ubiquitylated peptides during MS detection, an enrichment method is required. Ubiquitin enrichment can be performed at either the protein or peptide level through either reconstructed ubiquitin binding domains or antibodies. Peptide-level ubiquitin enrichment provides the advantage of enriching at the ubiquitylation site, therefore given a 100% enrichment efficiency, all detected peptides will include the ubiquitin modification. However,

like in our workflow the enrichment efficiency is never 100%. In an attempt to improve ubiquitin enrichment, we decided to modify the recommended K-ε-GG immunoprecipitation protocol for our ageing study in chapter 5. A recent publication had demonstrated that using less antibody-bound beads and adding 50% ACN with 0.01% CHAPS in the wash buffers improved the detection of ubiquitin-modified peptides [130]. Given that we originally suffered from less than 50% ubiquitin enrichment efficiency, we hoped that this modified protocol would enhance this number. Remarkably, we were able to achieve > 95% enrichment efficiency which suggests a stark reduction in non-specific binding (**Figure 6.2**). Surprisingly, we detected a lower number of diGly-modified peptides than before we modified the protocol. Therefore, it appears that the modified protocol removed diGly-modified peptides from the antibody. This likely occurred from the addition of 50% ACN, which is often included in elution buffers to disrupt hydrophobic peptide interactions [283]. Therefore, we recommend that future studies should optimise the optimal amount of ACN to remove non-specific peptides without disrupting diGly-modified peptides bound to the antibody.

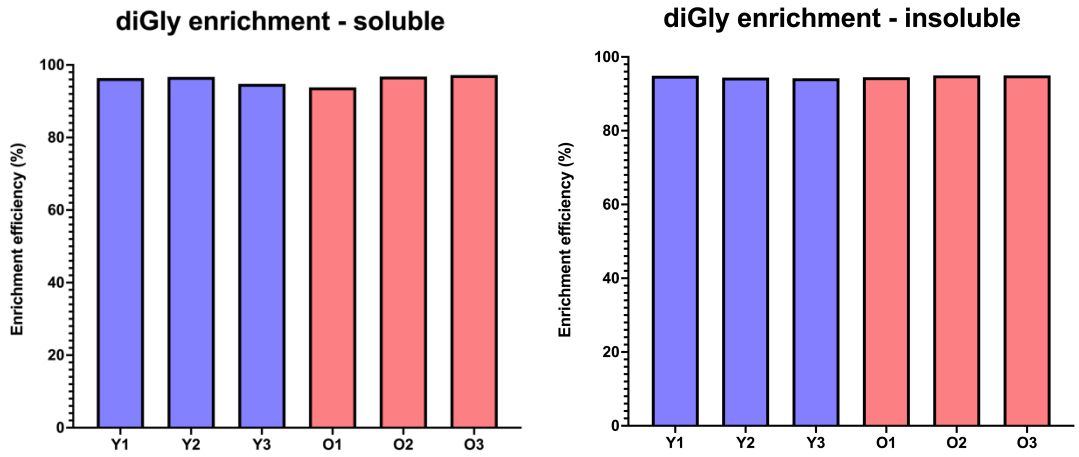

Figure 6. 2. Enrichment efficiency of diGly-modified peptides. The percentage of PSMs that contained a diGly modification in each sample following K-Ɛ-GG immunoprecipitation from the soluble and insoluble muscle fraction.

6.2 Key findings

6.2.1 Energy-regulating pathways

It is well-established that ageing skeletal muscle undergoes metabolic changes, however there are many factors which can alter the degree and even direction of change. Our findings have provided further insight into age-related changes in muscle metabolism, providing some additional input into sex-specific effects.

Decline in mitochondrial function is a prominent hallmark of ageing [17], and this is no different in skeletal muscle [19]. However, at the gene level it has been reported that whilst mitochondrial metabolic pathways are downregulated with age in both male and female human skeletal muscle, males experiences a more pronounced decline [284]. In a similar fashion, our proteomics data displayed a trend decline in mitochondrial proteins across both sexes, however the significance was greater in males. Many different studies have reported different causes for mitochondrial decline, including reduced mitochondrial volume, number or oxidative capacity [19]. An explanation for reduced mitochondrial number is a translational decline in mitochondrial-encoding proteins [249]. This study suggested that reduced mitochondrial translation is due to reduced engagement with the ribosome, dismissing the role of mitochondrial ribosome number. Interestingly, when searching into their supplementary data, we found whilst there was no significant change in mitochondrial ribosomes RNA level, 59 out of the 67 had a negative fold change indicating a trend decline. Our findings show an age-related decline in mitochondrial ribosomes at the protein level, suggesting their abundance likely does impact mitochondrial protein translation.

In human skeletal muscle, it has been shown that mitochondrial proteins decrease with age in both muscle fibre types, whilst glycolysis-regulating enzymes are downregulated in fast muscle fibres but upregulated in slow fibres [25]. Whilst our study did not differentiate between slow and fast fibre types, the gastrocnemius complex is predominantly fast-twitch [285]. We found an age-related decline in glycolysis-regulating enzymes across both male and female mice, supporting the concept that glycolysis is reduced with age in fast-twitch muscles. This is perhaps not surprising given that with age, fast-twitch glycolytic fibres undergo greater atrophy, therefore slow-oxidative muscle fibres are favoured [286].

We found an age-related increase of key enzymes involved in fatty acid oxidation in male mice. This ageing effect has previously been reported in both mouse and human skeletal muscle [29], [30]. A possible explanation for the age-related increase is fibre type composition, as slow-twitch fibres have a higher capacity to utilise fatty acids for energy production. To counter this, lipid accumulation is associated with ageing muscle, and whilst the mechanisms are unclear it has been linked with reduced mitochondria that are required for fatty acid oxidation [287]. Given the reduction in mitochondria in the older male mice, it is difficult to explain why fatty acid oxidation appears to counteract this. Sex specific differences in lipid metabolism have previously been observed, for instance non-oxidative fatty acid metabolism is higher in women suggesting they have a lower tendency to oxidise circulating fatty acids [288]. This could explain why female mice did not display the same increase in proteins associated with fatty acid oxidation as males. However, it is important to note that whilst the role of sex might have an effect, fatty acid oxidation is also affected by activity levels [289]. Unfortunately, no activity data was recorded on the mice we studied; therefore, we cannot determine if sex or activity levels were responsible for driving these differences.

6.2.2 Proteostasis

Proteostasis decline with age is another key hallmark of ageing [17], well researched in the neurodegenerative disorders such as Alzheimer's disease where protein aggregates accumulate [290]. There are studies which have shown that skeletal muscle undergoes dysregulated proteostasis, including sustained activation of mTOR [291], slower turnover of collagen proteins [23], and increased protein aggregates [281]. In skeletal muscle, proteostasis is often studied with regards to protein turnover with methods frequently employed to measure muscle protein synthesis and to a lesser degree, muscle protein degradation [280]. An area that has received less attention is the role of protein folding, but one that has large implications on muscle proteostasis.

In male mice, we found an age-related increase in folding enzymes such as heat shock proteins and protein disulphide isomerases, located in the endoplasmic reticulum. The upregulation of pro-folding proteins such as BiP and PDI in the endoplasmic reticulum of skeletal muscle has previously been demonstrated to be a male specific trait of ageing in mice [243]. It is important to note that this study utilised 18-month-old mice as their 'old' cohort, and we used 21- and 22-month-old mice. The C57BL/6 mice employed can live beyond 28 months [292], so it is possible that loss of endoplasmic reticulum proteostasis occurs in females at a later stage. Nevertheless, our results suggest that male mice experience an earlier age-reduction of impaired proteostasis in the endoplasmic reticulum of skeletal muscle.

One of the more apparent findings from our dataset, was an age-related increase in sHsp. These proteins are a class of ATP-independent chaperones that bind to exposed regions of unfolded proteins to prevent them from forming aggregates. Therefore, an age-related increase in sHsp likely suggests an adaptive response to increased accumulation of unfolded proteins. Hspb7

and Hspb5 (Cryab) facilitate sarcomeric proteostasis [26]. We found that Hspb7 increased in both sexes (significant in males only), and Hspb5 was predominantly upregulated in males. Increased sHsp response might suggest sarcomeric proteostasis is impaired in age mice. To test this hypothesis, it would be interesting to use immunohistochemistry to visualise the location of these sHsp in young and old muscle cross-sections. This would provide insight into whether sHsp are binding to the sarcomere, acting to protect against muscle filament protein aggregation.

6.2.3 Sarcomere solubility

The soluble and insoluble fraction were initially separated to increase the coverage of the proteome, but it can also provide some additional insight. Studies have previously used the detergent-insoluble fractions to try and capture insoluble aggregates [293]. We did not use the insoluble fraction as a means of identifying aggregates, as there are many confounding factors that would need to be considered. For instance, muscle proteins are difficult to solubilise so a large proportion of the insoluble protein would be functional muscle proteins. Interestingly, one of our key findings was an age-related increase in muscle proteins in the soluble fraction in male mice. These proteins are most likely not attached to the sarcomere, either due to their release for degradation or newly synthesised and awaiting chaperone-assisted formation. Muscle filament proteins can be released from the sarcomere through ubiquitin-mediated processes [261], [294]. Therefore, we speculated that soluble muscle proteins would be modified by ubiquitin. To our surprise, we did not find any correlation between the age-related abundance of muscle protein and their ubiquitin (diGly) modifications in the soluble fraction. Previous studies in muscle wasting conditions also found no clear relationship between muscle protein abundance and the extent of ubiquitylation [142], [143]. Therefore, ubiquitylation of soluble muscle proteins most likely do not signal for the same function. To better understand

the role of ubiquitylated soluble muscle proteins, it is important to characterise the type of ubiquitin modification i.e. mono- or poly-ubiquitylation and the specific ubiquitin chain type. However, methodological limitations mean it is difficult to characterise ubiquitin architecture on specific sites.

6.2.4 Extracellular matrix

Age-related changes towards muscle function are also brought about by processes outside the myofiber. Well established age-related changes occur at the neuromuscular junction, satellite cells and the extracellular matrix. From our GSEA data, we found that the extracellular matrix was one of the major pathways upregulated with age in both male and female mice. Typically with age, changes to the extracellular matrix are associated with collagen proteins. In mice, aged muscle experiences collagen accumulation and experiences an increase in insoluble collagen [23], [244]. We found collagen was amongst the proteins displaying age-related increases in skeletal muscle, which occurred in both the soluble and insoluble fraction. Therefore, our findings suggest the rise in skeletal muscle collagen does not appear to be solely attributed to insoluble aggregates. However, unlike those studies we did not use pepsin to determine the proportion of cross-linked collagen which gives an indication of those resistant to degradation. Another extracellular matrix protein which we found increased with age was the SLRPs. Previous proteomics research has identified SLRPs in 24 month old mice [295], and lumican and tenomodulin were significantly increased in 22-23 month old mice relative to 11 month [246]. However, this study only used male mice and so our finding provides additional insight revealing SLRPs increase with age in both male and female mice.

6.2.5 Splicing machinery

Two decades ago, gene expression profiling revealed RNA processing was affected by age in human skeletal muscle [296], [297]. Over the last few years, discovery proteomics research in human skeletal muscle has identified a number of age-related changes in RNA splicing proteins [30], [31]. In 2021, dysregulation of alternative splicing was proposed as a hallmark of myotonic dystrophy and ageing [262]. Our data showed an age-related change in the spliceosome, in which the older male and female mice experienced a rise in ribonucleoproteins. Interestingly, we also found two ribonucleoproteins experienced divergent age-related changes in protein ubiquitylation in male mice. Ubiquitylation of ribonucleoproteins has been shown to regulate spliceosome activity and assembly [298], [299]. To our knowledge, this is the first report of ribonucleoprotein ubiquitylation effected by ageing in skeletal muscle.

Age-related splicing dysregulation appears to occur across other cell types and tissues. In 2011, transcriptomics of human leukocytes revealed major pathways affected by age relate to RNA processing [300]. In the brain, alternative splicing patterns have been associated with neurodegenerative diseases during ageing [301]. Interestingly, a comprehensive map of the human genome across multiple tissues found the splicing profile is a better indicator of human age than gene expression profiles [302]. In 2022, an exploration of ageing research meant that splicing dysregulation was proposed as a new hallmark of ageing [303].

The question now being posed is why dysregulated splicing is associated with ageing. One study reported that muscle fibres positive for the senescence markers showed enrichment for differential alternative splicing [262]. Splicing factors affect multiple aspects of cellular senescence — a key hallmark of ageing [17] — regulating telomere maintenance, DNA repair and SASP (senescence-associated secretory phenotypes) [304]. Perturbations towards splicing machinery can trigger cells to enter senescence, implicating the spliceosome as a key regulator

[305]. However, the exact mechanisms linking the rise in splicing factors to skeletal muscle senescence are unknown.

6.2.6 Histone ubiquitylation

Remarkably, only 2 diGly sites were significantly regulated in both male and female mice – Moesin (Msn) at K79 and Histone H2B type 1-K (H2bc12) at K121. Msn (K79) significantly decreased in the male soluble fraction and significantly increased in the female insoluble fraction with age. H2bc12 (K121) significantly decreased in the insoluble fraction of both sexes with age. Interestingly, H2bc12 (K121) was the most and third most significantly regulated diGly-modified peptide in the male and female insoluble fraction, respectively. It was interesting to see no age-related change in the more prevalent H2B isoforms. There is an antibody from Cell Signaling Technology which only detects Histone H2B when it is ubiquitylated at K121, however it is designed to bind to a sequence containing Ser124 which is not present in the H2bc12 isoform. Therefore, we could not use this approach to validate our findings. Histone H2B is known to be monoubiquitylated by Bre1 (also known as RNF20/40 complex) [306], which can be removed by a range of DUBs (USP12, USP22, USP44 and USP46) [307], [308], [309], none of which were detected in our proteomics datasets. It is possible that different E3 ligases and DUBs are involved in the ubiquitylation of different H2B isoforms.

Previous studies reporting changes on Histone H2B K121 ubiquitylation have not differentiated between isoforms. There are 16 isoforms of Histone H2B in humans, and the only ones that seem to have been studied in depth are testis-specific [256]. Whilst each isoform only differ by a few amino acids, these changes could significantly affect the protein function. With regards to H2bc12 the serine-to-alanine swap creates a larger polar charged amino acid

which could alter the structure of the C-terminal tail. Given the sequence similarity, bottom-up proteomics approach cannot distinguish between all Histone H2B isoforms as many share the same peptide sequences. Top-down proteomics retains the complete intact amino acid sequence and is therefore capable of distinguishing between all histone H2B isoforms and their PTMs. Whilst this approach is much less routinely performed it could offer more clarity on age-related changes in histone H2B ubiquitylation.

6.3 Limitations

6.3.1 Ageing model

Mice are frequently used to study the mechanisms of human ageing. Mice are both genetically and anatomically similar to humans, with 99% of human genes represented by an identifiable mouse homologue [310]. Importantly, they suffer from various age-related diseases similar to humans, including sarcopenia [230]. Mice have the advantage of having a much shorter life expectancy to humans, with the common laboratory mouse C57BL/6 living around 2.5 years [311]. However, the mouse model of ageing does have some shortcomings, for instance there is heterogeneity of muscle fibres between mouse and human skeletal muscle, in which mice are composed of more type II (fast muscle) fibres which are more susceptible to atrophy during ageing [285], [286], [312]. Given that the gastrocnemius muscle (fast) is the predominant muscle employed in our study, our findings may not be reproduced in slower human muscle fibres. For instance, a key finding from our dataset was a loss of proteostasis, which has been reported in aged rodent studies but lacks the same support in humans [19]. Although, recent work in humans has reported age-related increase in the UPR (Michie et al., 2024 – published ahead of print). The translational impact of our findings could be greater if we/others were able to repeat this work in aged humans.

The ageing model we employed is one that uses two distinct timepoints classified as 'young' and 'old'. This design means we cannot detect the timepoint at which age-related changes occur. The inclusion of middle-aged (~12 months) and advanced age (> 24 months) mice would help determine how proteins and ubiquitylated proteins changed over the ageing time course. At the transcriptional level, nearly 50% of age-related changes in males were only seen in mice aged 25 months, not observed in mice aged 17 or 21 months old – the age of our old mice [242]. Therefore, it is likely that we are missing age-related protein changes which occur at later life. Another limitation of our ageing model was the lack of phenotype characteristics available for the mice. Measurements such as daily activity, muscle force and fibre cross-sectional area would have allowed us to map individual protein changes in mice to their phenotype. The only measure we obtained for sarcopenia was muscle mass, which when accounting for body weight was not significantly downregulated in either sex **(Figure 6.3a and Figure 6.3b)**. Therefore, it is likely that the aged mice we have worked with are not experiencing sarcopenia. This is not surprising, as whilst muscle function has been shown to decline by the age of 18 months, more pronounced deterioration is seen around 24-25 months [230]. The age-related protein changes identified in our study could be driving factors of sarcopenia at a later stage. It would be interesting to see which of our age-related changes become more pronounced in a model of sarcopenia.

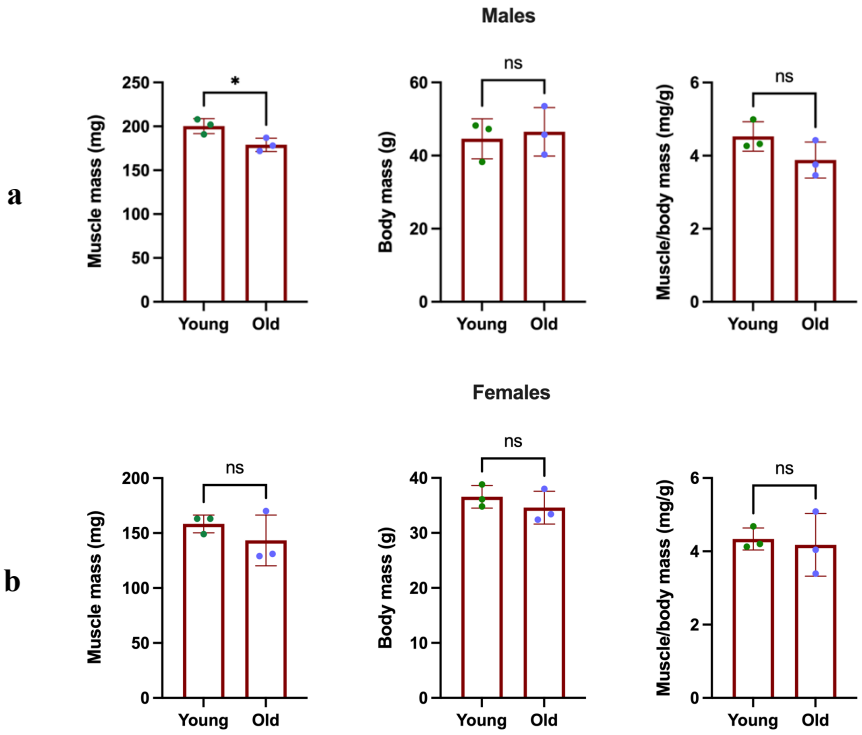

Figure 6. 3. Aged mice do not display muscle atrophy. Mass of the gastrocnemius complex muscle and whole body from the 3 young (6 month) and 3 old (21-22 month) a) male and b) female mice used for the proteomics and ubiquitylomics analysis. Data was visualised on GraphPad Prism using unpaired t-test to confirm significance (* = $P < 0.05$) with standard deviation bars.

Compared to the young mice, older mice displayed a much greater variation in protein abundance values. In the female mice, this meant that we suffered from low significance values despite certain protein abundance values showing a clear fold change difference between ages. By including a greater number of replicates, the impact that replicate variation has on statistical analysis would most likely be attenuated by reducing the effect of potential outliers. Whilst in theory this would have been beneficial, there are additional cost complications when increasing the sample number, for instance greater amount of antibody and TMT labels.

6.3.2 Separate male and female analysis

Due to sample availability, we had originally planned to conduct male analysis only. As a result, our female analysis was performed later on a separate LC-MS run. Typically, for TMT-

based quantification, you employ a reference channel to compare abundance values between LC-MS runs. Therefore, any technical variations which can influence LC-MS performance can be detected and adjusted for before comparison of protein abundances. In our study we had not anticipated comparing two separate LC-MS analyses, therefore we had not included a reference channel. This oversight meant we could not compare protein abundance values between sex. Of note, even if we had included a reference channel, TMT relies on DDA which is inherently stochastic and therefore you would still obtain unavoidable technical variation. Therefore, ideally this analysis would have been performed all in one run by using more TMT channels, or alternatively using DIA to remove stochasticity. The methodological constraint of our study highlights the importance of careful experimental design in proteomics studies.

6.4 User guide

Our ubiquitylomics protocol can be divided into five major stages: 1) tissue collection and lysis, 2) protein clean up, 3) protein digestion, 4) ubiquitin enrichment, and 5) LC-MS analysis.

1) During tissue collection we recommend using at least four biological replicates per ubiquitylomics experiment. If sample amounts permit, having more the 3 replicates allows you a) reduce the effect of biological variation in tissue samples and b) remove any outliers that may arise from technical variation during antibody enrichment. During tissue lysis it is important to include strong detergents e.g., SDS (or alternative solubilising agents e.g. urea) and DUB inhibitors e.g. PR-619 to extract and capture ubiquitylated proteins from tissue.
2) When performing SP4 clean-up for the first time, visualise protein content in both pellet and supernatant using a Coomassie protein stain. Small protein losses in the

supernatant are normal, but significant losses may indicate insufficient precipitation, agitation during washing or high content of hydrophilic proteins. For the latter, SP3 may be a more suitable option.

3) After protein digestion, we highly recommend checking that no protein is present by taking a small volume of sample (~10 µg) for a Coomassie protein stain. In the case of incomplete digestion, we advise performing an additional overnight digestion at room temperature. Checking complete digestion ensures equal peptide loading for ubiquitin enrichment, of note we do not recommend quantifying and normalising to peptide concentration given the suboptimal accuracy of available methods.
4) During ubiquitin enrichment, we recommend using magnetic beads to minimise agitation during wash steps. For TMT labelling, perform after enrichment and whilst peptides are still bound to the antibody. If feasible, we recommend users optimise both volume of antibody (e.g., 5, 10 and 20 µL) and volume of acetonitrile in wash stages (e.g., 0, 25 and 50 %). Both impact the level of unspecific peptide binding to the beads, impacting the number of ubiquitylated peptides identified during LC-MS.
5) As a guide we recommend injecting least 50% of the enriched sample to ensure sufficient peptide detection but also allow for a second run if needed. For TMT labelling, we advise using an orbitrap tribrid MS (e.g., Eclipse or Ascend) with FAIMS for high resolution spectra and MS^3 scanning with real time searching for improved quantitative accuracy. Given that ubiquitin is bound by a covalent bond, HCD can be used for fragmentation without loss of modification.

6.5 Future directions

Moving forward, we recommend a list of methodological techniques that future studies could harness to build upon our findings. To confirm the main findings of this work, it would be beneficial to employ targeted proteomics. Our work has used untargeted proteomics which benefits from high throughput but suffers from low reproducibility. Selected reaction monitoring (SRM) or parallel reaction monitoring (PRM) are targeted approaches which allow proteins to be studied in isolation with very little background noise, thereby achieving high sensitivity and reproducibility. Targeted proteomics also allows for absolute abundance to be determined by including reference peptides of known quantities. This has been used for quantifying ubiquitin chain types (Ub-AQUA) and could be used in future studies to quantify the absolute abundance of different ubiquitin chains between young and old skeletal muscle. To determine the biological impact of a ubiquitylation site, future studies could look to use site-directed mutagenesis in a cell model. Converting the amino acid site from a lysine to (typically) arginine, prevents the site from becoming ubiquitylated. By doing so, researchers can study whether this ubiquitylation site is critical for protein function. Finally, combining dynamic proteome profiling with ubiquitylomics provides a great opportunity to study those ubiquitin-modified proteins that are destined for degradation. Stable isotope labelling e.g., deuterated “heavy” water, in combination with MS measures individual rates of protein synthesis [313]. If combined with protein abundance measurements (a process known as dynamic proteome profiling), the mismatch between the synthesis and abundance can be attributed to degradation [314]. This could help identify which proteins are differentially degraded with age and whether this could be due to differences in ubiquitin modifications.

6.6 Final conclusions

This thesis has outlined methodology required to perform large-scale, untargeted analysis of the skeletal muscle proteome and ubiquitylome in addition to providing a resource of age-related changes that occur. We demonstrate that ageing is characterised by changes in many different biological pathways, most notably those involved in energy regulation, proteostasis, RNA processing and structural integrity both at the extracellular matrix and sarcomere. We have revealed specific ubiquitylation sites that are differentially modified with age, including those present on ribosomes, histones and proteasomes. We have addressed the sex-bias that is commonly seen in ageing rodent studies which has limited many ageing findings to males. In doing so, we highlight that the dysregulation of proteostasis in the endoplasmic reticulum is a male specific trait, at least at 21-22 months of age. This comprehensive analysis has generated an extensive dataset that serves as a valuable resource, enabling future investigations to delve deeper into the mechanistic significance of the age-related changes identified.

7. References

[1] A. Garmany, S. Yamada, and A. Terzic, “Longevity leap: mind the healthspan gap,” *NPJ Regen Med*, vol. 6, no. 1, pp. 1–7, 2021, doi: 10.1038/s41536-021-00169-5.
[2] K. Jin, J. W. Simpkins, X. Ji, M. Leis, and I. Stambler, “The critical need to promote research of aging and aging-related diseases to improve health and longevity of the elderly population,” *Aging Dis*, vol. 6, no. 1, pp. 1–5, 2015, doi: 10.14336/AD.2014.1210.
[3] K. D. Boudoulas, F. Triposkiadis, C. Stefanadis, and H. Boudoulas, “The endlessness evolution of medicine, continuous increase in life expectancy and constant role of the physician,” *Hellenic Journal of Cardiology*, vol. 58, no. 5, pp. 322–330, 2017, doi: 10.1016/j.hjc.2017.05.001.
[4] World Health Organization, *Decade of Healthy Ageing Decade of Healthy Ageing Functional Ability Intrinsic Capacity*, vol. 20, no. February. 2020. [Online]. Available: https://www.who.int/publications/i/item/9789240017900
[5] A. J. Cruz-Jentoft *et al.*, “Sarcopenia: Revised European consensus on definition and diagnosis,” *Age Ageing*, vol. 48, no. 1, pp. 16–31, 2019, doi: 10.1093/ageing/afy169.
[6] S. von Haehling, J. E. Morley, and S. D. Anker, “An overview of sarcopenia: Facts and numbers on prevalence and clinical impact,” *J Cachexia Sarcopenia Muscle*, vol. 1, no. 2, pp. 129–133, 2010, doi: 10.1007/s13539-010-0014-2.
[7] F. Landi *et al.*, “Sarcopenia and mortality risk in frail olderpersons aged 80 years and older: Results from iLSIRENTE study,” *Age Ageing*, vol. 42, no. 2, pp. 203–209, 2013, doi: 10.1093/ageing/afs194.
[8] P. Srikanthan and A. S. Karlamangla, “Relative muscle mass is inversely associated with insulin resistance and prediabetes. Findings from the Third National Health and Nutrition Examination Survey,” *Journal of Clinical Endocrinology and Metabolism*, vol. 96, no. 9, pp. 2898–2903, 2011, doi: 10.1210/jc.2011-0435.
[9] M. F. Xia *et al.*, “Sarcopenia, sarcopenic overweight/obesity and risk of cardiovascular disease and cardiac arrhythmia: A cross-sectional study,” *Clinical Nutrition*, no. xxxx, pp. 1–10, 2020, doi: 10.1016/j.clnu.2020.06.003.
[10] T. C. Peng, W. L. Chen, L. W. Wu, Y. W. Chang, and T. W. Kao, “Sarcopenia and cognitive impairment: A systematic review and meta-analysis,” *Clinical Nutrition*, vol. 39, no. 9, pp. 2695–2701, 2020, doi: 10.1016/j.clnu.2019.12.014.
[11] P. Srikanthan and A. S. Karlamangla, “Muscle mass index as a predictor of longevity in older adults,” *American Journal of Medicine*, vol. 127, no. 6, pp. 547–553, 2014, doi: 10.1016/j.amjmed.2014.02.007.
[12] E. J. Metter, L. A. Talbot, M. Schrager, and R. Conwit, “Skeletal muscle strength as a predictor of all-cause mortality in healthy men,” *Journals of Gerontology - Series A Biological Sciences and Medical Sciences*, vol. 57, no. 10, pp. B359–B365, 2002, doi: 10.1093/gerona/57.10.B359.
[13] R. Pinedo-Villanueva *et al.*, “Health Care Costs Associated With Muscle Weakness: A UK Population-Based Estimate,” *Calcif Tissue Int*, vol. 104, no. 2, pp. 137–144, 2019, doi: 10.1007/s00223-018-0478-1.
[14] B. T. Wall, M. L. Dirks, and L. J. C. Van Loon, “Skeletal muscle atrophy during short-term disuse: Implications for age-related sarcopenia,” *Ageing Res Rev*, vol. 12, no. 4, pp. 898–906, 2013, doi: 10.1016/j.arr.2013.07.003.
[15] G. D. Cartee, R. T. Hepple, M. M. Bamman, and J. R. Zierath, “Exercise Promotes Healthy Aging of Skeletal Muscle,” *Cell Metab*, vol. 23, no. 6, pp. 1034–1047, 2016, doi: 10.1016/j.cmet.2016.05.007.
[16] Y. Shen *et al.*, “Exercise for sarcopenia in older people: A systematic review and network meta-analysis,” *J Cachexia Sarcopenia Muscle*, vol. 14, no. 3, pp. 1199–1211, 2023, doi: 10.1002/jcsm.13225.

[17] C. López-Otín, M. A. Blasco, L. Partridge, M. Serrano, and G. Kroemer, “The hallmarks of aging,” *Cell*, vol. 153, no. 6, p. 1194, 2013, doi: 10.1016/j.cell.2013.05.039.
[18] C. López-Otín, M. A. Blasco, L. Partridge, M. Serrano, and G. Kroemer, “Hallmarks of aging: An expanding universe,” *Cell*, vol. 186, no. 2, pp. 243–278, 2023, doi: 10.1016/j.cell.2022.11.001.
[19] A. Granic, K. Suetterlin, T. Shavlakadze, M. D. Grounds, and A. A. Sayer, “Hallmarks of ageing in human skeletal muscle and implications for understanding the pathophysiology of sarcopenia in women and men,” *Clin Sci (Lond)*, vol. 137, no. 22, pp. 1721–1751, 2023, doi: 10.1042/CS20230319.
[20] A. S. Deshmukh, M. Murgia, N. Nagaraj, J. T. Treebak, J. Cox, and M. Mann, “Deep proteomics of mouse skeletal muscle enables quantitation of protein isoforms, metabolic pathways, and transcription factors,” *Molecular and Cellular Proteomics*, vol. 14, no. 4, pp. 841–853, 2015, doi: 10.1074/mcp.M114.044222.
[21] M. Gonzalez-Freire *et al.*, “The Human Skeletal Muscle Proteome Project: a reappraisal of the current literature,” *J Cachexia Sarcopenia Muscle*, vol. 8, no. 1, pp. 5–18, 2017, doi: 10.1002/jcsm.12121.
[22] C. T. Haun, C. G. Vann, B. M. Roberts, A. D. Vigotsky, B. J. Schoenfeld, and M. D. Roberts, “A critical evaluation of the biological construct skeletal muscle hypertrophy: Size matters but so does the measurement,” *Front Physiol*, vol. 10, no. MAR, pp. 1–23, 2019, doi: 10.3389/fphys.2019.00247.
[23] C. B. Abbott *et al.*, “A Novel Stable Isotope Approach Demonstrates Surprising Degree of Age-Related Decline in Skeletal Muscle Collagen Proteostasis,” *Function*, vol. 2, no. 4, pp. 1–11, 2021, doi: 10.1093/function/zqab028.
[24] C. L. O’Reilly, S. C. Bodine, and B. F. Miller, “Current limitations and future opportunities of tracer studies of muscle ageing,” *Journal of Physiology*, vol. 0, pp. 1–9, 2023, doi: 10.1113/JP285616.
[25] M. Murgia *et al.*, “Single Muscle Fiber Proteomics Reveals Fiber-Type-Specific Features of Human Muscle Aging,” *Cell Rep*, vol. 19, no. 11, pp. 2396–2409, 2017, doi: 10.1016/j.celrep.2017.05.054.
[26] P. Doran, J. Gannon, K. O’Connell, and K. Ohlendieck, “Aging skeletal muscle shows a drastic increase in the small heat shock proteins αB-crystallin/HspB5 and cvHsp/HspB7,” *Eur J Cell Biol*, vol. 86, no. 10, pp. 629–640, 2007, doi: 10.1016/j.ejcb.2007.07.003.
[27] P. Doran, K. O’Connell, J. Gannon, M. Kavanagh, and K. Ohlendieck, “Opposite pathobiochemical fate of pyruvate kinase and adenylate kinase in aged rat skeletal muscle as revealed by proteomic DIGE analysis,” *Proteomics*, vol. 8, no. 2, pp. 364–377, 2008, doi: 10.1002/pmic.200700475.
[28] M. Gueugneau *et al.*, “Proteomics of muscle chronological ageing in post-menopausal women,” *BMC Genomics*, vol. 15, no. 1, 2014, doi: 10.1186/1471-2164-15-1165.
[29] C. Y. Hwang *et al.*, “Quantitative proteome analysis of age-related changes in mouse gastrocnemius muscle using mTRAQ,” *Proteomics*, vol. 14, no. 1, pp. 121–132, 2014, doi: 10.1002/pmic.201200497.
[30] M. D. Roberts *et al.*, “A novel deep proteomic approach in human skeletal muscle unveils distinct molecular signatures affected by aging and resistance training,” *Aging*, pp. 6631–6651, 2024, doi: 10.18632/aging.205751.
[31] C. Ubaida-Mohien *et al.*, “Discovery proteomics in aging human skeletal muscle finds change in spliceosome, immunity, proteostasis and mitochondria,” *Elife*, vol. 8, pp. 1–27, 2019, doi: 10.7554/eLife.49874.

[32] M. J. Suskiewicz, “The logic of protein post-translational modifications (PTMs): Chemistry, mechanisms and evolution of protein regulation through covalent attachments,” *BioEssays*, vol. 46, no. 3, pp. 1–25, 2024, doi: 10.1002/bies.202300178.
[33] N. Kitamura and J. J. Galligan, “A global view of the human post-translational modification landscape,” *Biochemical Journal*, vol. 480, no. 16, pp. 1241–1265, 2023, doi: 10.1042/BCJ20220251.
[34] R. Aebersold *et al.*, “How many human proteoforms are there?,” *Nat Chem Biol*, vol. 14, no. 3, pp. 206–214, 2018, doi: 10.1038/nchembio.2576.
[35] S. Ramazi and J. Zahiri, “Post-translational modifications in proteins: Resources, tools and prediction methods,” *Database*, vol. 2021, no. 7, pp. 1–20, 2021, doi: 10.1093/database/baab012.
[36] Q. Zhong *et al.*, “Post-translational regulation of muscle growth, muscle aging and sarcopenia,” *J Cachexia Sarcopenia Muscle*, 2023, doi: 10.1002/jcsm.13241.
[37] D. J. Ryder, S. M. Judge, A. W. Beharry, C. L. Farnsworth, C. Silva, and A. R. Judge, “Identification of the Acetylation and Ubiquitin-Modified Proteome during the Progression of Skeletal Muscle Atrophy,” *PLoS One*, pp. 1–24, 2015, doi: 10.1371/journal.pone.0136247.
[38] K. Svensson *et al.*, “p300 and cAMP response element-binding protein-binding protein in skeletal muscle homeostasis, contractile function, and survival,” *J Cachexia Sarcopenia Muscle*, vol. 11, no. 2, pp. 464–477, 2020, doi: 10.1002/jcsm.12522.
[39] A. Lundby *et al.*, “Proteomic Analysis of Lysine Acetylation Sites in Rat Tissues Reveals Organ Specificity and Subcellular Patterns,” *Cell Rep*, vol. 2, no. 2, pp. 419–431, 2012, doi: 10.1016/j.celrep.2012.07.006.
[40] A. Hershko and A. Ciechanover, “THE UBIQUITIN SYSTEM,” *Annu Rev Biochem*, vol. 67, no. 1, pp. 425–479, Jun. 1998, doi: 10.1146/annurev.biochem.67.1.425.
[41] K. Haglund and I. Dikic, “Ubiquitylation and cell signaling,” *EMBO Journal*, vol. 24, no. 19, pp. 3353–3359, 2005, doi: 10.1038/sj.emboj.7600808.
[42] S. Ghosh and T. Saha, “Central Role of Ubiquitination in Genome Maintenance: DNA Replication and Damage Repair,” *ISRN Mol Biol*, vol. 2012, pp. 1–9, 2012, doi: 10.5402/2012/146748.
[43] L. Hicke and R. Dunn, “Regulation of Membrane Protein Transport by Ubiquitin and Ubiquitin-Binding Proteins,” *Annu Rev Cell Dev Biol*, vol. 19, pp. 141–172, 2003, doi: 10.1146/annurev.cellbio.19.110701.154617.
[44] I. R. Kelsall, “Non-lysine ubiquitylation: Doing things differently,” 2022. doi: 10.3389/fmolb.2022.1008175.
[45] I. Dikic and B. A. Schulman, “An expanded lexicon for the ubiquitin code,” *Nat Rev Mol Cell Biol*, vol. 0123456789, 2022, doi: 10.1038/s41580-022-00543-1.
[46] M. J. Clague, C. Heride, and S. Urbé, “The demographics of the ubiquitin system,” *Trends Cell Biol*, vol. 25, no. 7, pp. 417–426, 2015, doi: 10.1016/j.tcb.2015.03.002.
[47] K. N. Swatek and D. Komander, “Ubiquitin modifications,” 2016. doi: 10.1038/cr.2016.39.
[48] I. Dikic, S. Wakatsuki, and K. J. Walters, “Ubiquitin-binding domains from structures to functions,” *Nat Rev Mol Cell Biol*, vol. 10, no. 10, pp. 659–671, 2009, doi: 10.1038/nrm2767.
[49] M. Akutsu, I. Dikic, and A. Bremm, “Ubiquitin chain diversity at a glance,” *J Cell Sci*, vol. 129, no. 5, pp. 875–880, 2016, doi: 10.1242/jcs.183954.
[50] W. Kim *et al.*, “Systematic and Quantitative Assessment of the Ubiquitin-Modified Proteome,” *Mol Cell*, vol. 44, no. 2, pp. 325–340, 2011, doi: 10.1016/j.molcel.2011.08.025.

[51] D. Komander and M. Rape, “The Ubiquitin Code,” *Annu Rev Biochem*, vol. 81, no. 1, pp. 203–229, 2012, doi: 10.1146/annurev-biochem-060310-170328.
[52] M. Tracz and W. Bialek, “Beyond K48 and K63: non-canonical protein ubiquitination,” *Cell Mol Biol Lett*, vol. 26, no. 1, pp. 1–17, 2021, doi: 10.1186/s11658-020-00245-6.
[53] G. Dittmar and K. F. Winklhofer, “Linear Ubiquitin Chains: Cellular Functions and Strategies for Detection and Quantification,” *Front Chem*, vol. 7, no. January, pp. 1–16, 2020, doi: 10.3389/fchem.2019.00915.
[54] A. J. McClellan, S. H. Laugesen, and L. Ellgaard, “Cellular functions and molecular mechanisms of non-lysine ubiquitination,” *Open Biol*, vol. 9, no. 9, 2019, doi: 10.1098/rsob190147.
[55] A. Zuin, M. Isasa, and B. Crosas, “Ubiquitin signaling: Extreme conservation as a source of diversity,” *Cells*, vol. 3, no. 3, pp. 690–701, 2014, doi: 10.3390/cells3030690.
[56] P. M. Sharp and W. H. Li, “Molecular evolution of ubiquitin genes,” *Trends Ecol Evol*, vol. 2, no. 11, pp. 328–332, 1987, doi: 10.1016/0169-5347(87)90108-X.
[57] X. Hou *et al.*, “Mining and characterization of ubiquitin E3 ligases expressed in the mouse testis,” *BMC Genomics*, vol. 13, no. 1, pp. 1–12, 2012, doi: 10.1186/1471-2164-13-495.
[58] D. Cai, K. K. H. Lee, M. Li, M. K. Tang, and K. M. Chan, “Ubiquitin expression is up-regulated in human and rat skeletal muscles during aging,” *Arch Biochem Biophys*, vol. 425, no. 1, pp. 42–50, 2004, doi: 10.1016/j.abb.2004.02.027.
[59] S. Clavel, A. S. Coldefy, E. Kurkdjian, J. Salles, I. Margaritis, and B. Derijard, “Atrophy-related ubiquitin ligases, atrogin-1 and MuRF1 are up-regulated in aged rat Tibialis Anterior muscle,” *Mech Ageing Dev*, vol. 127, no. 10, pp. 794–801, 2006, doi: 10.1016/j.mad.2006.07.005.
[60] C. N. Chen, Y. H. Liao, S. C. Tsai, and L. D. V. Thompson, “Age-dependent effects of caloric restriction on mTOR and ubiquitin-proteasome pathways in skeletal muscles,” *Geroscience*, vol. 41, no. 6, pp. 871–880, 2019, doi: 10.1007/s11357-019-00109-8.
[61] L. M. Baehr *et al.*, “Age-related deficits in skeletal muscle recovery following disuse are associated with neuromuscular junction instability and ER stress, not impaired protein synthesis,” *Aging*, vol. 8, no. 1, pp. 127–146, 2016, doi: 10.18632/aging.100879.
[62] S. C. Bodine *et al.*, “Identification of Ubiquitin Ligases Required for Skeletal Muscle Atrophy,” 2001. Accessed: Apr. 01, 2019. [Online]. Available: https://www-jstor-org.ezproxye.bham.ac.uk/stable/pdf/3085298.pdf?refreqid=excelsior%3Aaf00ba1aeb2f31bef1633084dffca959
[63] M. D. Gomes, S. H. Lecker, R. T. Jagoe, A. Navon, and A. L. Goldberg, “Atrogin-1, a muscle-specific F-box protein highly expressed during muscle atrophy,” *Structure*, pp. 1–6, 2001.
[64] D. C. Hughes, L. M. Baehr, D. S. Waddell, and A. P. Sharples, “Ubiquitin Ligases in Longevity and Aging Skeletal Muscle,” pp. 1–23, 2022.
[65] J. Y. Seo *et al.*, “Maintenance of type 2 glycolytic myofibers with age by Mib1-Actn3 axis,” *Nat Commun*, vol. 12, no. 1, pp. 1–15, 2021, doi: 10.1038/s41467-021-21621-6.
[66] K. Yamano, N. Matsuda, and K. Tanaka, “The ubiquitin signal and autophagy: an orchestrated dance leading to mitochondrial degradation,” *EMBO Rep*, vol. 17, no. 3, pp. 300–316, 2016, doi: 10.15252/embr.201541486.
[67] C. C. W. Chen, A. T. Erlich, M. J. Crilly, and D. A. Hood, “Parkin is required for exercise-induced mitophagy in muscle: Impact of aging,” *Am J Physiol Endocrinol Metab*, vol. 315, no. 3, pp. E404–E415, 2018, doi: 10.1152/ajpendo.00391.2017.

[68] J. P. Leduc-Gaudet, O. Reynaud, S. N. Hussain, and G. Gouspillou, “Parkin overexpression protects from ageing-related loss of muscle mass and strength,” *Journal of Physiology*, vol. 597, no. 7, pp. 1975–1991, 2019, doi: 10.1113/JP277157.
[69] G. Gouspillou *et al.*, “Protective role of Parkin in skeletal muscle contractile and mitochondrial function,” *Journal of Physiology*, vol. 596, no. 13, pp. 2565–2579, 2018, doi: 10.1113/JP275604.
[70] L. C. Hunt *et al.*, “Antagonistic control of myofiber size and muscle protein quality control by the ubiquitin ligase UBR4 during aging,” *Nat Commun*, 2021, doi: 10.1038/s41467-021-21738-8.
[71] R. Tawo *et al.*, “The Ubiquitin Ligase CHIP Integrates Proteostasis and Aging by Regulation of Insulin Receptor Turnover,” *Cell*, vol. 169, no. 3, pp. 470-482.e13, 2017, doi: 10.1016/j.cell.2017.04.003.
[72] É. Kevei and T. Hoppe, “Ubiquitin sets the timer: Impacts on aging and longevity,” *Nat Struct Mol Biol*, vol. 21, no. 4, pp. 290–292, 2014, doi: 10.1038/nsmb.2806.
[73] J.-N. Min, R. A. Whaley, N. E. Sharpless, P. Lockyer, A. L. Portbury, and C. Patterson, “CHIP Deficiency Decreases Longevity, with Accelerated Aging Phenotypes Accompanied by Altered Protein Quality Control,” *Mol Cell Biol*, vol. 28, no. 12, pp. 4018–4025, 2008, doi: 10.1128/mcb.00296-08.
[74] M. Altun *et al.*, “Muscle wasting in aged, sarcopenic rats is associated with enhanced activity of the ubiquitin proteasome pathway,” *Journal of Biological Chemistry*, vol. 285, no. 51, pp. 39597–39608, 2010, doi: 10.1074/jbc.M110.129718.
[75] M. J. Lee, B. H. Lee, J. Hanna, R. W. King, and D. Finley, “Trimming of ubiquitin chains by proteasome-associated deubiquitinating enzymes,” *Molecular and Cellular Proteomics*, vol. 10, no. 5, p. R110.003871, 2011, doi: 10.1074/mcp.R110.003871.
[76] M. He *et al.*, “The emerging role of deubiquitinating enzymes in genomic integrity, diseases, and therapeutics,” *Cell Biosci*, vol. 6, no. 1, pp. 1–15, 2016, doi: 10.1186/s13578-016-0127-1.
[77] D. Komander, M. J. Clague, and S. Urbé, “Breaking the chains: Structure and function of the deubiquitinases,” *Nat Rev Mol Cell Biol*, vol. 10, no. 8, pp. 550–563, 2009, doi: 10.1038/nrm2731.
[78] N. Bédard *et al.*, “Inactivation of the ubiquitin-specific protease 19 deubiquitinating enzyme protects against muscle wasting,” *FASEB Journal*, vol. 29, no. 9, pp. 3889–3898, 2015, doi: 10.1096/fj.15-270579.
[79] E. S. Coyne *et al.*, “Knockout of USP19 deubiquitinating enzyme prevents muscle wasting by modulating insulin and glucocorticoid signaling,” *Endocrinology*, vol. 159, no. 8, pp. 2966–2977, 2018, doi: 10.1210/en.2018-00290.
[80] S. Koyuncu, R. Loureiro, H. J. Lee, P. Wagle, M. Krueger, and D. Vilchez, “Rewiring of the ubiquitinated proteome determines ageing in C . elegans,” *Nature*, no. November 2020, 2021, doi: 10.1038/s41586-021-03781-z.
[81] F. El Magraoui, C. Reidick, H. E. Meyer, and H. W. Platta, “Autophagy-related deubiquitinating enzymes involved in health and disease,” *Cells*, vol. 4, no. 4, pp. 596–621, 2015, doi: 10.3390/cells4040596.
[82] K. Tanaka, “The proteasome: Overview of structure and functions,” *Proc Jpn Acad Ser B Phys Biol Sci*, vol. 85, no. 1, pp. 12–36, 2009, doi: 10.2183/pjab.85.12.
[83] J. N. Keller, F. F. Huang, and W. R. Markesbery, “Decreased levels of proteasome activity and proteasome expression in aging spinal cord,” *Neuroscience*, vol. 98, no. 1, pp. 149–156, 2000, doi: 10.1016/S0306-4522(00)00067-1.
[84] A. L. Bulteau, I. Petropoulos, and B. Friguet, “Age-related alterations of proteasome structure and function in aging epidermis,” *Exp Gerontol*, vol. 35, no. 6–7, pp. 767–777, 2000, doi: 10.1016/S0531-5565(00)00136-4.

[85] A. L. Bulteau, L. I. Szweda, and B. Friguet, “Age-dependent declines in proteasome activity in the heart,” *Arch Biochem Biophys*, vol. 397, no. 2, pp. 298–304, 2002, doi: 10.1006/abbi.2001.2663.
[86] C. Behl, “BAG3 and friends: Co-chaperones in selective autophagy during aging and disease,” *Autophagy*, vol. 7, no. 7, pp. 795–798, 2011, doi: 10.4161/auto.7.7.15844.
[87] D. A. Ferrington, A. D. Husom, and L. V. Thompson, “Altered proteasome structure, function, and oxidation in aged muscle,” *The FASEB Journal*, vol. 19, no. 6, pp. 1–24, 2005, doi: 10.1096/fj.04-2578fje.
[88] K. H. Strucksberg, K. Tangavelou, R. Schröder, and C. S. Clemen, “Proteasomal activity in skeletal muscle: A matter of assay design, muscle type, and age,” *Anal Biochem*, vol. 399, no. 2, pp. 225–229, 2010, doi: 10.1016/j.ab.2009.12.026.
[89] L. Combaret *et al.*, “A leucine-supplemented diet restores the defective postprandial inhibition of proteasome-dependent proteolysis in aged rat skeletal muscle,” *Journal of Physiology*, vol. 569, no. 2, pp. 489–499, 2005, doi: 10.1113/jphysiol.2005.098004.
[90] A. D. Husom, E. A. Peters, E. A. Kolling, N. A. Fugere, L. D. V. Thompson, and D. A. Ferrington, “Altered proteasome function and subunit composition in aged muscle,” *Arch Biochem Biophys*, vol. 421, no. 1, pp. 67–76, 2004, doi: 10.1016/j.abb.2003.10.010.
[91] Z. Radák *et al.*, “Effect of aging and late onset dietary restriction on antioxidant enzymes and proteasome activities, and protein carbonylation of rat skeletal muscle and tendon,” *Exp Gerontol*, vol. 37, no. 12, pp. 1423–1430, 2002, doi: 10.1016/S0531-5565(02)00116-X.
[92] D. T. Hwee, L. M. Baehr, A. Philp, K. Baar, and S. C. Bodine, “Maintenance of muscle mass and load-induced growth in Muscle RING Finger 1 null mice with age,” *Aging Cell*, vol. 13, no. 1, pp. 92–101, 2014, doi: 10.1111/acel.12150.
[93] M. Bossola, F. Pacelli, P. Costelli, A. Tortorelli, F. Rosa, and G. B. Doglietto, “Proteasome activities in the rectus abdominis muscle of young and older individuals,” *Biogerontology*, vol. 9, no. 4, pp. 261–268, 2008, doi: 10.1007/s10522-008-9135-9.
[94] R. T. Hepple, M. Qin, H. Nakamoto, and S. Goto, “Caloric restriction optimizes the proteasome pathway with aging in rat plantaris muscle: Implications for sarcopenia,” *Am J Physiol Regul Integr Comp Physiol*, vol. 295, no. 4, pp. 1231–1237, 2008, doi: 10.1152/ajpregu.90478.2008.
[95] R. Fernando *et al.*, “Low proteasomal activity in fast skeletal muscle fibers is not associated with increased age-related oxidative damage,” *Exp Gerontol*, vol. 117, no. May 2018, pp. 45–52, 2019, doi: 10.1016/j.exger.2018.10.018.
[96] F. Bardag-Gorce, L. Farout, C. Veyrat-Durebex, Y. Briand, and M. Briand, “Changes in 20S proteasome activity during ageing of the LOU rat,” *Mol Biol Rep*, vol. 26, no. 1–2, pp. 89–93, 1999, doi: 10.1023/a:1006968208077.
[97] Y. Kitajima *et al.*, “Proteasome dysfunction induces muscle growth defects and protein aggregation,” *J Cell Sci*, vol. 127, no. 24, pp. 5204–5217, 2014, doi: 10.1242/jcs.150961.
[98] N. Mizushima and M. Komatsu, “Autophagy: Renovation of cells and tissues,” *Cell*, vol. 147, no. 4, pp. 728–741, 2011, doi: 10.1016/j.cell.2011.10.026.
[99] A. Khaminets, C. Behl, and I. Dikic, “Ubiquitin-Dependent And Independent Signals In Selective Autophagy,” *Trends Cell Biol*, vol. 26, no. 1, pp. 6–16, 2016, doi: 10.1016/j.tcb.2015.08.010.
[100] V. Rogov, V. Dötsch, T. Johansen, and V. Kirkin, “Interactions between Autophagy Receptors and Ubiquitin-like Proteins Form the Molecular Basis for Selective Autophagy,” *Mol Cell*, vol. 53, no. 2, pp. 167–178, 2014, doi: 10.1016/j.molcel.2013.12.014.

[101] C. Pohl and I. Dikic, “Cellular quality control by the ubiquitin-proteasome system and autophagy,” *Science (1979)*, vol. 366, no. 6467, pp. 818–822, 2019, doi: 10.1126/science.aax3769.
[102] L. García-Prat *et al.*, “Autophagy maintains stemness by preventing senescence,” *Nature*, vol. 529, no. 7584, pp. 37–42, 2016, doi: 10.1038/nature16187.
[103] G. Xie *et al.*, “Autophagy in sarcopenia: Possible mechanisms and novel therapies,” *Biomedicine and Pharmacotherapy*, vol. 165, no. June, p. 115147, 2023, doi: 10.1016/j.biopha.2023.115147.
[104] Z. Zeng, J. Liang, L. Wu, H. Zhang, J. Lv, and N. Chen, “Exercise-Induced Autophagy Suppresses Sarcopenia Through Akt/mTOR and Akt/FoxO3a Signal Pathways and AMPK-Mediated Mitochondrial Quality Control,” *Front Physiol*, vol. 11, no. November, 2020, doi: 10.3389/fphys.2020.583478.
[105] J. Liang *et al.*, “Lifelong Aerobic Exercise Alleviates Sarcopenia by Activating Autophagy and Inhibiting Protein Degradation via the AMPK/PGC-1α Signaling Pathway,” *Metabolites*, 2021.
[106] N. Raben *et al.*, “Suppression of autophagy in skeletal muscle uncovers the accumulation of ubiquitinated proteins and their potential role in muscle damage in Pompe disease,” *Hum Mol Genet*, vol. 17, no. 24, pp. 3897–3908, 2008, doi: 10.1093/hmg/ddn292.
[107] E. Masiero *et al.*, “Autophagy Is Required to Maintain Muscle Mass,” *Cell Metab*, vol. 10, no. 6, pp. 507–515, 2009, doi: 10.1016/j.cmet.2009.10.008.
[108] J. D. Fuqua *et al.*, “ULK2 is essential for degradation of ubiquitinated protein aggregates and homeostasis in skeletal muscle,” *FASEB Journal*, vol. 33, no. 11, pp. 11735–12745, 2019, doi: 10.1096/fj.201900766R.
[109] A. Sinha and M. Mann, “A beginner’s guide to mass spectrometry–based proteomics,” *Biochem (Lond)*, vol. 0, no. June, pp. 1–6, 2020, [Online]. Available: https://doi.org/10.1042/BIO20200034
[110] F. Trulsson *et al.*, “Deubiquitinating enzymes and the proteasome regulate preferential sets of ubiquitin substrates,” *Nat Commun*, vol. 13, no. 1, 2022, doi: 10.1038/s41467-022-30376-7.
[111] G. Prus, S. Satpathy, B. T. Weinert, and T. Narita, “Resource Global , site-resolved analysis of ubiquitylation occupancy and turnover rate reveals systems properties Global , site-resolved analysis of ubiquitylation occupancy and turnover rate reveals systems properties,” *Cell*, pp. 1–18, 2024, doi: 10.1016/j.cell.2024.03.024.
[112] J. Li *et al.*, “Proteome-wide mapping of short-lived proteins in human cells,” *Mol Cell*, vol. 81, no. 22, pp. 4722-4735.e5, 2021, doi: 10.1016/j.molcel.2021.09.015.
[113] C. H. Emmerich and P. Cohen, “Optimising methods for the preservation, capture and identification of ubiquitin chains and ubiquitylated proteins by immunoblotting,” *Biochem Biophys Res Commun*, vol. 466, no. 1, pp. 1–14, 2015, doi: 10.1016/j.bbrc.2015.08.109.
[114] N. Albornoz, H. Bustamante, A. Soza, and P. Burgos, “Cellular responses to proteasome inhibition: Molecular mechanisms and beyond,” *Int J Mol Sci*, vol. 20, no. 14, 2019, doi: 10.3390/ijms20143379.
[115] S. A. Wagner *et al.*, “A Proteome-wide, Quantitative Survey of In Vivo Ubiquitylation Sites Reveals Widespread Regulatory Roles,” *Molecular & Cellular Proteomics*, vol. 10, no. 10, p. M111.013284, 2011, doi: 10.1074/mcp.m111.013284.
[116] B. D. Silverman, “Hydrophobicity of transmembrane proteins: Spatially profiling the distribution,” *Protein Science*, vol. 12, no. 3, pp. 586–599, 2003, doi: 10.1110/ps.0214903.

[117] T. Masuda, S. Ito, and S. Ohtsuki, “Advances in sample preparation for membrane proteome quantification,” *Drug Discov Today Technol*, vol. 39, pp. 23–29, 2021, doi: 10.1016/j.ddtec.2021.06.005.
[118] H. E. Johnston *et al.*, “Solvent Precipitation SP3 (SP4) Enhances Recovery for Proteomics Sample Preparation without Magnetic Beads,” *Anal Chem*, vol. 94, no. 29, pp. 10320–10328, 2022, doi: 10.1021/acs.analchem.1c04200.
[119] N. Foot, T. Henshall, and S. Kumar, “Ubiquitination and the regulation of membrane proteins,” *Physiol Rev*, vol. 97, no. 1, pp. 253–281, 2017, doi: 10.1152/physrev.00012.2016.
[120] Q. Huang and X. Zhang, “Emerging Roles and Research Tools of Atypical Ubiquitination,” *Proteomics*, vol. 20, no. 9, pp. 1–9, 2020, doi: 10.1002/pmic.201900100.
[121] K. Newton *et al.*, “Ubiquitin Chain Editing Revealed by Polyubiquitin Linkage-Specific Antibodies,” *Cell*, vol. 134, no. 4, pp. 668–678, 2008, doi: 10.1016/j.cell.2008.07.039.
[122] M. D. Wilson, M. Saponaro, M. A. Leidl, and J. Q. Svejstrup, “MultiDsk: A Ubiquitin-Specific Affinity Resin,” *PLoS One*, vol. 7, no. 10, 2012, doi: 10.1371/journal.pone.0046398.
[123] R. Hjerpe, F. Aillet, F. Lopitz-Otsoa, V. Lang, P. England, and M. S. Rodriguez, “Efficient protection and isolation of ubiquitylated proteins using tandem ubiquitin-binding entities,” *EMBO Rep*, vol. 10, no. 11, pp. 1250–1258, 2009, doi: 10.1038/embor.2009.192.
[124] M. Zhang, J. M. Berk, A. B. Mehrtash, J. Kanyo, and M. H. Id, *A versatile new tool derived from a bacterial deubiquitylase to detect and purify ubiquitylated substrates and their interacting proteins*. 2022. doi: 10.1371/journal.pbio.3001501.
[125] G. Xu, J. S. Paige, and S. R. Jaffrey, “Global analysis of lysine ubiquitination by ubiquitin remnant immunoaffinity profiling,” *Nat Biotechnol*, vol. 28, no. 8, pp. 868–873, 2010, doi: 10.1038/nbt.1654.
[126] A. Subramanian *et al.*, “Gene set enrichment analysis: A knowledge-based approach for interpreting genome-wide expression profiles,” *Proc Natl Acad Sci U S A*, vol. 102, no. 43, pp. 15545–15550, 2005, doi: 10.1073/pnas.0506580102.
[127] J. Peng *et al.*, “A proteomics approach to understanding protein ubiquitination,” *Nat Biotechnol*, vol. 21, no. 8, pp. 921–926, 2003, doi: 10.1038/nbt849.
[128] N. D. Udeshi *et al.*, “Refined preparation and use of anti-diglycine remnant (k-ε-gg) antibody enables routine quantification of 10,000s of ubiquitination sites in single proteomics experiments,” *Molecular and Cellular Proteomics*, vol. 12, no. 3, pp. 825–831, 2013, doi: 10.1074/mcp.O112.027094.
[129] N. D. Udeshi *et al.*, “Rapid and deep-scale ubiquitylation profiling for biology and translational research,” *Nat Commun*, 2020, doi: 10.1038/s41467-019-14175-1.
[130] K. D. Rivera *et al.*, “Automating UbiFast for High-throughput and Multiplexed Ubiquitin Enrichment,” *Molecular and Cellular Proteomics*, vol. 20, p. 100154, 2021, doi: 10.1016/j.mcpro.2021.100154.
[131] V. Akimov *et al.*, “Ubisite approach for comprehensive mapping of lysine and n-terminal ubiquitination sites,” *Nat Struct Mol Biol*, vol. 25, no. 7, pp. 631–640, 2018, doi: 10.1038/s41594-018-0084-y.
[132] C. W. Davies *et al.*, “Antibody toolkit reveals N-terminally ubiquitinated substrates of UBE2W,” *Nat Commun*, vol. 12, no. 1, pp. 1–19, 2021, doi: 10.1038/s41467-021-24669-6.

[133] M. Mattern, J. Sutherland, K. Kadimisetty, R. Barrio, and M. S. Rodriguez, “Using Ubiquitin Binders to Decipher the Ubiquitin Code,” *Trends Biochem Sci*, vol. 44, no. 7, pp. 599–615, 2019, doi: 10.1016/j.tibs.2019.01.011.
[134] P. Xu and J. Peng, “Characterization of polyubiquitin chain structure by middle-down mass spectrometry,” *Anal Chem*, vol. 80, no. 9, pp. 3438–3444, 2008, doi: 10.1021/ac800016w.
[135] K. N. Swatek *et al.*, “Insights into ubiquitin chain architecture using Ub-clipping,” *Nature*, vol. 572, no. 7770, pp. 533–537, 2019, doi: 10.1038/s41586-019-1482-y.
[136] H. Tsuchiya *et al.*, “Ub-ProT reveals global length and composition of protein ubiquitylation in cells,” *Nat Commun*, vol. 9, no. 1, 2018, doi: 10.1038/s41467-018-02869-x.
[137] D. S. Kirkpatrick *et al.*, “Quantitative analysis of in vitro ubiquitinated cyclin B1 reveals complex chain topology,” *Nat Cell Biol*, vol. 8, no. 7, pp. 700–710, 2006, doi: 10.1038/ncb1436.
[138] T. Heunis, F. Lamoliatte, J. L. Marín-Rubio, A. Dannoura, and M. Trost, “Technical report: Targeted proteomic analysis reveals enrichment of atypical ubiquitin chains in contractile murine tissues,” *J Proteomics*, vol. 229, no. August, p. 103963, 2020, doi: 10.1016/j.jprot.2020.103963.
[139] S. E. Kaiser *et al.*, “Protein standard absolute quantification (PSAQ) method for the measurement of cellular ubiquitin pools,” *Nat Methods*, vol. 8, no. 8, pp. 691–696, 2011, doi: 10.1038/nmeth.1649.
[140] Amit Fulzele and Eric J. Bennett, “Ubiquitin diGLY Proteomics as an Approach to Identify and Quantify the Ubiquitin-Modified Proteome,” *Methods in Molecular Biology*, vol. 1844, pp. 101–103, 2018, doi: 10.31826/9781463211677-023.
[141] M. J. Emanuele *et al.*, “Global identification of modular cullin-RING ligase substrates,” *Cell*, vol. 147, no. 2, pp. 459–474, 2011, doi: 10.1016/j.cell.2011.09.019.
[142] L. M. Baehr *et al.*, “Identification of the MuRF1 skeletal muscle ubiquitylome through quantitative proteomics,” *American Physiological Society - Function*, vol. 2, no. May, pp. 14–27, 2021.
[143] C. A. Goodman, J. R. Davey, A. Hagg, B. L. Parker, and P. Gregorevic, “Dynamic Changes to the Skeletal Muscle Proteome and Ubiquitinome Induced by the E3 Ligase, ASB2β,” *Molecular & Cellular Proteomics*, vol. 20, p. 100050, 2021, doi: 10.1016/j.mcpro.2021.100050.
[144] A. Mansur *et al.*, “Dynamic regulation of inter-organelle communication by ubiquitylation controls skeletal muscle development and disease onset,” *Elife*, vol. 12, pp. 1–33, 2023, doi: 10.7554/eLife.81966.
[145] B. Bingol *et al.*, “The mitochondrial deubiquitinase USP30 opposes parkin-mediated mitophagy,” *Nature*, vol. 510, no. 7505, pp. 370–375, 2014, doi: 10.1038/nature13418.
[146] N. Elu *et al.*, “Identification of substrates for human deubiquitinating enzymes (DUBs): An up-to-date review and a case study for neurodevelopmental disorders,” *Semin Cell Dev Biol*, vol. 132, no. November 2021, pp. 120–131, 2022, doi: 10.1016/j.semcdb.2022.01.001.
[147] H. F. O’Connor *et al.*, “Ubiquitin-Activated Interaction Traps (UBAITs) identify E3 ligase binding partners,” *EMBO Rep*, vol. 16, no. 12, pp. 1699–1712, 2015, doi: 10.15252/embr.201540620.
[148] M. Watanabe *et al.*, “A substrate-trapping strategy to find E3 ubiquitin ligase substrates identifies Parkin and TRIM28 targets,” *Commun Biol*, vol. 3, no. 1, pp. 2–4, 2020, doi: 10.1038/s42003-020-01328-y.

[149] Y. Yoshida, Y. Saeki, A. Murakami, J. Kawawaki, H. Tsuchiya, and H. Yoshihara, “A comprehensive method for detecting ubiquitinated substrates using TR-TUBE,” *Proc Natl Acad Sci U S A*, vol. 112, no. 15, 2015, doi: 10.1073/pnas.1422313112.
[150] T. C. Branon *et al.*, “Efficient proximity labeling in living cells and organisms with TurboID,” *Nat Biotechnol*, vol. 36, no. 9, pp. 880–898, 2018, doi: 10.1038/nbt.4201.
[151] O. Barroso-Gomila *et al.*, “BioE3 identifies specific substrates of ubiquitin E3 ligases,” *Nat Commun*, vol. 14, no. 1, 2023, doi: 10.1038/s41467-023-43326-8.
[152] H. T. Huang *et al.*, “Ubiquitin-specific proximity labeling for the identification of E3 ligase substrates,” *Nat Chem Biol*, 2024, doi: 10.1038/s41589-024-01590-9.
[153] U. Mukhopadhyay *et al.*, “A ubiquitin-specific, proximity-based labeling approach for the identification of ubiquitin ligase substrates,” *Sci Adv*, vol. 10, no. 32, p. eadp3000, Aug. 2024, doi: 10.1126/sciadv.adp3000.
[154] L. Zhao, J. Zhao, K. Zhong, A. Tong, and D. Jia, “Targeted protein degradation: mechanisms, strategies and application,” *Signal Transduct Target Ther*, vol. 7, no. 1, 2022, doi: 10.1038/s41392-022-00966-4.
[155] J. Krönke *et al.*, “Lenalidomide causes selective degradation of IKZF1 and IKZF3 in multiple myeloma cells,” *Science (1979)*, vol. 343, no. 6168, pp. 301–305, 2014, doi: 10.1126/science.1244851.
[156] M. Leutert, S. W. Entwisle, and J. Villén, “Decoding post-translational modification crosstalk with proteomics,” *Molecular and Cellular Proteomics*, vol. 20, pp. 0–11, 2021, doi: 10.1016/j.mcpro.2021.100129.
[157] P. Mertins *et al.*, “Integrated proteomic analysis of post-translational modifications by serial enrichment,” *Nat Methods*, vol. 10, no. 7, pp. 634–637, 2013, doi: 10.1038/nmeth.2518.
[158] J. G. Abelin *et al.*, “Workflow enabling deepscale immunopepti- proteome , and acetylome analyses of sample-limited tissues,” *Nat Chem Biol*, pp. 1–22, 2023, doi: 10.1038/s41467-023-37547-0.
[159] K. R. Adoni, D. L. Cunningham, J. K. Heath, and A. C. Leney, “FAIMS Enhances the Detection of PTM Crosstalk Sites,” *J Proteome Res*, vol. 21, no. 4, pp. 930–939, 2022, doi: 10.1021/acs.jproteome.1c00721.
[160] C. M. Potel, S. Lemeer, and A. J. R. Heck, “Phosphopeptide Fragmentation and Site Localization by Mass Spectrometry: An Update,” *Anal Chem*, vol. 91, no. 1, pp. 126–141, 2019, doi: 10.1021/acs.analchem.8b04746.
[161] D. L. Swaney *et al.*, “Global analysis of phosphorylation and ubiquitylation cross-talk in protein degradation,” *Nat Methods*, vol. 10, no. 7, pp. 676–682, 2013, doi: 10.1038/nmeth.2519.
[162] H. Lu *et al.*, “Cell cycle-dependent phosphorylation regulates RECQL4 pathway choice and ubiquitination in DNA double-strand break repair,” *Nat Commun*, vol. 8, no. 1, 2017, doi: 10.1038/s41467-017-02146-3.
[163] S. Huntwork-Rodriguez *et al.*, “JNK-mediated phosphorylation of DLK suppresses its ubiquitination to promote neuronal apoptosis,” *Journal of Cell Biology*, vol. 202, no. 5, pp. 747–763, 2013, doi: 10.1083/jcb.201303066.
[164] H. Barbour *et al.*, “An inventory of crosstalk between ubiquitination and other post-translational modifications in orchestrating cellular processes,” *iScience*, vol. 26, no. 5, pp. 1–26, 2023, doi: 10.1016/j.isci.2023.106276.
[165] C. Caron, C. Boyault, and S. Khochbin, “Regulatory cross-talk between lysine acetylation and ubiquitination: Role in control of protein stability,” *BioEssays*, vol. 27, no. 4, pp. 408–415, 2005, doi: 10.1002/bies.20210.

[166] S. Varland *et al.*, “N-terminal acetylation shields proteins from degradation and promotes age-dependent motility and longevity,” *Nat Commun*, p. 2022.09.01.505523, 2023, doi: 10.1101/2022.09.01.505523.
[167] F. Ohtake *et al.*, “Ubiquitin acetylation inhibits polyubiquitin chain elongation,” *EMBO Rep*, vol. 16, no. 2, pp. 192–201, 2015, doi: 10.15252/embr.201439152.
[168] A. Rebelo-Marques *et al.*, “Aging hallmarks: The benefits of physical exercise,” *Front Endocrinol (Lausanne)*, vol. 9, no. MAY, pp. 1–15, 2018, doi: 10.3389/fendo.2018.00258.
[169] J. C. Campos *et al.*, “Exercise prevents impaired autophagy and proteostasis in a model of neurogenic myopathy,” *Sci Rep*, vol. 8, no. 1, pp. 1–14, 2018, doi: 10.1038/s41598-018-30365-1.
[170] J. J. S. VerPlank, S. Lokireddy, J. Zhao, and A. L. Goldberg, “26S Proteasomes are rapidly activated by diverse hormones and physiological states that raise cAMP and cause Rpn6 phosphorylation,” *Proc Natl Acad Sci U S A*, vol. 116, no. 10, pp. 4228–4237, 2019, doi: 10.1073/pnas.1809254116.
[171] B. Parker, B. Kiens, J. Wojtaszewski, E. Richter, and D. James, “Quantification of exercise-regulated ubiquitin signaling in human skeletal muscle identifies protein modification cross talk via NEDDylation,” *FASEB Journal*, no. February, pp. 1–11, 2020, doi: 10.1096/fj.202000075R.
[172] R. Blazev *et al.*, “Phosphoproteomics of three exercise modalities identifies canonical signaling and C18ORF25 as an AMPK substrate regulating skeletal muscle function.,” *Cell Metab*, pp. 1–17, 2022, doi: 10.1016/j.cmet.2022.07.003.
[173] L. Yang *et al.*, “Ubiquitylome study identifies increased histone 2A ubiquitylation as an evolutionarily conserved aging biomarker,” *Nat Commun*, vol. 10, no. 1, 2019, doi: 10.1038/s41467-019-10136-w.
[174] N. B. Basisty *et al.*, “Stable Isotope Labeling Reveals Novel Insights into Ubiquitin-Mediated Protein Aggregation with Age, Calorie Restriction, and Rapamycin Treatment,” *Journals of Gerontology - Series A Biological Sciences and Medical Sciences*, vol. 73, no. 5, pp. 561–570, 2017, doi: 10.1093/gerona/glx047.
[175] Y. R. Chen *et al.*, “Tissue-specific landscape of protein aggregation and quality control in an aging vertebrate,” *Dev Cell*, vol. 59, no. 14, pp. 1892-1911.e13, 2024, doi: 10.1016/j.devcel.2024.04.014.
[176] F. Lang *et al.*, “Dynamic changes in the mouse skeletal muscle proteome during denervation-induced atrophy,” *DMM Disease Models and Mechanisms*, vol. 10, no. 7, pp. 881–896, 2017, doi: 10.1242/dmm.028910.
[177] D. Neyroud *et al.*, “Blocking muscle wasting via deletion of the muscle-specific E3 ligase MuRF1 impedes pancreatic tumor growth,” *Commun Biol*, vol. 6, no. 1, pp. 1–17, 2023, doi: 10.1038/s42003-023-04902-2.
[178] I. L. Lemmer *et al.*, “Nfe2l1-mediated proteasome function controls muscle energy metabolism in obesity,” *bioRxiv*, vol. 1, p. 2023.04.20.537611, 2023, doi: https://doi.org/10.1101/2023.04.20.537611.
[179] S. Bachiller *et al.*, “The ubiquitin proteasome system in neuromuscular disorders: Moving beyond movement,” *Int J Mol Sci*, vol. 21, no. 17, pp. 1–20, 2020, doi: 10.3390/ijms21176429.
[180] F. Chen, Y. Sugiura, K. G. Myers, Y. Liu, and W. Lin, “Ubiquitin carboxyl-terminal hydrolase L1 is required for maintaining the structure and function of the neuromuscular junction,” *Proc Natl Acad Sci U S A*, vol. 107, no. 4, pp. 1636–1641, 2010, doi: 10.1073/pnas.0911516107.

[181] V. Tomaić and L. Banks, “Angelman syndrome-associated ubiquitin ligase UBE3A/E6AP mutants interfere with the proteolytic activity of the proteasome,” *Cell Death Dis*, vol. 6, no. 1, pp. 1–8, 2015, doi: 10.1038/cddis.2014.572.
[182] M. Benini *et al.*, “E3 Ligase RNF126 Directly Ubiquitinates Frataxin, Promoting Its Degradation: Identification of a Potential Therapeutic Target for Friedreich Ataxia,” *Cell Rep*, vol. 18, no. 8, pp. 2007–2017, 2017, doi: 10.1016/j.celrep.2017.01.079.
[183] A. Aghamaleky Sarvestany *et al.*, “Label-free quantitative proteomic profiling identifies disruption of ubiquitin homeostasis as a key driver of Schwann cell defects in spinal muscular atrophy,” *J Proteome Res*, vol. 13, no. 11, pp. 4546–4557, 2014, doi: 10.1021/pr500492j.
[184] N. E. Farrawell *et al.*, “Ubiquitin Homeostasis Is Disrupted in TDP-43 and FUS Cell Models of ALS,” *iScience*, vol. 23, no. 11, p. 101700, 2020, doi: 10.1016/j.isci.2020.101700.
[185] N. E. Farrawell *et al.*, “SOD1A4V aggregation alters ubiquitin homeostasis in a cell model of ALS,” *J Cell Sci*, vol. 131, no. 11, 2018, doi: 10.1242/jcs.209122.
[186] A. Siebert, V. Gattringer, J. H. Weishaupt, and C. Behrends, “ALS-linked loss of Cyclin-F function affects HSP90,” *Life Sci Alliance*, vol. 5, no. 12, pp. 1–17, 2022, doi: 10.26508/lsa.202101359.
[187] S. A. Wagner *et al.*, “Proteomic analyses reveal divergent ubiquitylation site patterns in murine tissues,” *Molecular and Cellular Proteomics*, vol. 11, no. 12, pp. 1578–1585, 2012, doi: 10.1074/mcp.M112.017905.
[188] B. Manadas, V. M. Mendes, J. English, and M. J. Dunn, “Peptide fractionation in proteomics approaches,” *Expert Rev Proteomics*, vol. 7, no. 5, pp. 655–663, 2010, doi: 10.1586/epr.10.46.
[189] Z. Cao, H. Y. Tang, H. Wang, Q. Liu, and D. W. Speicher, “Systematic comparison of fractionation methods for in-depth analysis of plasma proteomes,” *J Proteome Res*, vol. 11, no. 6, pp. 3090–3100, 2012, doi: 10.1021/pr201068b.
[190] L. Van Der Wal, K. Bezstarosti, K. A. Sap, D. H. W. Dekkers, and E. Rijkers, “Improvement of ubiquitylation site detection by Orbitrap mass spectrometry,” *J Proteomics*, vol. 172, no. October 2017, pp. 49–56, 2018, doi: 10.1016/j.jprot.2017.10.014.
[191] S. J. Hesketh, H. Sutherland, P. J. Lisboa, J. C. Jarvis, and J. G. Burniston, “Adaptation of rat fast-twitch muscle to endurance activity is underpinned by changes to protein degradation as well as protein synthesis,” *FASEB Journal*, vol. 34, no. 8, pp. 10398–10417, 2020, doi: 10.1096/fj.202000668RR.
[192] G. K. Potts *et al.*, “A map of the phosphoproteomic alterations that occur after a bout of maximal-intensity contractions,” *Journal of Physiology*, vol. 595, no. 15, pp. 5209–5226, 2017, doi: 10.1113/JP273904.
[193] M. D. Roberts *et al.*, “An optimized procedure for isolation of rodent and human skeletal muscle sarcoplasmic and myofibrillar proteins,” *J Biol Methods*, vol. 7, no. 1, p. e127, 2020, doi: 10.14440/jbm.2020.307.
[194] C. G. Vann *et al.*, “Higher in Resistance-Trained Men , and Aging in the Absence of Training May Have an Opposite Effect,” *Sports*, vol. 8, no. 1, pp. 1–17, 2020.
[195] F. M. Hansen *et al.*, “Data-independent acquisition method for ubiquitinome analysis reveals regulation of circadian biology,” *Nat Commun*, vol. 12, no. 1, 2021, doi: 10.1038/s41467-020-20509-1.
[196] M. Steger *et al.*, “Time-resolved in vivo ubiquitinome profiling by DIA-MS reveals USP7 targets on a proteome-wide scale,” *Nat Commun*, vol. 12, no. 1, 2021, doi: 10.1038/s41467-021-25454-1.

[197] A. Ordureau, C. Münch, and J. W. Harper, “Quantifying Ubiquitin Signaling,” *Mol Cell*, vol. 58, no. 4, pp. 660–676, 2015, doi: 10.1016/j.molcel.2015.02.020.
[198] M. Steger, Ö. Karayel, and V. Demichev, “Ubiquitinomics: history, methods and applications in basic research and drug discovery,” *Proteomics*, no. February, p. 2200074, 2022, doi: 10.1002/pmic.202200074.
[199] G. Vere, R. Kealy, B. M. Kessler, and A. Pinto-Fernandez, “Ubiquitomics: An overview and future,” *Biomolecules*, vol. 10, no. 10, pp. 1–22, 2020, doi: 10.3390/biom10101453.
[200] I. Sahu, H. Zhu, S. J. Buhrlage, and J. A. Marto, “Proteomic approaches to study ubiquitinomics,” *Biochim Biophys Acta Gene Regul Mech*, vol. 1866, no. 2, p. 194940, 2023, doi: 10.1016/j.bbagrm.2023.194940.
[201] D. J. Wilkinson, H. Crossland, and P. J. Atherton, “Metabolomic and proteomic applications to exercise biomedicine,” *Translational Exercise Biomedicine*, vol. 1, no. 1, pp. 9–22, 2024, doi: 10.1515/teb-2024-2006.
[202] M. E. Colley, A. B. Esselman, C. F. Scott, and J. M. Spraggins, “High-Specificity Imaging Mass Spectrometry,” *Annual Review ofAnalytical Chemistry*, pp. 1–24, 2024.
[203] D. Kohler *et al.*, “MSstatsShiny: A GUI for Versatile, Scalable, and Reproducible Statistical Analyses of Quantitative Proteomic Experiments,” *J Proteome Res*, 2022, doi: 10.1021/acs.jproteome.2c00603.
[204] Y. Liao, J. Wang, E. J. Jaehnig, Z. Shi, and B. Zhang, “WebGestalt 2019: gene set analysis toolkit with revamped UIs and APIs,” *Nucleic Acids Res*, vol. 47, no. W1, pp. W199–W205, 2019, doi: 10.1093/nar/gkz401.
[205] T. K. Phung *et al.*, “CURTAIN—A unique web- based tool for exploration and sharing of MS- based proteomics data,” *The Proceedings of the National Academy of Sciences*, 2024, doi: 10.1073/pnas.2312676121.
[206] Y. Perez-Riverol *et al.*, “The PRIDE database and related tools and resources in 2019: Improving support for quantification data,” *Nucleic Acids Res*, vol. 47, no. D1, pp. D442–D450, 2019, doi: 10.1093/nar/gky1106.
[207] R. J. Solaro, D. C. Pang, and F. N. Briggs, “The purification of cardiac myofibrils with Triton X-100,” *BBA - Bioenergetics*, vol. 245, no. 1, pp. 259–262, 1971, doi: 10.1016/0005-2728(71)90033-8.
[208] C. S. Hughes, S. Moggridge, T. Müller, P. H. Sorensen, G. B. Morin, and J. Krijgsveld, “Single-pot, solid-phase-enhanced sample preparation for proteomics experiments,” *Nat Protoc*, vol. 14, no. 1, pp. 68–85, 2019, doi: 10.1038/s41596-018-0082-x.
[209] R. R. Loo, N. Dales, and P. C. Andrews, “The effect of detergents on proteins analyzed by electrospray ionization.,” *Methods Mol Biol*, vol. 61, pp. 141–160, 1996, doi: 10.1385/0-89603-345-7:141.
[210] T. M. Annesley, “Ion suppression in mass spectrometry,” *Clin Chem*, vol. 49, no. 7, pp. 1041–1044, 2003, doi: 10.1373/49.7.1041.
[211] L. L. Manza, S. L. Stamer, A. J. L. Ham, S. G. Codreanu, and D. C. Liebler, “Sample preparation and digestion for proteomic analyses using spin filters,” *Proteomics*, vol. 5, no. 7, pp. 1742–1745, 2005, doi: 10.1002/pmic.200401063.
[212] J. R. Wiśniewski, A. Zougman, N. Nagaraj, and M. Mann, “Universal sample preparation method for proteome analysis,” *Nat Methods*, vol. 6, no. 5, pp. 359–362, 2009, doi: 10.1038/nmeth.1322.
[213] J. Rappsilber, M. Mann, and Y. Ishihama, “Protocol for micro-purification, enrichment, pre-fractionation and storage of peptides for proteomics using StageTips,” *Nat Protoc*, vol. 2, no. 8, pp. 1896–1906, 2007, doi: 10.1038/nprot.2007.261.

[214] G. Gan, X. Xu, X. Chen, X. F. Zhang, J. Wang, and C. Q. Zhong, "SCASP: A simple and robust SDS-aided sample preparation method for proteomic research," *Molecular and Cellular Proteomics*, vol. 20, p. 100051, 2021, doi: 10.1016/J.MCPRO.2021.100051.
[215] J. M. Conforti *et al.*, "Differences in Protein Capture by SP3 and SP4 Demonstrate Mechanistic Insights of Proteomics Cleanup Techniques," *J Proteome Res*, vol. 23, no. 9, pp. 3877–3889, Sep. 2024, doi: 10.1021/acs.jproteome.4c00206.
[216] J. L. Nickerson and A. A. Doucette, "Rapid and Quantitative Protein Precipitation for Proteome Analysis by Mass Spectrometry," *J Proteome Res*, vol. 19, no. 5, pp. 2035–2042, 2020, doi: 10.1021/acs.jproteome.9b00867.
[217] C. Bielow, G. Mastrobuoni, and S. Kempa, "Proteomics Quality Control: Quality Control Software for MaxQuant Results," *J Proteome Res*, vol. 15, no. 3, pp. 777–787, 2016, doi: 10.1021/acs.jproteome.5b00780.
[218] J. Cox and M. Mann, "MaxQuant enables high peptide identification rates, individualized p.p.b.-range mass accuracies and proteome-wide protein quantification," *Nat Biotechnol*, vol. 26, no. 12, pp. 1367–1372, 2008, doi: 10.1038/nbt.1511.
[219] J. T. Aguilan, K. Kulej, and S. Sidoli, "Guide for protein fold change and: P-value calculation for non-experts in proteomics," *Mol Omics*, vol. 16, no. 6, pp. 573–582, 2020, doi: 10.1039/d0mo00087f.
[220] M. E. Ritchie *et al.*, "Limma powers differential expression analyses for RNA-sequencing and microarray studies," *Nucleic Acids Res*, vol. 43, no. 7, p. e47, 2015, doi: 10.1093/nar/gkv007.
[221] G. K. Smyth, "Linear models and empirical bayes methods for assessing differential expression in microarray experiments," *Stat Appl Genet Mol Biol*, vol. 3, no. 1, 2004, doi: 10.2202/1544-6115.1027.
[222] N. Pappireddi, L. Martin, and W. Martin, "A Review on Quantitative Multiplexed Proteomics," pp. 1210–1224, 2019, doi: 10.1002/cbic.201800650.
[223] Y. O. Saw, M. Salim, J. Noirel, C. Evans, I. Rehman, and P. C. Wright, "iTRAQ underestimation in simple and complex mixtures: 'The good, the bad and the ugly,'" *J Proteome Res*, vol. 8, no. 11, pp. 5347–5355, 2009, doi: 10.1021/pr900634c.
[224] B. Ruprecht, J. Zecha, D. P. Zolg, and B. Kuster, "High pH Reversed-Phase Micro-Columns for Simple, Sensitive, and Efficient Fractionation of Proteome and (TMT labeled) Phosphoproteome Digests," *Methods in Molecular Biology*, vol. 1550, 2017, doi: 10.1007/978-1-4939-6747-6.
[225] S. Pfammatter, E. Bonneil, and P. Thibault, "Improvement of Quantitative Measurements in Multiplex Proteomics Using High-Field Asymmetric Waveform Spectrometry," *J Proteome Res*, vol. 15, no. 12, pp. 4653–4665, 2016, doi: 10.1021/acs.jproteome.6b00745.
[226] L. Ting, R. Rad, S. P. Gygi, and W. Haas, "MS3 eliminates ratio distortion in isobaric multiplexed quantitative proteomics," *Nat Methods*, vol. 8, no. 11, pp. 937–940, 2011, doi: 10.1038/nmeth.1714.
[227] B. K. Erickson *et al.*, "Active Instrument Engagement Combined with a Real-Time Database Search for Improved Performance of Sample Multiplexing Workflows," *J Proteome Res*, vol. 18, no. 3, pp. 1299–1306, 2019, doi: 10.1021/acs.jproteome.8b00899.
[228] C. Della Peruta *et al.*, "Sex Differences in Inflammation and Muscle Wasting in Aging and Disease," *Int J Mol Sci*, vol. 24, no. 5, pp. 1–20, 2023, doi: 10.3390/ijms24054651.

[229] H. H. Zhou, Y. Liao, Z. Peng, F. Liu, Q. Wang, and W. Yang, “Association of muscle wasting with mortality risk among adults: A systematic review and meta-analysis of prospective studies,” *J Cachexia Sarcopenia Muscle*, vol. 14, no. 4, pp. 1596–1612, 2023, doi: 10.1002/jcsm.13263.
[230] W. qing Xie *et al.*, “Mouse models of sarcopenia: classification and evaluation,” *J Cachexia Sarcopenia Muscle*, vol. 12, no. 3, pp. 538–554, 2021, doi: 10.1002/jcsm.12709.
[231] L. C. Hunt *et al.*, “Integrated genomic and proteomic analyses identify stimulus-dependent molecular changes associated with distinct modes of skeletal muscle atrophy,” *Cell Rep*, vol. 37, no. 6, p. 109971, 2021, doi: 10.1016/j.celrep.2021.109971.
[232] A. Marino, D. Di Fraia, D. Panfilova, A. Kumar Sahu, and A. Ori, “Remodeling of the protein ubiquitylation landscape in the aging vertebrate brain,” 2023, [Online]. Available: https://doi.org/10.1101/2023.12.02.569713
[233] S. Lord, H. Johnston, R. Samant, and Y. Lai, “Ubiquitylomics : An Emerging Approach for Profiling Protein Ubiquitylation in Skeletal Muscle,” *J Cachexia Sarcopenia Muscle*, 2024, doi: 10.1002/jcsm.13601.
[234] T. Huang *et al.*, “MSstatsTMT: Statistical Detection of Differentially Abundant Proteins in Experiments with Isobaric Labeling and Multiple Mixtures,” *Molecular and Cellular Proteomics*, vol. 19, no. 10, pp. 1706–1723, 2020, doi: 10.1074/mcp.RA120.002105.
[235] D. Kohler *et al.*, “MSstatsPTM: Statistical Relative Quantification of Posttranslational Modifications in Bottom-Up Mass Spectrometry-Based Proteomics,” *Molecular and Cellular Proteomics*, vol. 22, no. 1, p. 100477, 2023, doi: 10.1016/j.mcpro.2022.100477.
[236] S. Rath *et al.*, “MitoCarta3.0: An updated mitochondrial proteome now with sub-organelle localization and pathway annotations,” *Nucleic Acids Res*, vol. 49, no. D1, pp. D1541–D1547, 2021, doi: 10.1093/nar/gkaa1011.
[237] B. Medvar, V. Raghuram, T. Pisitkun, A. Sarkar, and M. A. Knepper, “Comprehensive database of human E3 ubiquitin ligases: Application to aquaporin-2 regulation,” *Physiol Genomics*, vol. 48, no. 7, pp. 502–512, 2016, doi: 10.1152/physiolgenomics.00031.2016.
[238] Z. Xue, J. X. Chen, Y. Zhao, B. Medvar, and M. A. Knepper, “Data integration in physiology using Bayes’ rule and minimum Bayes’ factors: Deubiquitylating enzymes in the renal collecting duct,” *Physiol Genomics*, vol. 49, no. 3, pp. 151–159, 2017, doi: 10.1152/physiolgenomics.00120.2016.
[239] I. Cvitkovic and M. S. Jurica, “Spliceosome database: A tool for tracking components of the spliceosome,” *Nucleic Acids Res*, vol. 41, no. D1, pp. 132–141, 2013, doi: 10.1093/nar/gks999.
[240] Y. Xie *et al.*, “IBS 2.0: an upgraded illustrator for the visualization of biological sequences,” *Nucleic Acids Res*, vol. 50, no. W1, pp. W420–W426, 2022, doi: 10.1093/nar/gkac373.
[241] M. M. Robinson *et al.*, “Enhanced Protein Translation Underlies Improved Metabolic and Physical Adaptations to Different Exercise Training Modes in Young and Old Humans,” *Cell Metab*, vol. 25, no. 3, pp. 581–592, 2017, doi: 10.1016/j.cmet.2017.02.009.
[242] J. C. B. C. de Jong *et al.*, “Translatability of mouse muscle-aging for humans: the role of sex,” *Geroscience*, vol. 46, no. 3, pp. 3341–3360, 2024, doi: 10.1007/s11357-024-01082-7.

[243] G. R. Keele *et al.*, “Global and tissue-specific aging effects on murine proteomes,” *Cell Rep*, vol. 42, no. 7, p. 2022.05.17.492125, 2023, doi: 10.1016/j.celrep.2023.112715.
[244] J. Fuqua *et al.*, “Impaired proteostatic mechanisms other than protein synthesis limit aged skeletal muscle recovery after disuse atrophy,” *Physiology*, vol. 38, no. S1, 2023, doi: 10.1152/physiol.2023.38.s1.5729708.
[245] L. Ameye and M. F. Young, “Mice deficient in small leucine-rich proteoglycans: Novel in vivo models for osteoporosis, osteoarthritis, Ehlers-Danlos syndrome, muscular dystrophy, and corneal diseases,” *Glycobiology*, vol. 12, no. 9, pp. 107–116, 2002, doi: 10.1093/glycob/cwf065.
[246] C. Y. C. Yeung *et al.*, “Proteome profiles of intramuscular connective tissue: influence of aging and physical training,” *J Appl Physiol*, vol. 134, no. 5, pp. 1278–1286, 2023, doi: 10.1152/japplphysiol.00675.2022.
[247] S. C. Schüler *et al.*, “Extensive remodeling of the extracellular matrix during aging contributes to age-dependent impairments of muscle stem cell functionality,” *Cell Rep*, vol. 35, no. 10, 2021, doi: 10.1016/j.celrep.2021.109223.
[248] E. McShane and L. S. Churchman, “Central dogma rates in human mitochondria,” *Hum Mol Genet*, vol. 33, no. R1, pp. R34–R41, 2024, doi: 10.1093/hmg/ddae036.
[249] R. Tharakan, C. Ubaida-Mohien, Y. Piao, M. Gorospe, and L. Ferrucci, “Ribosome profiling analysis of human skeletal muscle identifies reduced translation of mitochondrial proteins with age,” *RNA Biol*, vol. 18, no. 11, pp. 1555–1559, 2021, doi: 10.1080/15476286.2021.1875647.
[250] E. Blachly-Dyson and M. Forte, “VDAC channels,” *IUBMB Life*, vol. 52, no. 3–5, pp. 113–118, 2001, doi: 10.1080/15216540152845902.
[251] J. J. Ruprecht and E. R. S. Kunji, “The SLC25 Mitochondrial Carrier Family: Structure and Mechanism,” *Trends Biochem Sci*, vol. 45, no. 3, pp. 244–258, 2020, doi: 10.1016/j.tibs.2019.11.001.
[252] A. R. Wolf and V. K. Mootha, “Functional Genomic Analysis of Human Mitochondrial RNA Processing,” *Cell Rep*, vol. 7, no. 3, pp. 918–931, 2014, doi: 10.1016/j.celrep.2014.03.035.
[253] J. Demarquoy, “Crosstalk between mitochondria and peroxisomes,” *World J Biol Chem*, vol. 6, no. 4, p. 301, 2015, doi: 10.4331/wjbc.v6.i4.301.
[254] A. Al Saedi, D. A. Debruin, A. Hayes, and M. Hamrick, “Lipid metabolism in sarcopenia,” *Bone*, vol. 164, no. August, p. 116539, 2022, doi: 10.1016/j.bone.2022.116539.
[255] M. Maleszewska, J. S. P. Mawer, and P. Tessarz, “Histone Modifications in Ageing and Lifespan Regulation,” *Curr Mol Biol Rep*, vol. 2, no. 1, pp. 26–35, 2016, doi: 10.1007/s40610-016-0031-9.
[256] R. C. Molden, N. V. Bhanu, G. LeRoy, A. M. Arnaudo, and B. A. Garcia, “Multi-faceted quantitative proteomics analysis of histone H2B isoforms and their modifications,” *Epigenetics Chromatin*, vol. 8, no. 1, pp. 1–17, 2015, doi: 10.1186/s13072-015-0006-8.
[257] A. Luo *et al.*, “H2B ubiquitination recruits FACT to maintain a stable altered nucleosome state for transcriptional activation,” *Nat Commun*, vol. 14, no. 1, pp. 1–13, 2023, doi: 10.1038/s41467-023-36467-3.
[258] L. Moyal *et al.*, “Requirement of ATM-Dependent Monoubiquitylation of Histone H2B for Timely Repair of DNA Double-Strand Breaks,” *Mol Cell*, vol. 41, no. 5, pp. 529–542, 2011, doi: 10.1016/j.molcel.2011.02.015.

[259] V. Vethantham *et al.*, "Dynamic Loss of H2B Ubiquitylation without Corresponding Changes in H3K4 Trimethylation during Myogenic Differentiation," *Mol Cell Biol*, vol. 32, no. 6, pp. 1044–1055, 2012, doi: 10.1128/mcb.06026-11.
[260] B. H. Rhie, Y. H. Song, H. Y. Ryu, and S. H. Ahn, "Cellular aging is associated with increased ubiquitylation of histone H2B in yeast telomeric heterochromatin," *Biochem Biophys Res Commun*, vol. 439, no. 4, pp. 570–575, 2013, doi: 10.1016/j.bbrc.2013.09.017.
[261] S. Cohen, B. Zhai, S. P. Gygi, and A. L. Goldberg, "Ubiquitylation by Trim32 causes coupled loss of desmin, Z-bands, and thin filaments in muscle atrophy," *Journal of Cell Biology*, vol. 198, no. 4, pp. 575–589, 2012, doi: 10.1083/jcb.201110067.
[262] E. M. Solovyeva *et al.*, "New insights into molecular changes in skeletal muscle aging and disease: Differential alternative splicing and senescence," *Mech Ageing Dev*, vol. 197, p. 111510, 2021, doi: 10.1016/j.mad.2021.111510.
[263] G. Varani and K. Nagai, "RNA recognition by RNP proteins during RNA processing," *Annu Rev Biophys Biomol Struct*, vol. 27, pp. 407–445, 1998, doi: 10.1146/annurev.biophys.27.1.407.
[264] S. A. Rodríguez *et al.*, "Global genome splicing analysis reveals an increased number of alternatively spliced genes with aging," *Aging Cell*, vol. 15, no. 2, pp. 267–278, 2016, doi: 10.1111/acel.12433.
[265] M. N. O'Leary *et al.*, "The Ribosomal Protein Rpl22 Controls Ribosome Composition by Directly Repressing Expression of Its Own Paralog, Rpl22l1," *PLoS Genet*, vol. 9, no. 8, 2013, doi: 10.1371/journal.pgen.1003708.
[266] C. Hu *et al.*, "Heat shock proteins: Biological functions, pathological roles, and therapeutic opportunities," *MedComm (Beijing)*, vol. 3, no. 3, pp. 1–39, 2022, doi: 10.1002/mco2.161.
[267] H. Nakamoto and L. Vígh, "The small heat shock proteins and their clients," *Cellular and Molecular Life Sciences*, vol. 64, no. 3, pp. 294–306, 2007, doi: 10.1007/s00018-006-6321-2.
[268] I. Dimauro, A. Antonioni, N. Mercatelli, and D. Caporossi, "The role of αB-crystallin in skeletal and cardiac muscle tissues," *Cell Stress Chaperones*, vol. 23, no. 4, pp. 491–505, 2018, doi: 10.1007/s12192-017-0866-x.
[269] E. J. Mercer, Y. F. Lin, L. Cohen-Gould, and T. Evans, "Hspb7 is a cardioprotective chaperone facilitating sarcomeric proteostasis," *Dev Biol*, vol. 435, no. 1, pp. 41–55, 2018, doi: 10.1016/j.ydbio.2018.01.005.
[270] S. S. Cao and R. J. Kaufman, "Unfolded protein response," *Current Biology*, vol. 22, no. 16, pp. R622–R626, 2012, doi: 10.1016/j.cub.2012.07.004.
[271] H. C. Besche *et al.*, "Autoubiquitination of the 26S Proteasome on Rpn13 Regulates Breakdown of Ubiquitin Conjugates," *EMBO Journal*, vol. 33, no. 10, pp. 1159–1176, 2014, doi: 10.1002/embj.201386906.
[272] D. Gödderz, T. A. Giovannucci, J. Laláková, V. Menéndez-Benito, and N. P. Dantuma, "The deubiquitylating enzyme Ubp12 regulates Rad23-dependent proteasomal degradation," *J Cell Sci*, vol. 130, no. 19, pp. 3336–3346, 2017, doi: 10.1242/jcs.202622.
[273] X. Fu, V. Sokolova, K. J. Webb, W. Old, and S. Park, "Ubiquitin-dependent switch during assembly of the proteasomal ATPases mediated by Not4 ubiquitin ligase," *Proc Natl Acad Sci U S A*, vol. 115, no. 52, pp. 13246–13251, 2018, doi: 10.1073/pnas.1805353115.
[274] H. C. Nguyen, W. Wang, and Y. Xiong, "Cullin-RING E3 ubiquitin ligases: Bridges to destruction," *Subcell Biochem*, vol. 83, pp. 323–347, 2017, doi: 10.1007/978-3-319-46503-6_12.

[275] P. V. Hornbeck *et al.*, “PhosphoSitePlus: A comprehensive resource for investigating the structure and function of experimentally determined post-translational modifications in man and mouse,” *Nucleic Acids Res*, vol. 40, no. D1, pp. 261–270, 2012, doi: 10.1093/nar/gkr1122.
[276] T. Yao *et al.*, “Proteasome recruitment and activation of the Uch37 deubiquitinating enzyme by Adrm1,” *Nat Cell Biol*, vol. 8, no. 9, pp. 994–1002, 2006, doi: 10.1038/ncb1460.
[277] J. Rydström, “Mitochondrial NADPH, transhydrogenase and disease,” *Biochim Biophys Acta Bioenerg*, vol. 1757, no. 5–6, pp. 721–726, 2006, doi: 10.1016/j.bbabio.2006.03.010.
[278] J. Gannon, L. Staunton, K. O’Connell, P. Doran, and K. Ohlendieck, “Phosphoproteomic analysis of aged skeletal muscle,” *Int J Mol Med*, vol. 22, no. 1, pp. 33–42, 2008, doi: 10.3892/ijmm.22.1.33.
[279] A. Bareja, J. A. Draper, L. H. Katz, D. E. Lee, P. A. Grimsrud, and J. P. White, “Chronic caloric restriction maintains a youthful phosphoproteome in aged skeletal muscle,” *Mech Ageing Dev*, vol. 195, p. 111443, 2021, doi: 10.1016/j.mad.2021.111443.
[280] R. Fernando, C. Drescher, K. Nowotny, T. Grune, and J. P. Castro, “Impaired proteostasis during skeletal muscle aging,” *Free Radic Biol Med*, vol. 132, no. August 2018, pp. 58–66, 2019, doi: 10.1016/j.freeradbiomed.2018.08.037.
[281] S. Ayyadevara *et al.*, “Proteins that accumulate with age in human skeletal-muscle aggregates contribute to declines in muscle mass and function in Caenorhabditis elegans,” *Aging*, vol. 8, no. 12, pp. 3486–3497, 2016, doi: 10.18632/aging.101141.
[282] V. A. Duong and H. Lee, “Bottom-Up Proteomics: Advancements in Sample Preparation,” *Int J Mol Sci*, vol. 24, no. 6, 2023, doi: 10.3390/ijms24065350.
[283] M. Wacker *et al.*, “Immunoprecipitation methods impact the peptide repertoire in immunopeptidomics,” *Front Immunol*, vol. 14, no. July, pp. 1–11, 2023, doi: 10.3389/fimmu.2023.1219720.
[284] J. C. B. C. de Jong *et al.*, “Sex differences in skeletal muscle-aging trajectory: same processes, but with a different ranking,” *Geroscience*, vol. 45, no. 4, pp. 2367–2386, 2023, doi: 10.1007/s11357-023-00750-4.
[285] V. Augusto, C. R. Padovani, and G. E. R. Campos, “Skeletal Muscle Fiber Types in C57BL6J Mice,” *Brazilian Journal of Morphological Science*, vol. 21, no. 2, pp. 89–94, 2004.
[286] M. R. Deschenes, “Effects of aging on muscle fibre type and size,” *Sports Medicine*, vol. 34, no. 12, pp. 809–824, 2004, doi: 10.2165/00007256-200434120-00002.
[287] B. J. F. Gheller, E. S. Riddle, M. R. Lem, and A. E. Thalacker-Mercer, “Understanding Age-Related Changes in Skeletal Muscle Metabolism: Differences between Females and Males,” *Annu Rev Nutr*, vol. 36, pp. 129–156, 2016, doi: 10.1146/annurev-nutr-071715-050901.
[288] O. Varlamov, C. L. Bethea, and C. T. Roberts, “Sex-specific differences in lipid and glucose metabolism,” *Front Endocrinol (Lausanne)*, vol. 5, no. DEC, pp. 1–7, 2014, doi: 10.3389/fendo.2014.00241.
[289] N. F. Shur *et al.*, “Age-related changes in muscle architecture and metabolism in humans: The likely contribution of physical inactivity to age-related functional decline,” *Ageing Res Rev*, vol. 68, p. 101344, 2021, doi: 10.1016/j.arr.2021.101344.
[290] E. T. Powers, R. I. Morimoto, A. Dillin, J. W. Kelly, and W. E. Balch, “Biological and chemical approaches to diseases of proteostasis deficiency,” *Annu Rev Biochem*, vol. 78, pp. 959–991, 2009, doi: 10.1146/annurev.biochem.052308.114844.

[291] Paez HG, Pitzer CR, and Alway SE, "Age-Related Dysfunction in Proteostasis and Cellular Quality Control in the Development of Sarcopenia," *Cells*, vol. 12, no. 2, pp. 1–30, 2023.
[292] C. W. Baumann, D. Kwak, and L. D. V. Thompson, "Sex-specific components of frailty in C57BL/6 mice," *Aging*, vol. 11, no. 14, pp. 5206–5214, 2019, doi: 10.18632/aging.102114.
[293] M. Rai *et al.*, "Analysis of proteostasis during aging with western blot of detergent-soluble and insoluble protein fractions," *STAR Protoc*, vol. 2, no. 3, p. 100628, 2021, doi: 10.1016/j.xpro.2021.100628.
[294] S. Cohen *et al.*, "During muscle atrophy, thick, but not thin, filament components are degraded by MuRF1-dependent ubiquitylation," *Journal of Cell Biology*, vol. 185, no. 6, pp. 1083–1095, 2009, doi: 10.1083/jcb.200901052.
[295] P. Dowling, S. Gargan, M. Zweyer, M. Henry, P. Meleady, and K. Ohlendieck, "Proteomic reference map for sarcopenia research : mass spectrometric identification of key muscle proteins located in the sarcomere , cytoskeleton and the extracellular matrix," *Eur J Transl Myol*, 2024, doi: 10.4081/ejtm.2024.12564.
[296] P. G. Giresi *et al.*, "Identification of a molecular signature of sarcopenia," *Physiol Genomics*, vol. 21, pp. 253–263, 2005, doi: 10.1152/physiolgenomics.00249.2004.
[297] S. Welle, A. I. Brooks, J. M. Delehanty, N. Needler, and C. A. Thornton, "Gene expression profile of aging in human muscle," *Physiol Genomics*, vol. 14, pp. 149–159, 2003, doi: 10.1152/physiolgenomics.00049.2003.
[298] P. Bellare, E. C. Small, X. Huang, J. A. Wohlschlegel, J. P. Staley, and E. J. Sontheimer, "A role for ubiquitin in the spliceosome assembly pathway," *Nat Struct Mol Biol*, vol. 15, no. 5, pp. 444–451, 2008, doi: 10.1038/nsmb.1401.
[299] F. Wang *et al.*, "SPSB1-mediated HnRNP A1 ubiquitylation regulates alternative splicing and cell migration in EGF signaling," *Cell Res*, vol. 27, no. 4, pp. 540–558, 2017, doi: 10.1038/cr.2017.7.
[300] L. W. Harries *et al.*, "Human aging is characterized by focused changes in gene expression and deregulation of alternative splicing," *Aging Cell*, vol. 10, no. 5, pp. 868–878, 2011, doi: 10.1111/j.1474-9726.2011.00726.x.
[301] J. R. Tollervey *et al.*, "Analysis of alternative splicing associated with aging and neurodegeneration in the human brain," *Genome Res*, vol. 21, no. 10, pp. 1572–1582, 2011, doi: 10.1101/gr.122226.111.
[302] K. Wang *et al.*, "Comprehensive map of age-associated splicing changes across human tissues and their contributions to age-associated diseases," *Sci Rep*, vol. 8, no. 1, pp. 1–12, 2018, doi: 10.1038/s41598-018-29086-2.
[303] T. Schmauck-Medina *et al.*, "New hallmarks of ageing: a 2022 Copenhagen ageing meeting summary," *Aging*, vol. 14, no. 16, pp. 6829–6839, 2022, doi: 10.18632/aging.204248.
[304] M. Deschênes and B. Chabot, "The emerging role of alternative splicing in senescence and aging," *Aging Cell*, vol. 16, no. 5, pp. 918–933, 2017, doi: 10.1111/acel.12646.
[305] S. M. Kwon *et al.*, "Global spliceosome activity regulates entry into cellular senescence," *FASEB Journal*, vol. 35, no. 1, pp. 1–13, 2021, doi: 10.1096/fj.202000395RR.
[306] W. W. Hwang, S. Venkatasubrahmanyam, A. G. Ianculescu, A. Tong, C. Boone, and H. D. Madhani, "A conserved RING finger protein required for histone H2B monoubiquitination and cell size control," *Mol Cell*, vol. 11, no. 1, pp. 261–266, 2003, doi: 10.1016/S1097-2765(02)00826-2.
[307] X. Y. Zhang *et al.*, "The Putative Cancer Stem Cell Marker USP22 Is a Subunit of the Human SAGA Complex Required for Activated Transcription and Cell-Cycle

Progression," *Mol Cell*, vol. 29, no. 1, pp. 102–111, 2008, doi: 10.1016/j.molcel.2007.12.015.
[308] H. Y. Joo *et al.*, "Regulation of histone H2A and H2B deubiquitination and xenopus development by USP12 and USP46," *Journal of Biological Chemistry*, vol. 286, no. 9, pp. 7190–7201, 2011, doi: 10.1074/jbc.M110.158311.
[309] G. Fuchs *et al.*, "RNF20 and USP44 Regulate Stem Cell Differentiation by Modulating H2B Monoubiquitylation," *Mol Cell*, vol. 46, no. 5, pp. 662–673, 2012, doi: 10.1016/j.molcel.2012.05.023.
[310] Mouse Genome Consortium *et al.*, "Initial sequencing and comparative analysis of the mouse genome," *Nature*, vol. 420, no. 6915, pp. 520–562, 2002, [Online]. Available: http://www.nature.com/nature/journal/v420/n6915/full/nature01262.html
[311] R. Yuan, L. L. Peters, and B. Paigen, "Mice as a mammalian model for research on the genetics of aging," *ILAR J*, vol. 52, no. 1, pp. 4–15, 2011, doi: 10.1093/ilar.52.1.4.
[312] S. Schiaffino and C. Reggiani, "Fiber types in Mammalian skeletal muscles," *Physiol Rev*, vol. 91, no. 4, pp. 1447–1531, 2011, doi: 10.1152/physrev.00031.2010.
[313] J. C. Price *et al.*, "Measurement of human plasma proteome dynamics with 2H 2O and liquid chromatography tandem mass spectrometry," *Anal Biochem*, vol. 420, no. 1, pp. 73–83, 2012, doi: 10.1016/j.ab.2011.09.007.
[314] J. G. Burniston, "Investigating Muscle Protein Turnover on a Protein-by-Protein Basis Using Dynamic Proteome Profiling," *Omics Approaches to Understanding Muscle Biology*, pp. 171–190, 2019, doi: 10.1007/978-1-4939-9802-9_9.

8. Appendix

Title: Uncovering the mechanisms of MuRF1-induced ubiquitylation and revealing similarities with MuRF2 and MuRF3

Journal: Biochemistry and Biophysics reports

Year: 2024

DOI: https://doi.org/10.1016/j.bbrep.2023.101636

Biochemistry and Biophysics Reports 37 (2024) 101636

Contents lists available at ScienceDirect

Biochemistry and Biophysics Reports

journal homepage: www.elsevier.com/locate/bbrep

Uncovering the mechanisms of MuRF1-induced ubiquitylation and revealing similarities with MuRF2 and MuRF3

Samuel O. Lord [a,1], Peter W.J. Dawson [a,b,1], Jitpisute Chunthorng-Orn [a], Jimi Ng [a], Leslie M. Baehr [c,2], David C. Hughes [c,2], Pooja Sridhar [d], Timothy Knowles [d], Sue C. Bodine [c,2], Yu-Chiang Lai [a,b,*]

[a] School of Sport, Exercise and Rehabilitation Sciences, University of Birmingham, Birmingham, UK
[b] MRC Versus Arthritis Centre for Musculoskeletal Ageing Research, University of Birmingham, Birmingham, UK
[c] Division of Endocrinology and Metabolism, Department of Internal Medicine, Carver College of Medicine, University of Iowa, Iowa City, IA, USA
[d] School of Biosciences, University of Birmingham, Birmingham, UK

ARTICLE INFO

Keywords:
RING E3 Ligase
Ubiquitin Conjugating Enzyme (UBE2)
Ubiquitin
Autoubiquitylation
In vitro
Muscle Atrophy

ABSTRACT

MuRF1 (Muscle-specific RING finger protein 1; gene name TRIM63) is a ubiquitin E3 ligase, associated with the progression of muscle atrophy. As a RING (Really Interesting New Gene) type E3 ligase, its unique activity of ubiquitylation is driven by a specific interaction with a UBE2 (ubiquitin conjugating enzyme). Our understanding of MuRF1 function remains unclear as candidate UBE2s have not been fully elucidated. In the present study, we screened human ubiquitin dependent UBE2s in vitro and found that MuRF1 engages in ubiquitylation with UBE2D, UBE2E, UBE2N/V families and UBE2W. MuRF1 can cause mono-ubiquitylation, K48- and K63-linked polyubiquitin chains in a UBE2 dependent manner. Moreover, we identified a two-step UBE2 dependent mechanism whereby MuRF1 is monoubiquitylated by UBE2W which acts as an anchor for UBE2N/V to generate polyubiquitin chains. With the in vitro ubiquitylation assay, we also found that MuRF2 and MuRF3 not only share the same UBE2 partners as MuRF1 but can also directly ubiquitylate the same substrates: Titin (A168-A170), Desmin, and MYLPF (Myosin Light Chain, Phosphorylatable, Fast Skeletal Muscle; also called Myosin Light Regulatory Chain 2). In summary, our work presents new insights into the mechanisms that underpin MuRF1 activity and reveals overlap in MuRF-induced ubiquitylation which could explain their partial redundancy in vivo.

1. Introduction

MuRF1 (Muscle-specific RING finger protein 1) plays a critical role in skeletal muscle atrophy. Many studies in humans and rodents, demonstrate that MuRF1 gene (TRIM63) and protein expression increase following numerous atrophy models including disuse, denervation, cancer, renal failure, heart failure, burn injury, fasting, diabetes, corticosteroid treatment and cytokine exposure [1–7.] Importantly, suppression of MuRF1 expression perturbs atrophy induced by denervation, glucocorticoid treatment, limb unloading, and lung injury [2, 8–10]. These earlier studies have established MuRF1 as a key regulator of skeletal muscle mass. Nonetheless, insight into the molecular mechanisms of MuRF1-induced muscle atrophy is unclear, slowing the development of therapeutics that target MuRF1-induced muscle atrophy.

MuRF1 is an E3 ligase, which functions to target proteins for

Abbreviations: ELISA, enzyme-linked immunosorbent assay; HIS, Histidine; IPTG, Isopropyl β-D-1-thiogalactopyranoside; LB, Lysogeny Broth; MBP, Maltose Binding Protein; MuRF1, Muscle-specific RING finger protein 1; MuRF2, Muscle-specific RING finger protein 2; MuRF3, Muscle-specific RING finger protein 3; MYLPF, Myosin Light Chain Phosphorylatable Fast Skeletal Muscle Protein; RING, Really Interesting New Gene; SUMO, Small Ubiquitin-like Modifier; SPR, Surface Plasmon Resonance; TBS-T, Tris-buffered saline Tween-20; TRIM, Tripartite Motif-Containing; UBE1, E1 ubiquitin activating enzyme; UBE2, E2 ubiquitin-conjugating enzyme; VCP, Valosin-containing protein.

* Corresponding author. School of Sport, Exercise and Rehabilitation Sciences, University of Birmingham, Edgbaston, Birmingham, B15 2TT, UK.
E-mail address: y.lai.1@bham.ac.uk (Y.-C. Lai).

[1] Samuel O. Lord and Peter W.J. Dawson contributed equally to this work.
[2] Present Address: Aging and Metabolism Research Program, Oklahoma Medical Research Foundation, Oklahoma City, OK, USA.

https://doi.org/10.1016/j.bbrep.2023.101636
Received 6 November 2023; Received in revised form 12 December 2023; Accepted 29 December 2023

ubiquitylation. The process of protein ubiquitylation is a coordinated sequence of three enzymatic actions: by an E1 ubiquitin-activating enzyme (UBE1), an E2 ubiquitin-conjugating enzyme (UBE2), and finally an E3 ubiquitin-ligase. The UBE1 enzyme hydrolyses ATP to adenylate ubiquitin, which is transferred to an UBE2 active site. As MuRF1 is a RING-type (Really Interesting New Gene) E3 ligase, with no catalytic activity, it requires the interaction of a UBE2 to directly transfer ubiquitin to the substrate(s) [11]. UBE2s are responsible for the type of ubiquitylation (mono-, multi-mono-, or poly-ubiquitylation) and the structure of ubiquitin chains based on ubiquitin-ubiquitin attachment residue [12,13]. There are eight different polyubiquitin chain types (M1, K6, K11, K27, K29, K33, K48 and K63) and the topology of ubiquitin chain types ultimately determine the fate of the target protein, such as degradation, localisation, or other signalling events [14]. Therefore, to understand the functional role of MuRF1 ubiquitylation onto its substrate, one must identify the UBE2 that partners with MuRF1. Identifying MuRF1 partnering UBE2s would also provide a tool to directly explore substrates of MuRF1 in vitro and characterise their specific form of ubiquitylation.

Previous studies have attempted to identify UBE2s that interact with MuRF1. Polge et al. [15] applied yeast two-hybrid screen and SPR (surface plasmon resonance) technologies and identified several UBE2s, including UBE2E1, UBE2G1, UBE2J1, UBE2J2, and UBE2L3, as interacting with MuRF1. However, these two methods only measure protein-protein interaction without detecting ubiquitin E3 ligase activity of MuRF1. When MuRF1-UBE2 ubiquitylation activity has been studied using ELISA based methods, only 11 UBE2s have been explored [16]. Due to limited characterisation of MuRF1-UBE2 partners, studies have often used UBE2D (UBCH5) family when investigating MuRF1 substrates [17–20]. While this offers some insights into MuRF1-UBE2D ubiquitylation activity, it is worth noting that the UBE2D family may be promiscuous and can interact and produce ubiquitylation activity with most RING type E3 ligases [13]. Therefore, the current literature offers limited understanding of MuRF1-UBE2 partners and how they relate to MuRF1 ubiquitylation function. A study of all human UBE2s with MuRF1 is necessary to further understand the mechanism of MuRF1-mediated ubiquitylation.

MuRF1 shares high homology with two other TRIM family members, MuRF2 (TRIM55) and MuRF3 (TRIM54). Sequence alignment shows MuRF1 displays 62 % and 77 % overlap with MuRF2 and MuRF3 respectively [21]. Given their similar sequence it is possible that they share overlapping roles, a concept supported by genetic mouse models which highlight the redundancy of MuRF E3 ligases. For example, removal of MuRF1 has no detrimental effect on mice phenotype [2,20,22]. However, when MuRF2 or MuRF3 are also removed this causes severe detrimental effects on skeletal and cardiac muscle size and function. Double knockout (dKO) of MuRF1 and MuRF2 causes hypertrophic cardiomyopathy that resulted in the death of ~75 % of mice in their first few weeks [23,24]. MuRF1 and MuRF3 dKO mice experience skeletal muscle myopathy and hypertrophic cardiomyopathy [20]. Similar features were observed in human patients with mutations in MuRF1 (homozygous) and MuRF3 (heterozygous) [25]. These findings suggest that the loss of MuRF1 can be somewhat compensated by the presence of MuRF2 or MuRF3. Given the lack of molecular understanding surrounding MuRF-induced ubiquitylation, there is no comprehensive explanation for this response. Therefore, a study directly comparing MuRF1, MuRF2 and MuRF3 ubiquitylation is needed.

In the present study a full human UBE2 library (excluding ubiquitin-like UBE2s; see Table S1) were screened using a standard in vitro ubiquitylation assay. This revealed that UBE2D, UBE2E, UBE2N/V families and UBE2W partner with MuRF1 during ubiquitylation. We found that MuRF1 partners with UBE2W and UBE2N/V in a sequential two-step fashion, forming K63-linked ubiquitin chains. Moreover, we showed that MuRF2 and MuRF3 also function with these UBE2s during ubiquitylation and can target the same set of substrates as MuRF1 (Titin, Desmin and MYLPF), providing a molecular explanation for their functional redundancy in vivo.

2. Materials and methods

2.1. Constructs

MBP-MuRF1, MBP-MuRF2, MBP-MuRF3, Ubiquitin, HIS-UBE1 and the full library of human E2s were sourced from the Medical Research Council - Protein, Phosphorylation and Ubiquitylation Unit (MRC PPU) Reagents and Services (https://mrcppureagents.dundee.ac.uk/) (Table S3). Plasmids for HIS-Titin were provided by Prof. Olga Mayans (University of Konstanz). Titin was cloned into a pMEX3Cb vector to express His-Titin. Recombinant Desmin (A60041) and His-SUMO-MYLPF (A225264) were bought from antibodies.com.

2.2. Expression and purification of proteins

Plasmids were transformed into BL21 competent Escherichia Coli (E. Coli) cells. A single colony was selected and inoculated in Ampicillin-treated LB media expanding to 1 L (For MBP-MuRF1, MBP-MuRF2 and MBP-MuRF3 expression 200 μM ZnSO4 was also added prior to Isopropyl β-D-1-thiogalactopyranoside (IPTG) induction) at 37 °C 180 rpm. Bacteria were grown to OD 600 of 0.6 before the addition of 250 μM IPTG to induce protein expression. Growth was inhibited by reducing the temperature down to 18 °C and left overnight to continue protein expression. The cells were pelleted by centrifugation at 5000×*g* at 4 °C for 15 min. Pellets were resuspended in lysis buffer (HIS tag: 50 mM Tris-HCl pH 8.0, 150 mM NaCl, 50 mM Imidazole, 0.5 mM TCEP, 1 mM PMSF. MBP tag: 50 mM Tris-HCl pH 7.5, 150 mM NaCl, 5 % Glycerol, 1 mM TCEP, 1 mM PMSF) and lysed using an Emulsiflex C3 Cell Disruptor (Avestin Europe, Mannheim, Germany). Lysate was cleared at 5000×*g* 4 °C for 2 h and filtered using a 0.45 μm filter to remove any remaining cell debris. Recombinant proteins were purified using His-Trap (GE Healthcare) or Amylose resin (New England Biosciences) as per manufacturer's protocol. Protein purity was confirmed using a Coomassie blue stain (Thermo Fisher Scientific) and protein concentration was determined using a nanodrop. Protein samples were concentrated using 50 kDa centrifugal filters (Amicon, Merck) and stored at −80 °C.

2.3. In vitro ubiquitylation assay

In vitro reaction (50 μl) contained 50 mM HEPES pH 7.5, 1 mM DTT, 10 mM MgCl2, 1 mM ATP, 50 μg ubiquitin, 0.2 μg HIS-UBE1, 0.6 μg UBE2 and 2.5 μg MBP-MuRF1, MBP-MuRF2 or MBP-MuRF3. For experiments involving substrates (His-Titin fragment (A168-A170), Desmin or His-SUMO-MYLPF), 0.5 μg of substrate was included alongside 0.5 μg of MBP-MuRF1, MBP-MuRF2 or MBP-MuRF3. Reactions were performed at 37 °C for 1 h at 1000 rpm on the Thermoshaker (Eppendorf) and terminated with the addition of 4x LDS sample buffer (Thermo Fisher Scientific) containing 5 % β-mercaptoethanol to final concentration 1x and 1.25 % respectively. Samples were left overnight at room temperature to denature.

2.4. Western blotting

Samples were loaded on 8 % acrylamide Bis-Tris gels and separated using SDS-PAGE gel electrophoresis. Gels were run in 1x MOPS buffer for approximately 90 min at 140 V. Proteins were transferred onto PVDF membranes (Millipore, Hertfordshire, UK) for 2.5 h at 30 V based on an optimised protocol for detecting polyubiquitin chains [26]. Membranes were blocked in 5 % BSA diluted in Tris-buffered saline Tween-20 (TBS-T) for 1 h and incubated overnight at 4 °C with the appropriate primary antibody: Anti-MBP (E8038S, 1:60,000) from New England Biolabs, 6xHis (631212, 1:10,000) from Clontech, Anti-MYLPF (MF-5, 1:1000) from Developmental Studies Hybridoma Bank, Desmin (5332, 1:1000) from Cell Signalling Technology, Anti-ubiquitin P4D1 (646302,

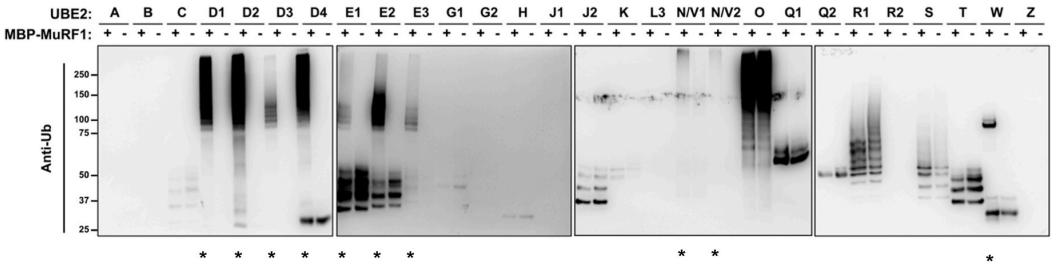

Fig. 1. In vitro ubiquitylation assay shows UBE2D, UBE2E, UBE2N/V, and UBE2W family members partnering with MuRF1 to form conjugated ubiquitin (mono- or poly-ubiquitin). A library of 28 human ubiquitin E2s (with exception to non-classical Ubiquitin E2s - listed in Table S1) were incubated with or without MBP-MuRF1 for 1 h during an in vitro ubiquitylation assay. Samples were subject to SDS-PAGE gel electrophoresis before western blot imaging to detect MuRF1-dependent ubiquitylation using anti-ubiquitylated proteins antibody. UBE2s that form MuRF1-dependent ubiquitylation are highlighted with an asterisk (*).

1:1000) from BioLegend, Anti-ubiquitylated proteins FK2 (04–263, 1:1000), Anti-Ubiquitin K48-Specific (05–1307, 1:1000) and Anti-Ubiquitin K63-Specific (05–1313, 1:1000) from Merck-Millipore. Membranes were washed in TBS-T three times prior to 1 h incubation at room temperature in horseradish peroxidase-conjugated secondary antibodies from Cell Signalling Technology (1:10,000). Membranes were washed a further three times in TBS-T prior to antibody detection using enhanced chemiluminescence horseradish peroxidase substrate detection kit (Millipore, Hertfordshire, UK). Imaging was undertaken using a G:BOX Chemi-XR5 (Syngene, Cambridgeshire, UK).

2.5. Study approval for animal experiments

The mice used in these studies were males from the C57BL/6 strain obtained from Charles River Laboratories at ages 3–4 month and used for experiments within 2 weeks of their arrival. Animals were housed in ventilated cages maintained in a room at 21 °C with 12-h light/dark cycles and had ad libitum access to standard chow (Harlan-Teklad formula 7913) and water throughout the study. Using the same samples obtained from previous published experiments [27], we undertook new analysis of UBE2 gene expression. Briefly, denervation-induced skeletal muscle atrophy was performed as previously described [27,28], through targeted denervation of the lower limb muscles of the right leg was accomplished via transection of the sciatic nerve in the midthigh region of mice using forceps. The procedure was completed under isoflurane anaesthesia (3 % inhalation) with the use of aseptic surgical techniques. Mice were given an analgesic (buprenorphine, 0.1 mg kg^{-1}) immediately, as well as for 48 h following surgery, and returned to their cage following recovery. Following completion of the appropriate time period (3, 7, 14, and 21 days; $n = 6$ per group), mice were anaesthetized with 3 % isoflurane, and the gastrocnemius complex (GSTC) muscles were excised, weighed, frozen in liquid nitrogen and stored at −80 °C for later analysis. On completion of tissue removal, mice were killed by exsanguination. A separate untreated cohort of animals ($n = 6$) was used as the relevant control. All animal procedures were approved by the Institutional Animal Care and Use Committee at the University of Iowa.

2.6. RNA isolation and qPCR

RNA isolation and qPCR were performed as previously described [29]. RNA was isolated from frozen gastrocnemius muscle powder using RNAzol RT reagent (Sigma-Aldrich, St Louis, MO). Complementary DNA (cDNA) was generated from 1 μg of RNA using the iScript Reverse Transcription Supermix kit (BioRad, Hercules, CA). qPCR experiments were performed using the Power SYBR Green master mix (Thermo Fisher Scientific) on a Quantstudio 6 Flex Real-time PCR System (Applied Biosystems, Foster City, CA). Gene expression values were normalised to muscle mass, as previously performed [29–31]. The mouse primers used in this study are shown in Table S2.

2.7. Statistical analysis

Data presented as ± SEM. The statistical analyses were performed using Prism (GraphPad Software). One-way ANOVA was performed with Tukey's post hoc test and p values $< .05$ were considered statistically significant.

3. Results

3.1. MuRF1 interacts with UBE2D, E, N/V families, and UBE2W to induce ubiquitylation

To investigate which UBE2s function with MuRF1, a full screen of 28 recombinant human UBE2s was undertaken to determine which catalyse MuRF1-dependent ubiquitylation in vitro. It is known that some UBE2s can build ubiquitin chains without the need of an E3 ligase, therefore we screened UBE2s with and without MuRF1 to detect MuRF1-dependent ubiquitylation. The results showed that MBP-MuRF1 interacts with UBE2D family (D1, D2, D3 and D4), UBE2E family (E1, E2, and E3), UBE2N/V1 and UBE2N/V2 by forming polyubiquitin chains (Fig. 1). We found that UBE2W monoubiquitylates MuRF1, illustrated by the single band ~90 kDa (Fig. 1). To ensure that ubiquitylation occurs on MuRF1 and not the MBP tag, we performed an in vitro ubiquitylation assay with either MBP-MuRF1 or MBP-alone which showed that ubiquitylation did not occur on MBP tag (Fig. S1). Some UBE2s can form unanchored ubiquitin chains [32], depicted by ubiquitin bands below the molecular weight of MBP-MuRF1 (~85 kDa). Overall, this data demonstrates MuRF1 produces distinct ubiquitylation in a UBE2 dependent manner.

3.2. MuRF1 autoubiquitylates by a sequential interaction with UBE2W then UBE2N/V family to form K63-linked polyubiquitin chains

Previous research has shown other TRIM E3 ligases, TRIM5α and TRIM21, partner with UBE2W to form monoubiquitin as an anchor to attach additional polyubiquitin chains [32,33]. As such, we proceeded to explore whether this mechanism also occurs with MuRF1. First, we determined which UBE2s were capable of attaching ubiquitin onto MuRF1 itself (autoubiquitylation). We found that unlike the other MuRF1 partnering UBE2s, UBE2N/V1 and UBE2N/V2 generated polyubiquitin chains unbound to MBP-MuRF1 (Fig. S2). This is evident from the level of unmodified MBP-MuRF1, which is dramatically reduced in the presence of UBE2D, E and W, but unchanged by UBE2N/V. Therefore, we hypothesised that the UBE2N/V family requires UBE2W to form anchored polyubiquitin chains. To test this hypothesis, we examined the ubiquitin chains formed by each MuRF1-interacting UBE2 in the presence or absence of UBE2W. We found that the combination of UBE2N/V1 or N/V2 with UBE2W causes polyubiquitylation of MBP-MuRF1 (Fig. 2A). This indicates that monoubiquitin is an anchor on MuRF1 to allow further polyubiquitin chains, generated by

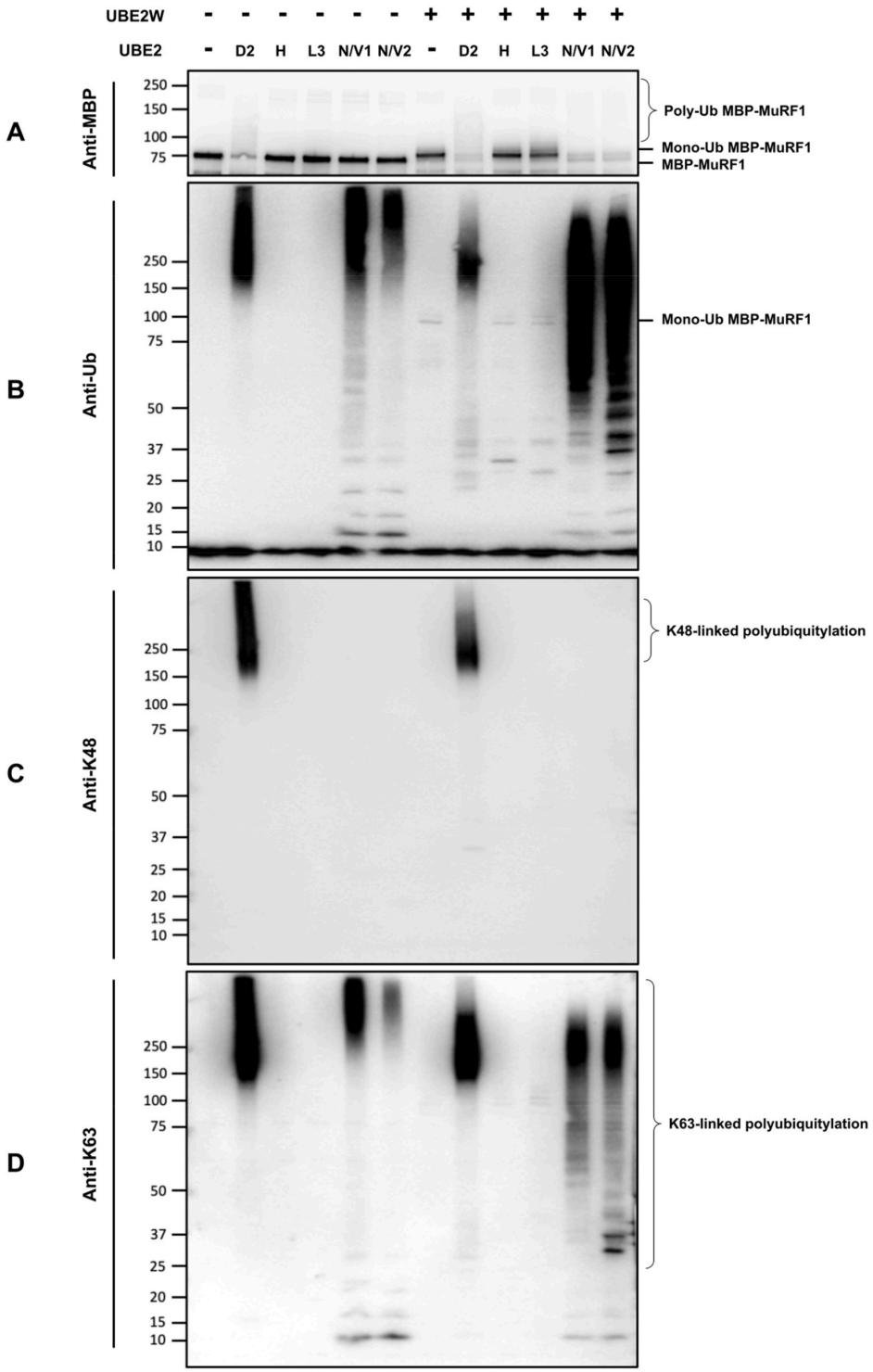

Fig. 2. Combination of UBE2W with other MuRF1-interacting UBE2s shows that UBE2W and UBE2N/V cooperate to generate MuRF1-anchored K63 polyubiquitin chains. In vitro ubiquitylation assay of MuRF1-interacting E2s: UBE2D2, N/V1 and N/V2, were incubated in the presence or absence of UBE2W. UBE2H and UBE2L3 were used as negative controls. The reaction mixtures were separated by SDS-PAGE and proteins detected by anti-MBP (A), anti-ubiquitin (B), anti-ubiquitin K48-Specific (C) and anti-ubiquitin K63-Specific (D).

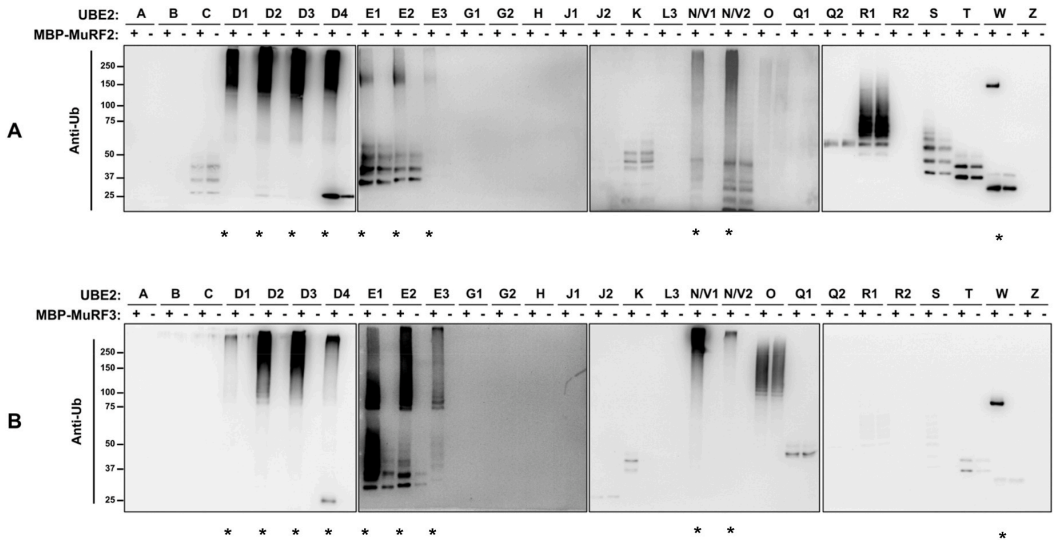

Fig. 3. In vitro ubiquitylation assay shows UBE2D, UBE2E, UBE2N/V, and UBE2W family members partnering with MuRF2 and MuRF3 to form conjugated ubiquitin (mono- or polyubiquitin). 28 different UBE2s were incubated with or without a) MBP-MuRF2 or b) MBP-MuRF3 for 1 h during an in vitro ubiquitylation assay. Samples were subject to SDS-PAGE gel electrophoresis before western blot imaging to detect MuRF2- and MuRF3-dependent ubiquitylation using anti-ubiquitylated proteins antibody. UBE2s that form MuRF2- and MuRF3-dependent ubiquitylation are highlighted with an asterisk (*).

UBE2N/V1 or N/V2, to attach. The polyubiquitin chains formed by UBE2D2 shifted to a lower molecular weight in the presence of UBE2W, suggesting the ubiquitin chain lengths were shortened (Fig. 2B). Therefore, whilst we can confirm that MuRF1 autoubiquitylation by UBE2D family is not UBE2W dependent, we cannot rule that UBE2W alters the topology of ubiquitin chains. Furthermore, probing for specific polyubiquitin chain types demonstrated that UBE2N/V1 and N/V2 can generate K63-linked, but not K48-linked, polyubiquitin chains (Fig. 2C and D). Consistent with previous experiments, UBE2D2 was able to form polyubiquitin chains on MBP-MuRF1 (Fig. 2A and B). UBE2D families are able to generate all eight different linkage types of polyubiquitin chains [34]. In similar fashion UBE2D2 was able to generate K48- and K63-linked polyubiquitin chains (Fig. 2C and D).

3.3. *MuRF2 and MuRF3 partner with the same UBE2s as MuRF1 to execute protein ubiquitylation*

Sequencing of each MuRF E3 ligase shows over 80 % alignment across their N-terminal residues, including the UBE2-binding RING finger domain [21]. Therefore, we hypothesised that MuRF1, MuRF2 and MuRF3 would share UBE2 partners. To investigate this, we screened MuRF2 and MuRF3 with 28 UBE2s to determine whether they partner with the same UBE2s as MuRF1. We found that as with MuRF1, MuRF2 and MuRF3 also function with the UBE2D, UBE2E, UBE2N/V and UBE2W family (Fig. 3). As expected, UBE2W attached a single ubiquitin molecule to MBP-MuRF2 and MBP-MuRF3, whereas UBE2D, UBE2E, and UBE2N/V produced polyubiquitin chains.

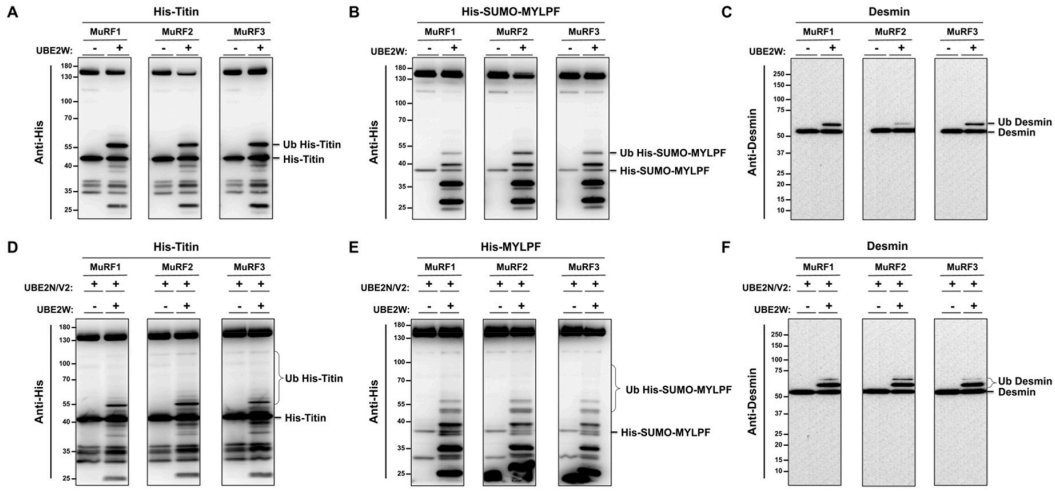

Fig. 4. MuRF1, MuRF2 and MuRF3 all target Titin, MYLPF and Desmin for ubiquitylation. A & D) His-Titin (A168-A170), B & E) His-SUMO-MYLPF and C & F) Desmin were incubated with MBP-MuRF1, MBP-MuRF2 or MBP-MuRF3 with or without UBE2s (W and N/V2) for 1 h during an in vitro ubiquitylation assay. Samples were subject to SDS-PAGE gel electrophoresis before western blot imaging. Anti-His antibody was used to detect His-Titin and His-SUMO-MYLPF and Anti-Desmin antibody was used to detect Desmin.

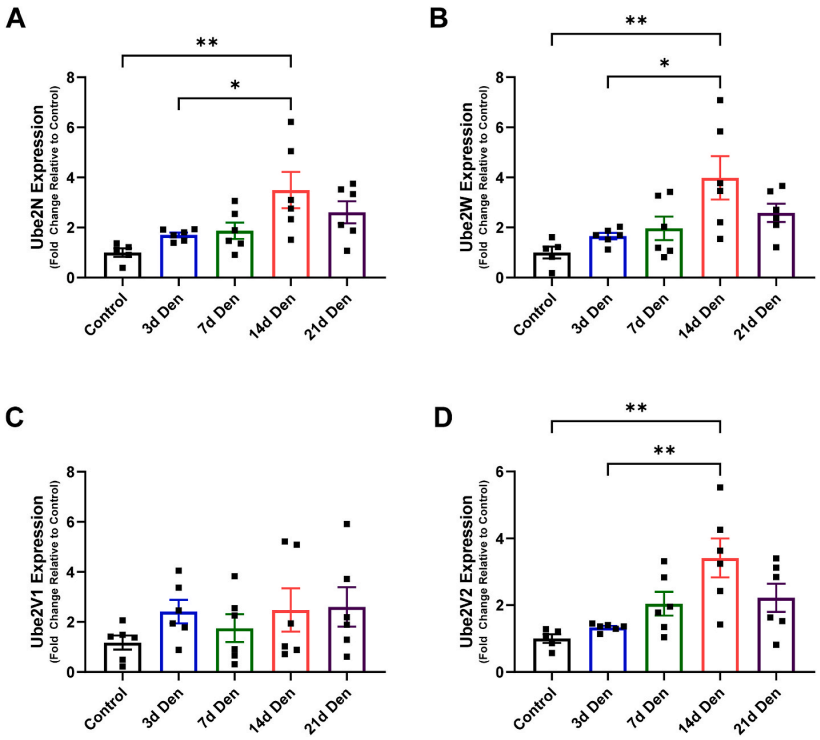

Fig. 5. UBE2N, UBE2W, UBE2V2, but not UBE2V1, mRNA expression increases following denervation of gastrocnemius complex muscle in mice. C57BL/6 mice were grown for 3–4 months and then had their right leg denervated through surgical ablation of the sciatic nerve. Mice were sacrificed (at days 3, 7, 14, and 21) and their gastrocnemius UBE2 mRNA expression was measured by rt-qPCR. P-values were calculated using a one-way ANOVA with Tukey's post hoc test, *P < .05; **P < .01. Data presented as means ± SEM (n = 6).

3.4. MuRF E3 ligases directly ubiquitylates Titin, MYLPF and Desmin in vitro

To provide further evidence for MuRF overlap during ubiquitylation, we next explored whether MuRF1, 2 and 3 can ubiquitylate the same substrates in vitro. The first substrate tested was Titin (A168-170) which is well established as a site of MuRF1 translocation and interaction [21, 35–37], and more recently a binding site for MuRF2 and MuRF3 [38]. Additionally, we included MYLPF and Desmin as in vitro substrates, previously identified as potential MuRF1 substrates [29,39,40]. The ubiquitylation assays revealed that MuRF1, MuRF2 and MuRF3 partner with UBE2W to ubiquitylate His-Titin (A168-A170) (Fig. 4A), His-SUMO-MYLPF (Fig. 4B) and Desmin (Fig. 4C), demonstrating them to be direct substrates of all MuRF E3 ligases. The two-step mechanism of UBE2W and UBE2N/V2 that had been identified during MuRF autoubiquitylation, is also seen with substrate ubiquitylation whereby UBE2N/V2 can only polyubiquitylated substrates once they have been monoubiquitylated by UBE2W (Fig. 4D, E and F). Notably, the poly-ubiquitylated substrates appeared more difficult to detect as each chain length gets diluted and subsequently becomes less sensitive to antibody detection. When blotting for His, we also detect His-tagged UBE1 and UBE2's, which also become ubiquitylated and appear near the predicted band for ubiquitylated His-Titin and His-SUMO-MYLPF (Fig. 4A, B, D and E). To confirm that the labelled bands in the His blots were in fact ubiquitylated Titin and MYLPF and not other His-tagged proteins present in the reaction, we also blotted for the ubiquitin and MYLPF respectively. These western blots showed the bands above His-Titin (A168-A170) and His-SUMO-MYLPF, confirming that these bands are the ubiquitylated substrates (Figs. S3 and S4). To ensure that our model of substrate ubiquitylation was valid, we wanted to confirm that substrate ubiquitylation did not occur just because of their close proximity to ubiquitin and ubiquitin-regulating enzymes. Using our model, we also tested Valosin-containing protein (VCP) - another potential MuRF1 substrate [29], and found that it is not directly ubiquitylated by MuRF1 (Fig. S5). Therefore, our model does not cause all proteins to be ubiquitylated and so we can take more confidence that Titin, MYLPF and Desmin are direct substrates of MuRF1, MuRF2 and MuRF3.

3.5. UBE2N, W, and V2 gene expression increases following denervation of mouse skeletal muscle

Having identified MuRF E3 ligases cooperating with UBE2W and UBE2N/V during autoubiquitylation and substrate ubiquitylation, we wanted to investigate the importance of these UBE2s in skeletal muscle. MuRF1 is best known for its increased expression during different atrophic conditions, therefore we were interested to see if UBE2W and UBE2N/V followed a similar pattern. Using denervated mouse muscle that experienced muscle atrophy and increased MuRF1 mRNA expression [27], we measured the mRNA expression of UBE2W, UBE2N, UBE2V1 and UBE2V2. We confirmed the presence of all these UBE2's in muscle and found that UBE2W, UBE2N and UBE2V2 are upregulated following 14 days of denervation (Fig. 5A, B and D). Therefore, the two-step mechanism of UBE2W and UBE2N/V could play an important role in regulating the function of MuRF1 during denervation-induced muscle atrophy.

4. Discussion

In vitro ubiquitylation assays allow us to study direct reactions/interactions of ubiquitin-regulating enzymes. With this assay, we

identified a list of UBE2s that can partner with MuRF1 during ubiquitylation. Further, we showed that MuRF1 partners with different UBE2s to form multiple chain types, including K48- and K63-linked polyubiquitin chains. We identified that MuRF1 can partner with UBE2W to monoubiquitylate itself (autoubiquitylation), which can then serve as an anchor for K63-linked polyubiquitylation. This two-step mechanism allows MuRF1 to directly ubiquitylate Titin (A168-A170), MYLPF and Desmin. Utilising this in vitro method, we also found that MuRF2 and MuRF3 share the same UBE2 partners as MuRF1 and can target the same substrates, providing a molecular explanation for their functional redundancy in vivo.

4.1. Sequential and overlapping mechanism in UBE2 interaction with MuRF1, MuRF2 and MuRF3

We identified that MuRF1 was able to partner with all the UBE2D and UBE2E members to form polyubiquitin chains. Previous research has already shown the capacity for MuRF1 to partner with UBE2D and E families to form polyubiquitin chains [16,19,20,41]. The mechanisms by which MuRF1 function with the UBE2D family are disputed, with yeast-two hybrid methods showing no physical interaction with UBE2D2 [42]. However, it is possible that UBE2 binding properties are altered when bound to ubiquitin, which is not included during these interaction-based methods. Therefore, it is important not to directly compare the findings of in vitro ubiquitylation studies to interaction-based studies. Our data highlights MuRF1 ubiquitylation activity through direct cooperation with the UBE2D and E family of enzymes and therefore aligns with the current literature. These two families of UBE2s make up a quarter of the ubiquitin-conjugating enzymes in humans, offering a substantial number of partners to facilitate MuRF1 activity.

Our data demonstrates a common familial function of MuRF1 with fellow TRIM E3s, TRIM21 and TRIM5α. Like these E3 Ligases, MuRF1 can form K63-linked polyubiquitin chains in a two-step fashion by partnering with UBE2N/V1, or V2 and UBE2W to form an anchor on the substrate [32,33]. It is crucial to understand the diversity of ubiquitin chain types generated by this mechanism, since chain types determine the fate of substrates. We were able to confirm that K48-linked polyubiquitin chains were not formed, however future work would benefit from screening all ubiquitin chain types. Having shown overlap of MuRF1-UBE2 partners with other TRIM E3 ligases, we hypothesised that this could occur with MuRF2 and MuRF3. Previous work using ELISA-based methods found MuRF1, MuRF2 and MuRF3 display autoubiquitylation activity with some individual UBE2s [16], here we demonstrated that MuRF1, MuRF2 and MuRF3 function with all the same UBE2 enzymes (UBE2Ds, Es, Ns/Vs and W) during in vitro ubiquitylation.

From a structural perspective, the reason for specific UBE2-MuRF interactions during ubiquitylation is likely due to the sequence of E3-binding surface present on UBE2 loop regions [12,13]. Sequence variations in these motifs therefore contribute to the specificity of E3 binding [43]. It is worth mentioning that the interaction strength between MuRF1 and UBE2's has been shown to increase in the presence of telethonin [15], so we cannot rule out the possibility that UBE2-MuRF1 binding would be altered in the presence of a substrate.

4.2. Overlap in MuRF1, MuRF2 and MuRF3 substrate ubiquitylation

Using our in vitro model, we demonstrated that Titin (A168-A170), MYLPF and Desmin are direct substrates of all MuRF E3 ligases. Recent work has alluded to MuRF1-dependent ubiquitylation of these substrates in cancer cachexia [44]. This demonstrates the importance of these substrates in MuRF1 ubiquitylation, however the importance of these substrates in MuRF2 and MuRF3 ubiquitylation is not known. Given that only MuRF1 plays a predominant role in targeting substrates for degradation during atrophy, it is possible that MuRF2 and MuRF3 contribute to the normal turnover of these cytoskeletal substrates. Studies have shown that MYLPF is degraded by MuRF1 after denervation-induced atrophy [40] and is reduced following 14 days of MuRF1 overexpression [29]. We found that MuRF1 directly ubiquitylates MYLPF, supporting the hypothesis that degradation of MuRF1 substrates is caused by direct ubiquitylation. By revealing that MuRF2 and MuRF3 can also ubiquitylate MYLPF, they may also contribute its degradation. Desmin has been previously shown to be degraded during fasting-induced atrophy in a TRIM32 dependent manner [45]. Their study showed that TRIM32 expression did not change by fasting-induced atrophy, whereas MuRF1 expression increased. Since revealing Desmin as a direct substrate of MuRF1, this raises the question whether both MuRF1 and TRIM32 are required to contribute to Desmin ubiquitylation, facilitating its degradation. MuRF2 may have a more protective role for Desmin ubiquitylation given its function for maintaining intermediate filament proteins [46]. In support, increased Desmin ubiquitylation was associated with increased protein abundance following ASB2β overexpression in which MuRF2 was also increased [47]. This study along with others have revealed 10 different ubiquitylation sites on Desmin [48]. Future work could investigate whether any of these sites are ubiquitylated by all MuRF E3 ligase which would imply some redundant role.

We showed that substrate ubiquitylation can occur by a two-step ubiquitylation with UBE2W and UBE2N/V enzymes. This offers a mechanistic link to previous work showing that MuRF E3 ligases regulate K63-linked ubiquitin chains on Titin to signal for the degradation via autophagy [38]. A recent study reported that MuRF1 ubiquitylation of Titin resulted in recruitment of NBR1 and P62, proteins that facilitate the autophagy of large protein cargo [49]. MuRF2 also interacts with NBR1/P62 on Titin [50]. These data build a causal chain of events that end with Titin autophagy by p62 and NBR1, mediated by K63-linked chains, instigated by the MuRF-UBE2 partners that we have elucidated.

4.3. Implications in muscle atrophy

Given the role of MuRF1 during muscle atrophy, we wanted to test whether the UBE2's they function with are also upregulated during muscle atrophy. In dexamethasone treated mice, UBE2E1 knockdown exacerbated muscle atrophy [51]. Therefore, UBE2E family may be important for protecting MuRF1 substrates from degradation. Furthermore, transcriptomics of mice treated with dexamethasone for 14 days have shown increased expression of UBE2D2, D3, N, V1, and V2 [52]. The UBE2D family are highly promiscuous, interacting with most E3's to form all ubiquitin-linkage types, as such the biological importance of increased UBE2D expression is difficult to address. Following denervation-induced atrophy in mice, we found that mRNA expression of UBE2N, W, and V2 transiently increased at 14 days post-denervation. However, the peak mRNA expression of these UBE2 enzymes occurs later than MuRF1 mRNA, which occurs 3–7 days post denervation [27]. The loss of muscle mass is significantly greater after 14 days denervation when compared to 3–7 days, which could suggest that these UBE2's only increase in response to more severe muscle wasting. The delayed transient expression of UBE2s shown in our work highlights the importance of screening multiple time points of atrophy when studying UBE2s. In the perspectives of drug discovery, disrupting MuRF1-E2 interactions at their peak expression could offer an efficient therapeutic approach to diminish MuRF1's effect on muscle atrophy.

5. Conclusion

The data presented here offers molecular insight into MuRF-induced ubiquitylation. We show that MuRF1 can interact with the UBE2D, E, N/V families and UBE2W during ubiquitylation. MuRF1 forms monoubiquitylation and creates K48- and K63-linked polyubiquitin chains in a UBE2 dependent manner. We provide evidence of direct substrates of MuRF1 ubiquitylation, namely Titin, MYLPF, and Desmin. Additionally,

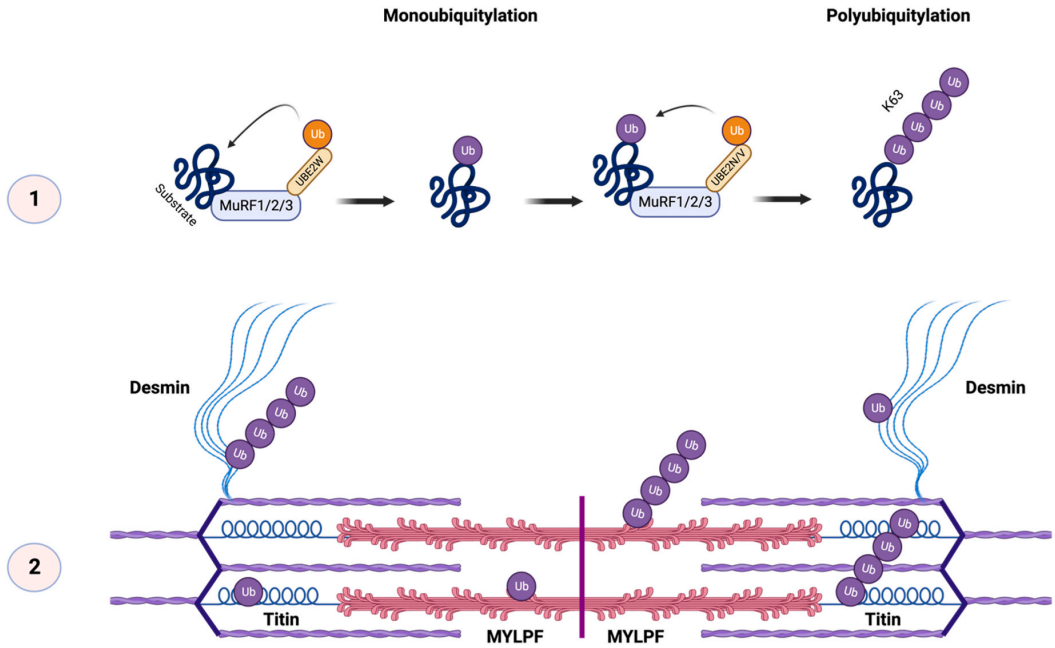

Fig. 6. Schematic of proposed explanation for MuRF E3 ligase functional redundancy. 1) MuRF3 E3 ligases bind with UBE2W to transfer a single ubiquitin onto the substrate (monoubiquitylation). This ubiquitin modification acts as an anchor for K63-linked ubiquitin chain formation (polyubiquitylation) by UBE2N/V. 2) We propose that each MuRF E3 ligase can perform the above mechanism of ubiquitylation on Titin (A168-A170), MYLPF and Desmin. Created with BioRender.com.

we show that these mechanisms are not specific to MuRF1, but also occur with MuRF2 and MuRF3. We propose that these findings are important for partial MuRF functional redundancy in vivo. Therefore, we have put forward a working hypothesis that under basal conditions MuRF1, MuRF2 and MuRF3 are co-ordinately involved in the ubiquitylation of certain substrates to ensure that individual loss of MuRF E3 ligase function does not impair the function of skeletal muscle (Fig. 6).

Funding

S.L. was supported by the Biotechnology and Biological Sciences Research Council (BBSRC) and University of Birmingham-funded Midlands Integrative Biosciences Training Partnership (MIBTP) (BB/T00746X/1). P.D. was supported by MRC Versus Arthritis Centre for Musculoskeletal Aging Research (MR/P021220/1). J.C–O. was supported by Ministry of Higher Education, Science, Research and Innovation, Thailand and Department of Applied Thai Traditional Medicine, Faculty of Medicine, Thammasat University, Thailand. Y–C.L. was supported by MRC Versus Arthritis Centre for Musculoskeletal Aging Research (MR/P021220/1).

CRediT authorship contribution statement

Samuel O. Lord: Writing – review & editing, Writing – original draft, Visualization, Methodology, Investigation, Conceptualization. **Peter W. J. Dawson:** Writing – original draft, Visualization, Methodology, Investigation, Conceptualization. **Jitpisute Chunthorng-Orn:** Writing – review & editing, Resources. **Jimi Ng:** Visualization, Writing – review & editing. **Leslie M. Baehr:** Visualization, Methodology, Investigation, Formal analysis. **David C. Hughes:** Writing – review & editing, Visualization, Methodology, Investigation, Formal analysis. **Pooja Sridhar:** Resources. **Timothy Knowles:** Supervision. **Sue C. Bodine:** Supervision. **Yu-Chiang Lai:** Writing – review & editing, Writing – original draft, Visualization, Supervision, Methodology, Investigation, Conceptualization.

Declaration of competing interest

We declare no conflicts of interest, financial or otherwise.

Acknowledgements

The authors gratefully acknowledge the MRC protein phosphorylation and ubiquitylation unit, University of Dundee for providing recombinant proteins required for in vitro ubiquitylation assays. We also thank Prof. Olga Mayans (University of Konstanz) for providing the His-Titin plasmid.

Appendix A. Supplementary data

Supplementary data to this article can be found online at https://doi.org/10.1016/j.bbrep.2023.101636.

References

[1] S.W. Jones, R.J. Hill, P.A. Krasney, B.O. Conner, N. Peirce, P.L. Greenhaff, Disuse atrophy and exercise rehabilitation in humans profoundly affects the expression of genes associated with the regulation of skeletal muscle mass, Faseb. J. 27 (4) (2004) 1–27.
[2] S.C. Bodine, et al., Identification of ubiquitin ligases required for skeletal muscle atrophy, Apr. 01, 2019. [Online]. Available: https://www-jstor-org.ezproxye.bham.ac.uk/stable/pdf/3085298.pdf?refreqid=excelsior%3Aaf00ba1aeb2f31bef1633084dffca959, 2001.
[3] J. Aniort, et al., Muscle wasting in patients with end-stage renal disease or early-stage lung cancer: common mechanisms at work, J. Cachexia. Sarcopenia Muscle 10 (2) (2019) 323–337, https://doi.org/10.1002/jcsm.12376.
[4] R.F. Carvalho, et al., Heart failure increases atrogin-1 and MuRF1 gene expression in skeletal muscle with fiber type-specific atrophy, J. Mol. Histol. 41 (1) (2010) 81–87, https://doi.org/10.1007/s10735-010-9262-x.
[5] E.K. Merritt, A. Thalacker-Mercer, J.M. Cross, S.T. Windham, S.J. Thomas, M. M. Bamman, Increased expression of atrogenes and TWEAK family members after severe burn injury in nonburned human skeletal muscle, J. Burn Care Res. 34 (5) (2013) 5–8, https://doi.org/10.1097/BCR.0b013e31827a2a9c.
[6] B.A. Clarke, et al., The E3 ligase MuRF1 degrades Myosin heavy chain protein in dexamethasone-treated skeletal muscle, Cell Metabol. 6 (5) (2007) 376–385, https://doi.org/10.1016/j.cmet.2007.09.009.

[7] O. Schakman, et al., Role of IGF-I and the TNFα/NF-κB pathway in the induction of muscle atrogenes by acute inflammation, Am. J. Physiol. Endocrinol. Metab. 303 (6) (2012), https://doi.org/10.1152/ajpendo.00060.2012.

[8] L.M. Baehr, J.D. Furlow, S.C. Bodine, Muscle sparing in muscle RING finger 1 null mice: response to synthetic glucocorticoids, J. Physiol. 589 (19) (2011) 4759–4776, https://doi.org/10.1113/jphysiol.2011.212845.

[9] S. Labeit, C.H. Kohl, C.C. Witt, D. Labeit, J. Jung, H. Granzier, Modulation of muscle atrophy, fatigue and MLC phosphorylation by MuRF1 as indicated by hindlimb suspension studies on MuRF1-KO mice, J. Biomed. Biotechnol. 2010 (2010), https://doi.org/10.1155/2010/693741.

[10] D.C. Files, et al., A critical role for muscle ring finger-1 in acute lung injury-associated skeletal muscle wasting, Am. J. Respir. Crit. Care Med. 185 (8) (2012) 825–834, https://doi.org/10.1164/rccm.201106-1150OC.

[11] R. Budhidarmo, Y. Nakatani, C.L. Day, RINGs hold the key to ubiquitin transfer, Trends Biochem. Sci. 37 (2) (2012) 58–65, https://doi.org/10.1016/j.tibs.2011.11.001.

[12] Y. Ye, M. Rape, Building ubiquitin chains: E2 enzymes at work, Nat. Rev. Mol. Cell Biol. 10 (11) (2009) 755–764, https://doi.org/10.1038/nrm2780.

[13] M.D. Stewart, T. Ritterhoff, R.E. Klevit, P.S. Brzovic, E2 enzymes : more than just middle men, Nat. Publ. Gr. 26 (4) (2016) 423–440, https://doi.org/10.1038/cr.2016.35.

[14] D. Komander, M. Rape, The ubiquitin code, Annu. Rev. Biochem. 81 (1) (2012) 203–229, https://doi.org/10.1146/annurev-biochem-060310-170328.

[15] C. Polge, et al., A muscle-specific MuRF1-E2 network requires stabilization of MuRF1-E2 complexes by telethonin, a newly identified substrate, J. Cachexia. Sarcopenia Muscle 9 (1) (2018) 129–145, https://doi.org/10.1002/jcsm.12249.

[16] J.G. Marblestone, et al., Comprehensive ubiquitin E2 profiling of ten ubiquitin E3 ligases, Cell Biochem. Biophys. 67 (1) (2013) 161–167, https://doi.org/10.1007/s12013-013-9627-3.

[17] Y. Maejima, et al., Muscle-specific RING finger 1 negatively regulates pathological cardiac hypertrophy through downregulation of calcineurin A, Circ. Hear. Fail. 7 (3) (2014) 479–490, https://doi.org/10.1161/CIRCHEARTFAILURE.113.000713.

[18] V. Kedar, H. McDonough, R. Arya, H.H. Li, H.A. Rockman, C. Patterson, Muscle-specific RING finger 1 is a bona fide ubiquitin ligase that degrades cardiac troponin I, Proc. Natl. Acad. Sci. U. S. A. 101 (52) (2004) 18135–18140, https://doi.org/10.1073/pnas.0404341102.

[19] C. Polge, et al., " Muscle actin is polyubiquitinylated in vitro and in vivo and targeted for breakdown by the E3 ligase MuRF1 ,", Faseb. J. 25 (11) (2011) 3790–3802, https://doi.org/10.1096/fj.11-180968.

[20] J. Fielitz, et al., Myosin accumulation and striated muscle myopathy result from the loss of muscle RING finger 1 and 3, J. Clin. Invest. 117 (9) (2007) 2486–2495, https://doi.org/10.1172/JCI32827.

[21] T. Centner, et al., Identification of muscle specific ring finger proteins as potential regulators of the titin kinase domain, J. Mol. Biol. 306 (4) (2001) 717–726, https://doi.org/10.1006/jmbi.2001.4448.

[22] M.S. Willis, C. Ike, L. Li, D.Z. Wang, D.J. Glass, C. Patterson, Muscle ring finger 1, but not muscle ring finger 2, regulates cardiac hypertrophy in vivo, Circ. Res. 100 (4) (2007) 456–459, https://doi.org/10.1161/01.RES.0000259559.48597.32.

[23] M.S. Willis, et al., Muscle ring finger 1 and muscle ring finger 2 are necessary but functionally redundant during developmental cardiac growth and regulate E2F1-mediated gene expression in vivo, Cell Biochem. Funct. 32 (1) (2014) 39–50, https://doi.org/10.1002/cbf.2969.

[24] C.C. Witt, S.H. Witt, S. Lerche, D. Labeit, W. Back, S. Labeit, Cooperative control of striated muscle mass and metabolism by MuRF1 and MuRF2, EMBO J. 27 (2) (2008) 350–360, https://doi.org/10.1038/sj.emboj.7601952.

[25] M. Olivé, et al., New cardiac and skeletal protein aggregate myopathy associated with combined MuRF1 and MuRF3 mutations, Hum. Mol. Genet. 24 (13) (2015) 3638–3650, https://doi.org/10.1093/hmg/ddv108.

[26] C.H. Emmerich, P. Cohen, Optimising methods for the preservation, capture and identification of ubiquitin chains and ubiquitylated proteins by immunoblotting, Biochem. Biophys. Res. Commun. 466 (1) (2015) 1–14, https://doi.org/10.1016/j.bbrc.2015.08.109.

[27] D.C. Hughes, L.M. Baehr, J.R. Driscoll, S.A. Lynch, D.S. Waddell, S.C. Bodine, Identification and characterization of Fbxl22, a novel skeletal muscle atrophy-promoting E3 ubiquitin ligase, Am. J. Physiol. - Cell Physiol. 319 (4) (2020) C700–C719, https://doi.org/10.1152/ajpcell.00253.2020.

[28] R.A. Seaborne, et al., UBR5 is a novel E3 ubiquitin ligase involved in skeletal muscle hypertrophy and recovery from atrophy, J. Physiol. 597 (14) (2019) 3727–3749, https://doi.org/10.1113/JP278073.

[29] L.M. Baehr, et al., Identification of the MuRF1 skeletal muscle ubiquitylome through quantitative proteomics, Am. Physiol. Soc. - Funct. 2 (May) (2021) 14–27.

[30] D.C. Hughes, et al., Alterations in the muscle force transfer apparatus in aged rats during unloading and reloading: impact of microRNA-31, J. Physiol. 596 (14) (2018) 2883–2900, https://doi.org/10.1113/JP275833.

[31] L.M. Baehr, et al., Age-related deficits in skeletal muscle recovery following disuse are associated with neuromuscular junction instability and ER stress, not impaired protein synthesis, Aging (Albany. NY) 8 (1) (2016) 127–146, https://doi.org/10.18632/aging.100879.

[32] A.J. Fletcher, et al., " TRIM 5α requires Ube2W to anchor Lys63-linked ubiquitin chains and restrict reverse transcription ,", EMBO J. 34 (15) (2015) 2078–2095, https://doi.org/10.15252/embj.201490361.

[33] A.J. Fletcher, D.L. Mallery, R.E. Watkinson, C.F. Dickson, L.C. James, J. Luban, Sequential ubiquitination and deubiquitination enzymes synchronize the dual sensor and effector functions of TRIM21, Proc. Natl. Acad. Sci. U. S. A. 112 (32) (2015) 10014–10019, https://doi.org/10.1073/pnas.1507534112.

[34] P.S. Brzovic, R.E. Klevit, Ubiquitin transfer from the E2 perspective: why is UbcH5 so promiscuous? Cell Cycle 5 (24) (2006) 2867–2873, https://doi.org/10.4161/cc.5.24.3592.

[35] A.S. McElhinny, K. Kakinuma, H. Sorimachi, S. Labeit, C.C. Gregorio, Muscle-specific RING finger-1 interacts with titin to regulate sarcomeric M-line and thick filament structure and may have nuclear functions via its interaction with glucocorticoid modulatory element binding protein-1, J. Cell Biol. 157 (1) (2002) 125–136, https://doi.org/10.1083/jcb.200108089.

[36] C.C. Gregorio, C.N. Perry, A.S. Mcelhinny, Functional properties of the titin/connectin-associated proteins, the muscle-specific RING finger proteins (MURFs), in striated muscle, J. Muscle Res. Cell Motil. 26 (6–8) (2005) 389–400, https://doi.org/10.1007/s10974-005-9021-x.

[37] M. Mrosek, et al., Molecular determinants for the recruitment of the ubiquitin-ligase MuRF-1 onto M-line titin, Faseb. J. 21 (7) (2007) 1383–1392, https://doi.org/10.1096/fj.06-7644com.

[38] E. Müller, S. Salcan, S. Bongardt, D.M. Barbosa, M. Krüger, S. Kötter, E3-ligase knock down revealed differential titin degradation by autopagy and the ubiquitin proteasome system, Sci. Rep. 11 (1) (2021) 1–13, https://doi.org/10.1038/s41598-021-00618-7.

[39] S.H. Witt, H. Granzier, C.C. Witt, S. Labeit, MURF-1 and MURF-2 Target a Specific Subset of Myofibrillar Proteins Redundantly: towards Under-standing MURF-dependent Muscle Ubiquitination, 2005, https://doi.org/10.1016/j.jmb.2005.05.021.

[40] S. Cohen, et al., During muscle atrophy, thick, but not thin, filament components are degraded by MuRF1-dependent ubiquitylation, J. Cell Biol. 185 (6) (2009) 1083–1095, https://doi.org/10.1083/jcb.200901052.

[41] T.K. Hyoung, et al., Certain pairs of ubiquitin-conjugating enzymes (E2s) and ubiquitin-protein ligases (E3s) synthesize nondegradable forked ubiquitin chains containing all possible isopeptide linkages, J. Biol. Chem. 282 (24) (2007) 17375–17386, https://doi.org/10.1074/jbc.M609659200.

[42] C. Polge, et al., UBE2D2 is not involved in MuRF1-dependent muscle wasting during hindlimb suspension, Int. J. Biochem. Cell Biol. 79 (2016) 488–493, https://doi.org/10.1016/j.biocel.2016.06.019.

[43] D.E. Christensen, R.E. Klevit, Dynamic interactions of proteins in complex networks: identifying the complete set of interacting E2s for functional investigation of E3-dependent protein ubiquitination, FEBS J. 276 (19) (2009) 5381–5389, https://doi.org/10.1111/j.1742-4658.2009.07249.x.

[44] D. Neyroud, et al., Blocking muscle wasting via deletion of the muscle-specific E3 ligase MuRF1 impedes pancreatic tumor growth, Commun. Biol. 6 (1) (2023) 1–17, https://doi.org/10.1038/s42003-023-04902-2.

[45] S. Cohen, B. Zhai, S.P. Gygi, A.L. Goldberg, Ubiquitylation by Trim32 causes coupled loss of desmin, Z-bands, and thin filaments in muscle atrophy, J. Cell Biol. 198 (4) (2012) 575–589, https://doi.org/10.1083/jcb.201110067.

[46] A.S. McElhinny, C.N. Perry, C.C. Witt, S. Labeit, C.C. Gregorio, Muscle-specific RING finger-2 (MURF-2) is important for microtubule, intermediate filament and sarcomeric M-line maintenance in striated muscle development, J. Cell Sci. 117 (15) (2004) 3175–3188, https://doi.org/10.1242/jcs.01158.

[47] C.A. Goodman, J.R. Davey, A. Hagg, B.L. Parker, P. Gregorevic, Dynamic changes to the skeletal muscle proteome and ubiquitinome induced by the E3 ligase, ASB2β, Mol. Cell. Proteomics 20 (2021) 100050 https://doi.org/10.1016/j.mcpro.2021.100050.

[48] G. Agnetti, H. Herrmann, S. Cohen, New roles for desmin in the maintenance of muscle homeostasis, FEBS J. 289 (10) (2022) 2755–2770, https://doi.org/10.1111/febs.15864.

[49] J. Bogomolovas, et al., Titin kinase ubiquitination aligns autophagy receptors with mechanical signals in the sarcomere, EMBO Rep. 22 (10) (2021) 1–14, https://doi.org/10.15252/embr.201948018.

[50] S. Lange, et al., The kinase domain of titin, Science 308 (June) (2005) 1599–1603.

[51] P. Cécile, et al., UBE2E1 is preferentially expressed in the cytoplasm of slow-twitch fibers and protects skeletal muscles from exacerbated atrophy upon dexamethasone treatment, Cells 7 (11) (2018), https://doi.org/10.3390/cells7110214.

[52] L.C. Hunt, et al., Integrated genomic and proteomic analyses identify stimulus-dependent molecular changes associated with distinct modes of skeletal muscle atrophy, Cell Rep. 37 (6) (2021) 109971, https://doi.org/10.1016/j.celrep.2021.109971.